MARMARA UNIVERSITY
INSTITUTE FOR GRADUATE STUDIES
IN PURE AND APPLIED SCIENCES

FILTER BACKWASH HYDRAULICS: AN INVESTIGATION ON POROUS AND NON-SPHERICAL MEDIA

SELDA YİĞİT HUNCE

Ph.D. THESIS

Department of Environmental Engineering

Thesis Supervisor

Prof. Dr. Ömer AKGİRAY

Thesis Co-supervisor

Assist. Prof. Dr. Elif SOYER

ISTANBUL, 2016

MARMARA UNIVERSITY
INSTITUTE FOR GRADUATE STUDIES
IN PURE AND APPLIED SCIENCES

FILTER BACKWASH HYDRAULICS: AN INVESTIGATION ON POROUS AND NON-SPHERICAL MEDIA

SELDA YİĞİT HUNCE

724310002

Ph.D. THESIS

Department of Environmental Engineering

Thesis Supervisor

Prof. Dr. Ömer AKGİRAY

Thesis Co-supervisor

Assist. Prof. Dr. Elif SOYER

ISTANBUL, 2016

ACKNOWLEDGEMENT

Foremost, I would like to express my sincere thanks to my advisors Prof. Dr. Ömer Akgiray and Assist. Prof. Dr. Elif Soyer for the continuous support to my phD study and research, for their endless encouragement, patience, constructive comments, understanding and immense knowledge. Working with them was a great opportunity for me.

I would like to express my special thanks to members of the thesis committee, Assoc Prof Dr Ayşe Çeçen Erbil and Assoc Prof Dr Adile Evren Tuğtaş Karnabat for their valuable advices, contributions and guidance during this work.

This study is supported by the Marmara University Scientific Research Committee (Project No: FEN-C-DRP-100713-0332). This financial support is greatly acknowledged.

I am grateful to all my friends working at the laboratories of the MU Environmental Engineering Department for their friendship and cooperation. I also thank to all my colleagues from Istanbul University, especially İberia and Burak, for their kindly support to complete this work.

I wish to thank my parents for their support and encouragement throughout my life. Also, I would like to thank my sisters Sema and Seda and their lovely families.

Lastly, and most importantly, I wish to thank my husband Özgür Hunce for his love, support, patience and encouragement.

January 2017 **Selda Yiğit Hunce**

TABLE OF CONTENTS

ACKNOWLEDGEMENT i

ABSTRACT iv

ÖZET vi

CLAIM OF ORIGINALITY viii

SYMBOLS ix

ABBREVIATIONS xiii

LIST OF FIGURES xiv

LIST OF TABLES xvii

1 INTRODUCTION 1

1.1 Particle Characterization 2

1.1.1 Particle Density 2

1.1.2 Particle Size 3

1.1.3 Particle shape 4

1.1.4 Sieve Analysis for the Characterization of Size and Size Distribution 6

1.1.5 Particle Characterization of porous materials 8

1.2 Fluid dynamics of a single particle 12

1.2.1 Particle Drag coefficient 12

1.2.2 The Stokes law regime and the Stokes free fall velocity 13

1.2.3 Empirical drag coefficient expression 14

1.3 Fixed bed hydraulics 15

1.3.1 Flow Through Packed Beds 16

1.3.2 Correlations for fixed bed porosity 19

1.3.3 Correlations for flow through packed beds 19

1.4 Filter Backwash Hydraulics and Fluidization 23

1.4.1 Filter Backwash Hydraulics 23
1.4.2 Liquid-Solid Fluidization 25
1.4.3 Fluidization of Binary Mixtures 39
2 MATERIALS and METHODS 42
2.1 Filter Materials 42
2.1.1 Spherical Particles 42
2.1.2 Non-spherical particles 43
2.2 Fluidization System 44
2.3 Fluidization of Binary Mixtures 47
2.4 Characterization of particles 49
2.4.1 Density 49
2.4.2 Particle Size 58
2.4.3 Sieving 61
2.4.4 Permeability Experiments 63
3 RESULTS AND DISCUSSION 66
3.1 Spherical Particles 66
3.2 Binary Mixtures of Spherical Particles 75
3.3 Non-spherical Particles 81
3.3.1 Non-spherical Non-porous Particles 81
3.3.2 Non-spherical Porous Particles 90
4 CONCLUSIONS 108
REFERENCES 112
ÖZGEÇMİŞ 155

ABSTRACT

FILTER BACKWASH HYDRAULICS: AN INVESTIGATION ON POROUS AND NON-SPHERICAL MEDIA

Liquid-solid fluidization is involved in many of the processes and operations in Environmental Engineering. The expansion of granular medium filter beds during backwashing is a significant example among these applications. The objective of this study is to investigate the overall expansion of fluidized granular beds containing different types of filter materials. Expansion of uniform and non-uniform spherical and non-spherical beds have been studied.

In this study, both spheres with different size and density values, and non-spherical (porous and non-porous) materials have been studied experimentally and the results have been analyzed. The fluidization experiments were conducted on uniform beds comprised of twenty different spherical particles (6 glass, 6 cellulose acetate, 4 delrin, 1 PVC and 3 plastics), thirty three different binary mixtures of spherical particles, twenty sieved fractions of four different non-spherical non-porous materials (sand, garnet, perlite and crushed glass) and fifteen sieved fractions of non-spherical porous materials (zeolite, activated carbon and anthracite). Density, equivalent diameter and sphericity measurements were employed to characterize the particles. Sphericity values were determined using fixed bed headloss data and calculated for each non-spherical materials used in this work. Permeability experiments for non-spherical particles were performed in different porosity values to determine the effect of porosity on sphericity.

The findings of the fluidization experiments of spherical particles reveal that Garside and Al-Dibouni (1977) and Akgiray and Soyer (2006) equations are the most reliable correlations for the prediction of bed expansion of spherical particles. The percent error values on predicted bed porosity for Garside and Al-Dibouni (1977) and Akgiray and Soyer (2006) correlations are found as 1.97 and 2.07, respectively. The well known equations proposed by Richardson and Zaki (1954) and Wen and Yu (1966) have error results as 6.96% and 6.93% based on porosity, respectively. Serial model provides the most reliable results for the prediction of fluidized bed expansion of binary mixtures of spheres.

A new experimental technique has been proposed to measure hydraulic density of porous filter materials considering the water in the pores of particles. Four different density measurement methods (skeletal, soak and strain, Le Chatelier and cone test) were evaluated for these materials. The results show that the standard cone test is the most suitable method for the type of applications considered in this work whereas the use of other simpler methods leads to varying degrees of error. An important finding of this work is that the fluidized-bed expansion data of the porous media studied here are in excellent agreement with the predictions of the correlation that Soyer and Akgiray (2009) developed by testing non-porous materials only.

January, 2017 **Selda Yiğit Hunce**

ÖZET

FİLTRE GERİ YIKAMA HİDROLİĞİ: KÜRESEL OLMAYAN VE GÖZENEKLİ YATAKLARIN İNCELENMESİ

Sıvı katı akışkanlaşma Çevre Mühendisliği'nde kullanılan birçok proses ve işlemde yer almaktadır. Granül filtre yataklarının akışkanlaşma sırasındaki genişlemesi bu uygulamalara önemli bir örnektir. Bu çalışmanın amacı, farklı filtre malzemeleri içeren akışkan granüler yatakların genişlemesini incelemektir. Yeknesak ve yeknesak olmayan küresel ve küresel olmayan yataklarda genişleme araştırılacaktır.

Bu çalışmada, farklı boyut ve yoğunluk değerlerine sahip küreler ve küresel olmayan (gözenekli ve gözeneksiz) malzemeler, deneysel olarak incelenmiş ve sonuçlar analiz edilmiştir. Akışkanlaşma deneyleri yirmi farklı küresel malzeme (6 cam, 6 selüloz asetat, 4 delrin, 1 PVC ve 3 plastik), otuz üç farklı ikili küresel malzeme karışımı, dört farklı küresel olmayan gözeneksiz malzemenin (kum, garnet, perlit ve kırık cam) yirmi elenmiş fraksiyonu ve küresel olmayan üç farklı gözenekli malzemenin (zeolit, aktif karbon, antrasit) on beş elenmiş fraksiyonu ile oluşturulan uniform yataklar ile yürütülmüştür. Parçacıkların özelliklerini belirlemek için yoğunluk, eşdeğer çap ve küresellik ölçümleri uygulanmıştır. Küresel olmayan malzemeler için geçirgenlik deneyleri gözenekliliğin küresellik üzerindeki etkisini belirlemek amacıyla farklı porozite değerlerinde gerçekleştirildi.

Küresel parçacıkların akışkanlaştırma deneylerinin bulguları, Garside ve Al-Dibouni (1977) ve Akgiray ve Soyer (2006) denklemlerinin, küresel parçacıkların yatak genişlemelerinin tahmini için en güvenilir korelasyonlar olduğunu ortaya koymaktadır. Garside ve Al-Dibouni (1977) ve Akgiray ve Soyer (2006) korelasyonları için tahmin edilen yatak gözenekliliğinde yüzde hata değerleri sırasıyla 1.97 ve 2.07 olarak bulunmuştur. Richardson ve Zaki (1954) ve Wen ve Yu (1966) tarafından önerilen iyi bilinen denklemler yatak gözenekliliği tahmini için sırasıyla % 6.96 ve % 6.93 hata değerlerine sahiptir. Seri model, ikili küresel malzeme karışımlarının akışkan yatak genişlemesinin tahmininde en güvenilir sonuçları sağlamaktadır.

Gözenekli filtre malzemelerinin hidrolik yoğunluğunu, parçacıkların gözeneklerindeki su dikkate alınarak ölçmek için yeni bir deney tekniği önerilmiştir. Bu malzemeler için dört

farklı yoğunluk ölçüm yöntemi değerlendirilmiştir. Sonuçlar, standart koni testinin, bu çalışmada ele alınan uygulama tipleri için en uygun yöntem olduğunu, diğer basit yöntemlerin kullanılmasının çeşitli derecelerde hata oluşturduğunu göstermektedir. Çalışmanın önemli bir bulgusu, incelenen gözenekli malzemelerden oluşturulan akışkan yatakların genişleme verisi Soyer ve Akgiray (2009)'ın sadece gözenekli olmayan malzemeleri test ederek geliştirdiği korelasyonunun tahminleriyle mükemmel bir uyum içerisinde olmasıdır.

Ocak, 2017 **Selda Yiğit Hunce**

CLAIM OF ORIGINALITY

FILTER BACKWASH HYDRAULICS: AN INVESTIGATION ON POROUS AND NON-SPHERICAL MEDIA

One of the significant problems in filter design is choosing an appropriate backwash velocity. The expansion of a filter bed at a particular velocity depends on the density, size distribution, shape characteristics of the material and the temperature of the water. The objective of this study is to investigate the overall expansion of fluidized granular beds containing different types of filter materials.

In this study, both spheres with different size and density values and non-spherical materials were studied experimentally and the results have been analyzed using existing correlations in the relevant literature. Also, experiments were performed with different porous filter materials. Penetration of the fluid employed into the pores of the grains is critical since it directly affects the density of particles. Particle and bed characteristics (such as particle density, particle equivalent diameter, mass of a sample placed into the bed, bed porosity) should be carefully determined before being used in hydraulic calculations for fixed and fluidized beds of porous particles. A new experimental technique (Le Chatelier test) has been developed and tested to measure hydraulic density of porous filter materials considering the water in the pores of particles. Four different density measurement methods (skeletal, soak and strain, Le Chatelier and cone test) were evaluated for these materials. The density of each of the fifteen fractions of porous materials was determined using these methods. The results show that the standard cone test is the most reliable method for the type of applications considered in this work whereas the use of other methods leads to varying degrees of error. An important finding of this work is that the fluidized-bed expansion data of the porous media studied here are in excellent agreement with the predictions of a correlation that Soyer and Akgiray (2009) developed by testing non-porous materials only.

This work contains original data, measurement techniques, calculation and assessment methods and the results will provide valuable insights into the relavant literature.

Ocak, 2017 **Prof. Dr Ömer Akgiray** **Selda Yiğit Hunce**

SYMBOLS

A: Bed area

A_p : Surface area of sphere of equal volume to the particle

A_{pr} : Particle projected area

B : Buoyancy

C_D : Particle drag coefficient

D = Column diameter

d_a: Projected area

d_c : Diameter of a circle equal in area to the projected area of the particle

d_{eq} : Equivalent volume diameter

d_{10}: Particle size, in millimeters, such that 10 % of the particles by weight are smaller

d_{60} : Particle size, in millimeters, such that 60 % of the particles by weight are smaller

d_p : Particle diameter

d_{pi} : Diameters of particles

ΔP : Pressure difference

dP_f/dz : Frictional pressure gradient

ε : Porosity

ε_0 : Porosity of fixed bed

ε_c : porosity at the core

ε_{mf} : Minimum fluidization porosity

ε_w : Porosity close to the wall

F : Fluid dynamic pressure

f_B : Blake's friction factor

F_D : Drag force

Fs : Force acting on a sphere

g : Gravitational acceleration (9.81 m/sec^2),

Ga : Galileo number

h : Headloss

k : Heywood shape factor

K : Ratio between the settling velocity of volume equivalent sphere and the settling velocity of the particle

L : Depth of the expanded bed

L_0 : Depth of the fixed bed

M : Mass of particles

$(M_{DW})_{OD}$: Mass of water displaced by OD material in 24 hours

$(M_{DW})_{SSD}$: Mass of the water displaced by the SSD sample

$(M_{DW})_{wet}$: Mass of water displaced by wet sample

M_{OD} : Oven dry mass of particles

M_{SSD} : Saturated surface dry mass of the sample

M_p = Mass of particles

M_{Pore} : Mass of pore water

M_{wet} : Mass of wet sample after straining

μ : Dynamic viscosity of fluid

n : Richarson-Zaki coefficient

N : Number of sieve sizes

N_p : Number of spheres

P : Pressure

Q : Flow rate through the filter bed

Re : Reynolds number

Re_1 : Modified Reynolds number

Re_B : Blake's Reynolds number

Re_{mf} : Reynolds number based on minimum fluidization

Re_t : Reynolds number based on terminal settling velocity

$Re_{t\infty}$: Reynolds number based on terminal settling velocity in an infinite column

Re_p : Particle Reynolds number

ρ : Density of fluid

ρ_B : Density of fluidized bed suspension

ρ_p : Particle density

ρ_w: Density of water at the test temperature

S : Particle surface area

S_p : Surface area of the particle

S_v : Specific surface

T : Temperature

u : Superficial velocity

U_r : Relative velocity of the particle

V : Velocity

$V_{1,SSD}$: Initial level volume of water for SSD particles

$V_{2,SSD}$: Final level volume of water for SSD particles

$V_{1,OD}$: Initial level volume of water for OD particles

$V_{2,OD}$: Final level volume of water for OD particles

V_i : Intercept velocity

$V_{material}$: Volume of material

V_{mf} : Minimum fluidization velocity

V_p : Volume of the particle

V_{Pore} : Volume of water in pores of material

$V_{t\infty}$: Settling velocity of the particle in an infinite column

V_{total} : Total volume of bed

V_{voids} : Volume of voids of bed

ϕ : Voidage function

Φ : Dimensionless group as a function of Re_l

w_i : Weight ratio of particles

ψ : Sphericity coefficient

ABBREVIATIONS

ASTM : American Society of Testing Materials

AWWA : American Water Works Association

DIN : German Institute for Standardization

ES : Effective size

hp : Horse power

OD : Oven dry

PVC : Polyvinyl chloride

SSD : Saturated surface dry

UC : Uniformity coefficient

LIST OF FIGURES

Figure 1.1 Evaluation of sieve analysis results..... 6

Figure 1.2 Illustrations of oven dry (OD) and saturated surface dry (SSD) particles 9

Figure 1.3 The illustration of the definition of particle drag coefficient..... 12

Figure 1.4 Two basic packing layers of mono-sized spheres 16

Figure 1.5 Darcy's experiment 20

Figure 1.6 Semi batch liquid fluidization system (Yang, 2003)..... 26

Figure 1.7 Frictional pressure drop graph for homogenous monodisperse particles as a function of linear velocity 31

Figure 1.8 Frictional pressure drop versus liquid superficial velocity for particles of mixed sizes shapes and densities (Yang, 2003)..... 31

Figure 2.1. Schematic view of experimental set-up 45

Figure 2.2 The electromagnetic flowmeters used in experiments 46

Figure 2.3. Fluidization graph of spheres used in the study 48

Figure 2.4 Different materials prepared for density measurements. 49

Figure 2.5 Air bubbles in material surface 51

Figure 2.6 Illustrations of saturated surface dry (SSD) and oven dry (OD) particles ... 51

Figure 2.7 A photo of mold and tamper used in the study 52

Figure 2.8 Illustration of the procedure of Le Chatelier Flask Method..... 54

Figure 2.9 A photo of Le Chatelier flask..... 55

Figure 2.10 A photo of materials counted for equivalent diameter measurement..... 59

Figure 2.11 A photo of diameter measurement using micrometer 60

Figure 2.12 Standard sieves and sieve shaker 62

Figure 2.13 A photo from coning and quartering process..... 62

Figure 2.14 A photo of modified "Armfield W3 Permeability/Fluidization Study

Apparatus” 64

Figure 3.1 An example graph of fixed bed experiments for the determination of sphericities (2mm glass spheres) 69

Figure 3.2 Example graphs of percent bed expansion and fluidized bed porosity depending on fluidization velocity (1mm glass spheres) 69

Figure 3.4 The evaluation of all fluidization data of spheres 71

Figure 3.5 The evaluation of fluidization data of spheres with some limitations..... 73

Figure 3.6 Results of fluidization experiment of Bin8 mixture of spheres 78

Figure 3.7. An example graph of fixed bed experiments for the determination of sphericities (Sand 1.00-0.85) 82

Figure 3.8. The porosity versus fluidization velocity graph of sand 0.85-0.71 fraction as an example graph of Appendix III..... 85

Figure 3.9 The fluidization data of sand fractions based on dimensionless groups 88

Figure 3.10 The fluidization data of garnet fractions based on dimensionless groups. 89

Figure 3.11 The fluidization data of crushed glass fractions based on dimensionless groups 89

Figure 3.12 The fluidization data of perlite fractions based on dimensionless groups 90

Figure 3.13 Particle density of zeolite, activated carbon, and anthracite fractions 91

Figure 3.14 Water absorption of porous material fractions..... 92

Figure 3.15 Particle equivalent diameters of porous material fractions 94

Figure 3.16 Sphericities of porous material fractions..... 95

Figure 3.17 Median fixed-bed porosities of porous material fractions (loose-bed and compacted-bed porosities are shown as variation on the bars) 97

Figure 3.18 Fluidization data for anthracite, zeolite, and activated carbon fractions.... 99

Figure 3.19. Predicted versus actual bed porosity based on two methods of determining wet sample mass and effective density..... 100

Figure 3.20 Experimental data for anthracite coal fractions and model lines for different sphericity values (properties based on the standard cone test)..... 101

Figure 3.21 Experimental data for zeolite fractions and model lines for different sphericity values (properties based on the standard cone test)..... 101

Figure 3.22 Experimental data for activated carbon fractions and model lines for different sphericity values (properties based on the standard cone test)..... 102

Figure 3.23 Experimental versus predicted bed expansions based on three different correlations (properties based on the standard cone test)..... 105

LIST OF TABLES

Table 1.1 Particle diameter definitions (Allen, 2003)..... 4

Table 1.2. Common particle shape descriptions (Holdich, 2002)..... 5

Table 1.3. Sphericities of different non-spherical particles (Geldart, 1986; AWWA, 1999) 6

Table 1.4 Types of standard sieves and sieve openings..... 7

Table 1.5 Empirical drag correlations ($w = log10Rep$) (Yang, 2003) 14

Table 1.6 Packing Characteristics of regular uniform mono-sized spheres (Yang, 2003) 17

Table 1.7 Rough Estimate of Bed Porosity (Yang, 2003) 18

Table 1.8 Comparison of Backwash Alternatives for Granular Bed Filters (AWWA, 1999)..... 24

Table 1.9 C_1 and C_2 parameters according to different studies (Yang, 2003)..... 29

Table 1.10. Porosity-velocity correlations for the liquid-solid fluidization of spheres . 33

Table 2.1 Spherical particles used in experiments..... 42

Table 2.2 Fractions of natural materials used in this study 43

Table 2.3 Fractions of non-spherical porous materials..... 44

Table 2.4 Binary mixtures of different spherical materials 48

Table 2.5 The procedure of density measurement of spherical particles and calculations 50

Table 2.6 The calculations of density using cone test method 53

Table 2.7 The calculations of density using Le Chatelier flask method..... 56

Table 2.8 The calculations of density using soak-and-strain method..... 57

Table 2.9 The calculations of skeletal density..... 58

Table 2.10 An example of equivalent diameter measurement..... 59

Table 2.11 An example of diameter measurement using micrometer (3.5mm Cellulose

Acetate beads)..... 61

Table 3.1 The results of density measurements..... 66

Table 3.2 Equivalent diameters of spherical materials..... 67

Table 3.3 Results of diameter measurements using micrometer of spherical materials 68

Table 3.4 Percent errors in porosity of spheres according to different correlations..... 72

Table 3.5 Percent errors in porosity of spheres according to different correlations (with some limitations in data) 74

Table 3.6. The binary mixtures of spheres produced from same material having relatively same density 76

Table 3.7 The binary mixtures of spheres produced from different material having slightly different densities 76

Table 3.8 The binary mixtures of spheres produced from different material having highly different particle sizes and densities..... 77

Table 3.9. Absolute mean percent errors in predicted fluidized bed height for the type 1 binary mixtures of spheres..... 79

Table 3.10 Absolute mean percent errors in predicted fluidized bed height for the type 2 binary mixtures of spheres..... 79

Table 3.11 Absolute mean percent errors in predicted fluidized bed height for the type 3 binary mixtures of spheres..... 80

Table 3.12 The results of density measurements of non-spherical non-porous particles 83

Table 3.13 The results of equivalent diameter measurements of non-spherical non-porous particles..... 84

Table 3.14 Sphericity values of sand fractions at different bed porosities..... 85

Table 3.15 Sphericity values of garnet fractions at different bed porosities 85

Table 3.16 Sphericity values of crushed glass fractions at different bed porosities..... 86

Table 3.17 Sphericity values of perlite fractions at different bed porosities 86

Table 3.18 Mean percent error values of non spherical material fractions..... 87

Table 3.19 Sphericities at different porosities for anthracite fractions using cone test and Le Chatelier flask density measurement methods 103

Table 3.20 Sphericities at different porosities for zeolite fractions using cone test and Le Chatelier flask density measurement methods. 104

Table 3.21 Sphericities at different porosities for activated carbon fractions using cone test and Le Chatelier flask density measurement methods..... 104

Table 3.22 Mean percent errors in expansion and porosity predicted with Equation 1.116 106

1 INTRODUCTION

Granular filtration is an extensively used method for the removal of particles from surface waters and groundwaters. The porous medium of different granular materials is used in granular filtration. Sand, garnet, ilmenite, activated carbon, and anthracite coal are commonly used in granular bed filters in monomedium, dual media and triple media configurations. Three main types of filtration are generally used in water treatment: rapid filtration, slow sand filtration and depth filtration.

Rapid filtration is one of the most important processes in drinking water treatment and advanced treatment of wastewaters. In rapid filtration, particles that cause turbidity and constitute suspended solids accumulate in the filter bed and the filters get clogged over time. When head loss in a filter reaches a certain level or the effluent water turbidity exceeds a specified value, the filter is cleaned by backwashing and returned back to service. It is possible to backwash a mono-medium filter with simultaneous water and air backwash and without fluidization. Another widely used method is fluidized bed backwashing using only water. Most of the existing mono-medium filters are backwashed with fluidization. In addition, a final backwashing step using water only is required especially for the stratification of multi-media filters (for example, dual-media filters using anthracite and sand), even when air is used for effective cleaning, a final backwashing step using water only is necessary to ensure the stratification of the multimedia filters cleaned with air-scouring.

One of the significant problems in filter design is choosing an appropriate backwash velocity. Selection of the appropriate bakwash velocity and pump capacity in rapid filters is critical for an effective operation. The amount of expansion of the filter bed depends on the backwash velocity. When backwashing is inadequate, the filter bed will never fluidize, or it will partially fluidize and will not be cleaned effectively. In this case, the desired stratification will not be provided for a multi-media filter. On the other hand, if too high a backwash velocity is used, loss of material into the backwash water collection channels may result. Also, unnecessarily high backwash velocities will cause waste of energy and water. The expansion of a filter bed at a particular velocity depends on the density, size distribution, shape characteristics of the material and the temperature of the water. In order to choose an appropriate backwash velocity, a calculation method is needed to estimate the expansion of

the bed as a function of the backwash velocity. Such a calculation method should be applicable to uniform filters as well as non-uniform and multi-media filters.

In this study, both spheres and non-spherical materials were studied experimentally and the results have been analyzed using existing correlations in relevant literature. Also, the experiments were performed with porous filter materials. Penetration of the fluid employed in reactions into the micro and macro pores of the grains is critical since it directly affects density of particles. Particle and bed characteristics should be carefully determined before being used in hydraulic calculations for fixed and fluidized beds of porous particles. For the measurement of hydraulic density of porous filter materials, four different density measurement methods (skeletal, soak and strain, Le Chatelier and cone test) were evaluated for these materials. The objective of this study is to investigate the overall expansion of liquid fluidized granular beds containing materials with different physical properties. This study is focused on the total expansion of mono-medium and multimedia beds during fluidization.

1.1 Particle Characterization

The measurement methods used in characterization differ according to special properties of particles. For instance, the size of a spherical particle can be defined as only its diameter. However, the particles used in filtration process are generally irregular in shape. There are different methods in order to characterize such particles. The results of all these methods may not be consistent. The selection of appropriate method for the particle has importance for the characterization.

1.1.1 Particle Density

Density of a particle affects the fluidization behaviour of a filter medium by means of backwash flow requirements. Particles having higher density but same diameter require higher backwash rates to fluidize. For the prediction models used in fixed and fluidized beds, density must be determined prior to bed porosity and equivalent diameter determinations.

Different definitions of density are available in the literature, however the convenience of the method differs in applications where particle density is included in evaluations. Density definition is given as mass per volume of material for the non-porous granular materials:

$$\rho_p = \frac{M_p}{V_p} \tag{1.1}$$

M_p : weight of particles

ρ_p : density of particles

V_p : water displacement volume of particles

Methods employed in density determination of porous solids are given in following section.

1.1.2 Particle Size

The particle size of regular shaped particles are characterized by only one (for spheres), two or three dimensions. In many of the fixed and fluidized bed applications, irregular shaped are involved. The sizes of irregular shaped particles are generally characterized depending on reference properties and simple size measurement methods such as the use of a micrometer or calipper. The most commonly used sizes for the characterization of irregular materials are given in Table 1.1.

The mostly used ones among these diameter definitions in fixed and fluidized bed applications are sieve, volume equivalent and surface equivalent diameter (including surface are and surface volume).

The volume diameter or volume equivalent diameter (d_{eq}) is defined as the diameter of a sphere having the same volume as the particle. It is the most relevant diameter for applications in fluidized beds. The mathematical expression of this diameter is as following where V_p is the volume of the particle.

$$d_{eq} = \sqrt[3]{\frac{6 \times V_p}{\pi}} \tag{1.2}$$

This formula is generally used to define particle size in filtration and fluidization studies. The experimental determination of equivalent diameter using this formula will be explained in following chapter of the study.

1.1.3 Particle shape

Many empirical factors have been proposed for the particle shape of non-spherical particles. This empirical definitions of particle shape are obtained by the use of several parameters including: i) volume ii) surface area iii) projected area iv) projected perimeter of the particle.

There is no consensus among the all proposed shape factor definitions up to date, since some particles having significantly different shapes may result with the same shape factor. The use of a single shape factor for highly comlex shaped materials would fail and lead ineduquate characterization. If the complex shapes are described merely by a single parameter, this situation is ineluctable.

Table 1.1 Particle diameter definitions (Allen, 2003)

Diameter	Symbol	Definition
Sieve diameter	d_A	Smallest sieve aperture through which the particle will pass
Volume diameter (Equivalent spherical diameter)	d_{eq}	Diameter of a sphere having the same volume as the particle
Surface diameter	d_s	Diameter of a sphere having the same surface area as the particle
Surface-volume diameter	d_{Sv}	Diameter of a sphere having the same external-surface-to-volume ratio as the particle
Drag diameter	d_d	Diameter of a sphere having the same resistance to motion, ie., drag force, as the particle in a fluid of the same density and viscosity and at the same relative velocity
Free-falling diameter	d_h	Diameter of a sphere having the same density and the same free-falling speed as the particle in a fluid of the same density and viscosity
Stoke's diameter	d_{st}	The diameter of a free-falling particle in the laminar flow region, i.e. Re < 0.2
Projected area diameter 1	d_a	Diameter of a circle having the same area as the projected area of the particle resting in a stable position
Projected area diameter 2	d_p	Diameter of a circle having the same area as the projected area of the particle resting in random position
Perimeter diameter	d_c	Diameter of a circle having the same perimeter as the projected outline of the particle
Feret's diameter	d_f	The mean value of the distance between parallel tangents on opposite sides of the particle measured in a fixed direction for a number of particles
Martin's diameter	d_M	The chord length of the projected outline of the particle.i.e.,the length of the line that bisects the image of the particle; the line may be drawn in any direction, which must be maintained constant for all the image measurements

1.1.3.1 Sphericity

Sphericity is one of the most widely used parameters for characterising shape of irregular particles. The sphericity (ψ) is a parameter that is used to define the shape of a particle. The sphericity of a particle is defined by Wadell (1933) as the ratio of the surface area of a sphere having equal volume with the particle to the surface area of the particle (S_p) (Eq. 1.3 and Eq. 1.4). Sphericity of a perfect sphere is equal to 1 and it differs between 0-1 for all shapes. The calculated sphericities of several different shapes are displayed in Table 1.2.

$$\psi = \frac{Surface\ area\ of\ sphere\ of\ equal\ volume\ to\ the\ particle}{Surface\ area\ of\ the\ particle} \tag{1.3}$$

$$= \frac{A_p}{S_p} = \frac{\pi d_{eq}^2}{S_p} \tag{1.4}$$

Table 1.2. Common particle shape descriptions (Holdich, 2002)

Descriptor	Wadell's sphericity (ψ)	Example
Spherical	1.000	Glass beads, calibration latex
Rounded	0.820	Water worn solids, atomized drops
Cubic	0.806	Sugar, calcite
Angular	0.660	Crushed minerals
Flaky	0.540	Gypsum, talc
Platelet	0.220	Clays, kaolin, mica, graphite

The sphericities of several non-spherical particles are included in Table 1.3 (Geldart, 1986; AWWA, 1999).

Leva (1959) and Subramanian and Arunachalam (1980) proposed experimental methods for the evaluation of sphericity. In this method, headloss of a particle bed is recorded at different linear velocities. Then the Ergun (1952) equation (Eq. 1.5) is employed to find out particle specific surface (and hence particle sphericity see Eq. 1.4).

$$\frac{h_L}{L} = 150\frac{\mu}{\rho g}\frac{(1-\varepsilon)^2}{\varepsilon^3}\left(\frac{S_v}{6}\right)^2 V + 1.75\frac{1}{g}\frac{(1-\varepsilon)}{\varepsilon^3}\left(\frac{S_v}{6}\right)V^2 \tag{1.5}$$

h : Headloss (m), L : Bed height (m), μ : Dynamic viscosity of fluid (kg/m/s), ρ : Density of fluid (kg/m^3), g : Gravitational acceleration (9.81 m/sec^2), ε : Porosity, S_v : Specific surface, V : Velocity, m/sec

Table 1.3. Sphericities of different non-spherical particles (Geldart, 1986; AWWA, 1999)

Material	Sphericity (ψ)
Round sand	0.86
Sharp sand	0.66
Crushed sandstone	0.8-0.9
Pulverized coal	0.73
Crushed coal	0.63-0.75
Activated Carbon	0.70-0.90
Garnet	0.60
Mica flakes	0.28
Common salt	0.84
Crushed glass	0.65
Silica gels	0.70-0.90
Tungsten powder	0.89

1.1.4 Sieve Analysis for the Characterization of Size and Size Distribution

Sieve analysis is the most common method for the classification of granular particles. US sieve sizes and Tyler sieve sizes are generally employed in the US practice. German DIN sieve sizes and British sieve sizes are used in relevant applications in the Europe. The mesh number of a standard sieve is the number of parallel wires per inch in the grid of sieve. The types of standard sieves and sieve openings specified by American Society of Testing Materials (ASTM C136, 2005) are compared in Table 1.4. The results of sieve analysis are generally plotted as shown in Figure 1.1. It is useful to state the particle size as the ordinate and the cumulative weight percentage under size as the abscissa.

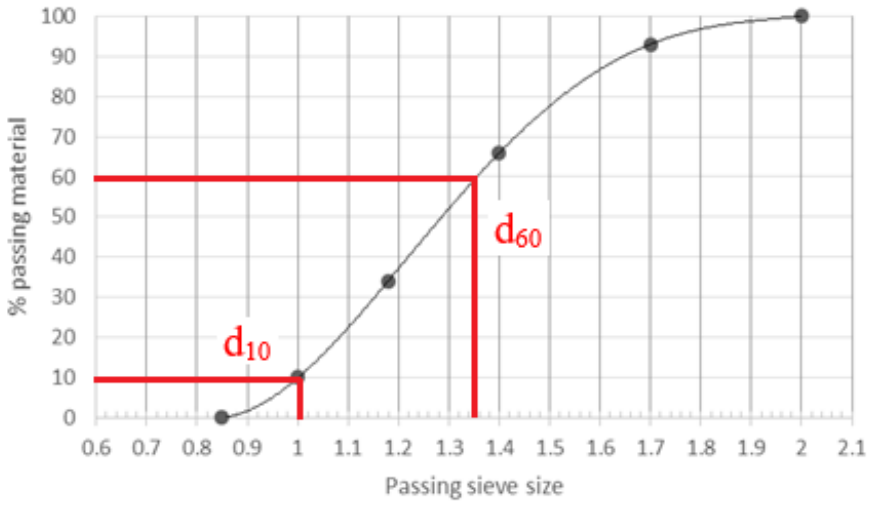


Figure 1.1 Evaluation of sieve analysis results

Table 1.4 Types of standard sieves and sieve openings

US mesh No.	Standard opening, mm	Tyler mesh No.	British mesh No.	Standard opening, mm	German DIN No.	Standard opening, mm
3 ½	5.66	3 ½	–	–	1	6
4	4.76	4	–	–	–	–
5	4	5	–	–	–	–
6	3.36	6	5	3.353	2	3
7	2.83	7	6	2.812	–	–
–	–	–	–	–	–	–
8	2.38	8	7	2.411	2 ½	2.4
10	2	9	8	2.057	3	2
12	1.68	10	10	1.676	4	1.5
–	–	–	–	–	–	–
14	1.41	12	12	1.405	–	–
–	–	–	–	–	–	–
16	1.19	14	14	1.204	5	1.2
–	–	–	–	–	–	–
18	1	16	16	1.003	6	1.02
20	0.84	20	18	0.853	–	–
–	–	–	–	–	8	0.75
25	0.71	24	22	0.699	–	–
–	–	–	–	–	–	–
30	0.59	28	25	0.599	10	0.6
–	–	–	–	–	11	0.54
35	0.5	32	30	0.5	12	0.49
40	0.42	35	36	0.422	14	0.43
45	0.35	42	44	0.353	16	0.385
–	–	–	–	–	–	–
50	0.297	48	52	0.295	20	0.3
60	0.25	60	60	0.251	24	0.25
70	0.21	65	72	0.211	30	0.2
80	0.177	80	85	0.178	–	–
100	0.149	100	100	0.152	40	0.15
–	–	–	–	–	–	–
120	0.125	115	120	0.124	50	0.12
140	0.105	150	150	0.104	60	0.102
170	0.088	170	170	0.089	70	0.088
–	–	–	–	–	–	–
200	0.074	200	200	0.076	80	0.075
230	0.062	250	240	0.066	100	0.06
270	0.053	270	300	0.053	–	–
325	0.044	325	–	–	–	–
400	0.038	400	–	–	–	–
635	0.02	–	–	–	–	–

A filter bed or in general a particle system, is characterized by stating its effective size and uniformity coefficient. Effective size (ES, d_{10}) is the particle size, in millimeters, such that 10% of the particles by weight are smaller and 90% are larger. Also, d_{60} is the size of aperture, in millimeters, through when 60% of particles passes. Uniformity coefficient (UC) is the ratio of d_{60} to d_{10} particle sizes (Eq. 1.6).

$$UC = \frac{d_{60}}{d_{10}} \tag{1.6}$$

The effective size and uniformity coefficient of a sample of material can be determined using sieve analysis. However, the information about the largest and smallest particle sizes cannot be obtained from sieve analysis. The size range provide a rough value for the average particle size. Also, it is not possible to distinguish the grain shape by sieve analysis. For example, a needle shaped particle can pass through a mesh or retain on the sieve, based on the orientation of particle during sieving. The effectiveness of sieving process are also depend on time of sieving, amount of material on the sieve and blinding or clogging of sieve. Agglomeration of small particles resulting from moisture or static electricity also might cause misleadings.

1.1.5 Particle Characterization of porous materials

Particle characterization of porous particles for hydraulic processes differs from the non-porous materials. Different definitions of density and corresponding methods of determination are described in the literature and the method selected, in principle, should depend on the area of application. However, a porous particle contains open and/or closed pores. An open pore has connections to the exterior surface of the particle, while a closed pore has no connections to the surface. Therefore, a fluid flowing around a particle can penetrate into an open pore (Figure 1.2). As a result, it is possible to define more than one type of density for a porous particle that is immersed in a fluid. A density based on the total mass of both solid and fluid contained within an imaginary envelope surrounding the particle and the total volume of that envelope (which contains the solid matrix and open and closed pores) will be different than the skeletal density (average density of the solid matrix including the closed pores) and is referred to as “wet density,” “effective density,” “envelope density,” or “hydraulic density” (Inglezakis and Poulopoulos, 2006; Stevenson, 1994; Tilton, 2008). Effective density is the same as skeletal density for non-porous materials, but skeletal density will be higher than the effective density for porous materials.

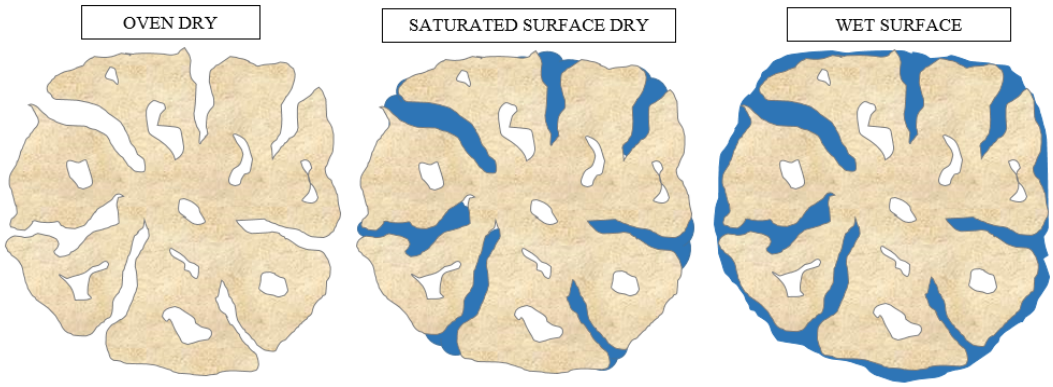


Figure 1.2 Illustrations of oven dry (OD) and saturated surface dry (SSD) particles

Leva et al. (1949) remarked that when working with porous materials like coal, the voidage and pycnometer density will contain the voids inside the particles. So the effective voidage and fluid flow characteristics could not be represented truly. Ergun (1951) noted that porous particles may be thought as having impervious envelope surroundings and that a fluid flowing through such a bed passes wholly through the void space, i.e. around the imaginary impervious envelopes surrounding the particles. Yang (2003) also explains that for porous materials the volume of a particle should be replaced with the envelope volume of the particle and that this approach would be more hydro-dynamically correct. All of these authors were considering gas-solid systems and therefore discussed only the measurement of "envelope volume," the effective density being based on the dry weight of the particles. In a liquid-solid system, however, the "wet weight" must also be determined and this introduces an additional complication in the determination of particle density.

Inglezakis and Poulopoulos (2006) explained that "hydraulic density is essential to many calculations involving fluidization and the suspension of particles" and added that "it is characteristic that in the related literature, authors use the terms "particle density" or "solid density" without specifying if the fluid in the pores has been taken into account." Stevenson (1994) noted that "porous materials are difficult to characterize" and "an approximate estimate of effective density can be obtained by soaking the grains and blotting them dry, leaving the internal pores filled, then using the specific-gravity bottle in the usual way." Morcom (1946) described a similar procedure (for measurement of particle volume including internal pores) involving "particles rolled on blotting paper until no water remained visible on the surface" reporting "fairly reproducible results" except for broken

coke. Benyahia and O'Neill (2005) also determined fixed-bed porosities using a soaking-blotting procedure. These authors stated that "particles that were porous were soaked in water to fill the pores and then were blotted with tissue paper to remove excess water on the surface before being used in the voidage measurement experiments." The step expressed as "blotting them dry" or "blotted to remove excess water" is ambiguous, however, and it is not clear how consistent and reproducible results can be obtained using such a procedure. This procedure may be successful with coarse particles (say, much larger than a few millimeters), but is very difficult to apply with fine materials. One practical difficulty is that fine particles tend to agglomerate when wet, and, even if this difficulty is somehow overcome, a sample of fine particles presents a large surface area per unit mass and it is not practical to blot such a large surface area uniformly and consistently. With both coarse and fine materials, too aggressive blotting may possibly lead to drainage of some of the liquid from the pores, whereas, especially with fine particles, it may be very difficult to apply blotting uniformly to all the particles in a sample leaving a fraction of particles with excessively wet external surfaces.

A standard density determination procedure for porous materials is detailed in ASTM Standard Test C128 (ASTM C128-12, 2012) and is recommended in AWWA Standard for Granular Filter Material (B100-01, 2001). This procedure is based on the "saturated surface dry" (SSD) condition of porous particles. This standard defines the SSD condition as the state in which the pores of particles are filled with water to the extent obtained by submerging in water for a specified period of time, however there should be no free water on the surface of particles. The SSD particle density is also defined as the mass of SSD material per unit volume of material. It includes the volume of impermeable pores, permeable pores and water-filled pores. But, it does not include the voids between the particles (ASTM C128-12, 2012). Although this density measurement method appears to be theoretically the most correct method for fixed and fluidized bed applications, it is reported that a reproducible SSD condition is difficult achieve (Edzwald, 2011; Logsdon, et al. 2002). Furthermore, the method is somewhat tedious and requires a certain level of experience and skill to perform.

There are only a few systematic studies of water fluidization of porous filter media (Amirtharajah and Cleasby, 1972; Amirtharajah, 1970; Carvalho, 1970; Cleasby and Baumann, 1976; Cleasby and Fan, 1981; Cleasby and Woods, 1975; Cleasby, 1973;

Dharmarajah and Cleasby, 1986; Dharmarajah, 1982; Gunasingham et al., 1978; Sholji and Johnson, 1987). In addition to typical non-porous filter materials such as silica sand and garnet sand, the only porous medium tested in all of these studies was anthracite coal which is of particular interest because it is used widely in water filtration. Gunasingham et al. (1978) did not give any information about how the density was measured, and, as a matter of fact, they did not even report the measured density values. Sholji and Johnson (1987) reported coal density values but did not describe how they were obtained. All of the other mentioned studies were carried out by Cleasby and co-workers over a period that spanned nearly two decades. One of the earlier of those studies is that by Carvalho (1970) and is of particular interest as it focuses on the fluidization of anthracite coal. From the description of density measurement method (on p. 54 and p. 96 of the thesis Carvalho (1970)), it is clear that density determinations were based on dry sample masses. Similarly, from the description of fixed-bed porosity measurements (on p. 103 of the thesis Carvalho (1970)), it is seen that the calculated porosity includes the internal pores of the coal particles. The density and porosity determination methods described by Amirtharajah (1970) are the same as those of Carvalho (1970) and would lead to the same errors, i.e. these methods would yield skeletal density (instead of effective density) values and porosities larger than true effective porosities, respectively. Cleasby and Fan (1981) explicitly stated that dry weights were used in the calculation of equivalent diameters and bed porosity. The latest and the most refined of these studies is that by Dharmarajah (1982) and Dharmarajah and Cleasby (1986) who also, as already mentioned, calculated equivalent diameters and porosities of anthracite coal fractions using dry weights of samples. In some of the above mentioned studies, it is stated that "coal samples were submerged for 24 hours before final weighings to allow the water to penetrate the pore space." This may be construed to mean (incorrectly) that coal samples were soaked in water for 24 hours and then separated from water and weighed in some approximate SSD condition. Even if this were true (which it is not, because samples were always weighed in bottles filled with water and were not weighed in isolation to determine their wet weights), there is no mention of a blotting or other surface drying procedure to prepare saturated samples before weighing. There is also no mention of the ASTM standard or the SSD condition described in the ASTM standard. As will be seen later in this work, simple draining of water by straining the media after soaking in water yields considerably different estimates of particle properties when compared to the results obtained

using the standard SSD condition.

The equivalent diameter measurement depends on the density results as can be seen from equations 1.1 and 1.2. Simply, particle density is required to calculate equivalent volume of a mass known particle. Also, particle density is required in order to calculate porosity and sphericity values. For this reason, the density measurement method has a key role on characterization of porous particles.

1.2 Fluid dynamics of a single particle

1.2.1 Particle Drag coefficient

The particle drag coefficient (C_D) is the ratio between the force on the particle and the fluid dynamic pressure (F) times the particle projected area (A_{pr}). C_D is a function of particle Reynolds number ($Re_p = U_r^2 \rho d_p / \mu$) for spheres and is given below (Figure 1.3):

$$C_D = \frac{F}{(1/2)\rho U_r^2 A_{pr}} \quad \text{or} \quad F = \frac{1}{2} C_D \rho U_r^2 A_{pr} \tag{1.7}$$

U_r is the relative velocity of the particle. Three different regimes exist based on the particle's Reynolds number: the Stokes regime, the intermediate regime and the Newton's law regime.

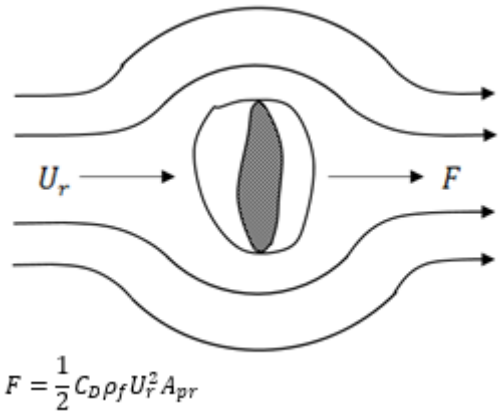


Figure 1.3 The illustration of the definition of particle drag coefficient

In the Stokes law regime, the viscosity of fluid is predominant and the particle Reynolds number is less than 0.2 ($Re_p < 0.2$). Also, the definition of drag coefficient is given by the following equation:

$$C_D = \frac{24}{Re_p} \tag{1.8}$$

The Reynolds number range for the intermediate regime is $0.2<Re_p<500$. In this type of regime, the drag coefficient is a function of particle Reynolds number and the mathematical expression is as given in below:

$$C_D = f\lfloor Re_p \rfloor \tag{1.9}$$

C_D is relatively constant ($C_D = 0.44$) in the Newton's law regime. The particle Reynolds number is larger than 500 ($Re_p > 500$) for this flow regime.

1.2.2 The Stokes law regime and the Stokes free fall velocity

The theoretical models used in the evaluation of $C_D$is valid only in the Stokes law regime. The theoretical analysis starts with the viscous flow around a sphere. Fs is the force acting on a sphere and it is expressed as:

$$F_s = 3\pi\mu d_p U_r \tag{1.10}$$

Viscous shear stress acting on the particle surface is the 2/3 of the drag force. Remaining 1/3 is caused by the pressure difference (drag) on particle surface. The following final form of equation is obtained by equating equations 1.7 and 1.10:

$$F_s = 3\pi\mu d_p U_r = \frac{1}{2} C_D \rho U_r^2 \frac{1}{4}\pi d_p^2 \quad \text{or} \quad C_D = 24\left(\frac{\mu}{d_p U_R \rho}\right) = \frac{24}{Re_P} \tag{1.11}$$

The linear relation between F_s and U_r is a significant feature of Stokes law, since it provides some simplifications for various problems.

Stokes free fall velocity is obtained by equating drag force of a single spherical particle to gravitational force and is expressed is as below:

$$F_s = \frac{\pi}{8} C_D \rho U_r^2 d_p^2 = \frac{\pi d_p^3}{6}(\rho_p - \rho)g \quad \text{or} \tag{1.12a}$$

$$C_D = \frac{4}{3}\frac{d_p(\rho_p - \rho)g}{\rho U_r^2} \quad \text{or} \tag{1.12b}$$

$$U_r = U_t = \frac{d_p^2(\rho_p - \rho)g}{18\mu} \tag{1.12c}$$

1.2.3 Empirical drag coefficient expression

The recommended drag correlations (Clift et al., 1978) for different ranges of particle Reynolds numbers are summarized in Table 1.5 (Yang, 2003).

Table 1.5 Empirical drag correlations ($w = log_{10}Re_p$) (Yang, 2003)

Particle Re number range	Drag coefficient expressions
$(\mathrm{Re})_p < 0.01$	$C_D = \frac{3}{16} + \frac{24}{(\mathrm{Re})_p}$
$0.01 < (\mathrm{Re})_p \le 20$	$\log_{10}\left[\frac{C_D(\mathrm{Re})_p}{24} - 1\right] = -0.881 + 0.82w - 0.05w^2$ $C_D = \frac{24}{(\mathrm{Re})_p}\left[1 + 0.1315(\mathrm{Re})_p^{(0.82-0.05w)}\right]$
$20 \le (\mathrm{Re})_p \le 260$	$\log_{10}\left[\frac{C_D(\mathrm{Re})_p}{24} - 1\right] = -0.7133 + 0.6305w$ $C_D = \frac{24}{(\mathrm{Re})_p}\left[1 + 0.1935(\mathrm{Re})_p^{0.6305}\right]$
$260 \le (\mathrm{Re})_p \le 1500$	$\log_{10} C_D = 1.6435 - 1.1242\ w + 0.1558\ w^2$
$1.5x10^3 \le (\mathrm{Re})_p \le 1.2x10^4$	$\log_{10} C_D = -2.4571 + 2.5558\ w - 0.9295\ w^2 + 0.1049\ w^3$
$1.2x10^4 \le (\mathrm{Re})_p \le 4.4x10^4$	$\log_{10} C_D = -1.9181 + 0.6370\ w - 0.0636\ w^2$
$4.4x10^4 \le (\mathrm{Re})_p \le 3.38x10^5$	$\log_{10} C_D = -4.3390 + 1.5809\ w - 0.1546\ w^2$
$3.38x10^5 \le (\mathrm{Re})_p \le 4x10^5$	$C_D = 29.78 - 5.3w$
$4x10^5 \le (\mathrm{Re})_p \le 10^6$	$C_D = 0.1w - 0.49$
$10^6 < (\mathrm{Re})_p$	$C_D = 0.19 - \frac{8x10^4}{(\mathrm{Re})_p}$

For the all ranges of Reynolds numbers Turton and Levenspiel (1986) recommended a correlation that simplifies the calculation of single particle drag coefficient. The equation proposed by Turton and Levenspiel (1986) is as following:

$$C_D = \frac{24}{Re_p}\left[1 + 0.173Re_p^{\,0.657}\right] + \frac{0.413}{1 + 16.3Re_p^{\,-1.09}} \tag{1.13}$$

Haider and Levenspiel (1989) proposed a developed version of the equation which is also valid for non-spherical particles.

$$C_D = \frac{24}{Re_p}\left[1 + (8.1716e^{-4.0655\psi})Re_p{}^{0.0964+0.5565\varphi}\right] + \frac{73.69\, e^{-5.0748\psi} Re_p}{Re_p + 5.378\, e^{6.2122\psi}} \qquad (1.14)$$

For the spherical particles the equation reduces into the following form:

$$C_D = \frac{24}{Re_p} + 3.3643 Re_p{}^{0.3471} + \frac{0.4607 Re_p}{Re_p + 2682.5} \qquad (1.15)$$

Pettyjohn and Christiansen (1948) investigated the free-settling rates of isometric particles having different shapes and sphericities (spheres (ψ=1), cube (ψ=0.806), octahedron (ψ=0.846), cube octahedron (ψ=0.906), and tetrahedron (ψ=0.670)). They suggested a correction factor in the following form:

$$K = 0.8431 log\left(\frac{\psi}{0.065}\right) \qquad Re_t < 0.05 \qquad 0.67 < \psi < 1 \qquad (1.16)$$

Here, K is the ratio of the settling velocity of volume equivalent sphere to the actual settling velocity of the particle.

1.3 Fixed bed hydraulics

Flow through packed beds had been investigated by a large number of investigators. These studies and models are based on two main approaches: the discrete particle model and the pipe flow analogy. Both of the models yielded valid predictions for pressure drop of flow through packed beds for spherical and almost-spherical particles, however they are not appropriate for the beds with irregular particles.

The pressure drop through the packed bed is resulted from the frictional resistance at the particle surface and from the expansion and contraction of flow through the spaces between the particles. The pipe flow analogy model (capillary tube model or channel model) is the most popular approach. Further refinement produced the constricted tube model. In this model, an assembly of tortuous channels of varying cross sections simulates the varying dimensions and curvatures of pores in the packed bed. The main studies based on this approach involve Blake (1922), Carman (1937), Ergun (1952) and Kozeny (1927). The discrete particle model accepts that the packed bed made up of a group of discrete particles which have their individual boundary layer. Although the pipe flow analogy model is more widely employed, the discrete particle model is more convenient to the physical definition of the flow through packed bed. The pipe flow analogy models are generally applicable for

the particles having sphericity values larger than about 0.6. The discrete particle models have wide applications for the particles having sphericity values less than 0.6.

1.3.1 Flow Through Packed Beds

Many chemical and environmental operations such as filtration and adsorption involve the use of packed bed or in other words fixed bed reactors. Packing characteristics of particles and the pressure drop through the packed bed of solids are the key subjects for the design and the operation of packed beds.

1.3.1.1 Packing Characteristics of Uniform-Sized Spheres

Packing of uniform and regular uniform-sized spherical particles is the most simple packing bed system. The porosity of such an ordered arrangement of uniform spheres can be calculated ideally by using mathematical considerations. The mathematical description of random packing of mono-sized spheres is more complicated and also the porosity of random packing of uniform spheres should be determined by carrying out experiments on the beds including these particles.

The regular packing is an organized form of particles composed of regular layers and rows. The square layer with a 90° angle and the simple rhombic layer with a 60° angle between the centers of spheres are the two basic layers (Figure 1.4). Six possible regular packings is yielded by the vertical stacking of these basic packings.

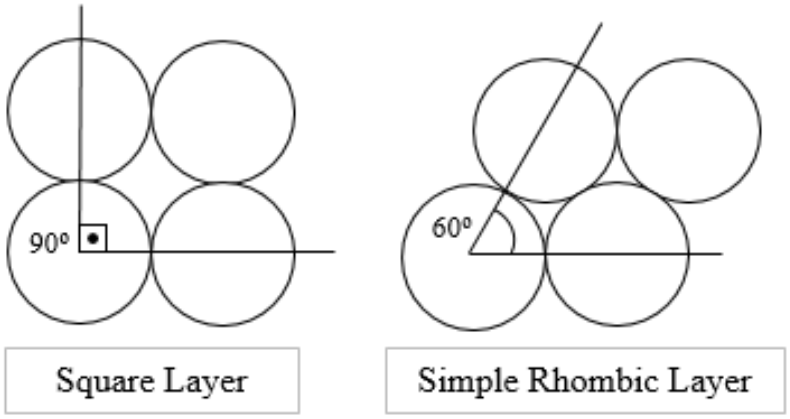


Figure 1.4 Two basic packing layers of mono-sized spheres

Bed porosity is independent of the size of particles spherical in shape. It only depends on the packing arrangement particles. Porosities calculated for these arrangements are given in Table 1.6 (Yang, 2003).

Table 1.6 Packing Characteristics of regular uniform mono-sized spheres (Yang, 2003)

Packing Type	Points of contact	Porosity
Cubic	6	0.4764
Orthorombic	8	0.3954
Tetragonal-Spheroidal	10	0.3019
Rhombohedral	12	0.2595

A random packing of uniform-sized spheres is obtained by random placement of particles. The two experimentally reproducible packings are loose random packing and dense random packing (Scott, 1960).

The porosity of loose random packing is in the range of 0.40 to 0.42, which is close to value obtained in cubic packing and orthorhombic packing. The density of dense random packing is between 0.61 and 0.63, and the porosity of this type of packing is in the range of 0.37 and 0.39 which is close to orthorhombic packing with a porosity of 0.3954.

Haughey and Beveridge (1966) reported a detailed classification of random packings: i) very loose random packing, ii) loose random packing, iii) poured random packing, and iv) close random packing. In this definition, the very loose random packing is the state that the bed is first fluidized and then the fluid flow is decreased until the fluid velocity is below the minimum fluidization velocity. Generally, the bed having this type of packing has a porosity of about 0.44.

Specific surface area is defined as the ratio of the total particle surface area and total bed volume. The number of spheres (N_p) per volume of bed and the specific surface area (S) are defined as follows:

$$N_p = \frac{6\,(1-\varepsilon)}{\pi\, d_p^3} \tag{1.17}$$

$$S = \frac{6\,(1-\varepsilon)}{d_p} \tag{1.18}$$

1.3.1.2 Packing characteristics of non-spherical particles

There are very few theoretical and experimental studies due to the complexity of packing in a non-spherical particle system. Oman and Watson (1944) performed experiments with different shaped particles and they found that the bed porosity increases in this order: cylinder, sphere, granule, Raschig rings and Berl saddles. Coulson (1949) worked on packed beds with cylinders and tablets and found that the packing depends on the height from which the particles were dropped in the column. The results are shown in Table 1.7.

Table 1.7 Rough Estimate of Bed Porosity (Yang, 2003)

Particle type	Normal packed	Dense packed	Multiplier for small tubes
Tablets	0.36	0.31	$1 + 0.43\ d_p/D$
Short extrudates	0.40	0.33	$1 + 0.46\ d_p/D$
Long extrudates	0.46	0.40	$1 + 0.46\ d_p/D$
Uniform-sized spheres	0.40	0.36	$1 + 0.42\ d_p/D$
Mixed-sized spheres	0.36	0.32	
Irregular	0.42 (average)	0.42 (average)	$1 + 0.3\ d_p/D$

Brown (1966) proposed that the bed porosity depends on the sphericity of the particles for random packed beds of uniform-sized particles. Wadell (1935) proposed a method to determine sphericity (ψ) for small grains that are observable under the microscope. After observing a sample of particles under microscope, the average values can be obtained from the following equation using this model:

$$\psi = \frac{d_c}{D_c} \tag{1.19}$$

Here, D_c is the diameter of the smallest circle circumscribing the projection of the particle, and d_c is diameter of a circle equal area to the projected area of the particle.The average sphericity is generally calculated from the mean of the different sphericities for the packed beds composed of a mixture of particles having various shapes.

Loose and dense random packing of mono-sized non-spherical particles are investigated by Zou and Yu (1996). They reported that the porosity is strongly depended on the particle

shape and the packing method. The initial porosities of loose and dense random packings were expressed with equations based on sphericity.

1.3.2 Correlations for fixed bed porosity

Bed porosity is determined by using experimental procedures as water displacement technique. The effect of wall on the particle packing characteristics was first studied by Furnas (1929). He suggested the equations given below to predict porosity near walls and in the centre of the bed:

$$\varepsilon_w = \left[1 + 0.6\left(\frac{d_p}{D}\right)\right]\varepsilon - 0.6\left(\frac{d_p}{D}\right) \tag{1.20}$$

$$\varepsilon_c = [\varepsilon + 0.3(1-\varepsilon)]\left[1 + 0.6\left(\frac{d_p}{D}\right)\right] - 0.6\left(\frac{d_p}{D}\right) \tag{1.21}$$

Here, ε_w is the porosity near the walls and ε_c represents the porosity in the centre of the bed. Experimentally determined average porosity (ε) is expressed as the ratio of void volume to total volume of the bed. Wall effect correction on porosity was neglected for the beds with a dp/D ratio less than 0.02 (Furnas, 1929).

Dixon (1988) studied the wall effects by experiments on low column/particle diameter systems. The following equations are proposed by Dixon (1988) for spherical particles:

$$\varepsilon = 0.4 + 0.05\left(\frac{d_p}{D}\right) + 0.412\left(\frac{d_p}{D}\right)^2 \qquad \left(\frac{d_p}{D}\right) \leq 0.5 \tag{1.22}$$

$$\varepsilon = 0.528 + 2.464\left(\frac{d_p}{D} - 0.5\right) \qquad 0.5 \leq \left(\frac{d_p}{D}\right) \leq 0.536 \tag{1.23}$$

$$\varepsilon = 1 - 0.667\left(\frac{d_p}{D}\right)^3\left[2\left(\frac{d_p}{D}\right) - 1\right]^{-0.5} \qquad \left(\frac{d_p}{D}\right) \geq 0.536 \tag{1.24}$$

1.3.3 Correlations for flow through packed beds

1.3.3.1 Darcy's Correlation

Darcy (1856) performed a classical experiment that explains the theory of laminar flow through homogenous porous media. The sketch describing Darcy's experiment is given in Figure 1.5. By this experiment, Darcy observed the flow through a filter bed was directly

proportional to the hydraulic head acting on the filter bed and inversely proportional to the depth of filter bed. Darcy (1856) proposed the following equation (Eq. 1.25) where h, Q, A and K are depth of the filter bed, flow rate through the filter bed, bed area and a constant based on the properties of the porous medium and of the fluid, respectively.

$$Q = -\frac{K\ A\ (h_2 - h_1)}{h} \tag{1.25}$$

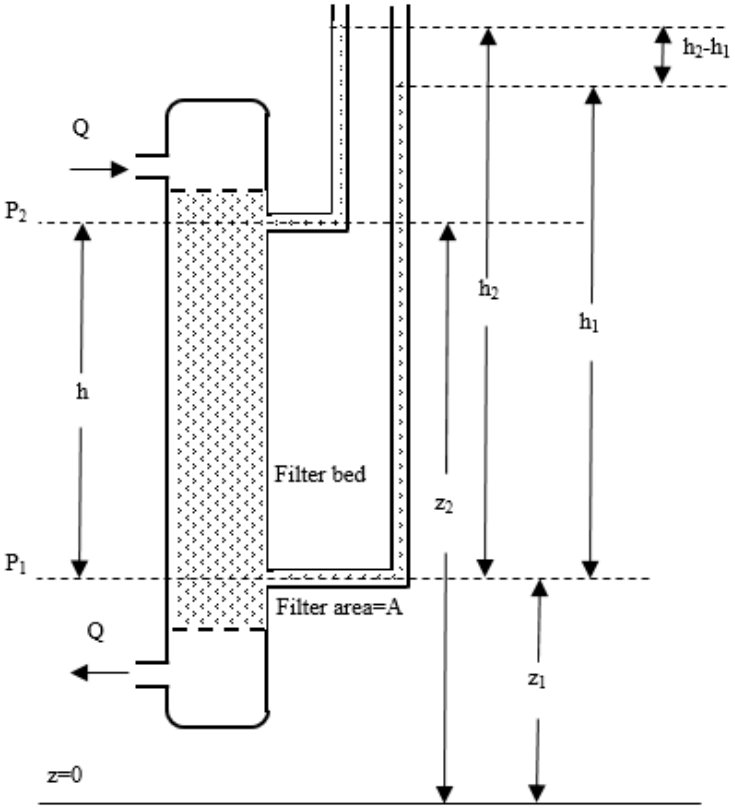


Figure 1.5 Darcy's experiment

Assuming that the liquid density is constant, Darcy's equation can be rewritten in terms of density of the fluid (ρ_f) and pressure (P) as following:

$$Q = -\frac{K\ A\ (P_2 - P_1 + \rho_f g\ h)}{h} \tag{1.26}$$

$$P = \rho_f g\ (h_1 - z_1) \qquad P = \rho_f g\ (h_2 - z_2) \tag{1.27}$$

Darcy's law is valid for the flow of Newtonian fluids at low Reynolds numbers. Darcy's law become invalid for the gases (at very low and very high velocities) and for the liquids at high velocities (Chang et al., 1999).

1.3.3.2 Blake's Correlation

Blake (1922) suggested a dimensionless group including the porosity in a particulate system. He proposed the use of the pore velocity, instead of the superficial velocity. Also, the total particle surface area per unit volume used in this definition instead of the particle diameter as the characteristic length. Blake (1922) proposed a modified Reynolds number (Re_B), a dimensionless group and a friction factor (f_B):

$$Re_B = \frac{U\, d_p\, \rho_f}{\mu\,(1-\varepsilon)} \tag{1.28}$$

$$f_B = \frac{\Delta P}{L}\frac{d_p}{\rho_f U^2\, g}\frac{\varepsilon^3}{(1-\varepsilon)} \tag{1.29}$$

The modified (Re_B) includes the pore velocity or interstitial velocity instead of superficial velocity. Particle diameter in regular particle Reynolds number definition was replaced with a characteristic length representing the totalparticle surface area per unit volume. These dimensionless groups are used in packed bed correlations.

1.3.3.3 Carman and Kozeny Correlations

Carman (1937) examined fluid flow through the different fixed-bed packings in viscous flow regime, and proposed the following equation:

$$f = \frac{90\,(1-\varepsilon)^2}{\varepsilon^3\,(Re)_p} \qquad \text{for} \quad 0.26 < \varepsilon < 0.89 \tag{1.30}$$

It is also found that this equation can be applied to regular shaped particles where the particle surface area was determined correctly.V_p is the volume of the particle, S_p is the surface area of the particle and d_p is defined as $6V_p/S_p$. For mixtures of particles in different sizes and shapes, V_p and S_p should be taken as averages of all packed particles in filter bed. The equation proposed by Kozeny (1927) is expressed as follows:

$$\frac{\Delta P}{L} = \frac{180\,(1-\varepsilon)^3 \mu\, U}{g\,\varepsilon^3 d_p^2} = \frac{5(1-\varepsilon)^2 \mu\, U}{g\,\varepsilon^3 (V_p/S_p)^2} \tag{1.31}$$

The specific surface that is defined as S_p/V_p can be calculated from:

$$\frac{S_p}{V_p} = \sqrt{\frac{g\,\Delta P\,\varepsilon^3}{5(1-\varepsilon)^2 \mu\, U\, L}} \tag{1.32}$$

1.3.3.4 Ergun Correlation

Ergun (1952) is the most widely used empirical correlation employing Blake's definition for drag coefficient and the Reynolds number. It is defined as:

$$\frac{\Delta P}{L} = \frac{g\, d_p\, \psi}{2\, \rho_f U^2} \cdot \frac{\varepsilon^3}{(1-\varepsilon)} = 75\, \frac{(1-\varepsilon)}{\psi\, (Re)_p} + 0.875 \tag{1.33}$$

The Ergun (1952) equation is expressed with sphericity (ψ) by substituting ψd_p for d_p for general applications. d_p, is the diameter of the irregular particle which is determined by using particle measurement techniques (such as sieving). For the better results different modifications of the Ergun equation have been proposed in the literature (Handley and Heggs, 1968; Hicks, 1970; Leva, 1947; Rose and Rizk, 1949; Tallmadge, 1970). The correlations suggested by Tallmadge (1970) and Leva (1947) are valid for high Reynolds numbers, where the Ergun equation does not fit the data well.

Gibilaro et al. (1985) proposed a modified form of Ergun equation as an alternative pressure drop equation. This equation is given below:

$$\Delta P = \left(\frac{17.3}{(Re)_p} + 0.336\right) \frac{\rho U^2 L}{d_p} (1-\varepsilon)\varepsilon^{-4.8} \tag{1.34}$$

The authors compared their proposed equation with experimental data taken from previous studies obtained with fixed beds of spheres having high bed porosities. This modified equation consists of two equations for the laminar and for fully turbulent flow. The equation for the laminar flow is derived from Blake– Kozeny equation at a porosity equal to 0.4.
For the turbulent flow condition following equation was obtained:

$$\Delta P = -0.336 \frac{\rho U^2 L}{d_p} (1-\varepsilon)\varepsilon^{-4.8} \tag{1.35}$$

The following equation describes the headloss in a normal fixed bed magnificently.

$$\Delta P = -1.75 \frac{\rho U^2 L}{d_p} \frac{(1-\varepsilon)}{\varepsilon^3} \tag{1.36}$$

Subramanian and Arunachalam (1980) proposed a technique in order to determine the sphericity of irregular particles using Ergun equation. According to this approach, the Ergun

equation can be reformulated definitively for very low flow rates to determine sphericity as following:

$$\psi = \left[\frac{\frac{150\ L\ (1-\varepsilon)^2 B\mu}{d_p^2 \varepsilon^3 \rho_f g}}{\frac{1-L}{H_1}}\right]^{1/2} \tag{1.37}$$

$$B = \frac{lnH_0 - lnH_1}{t} \qquad H_0 > H_1 > L \tag{1.38}$$

The time (t) required to pass from H_0 to h_1 can be obtained by carrying out a fixed bed experiment with irregular particles in a laminar flow condition. The sphericity of irregular particles can be determined by the use of these two equations given above. To carry out this experiment, a simple and sensitive setup was detailed in the study of Subramanian and Arunachalam (1980).

1.4 Filter Backwash Hydraulics and Fluidization

1.4.1 Filter Backwash Hydraulics

In conventional water treatment, filtration is the process used for the removal of solid particles from water by passage of water through a porous medium. The porous medium of granular filtration is a thick bed of granular material such as sand, garnet, activated carbon or ilmenite. Some of ground water treatment plants and most of the surface water treatment plants use filtration. Filtration improves the clarity of water by removing clay and silt particles, bacteria, protozoa, viruses and other organic and inorganic substances.

Rapid filtration is the most common granular filtration technology in water treatment. Media uniformity achieved in rapid filters enables the filters to operate at a higher hydraulic loading rate and lower headloss. Since, the void spaces in a rapid filter are substantially larger than the particles of filter material. There is another removal mechanism in the operation of rapid filters. The solids in water adhere to the filter materials or previously deposited solids. The solids are removed throughout depth of filter and it gives a high solid retention capacity to filters by increasing the clogging time.

The rapid filtration cycle consists of a filtration stage and backwash stage. Particles are accumulated in filter bed during filtration stage and they are removed from the system in

backwash stage. In filtration stage, water flows downward through the filter media and it lasts 1 to 4 days. The filter is cleaned by backwashing with an upflow of water. It is sometimes assisted by air flow and/or any auxiliary scouring system. The operating time of filters between two backwashes is called as a filter run. The total head loss at the end of the each filter run is referred to the terminal head loss.

Filter failures in treatment plants are mostly caused improper backwashing. Filters operating with a high efficiency of particle capture at a reasonable headloss development can be obtained with appropriate design, construction and operation of backwash system. Backwashing methods with and without fluidization are compared in Table 1.8.

Table 1.8 Comparison of Backwash Alternatives for Granular Bed Filters (AWWA, 1999)

	Backwash method	
	With fluidization	Without fluidization
Applications	1. Fine sand 2. Dual media 3. Triple media	Coarse single-media sand or anthracite
Routines used	1. Water wash + surface wash 2. Water wash + air scour	
Fluidization	During water wash	No
Bed Expansion	15–30 percent	Negligible
Wash troughs	Usually used	Usually not used
Horizontal water travel to overflow	Up to 0.9 m	Up to 4 m
Vertical height to overflow	0.76–0.91 m	0.6 m

The need for backwashing of granular filters is determined by one of the following three criteria (AWWA, 1999):

- The head loss through filter increases to the maximum allowed limit usually set as 2.4 m to 3.0 m.
- The quality of filtrate deteriorates.
- The maximum time limit established by operator has been reached.

A typical filter run lasts from 12 hours to 96 hours. Backwashing of a filter which operates very long hours due to the low levels of headloss can be difficult. In order to improve filter

performance by increasing the attachment of particlesto the filter media, filter aids may be added to the water before filtration operation. Also, chemical coagulation as a pretreatment step is essential for the efficient removal of solid particles in granular filtration.

The fundamentals of liquid solid fluidization should be known to understand backwash mechanisms of filter beds. Also the factors effecting fluidization and the importance of filter media characteristics should be recognized. For this reason, the liquid solid fluidization subject is detailed in the following section.

1.4.2 Liquid-Solid Fluidization

The components and the operational parameters should be analyzed carefully to understand and operate a solid-liquid fluidized bed. Epstein (2003) classified the applications of liquid-solid fluidization. These include: particle classification, backwashing of particle beds, in situ fluidized washing, crystal growth, leaching and washing processes, adsorption, ion exchange, flocculation, electrolysis, fluidized bed electrodes, heat exchangers, thermal energy storage and bioreactors. Some of them are the operations and processes employed in water and wastewater treatment.

To understand liquid solid fluidization, the conventional liquid fluidized bed system should be analyzed. Figure 1.6 represents the semi batch liquid fluidization system. The fluidization column may be in circular, rectangular or square in shape. A calming section placed before the fluidization section is necessary to obtain a uniform liquid velocity distribution throughout the bed. This section also helps minimizing the channeling problem in fluidization columns.

Various non-porous particles with uniform size, shape and density were used in the earlier fluidization studies. Handley et al. (1966) studied the motion of individual particle in a liquid fluidized bed. They found that the “uniform fluidization” occurs in the absence of bulk circulation and this uniform fluidization is characterized by a homogenous motion of the particles and by a fixed average liquid velocity and momentum distribution throughout the particle bed. Furthermore, the axial particle velocity fluctuations and displacements in vertical direction are higher than horizontal ones (Carlos and Richardson, 1968; Kmiec, 1978; Latif and Richardson, 1972). In a particulate fluidization system, the particle bed is a homogenous and a uniformly distributed liquid solid mixture (Couderc, 1985).

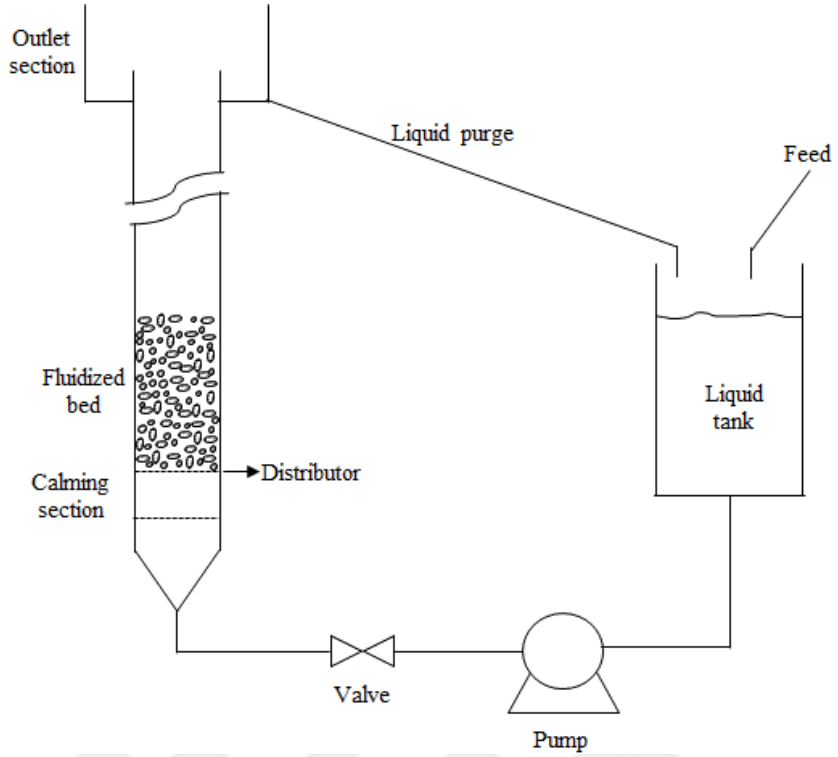


Figure 1.6 Semi batch liquid fluidization system (Yang, 2003)

1.4.2.1 Drag force and buoyancy

In a steady state condition, downward gravitational force is equal to the sum of upward buoyant force and drag force acting on a spherical particle with a volume V and density ρ_p:

$$V\rho_p g = B + F_D \tag{1.39}$$

In the literature there is a major disagreement in expressing buoyancy (B). The conventional formula is advocated by the researchers for example (Clift et al., 1987) and (Jean and Fan, 1998) and the buoyant force under static (means no flow) conditions is defined as:

$$B = V\rho g \tag{1.40}$$

The counterargument about the definition of buoyancy (B) that defines ρ_B as the density of fluidized bed suspension, presented by some researchers (Astarita, 1993; Gibilaro et al., 1987, 1984) and states that:

$$B = V\rho_B g \tag{1.41}$$

$$\rho_B = \rho_p(1-\varepsilon) + \rho\varepsilon \tag{1.42}$$

The main part of this equation is that the total pressure gradient under fluidized bed condition is given as following:

$$-\frac{dP}{dz} = \rho_B g \tag{1.43}$$

When equation 1.39 and equation 1.40 are combined the following equation is yielded:

$$V\rho_p g - F_D = V\rho g$$

$$F_D = V(\rho_p - \rho)g \tag{1.44}$$

Combination of equation 1.39, equation 1.41 and equation 1.42 gives the equation 1.45.

$$F_D = V(\rho_p - \rho)\varepsilon g \tag{1.45}$$

Because of the significance of the calculation of buoyancy (B) using equation 1.40 or 1.41; the drag force calculated using equation 1.45 is less than by a factor of ε ($\varepsilon_{mf} < \varepsilon < 1$). The supporters of equation 1.44 asserted that F_D causes the dissipation of mechanical energy. Also this dissipation should involve the energy required to convert to static buoyancy of particle under unfluidized condition to the dynamic buoyancy in fluidized condition. The researchers on both sides of disaggrement expresses the frictional pressure gradient (dP_f/dz) as below:

$$\begin{aligned} -\frac{dP_f}{dz} &= \rho_B g - \rho g \\ &= \left[\rho_p(1-\varepsilon) + \rho\varepsilon\right]g - \rho g \\ &= (1-\varepsilon)\left(\rho_p - \rho\right)g \end{aligned} \tag{1.46}$$

As previously given, V is the volume of particle in a homogenous solid-liquid fluidized bed. Then, the representative volume of liquid coupled with this particle and the representative volume of bed will be $V\varepsilon/(1-\varepsilon)$, $V\varepsilon/(1-\varepsilon)+V = V/(1-\varepsilon)$, respectively. Frictional pressure gradient should be described in different ways to obtain the same final expression (Eq 1.49). These are shown below:

$$-\frac{dP_f}{dz} = \frac{\begin{array}{c}drag\ force\ on \\ representative\ particle\end{array}}{\begin{array}{c}volume\ of\ bed\ associated\ with \\ representative\ particle\end{array}} = \frac{F_D}{\frac{V}{1-\varepsilon}} = (1-\varepsilon)\left(\rho_p - \rho\right)g \tag{1.47}$$

Also, the correlation to obtain from equation 1.45 to equation 1.46 is as following:

$$-\frac{dP_f}{dz} = \frac{\begin{matrix} drag\ force\ on \\ representative\ particle \end{matrix}}{\begin{matrix} volume\ of\ liquid\ associated\ with \\ representative\ particle \end{matrix}} = \frac{F_D}{\frac{V\varepsilon}{1-\varepsilon}} = (1-\varepsilon)(\rho_p - \rho)g \qquad (1.48)$$

$-dP_f/dz$ is commonly assumed to represent frictional force per bed volume including particles and liquid.

1.4.2.2 Minimum Fluidization

In order to determine the minimum fluidization velocity (V_{mf}), the minimum fluidization porosity (ε_{mf}) should be known for solid, non-porous particles having uniform size shape and density. This approach is same for the gas fluidization and liquid fluidization. At the point of incipient fluidization ($\varepsilon=\varepsilon_{mf}$), equating the frictional pressure gradient given in equation 1.46 with Ergun equation for a single phase Newtonian fluid flow through the loose bed:

$$\frac{-dp_f}{dz} = (1-\varepsilon_{mf})(\rho_p - \rho)g = \frac{150V_{mf}\mu(1-\varepsilon_{mf})^2}{\psi d_p^2 {\varepsilon_{mf}}^3} + \frac{1.75{V_{mf}}^2\rho(1-\varepsilon_{mf})}{\psi d_p {\varepsilon_{mf}}^2} \qquad (1.49)$$

Here, equivolume sphere diameter, d_p, is the product of sphericity and the equivalent surface volume sphere diameter d_{sv}. By rearranging the equation:

$$Re_{mf}^2 + \frac{150}{1{,}75}\frac{1-\varepsilon_{mf}}{\psi}Re_{mf} - \frac{\psi Re_{mf}^3 Ar}{1.75} = 0$$
$$where\ Ar = \frac{d_p^3\rho(\rho_p-\rho)g}{\mu^2}\ and\ \ Re_{mf} = \frac{d_p V_{mf}\rho}{\mu} \qquad (1.50)$$

By solving quadratic equation (1.50), the following equations are yielded:

$$Re_{mf} = (C_1^2 + C_2 Ar)^{1/2} - C_1 \qquad (1.51)$$

$$C_1 = \frac{150(1-\varepsilon_{mf})}{2\psi(1.75)} = 42.86\frac{(1-\varepsilon_{mf})}{\psi} \qquad (1.52)$$

$$C_2 = \frac{\psi{\varepsilon_{mf}}^3}{1.75} = 0.5714\psi{\varepsilon_{mf}}^3 \qquad (1.53)$$

$\rho_p, d_p, \mu, \rho, \varepsilon_{mf}$ and ψ should be known to solve equation 1.51 for Re_{mf} and V_{mf}. ψ is only known for the uniform perfect spheres ($\varepsilon_{mf} \approx 0.4$ and ψ=1). Eastwood et al. (1969) reported that determination of ε_{mf} is relatively simple.

Table 1.9 shows the C_1 and C_2 values defined in different studies. Many researchers proposed different values for C_1 and C_2 by assuming values for $\varepsilon_{mf}$and ψ or by using correlations between two values or by empirical solution using experimental data.

Table 1.9 C_1 and C_2 parameters according to different studies (Yang, 2003)

Study	C_1	C_2	Applicability
Wen and Yu, 1966	33.7	0.0408	Various particle shapes
Bourgeois and Grenier, 1968	25.46	0.0382	Spheres only
Richardson, 1971	25.7	0.0365	Spheres only
Saxena and Vogel, 1977	25.28	0.0571	Various particle shapes
Babu et al., 1978	25.25	0.0651	Various particle shapes
Grace, 1982	27.2	0.0408	Various particle shapes
Foscolo et al., 1983	25.74	$\varepsilon_{mf}^{4.8}$ / 0.336	Spheres
Chitester et al., 1984 Lin and Fan, 1997	28.7	0.0494	High pressure; spheres only for liquid fluidization
Nakamura et al., 1985	33.95	0.0465	High temperature and pressure; spheres
Lucas et al., 1986	29.5	0.0357	"Round" granular particles 0.8< ϕ<1
	32.1	0.0571	"Sharp" jagged particles 0.5< ϕ<0.8
	25.2	0.0672	"Other" particles e.g. rings 0.1< ϕ<0.5
Chen, 1987	33.67 $\phi^{0.1}$	$0.0408\phi^{0.45}$	All particle shapes
Chyang and Huang, 1988	33.3	0.0333	Granular particles

This solution is possible by using the correct predictions $\varepsilon_{mf}$and ψ. Alternatively, Chen (1987) is proposed the following equation for d_p>0.05mm and 0.2< ψ≤1.

$$\varepsilon_{mf} = \frac{0.415}{\psi^{0.483}} \tag{1.54}$$

The effective determination of $\varepsilon_{mf}$is performed by suddenly cutting of flow for an expanded bed system and allowing it to settle. Then, (1-ε_{mf}) is calculated by dividing volume of particles (M/ρ_p) to settled bed volume (AL_{mf}). If this method is not applicable, random loose porosity method should be used to predict ε_{mf} for the particles having relatively high sphericity ($\psi > 0.8$). A capped graduate cylinder which contains particles and water, is immediately reversed and then straightened to determine this porosity ratio. If the diameter of graduated cylinder is lower than the diameter of fluidization column, the wall effect correction is needed (Eastwood et al., 1969). The bed height should be higher than two times of diameter of graduated cylinder ($L_{mf} \geq 2D_c$) for both of the methods.

Another alternative method for V_{mf}, equating V to V_{mf} ($V=V_{mf}$) and equating ε to ε_{mf} ($\varepsilon=\varepsilon_{mf}$) in the bed expansion equations which is relating ε to V. However, bed expansion equations generally covers the all porosity (ε) intervals from ε_{mf} to ε_c, so for the ε_{mf} extremity give less correct results than some equations such as equation 1.51.

A third alternative for the V_{mf}, the use of empirical equations that are developed for limited conditions instead of equation 1.51. An empirical equation proposed by Riba et al. (1978) for the different combinations of liquid fluidization with spheres in Re_{mf} = 10-1000 interval, are as following:

$$Re_{mf} = 0.0154\, Ar^{0.66} = \left(\frac{\rho_p - \rho}{\rho}\right)^{0.04} \tag{1.55}$$

The advantage of the equation, it is not required any specification for ε_{mf} and ψ. By examining the equations 1.51 to 1.53, it is shown that the equations are very sensitive to ε_{mf} and even it is so hard to find an exact specification of ε_{mf} for spheres ($\psi = 1$) (Eastwood et al., 1969). Density ratio should be eliminated from the equation for the all studied liquid solid combinations, because $\left(\frac{\rho_p-\rho}{\rho}\right)^{0.04}$ factor is not higher than the experimental data deviation in all circumstances.

V_{mf} and ε_{mf} substantially diminished by fluidization liquid (El-Temtamy and Epstein, 1986). For solid particles having different sizes, it is assumed that any hysteresis effects have been eliminated. As shown in Figure 1.7, there is no exact transition from a fixed bed to a fluidized bed by first fluidizing the particles and then slowly diminishing the velocity of fluid to zero. A gradually transition takes place from the fixed bed to fluidized bed as shown in Figure 1.8. The values of V_{bf} and V_{tf} can be calculated from Equation 1.51 taking smallest and largest dimeter values as d_p. Using same equation, V_{mfa} can be predicted taking Sauter or reciprocal diameter as d_p (Jean and Fan, 1998). This value equals to surface volume mean diameter for fixed shape particles.

$$d_p = \frac{V_i}{\sum_{i=1}^{N} d_{pi}} \tag{1.56}$$

Figure 1.8 is valid for particles of mixed shapes and densities as well as mixed sizes. For the prediction of V_{bf} and V_{tf}, the particle characteristics in Equation 1.51 are taken as the lowest and the highest values of V_{mf}. Also, for the calculation of V_{amf} Equation 1.51 is needed the

mean particle density:

$$\rho_p = \frac{\sum_{i=1}^{N} M_i}{\sum_{i=1}^{N} \frac{M_i}{\rho_{pi}}} \tag{1.57}$$

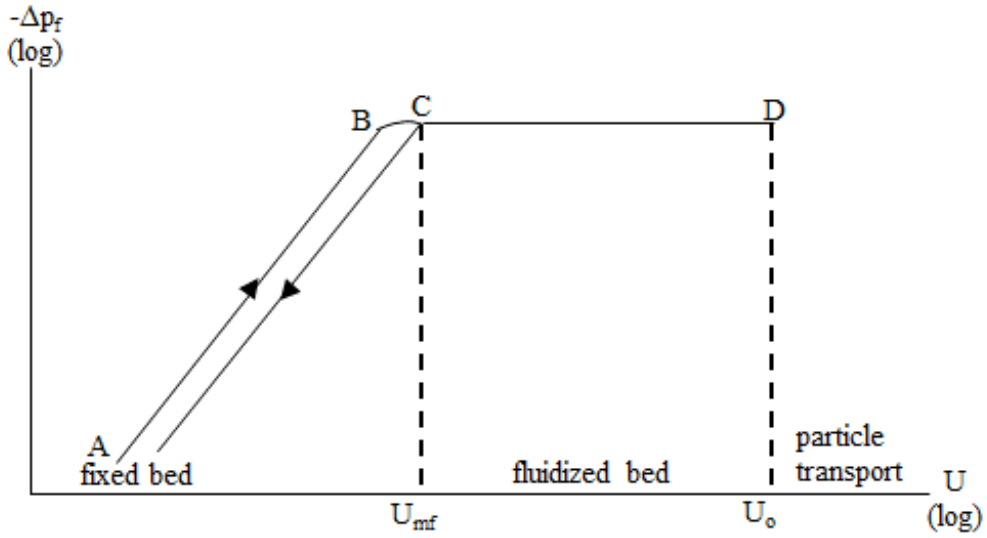


Figure 1.7 Frictional pressure drop graph for homogenous monodisperse particles as a function of linear velocity

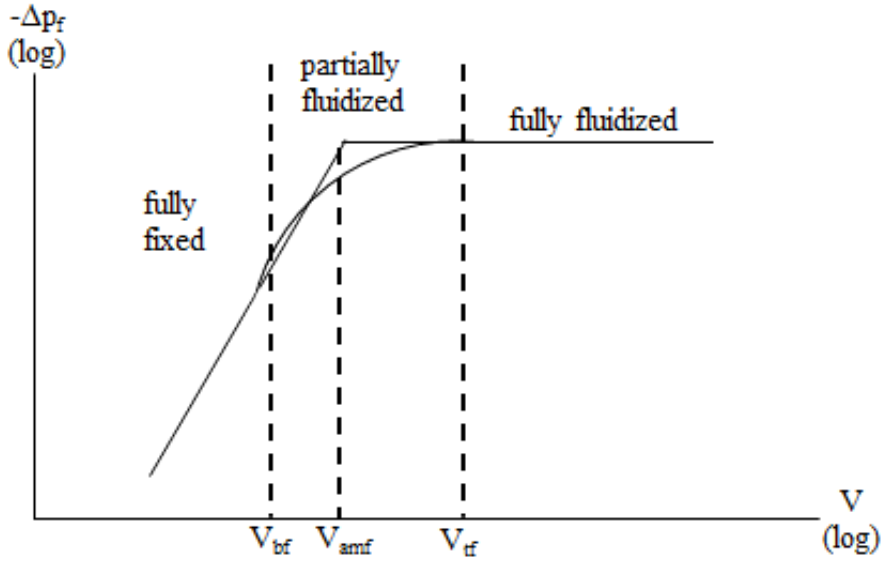


Figure 1.8 Frictional pressure drop versus liquid superficial velocity for particles of mixed sizes shapes and densities (Yang, 2003)

Wen and Yu (1966) are also developed correlations about minimum fluidization velocity. In their correlations, particle diameter is taken as an average of consecutive two sieve sizes. They reported that this approach does not cause any serious problem. The researchers stated that minimum fluidization porosity becomes independent for spherical particles when the wall effects are negligible. The porosity differs between 0.36-0.46 and these values are compatible with the data given in literature according to researchers. Also they reported that the 0.35 value proposed by Narsimhan (1965) is too low. The minimum fluidization porsity correlation proposed by Narsimhan (1965) is as following:

$$\varepsilon_{mf} = 0.768 - 0.42\psi \qquad 0.35 < \varepsilon_{mf} < 0.55 \tag{1.58}$$

When Wen and Yu (1966) created ε_{mf} and ψ fluctuations graph for spherical and non-spherical particles, they are recognized that although there are some deviations, a general correlation can be formed between two parameters and they proposed the following two equations for the defined experimental conditions (dp=0.05mm-5cm; ε_{mf} =0.385-0.935; ψ=0,136-1; d/D=0.000807-0.25):

$$\frac{1-\varepsilon_{mf}}{\psi^2 {\varepsilon_{mf}}^3} \cong 11 \qquad \frac{1}{\psi {\varepsilon_{mf}}^3} \cong 14 \tag{1.59}$$

1.4.2.3 Fluidized bed

One of the important problems in filtration design is the selection of water velocity for the backwash process. The expansion of filter bed depends on backwash velocity. Backwashing with inadequate velocity results unfluidized or partially fluidized filter bed and so filter bed retains unclean. In this case, the expected stratification will not be obtained in a multi-layered filter.

On the other hand, the escape of filter material to backwash channels and the discharge of them will be a matter in the case of very high backwash velocities. Even though the amount of escaped material is not considerable, the high velocity backwashing causes energy and water dissipation. The expansion of filter bed in a known veolocity differs depending on density, size distribution and shape properties of filter material and also temperature of water. In order to select an appropriate backwash velocity, there is a requirement for a calculation method to predict filter bed expansion depending on the filter backwash velocity.

Such a calculation method should be applicable for both non-spherical materials and non-uniform filter beds.

In fluidization literature, Richardson-Zaki equation is the most commonly used method for the prediction of bed expansion depending on velocity (Lewis and Bowerman, 1952; Richardson and Zaki, 1954):

$$\frac{V}{V_i} = \varepsilon^n \tag{1.60}$$

Here, V is the liquid velocity based on empty column area (flowrate/area), V_i is the intercept velocity and ε is the average porosity of the expanded bed. Average porosity is calculated using following correlation:

$$L(1-\varepsilon) = L_0(1-\varepsilon_0) \tag{1.61}$$

In this correlation L is the depth of the expanded bed, L_0 is the depth of the fixed bed and ε_0 represents the porosity of fixed bed. Richardson and Zaki proposed $V_i = V_{t\infty}$ equality for settling experiments and $\log V_i = \log V_{t\infty} - d/D$ equation for fluidization. Here, $V_{t\infty}$ is the settling velocity of the particle in an infinite column (no wall effect), d is the particle diameter and D is the inner diameter of the column.

n superscript of equation 1.60 is calculated from the equations given in Table 1.10 (Richardson, 1971). In more recent times, Khan and Richardson (1990) proposed an alternative correlation to Richardson-Zaki correlation. These two correlations and the other commonly used equations is given in Table 1.10.

Table 1.10. Porosity-velocity correlations for the liquid-solid fluidization of spheres

Study	**Correlations**		**#**
	$\frac{V}{V_i} = \varepsilon^n$		(1.60)
Richardson and Zaki (1954)	$n = 4.65 + 20\frac{d}{D}$	$(Re_{t\infty} < 0.2)$	(1.62)
	$n = \left(4.4 + 18\frac{d}{D}\right) {Re_{t\infty}}^{-0.03}$	$(0.2 < Re_{t\infty} < 1)$	(1.63)
Richardson (1971)	$n = (4.4 + 18\frac{d}{D}) {Re_{t\infty}}^{-0.1}$	$(1 < Re_{t\infty} < 200)$	(1.64)
	$n = 4.4\, {Re_{t\infty}}^{-0.1}$	$(200 < Re_{t\infty} < 500)$	(1.65)
	$n = 2.4$	$(Re_{t\infty} > 500)$	(1.66)

Table 1.10. (Continued)

Study	Correlations		#
Wen and Yu (1966)	$Ga = \frac{d^3 \rho_f^2 g}{\mu^2}$		(1.67)
	$\varepsilon^{4.7} Ga = (18Re + 2.7Re^{1.687})$		(1.68)
Garside and Al-Dibouni (1977)	$\varepsilon^{5.14} + 0.048\varepsilon^{2.28} Re_t^{\varepsilon+0.2} = \frac{Re\left(1 + 0.06{Re_t}^{\varepsilon+0.2}\right)}{Re_t}$	$\varepsilon \leq 0.85$	(1.69)
	$\varepsilon^{5.14} + 0.06\varepsilon^{3.65} Re_t^{\varepsilon+0.2} = \frac{Re\left(1 + 0.06{Re_t}^{\varepsilon+0.2}\right)}{Re_t}$	$\varepsilon > 0.85$	(1.70)
	$Re_{t\infty}/Re_t = 1 + 2.35(d/D)$		(1.71)
Gibilaro et al., (1986)	$\varepsilon^{4.8} Ga = Re^2((17.3/Re)^{\alpha} + 0.336^{\alpha})^{1/\alpha}$		(1.72)
	$\alpha = 2.55 - 2.1\left[\tan h\,(20\varepsilon - 8)^{1/3}\right]^3$		(1.73)
Khan and Richardson (1990)	$\frac{V}{V_t} = \varepsilon^n$		(1.74)
	$\frac{V}{V_{t\infty}} = 1 - 1.15\left(\frac{d}{D}\right)^{0.6}$		(1.75)
	$\frac{4.8 - n}{n - 2.4} = 0.043\, Ga^{0.57}\left[1 - 1.24\left(\frac{d}{D}\right)^{1.27}\right]$		(1.76)
Akgiray and Saatçı (2001)	$\varepsilon = \sqrt[3]{R + \sqrt[2]{R^2 + Q^3}} + \sqrt[3]{R - \sqrt[2]{R^2 + Q^3}}$		(1.77)
	$Q = \frac{12k_1 Re}{\psi^3 Ga}$		(1.78)
	$R = \frac{3Re}{\psi^3 Ga}(k_2 Re + 6k_1)$		(1.79)
	$Re = \frac{\psi d_{eq} \rho V}{\mu}$		(1.80)
	$Re = \frac{{d_{eq}}^3 \rho(\rho_p - \rho)g}{\mu^2}$		(1.81)
Lewis et al. (1949)	$f = \frac{4}{3}\frac{gd(\rho_P - \rho)}{v^2 \rho}\varepsilon^{4.65}$		(1.82)
	$\varepsilon = 2.00\left[\frac{\mu\, v}{gd^2(\rho_P - \rho)}\right]^{0.215}$	Re<2	(1.83)
Lewis and Bowerman (1952)	$\varepsilon = 1.95\left[\frac{\mu^{0.43} v\, \rho^{0.29}}{g^{0.71} d^{1.14}(\rho_P - \rho)^{0.71}}\right]^{0.337}$	2<Re<500	(1.84)
	$\varepsilon = 0.907\left[\sqrt[u]{\frac{\rho}{(\rho_P - \rho)gd}}\right]^{0.43}$	Re>500	(1.85)

Table 1.10. (Continued)

Study	Correlations		#
	$Mv = \frac{\rho_p - \rho}{\rho}$	$f(\varepsilon) = \left[1 - 1.21(1-\varepsilon)^{2/3}\right]^{-1}$ n=1.56	(1.86)
Ramamurthy and Subbaraju (1973)	$[f(\varepsilon)]^n = \frac{Ga\ Mv}{18\ Re}$	$Ga\ Mv < 18$	(1.87)
	$[f(\varepsilon)^{1.4}]^n$	$18 < Ga\ Mv < 10^5$	(1.88)
	$Ga\ Mv$ $[f(\varepsilon)^2]^n = \frac{3Ga\ Mv}{Re^2}$	$Ga\ Mv > 10^5$	(1.89)
	$C_{D(1-\varepsilon)} = \left(0.63 + \frac{4.8}{\sqrt{Re(1-\varepsilon)}}\right)^2$		(1.90)
Barnea and Mizrahi (1973)	$C_{D(1-\varepsilon)} = \frac{4}{3}\frac{d(\rho_P - \rho)g}{\rho u^2}\frac{\varepsilon^3}{(1+(1-\varepsilon)^{1/3})}$		(1.91)
	$Re_{(1-\varepsilon)} = \frac{Re}{\varepsilon\ \exp(\frac{5\ (1-\varepsilon)}{3\ \varepsilon})}$		(1.92)
Riba and	$\varepsilon = 1.58Re^{0.33}Ga^{-0.21}Mv^{-0.22}$	$\varepsilon \leq 0.85$	(1.93)
Couderc (1977)	$\varepsilon = 1.20Re^{0.17}Ga^{-0.11}Mv^{-0.12}$	$\varepsilon > 0.85$	(1.94)

A significant part of the most commonly used Environmental Engineering course books (having subjects of water treatment, wastewater treatment, unit operations etc.) are used the more simplified version of the Richardson Zaki equation (Droste, 1997; Fair et al., 1971; Metcalf and Eddy, 2004; Peavy et al., 1985; Reynolds, 1996; Weber, 1972):

$$\varepsilon = \left(V/V_{t\infty}\right)^{0.22} \tag{1.95}$$

Here, 0.22 (≈ 1/4.4) coefficient is obtained using d/D = 0 ve $Re_{t\infty}$ = 1 values in Richardson-Zaki equation (Table 1.10). Although it is the most widely used equation, the correct results of this equation should not be expected for different filter materials: (i) Richardson and Zaki (1954) is proposed this correlation based on the experiments with spherical particles, the equation is not valid for non-spherical materials (Cleasby and Fan, 1981; Dharmarajah and Cleasby, 1986; Richardson, 1971). (ii) in a recent evaluation concerning literature data and new fluidization experiments using spherical particles, it is reported that Richardson-Zaki correlation does not give exact results for spherical particles as well (Akgiray and Soyer, 2006). (iii) Equation 1.95 is based on more restricted assumption ($Re_{t\infty} \approx 1$).

Dharmarajah and Cleasby (1986) defines a fluid system basically depending on eight parameters. These are superficial velocity (u), fluid density (ϱ), fluid viscosity (μ), particle density (ϱ_s), particle surface area (S), porosity (ε), gravitational accelaration (g) and sphericity (ψ).

$$Characteristic\ velocity = \frac{u}{\varepsilon} \tag{1.96}$$

$$Characteristic\ length = \frac{mean\ cross\ sectional\ area\ of\ flow\ channels\ through\ bed}{mean\ wetted\ perimeter\ of\ flow\ channels} \tag{1.97}$$

Numerator and denominator are multiplyed with length:

$$Characteristic\ length = \frac{\varepsilon}{S\ (1-\varepsilon)} \tag{1.98}$$

Blake's modified Reynolds number:

$$Re_1 = \left(\frac{u}{\varepsilon}\right)\left(\frac{\varepsilon}{(1-\varepsilon)s}\right)\left(\frac{\varrho}{\mu}\right) = \frac{\varrho\ u}{S\ \mu\ (1-\varepsilon)} \tag{1.99}$$

To correlate the pressure drop through fixed beds, Blake (1922) and Carman (1937) used the modified Re number Re_1 and the following voidage function

$$\emptyset = \left(\frac{\Delta P}{L}\right)\left(\frac{1}{S\ \varrho\ u^2}\right)\left(\frac{\varepsilon^3}{(1-\varepsilon)}\right) \tag{1.100}$$

$$\left(\frac{\Delta P}{L}\right) = (\varrho_s - \varrho)(1-\varepsilon)g \tag{1.101}$$

$$\phi = (\varrho_s - \varrho)(1-\varepsilon)\left(\frac{g}{S\ \varrho\ u^2}\right)\left(\frac{\varepsilon^3}{(1-\varepsilon)}\right) \tag{1.102}$$

$$\phi = \frac{g\ (\varrho_s - \varrho)\ \varepsilon^3}{S\ \varrho\ u^2} \tag{1.103}$$

A1 is defined which is not a function of u.

$$A1 = \phi\ {Re_1}^2 \tag{1.104}$$

$$A1 = \frac{g\ (\varrho_s - \varrho)\ \varepsilon^3}{S\ \varrho\ u^2}\ \frac{u^{\,2}\varrho^2}{S^2\ \mu^2\ (1-\varepsilon)^2} \tag{1.105}$$

$$A1 = \frac{\varepsilon^3}{(1-\varepsilon)^2}\ \frac{\varrho\ (\varrho_s - \varrho)\ g}{S^3\ \mu^2} \tag{1.106}$$

In the study of Dharmarajah and Cleasby (1986), coarse sand, coarse and light coal, cube shaped polyvinyl plastics with different densities, circular disc shaped metal punchings of

brass, stainless steel and aluminum were used as filter material. The use of various materials gives an opportunity to produce a wide range of data in terms of equivalent diameter, density and sphericity. They reported that the sphericity of the material should be calculated using the fixed bed pressure drop data. The use of loose bed pressure drop data is better than a tightly compacted state.

Some investigators reported that d/D_t is only important parameter for the definition of the wall effect. However, Fidleris and Whitmore (1961) reported that Re_t is also significant as d/D_t in order to evaluate wall effect. Richardson and Zaki (1954) recognized the significance of d/D_t and Re_t for wall effect correction.

Loeffler (1953) performed fluidization experiments using same material in two different columns. Using the data of Loeffler (1953), Dharmarajah and Cleasby (1986) derived a hypothetical velocity which is independent from wall effect.

$$u_0 = u\ 10^{\alpha(\frac{d}{Dt})} \tag{1.107}$$

$$\alpha = \frac{5.18}{(Re_{t\alpha})^{0.585}} \cong \frac{5.2}{(Re_{t\alpha})^{0.6}} \tag{1.108}$$

u_0 is the velocity to achieve same porosity in an infinite larger container which is obtained in a container of diameter D_t.

Dharmarajah and Cleasby (1986) corrected all data of Loeffler (1953) and Wilhelm and Kwauk (1948) for wall effect. The particle reynolds number range of this data is about Re_t=1-2769 and in the evaluation the data which porosities are less than 0.85 is used. When Re_t < 100 and porosity>0.85, the points deviated from the trendline. If Re_1<0.2 , the data fell on a straight line.

$$A1 = 3.01Re1 \tag{1.109}$$

If Re_1>0.2

$$\log A1 = a_0 + a_1\ logRe1 + a_2(\log Re1)^2 + a_3(\log Re1)^3 + a_4(\log Re1)^4 \tag{1.110}$$

The general equation to describe the expansion behavior of spherical particles as well as non-spherical particles.

When Re_1>0.2

$$\log A1 = 0.56543 + 1.09348\ logRe1 + a_2(\log Re1)^2 + 0{,}17979(\log Re1)^3 - 0{,}00392(\log Re1)^4 - 1.5\ (log\ \psi)^2 \tag{1.111}$$

This equation tested using data of Dharmarajah (1982), Cleasby and Fan (1981) and Gunasingham et al. (1978). The correlation of Dharmarajah and Cleasby (1986) provides an alternative approach to predicting the velocity-voidage relationship of particulately fluidized systems. This correlation predicts the expanded bed porosity up to 0.85 when Re_t number is less than 100 and it is also satisfactory up to an expanded bed porosity of 0.9 if Re_t number is higher than 100.

Akgiray and Soyer (2006) was studied the most commonly used correlations in fluidization literature and they found that the correlation proposed by Garside and Al-Dibouni (1977) gives the more correct predictions among the existing corelations. In the mentioned study of Akgiray and Soyer (2006), they developed a new equation and they reported that this new equation gives better results than the equations given in Table 1.10:

$$\varphi = 3.137Re_1 + 0.673\,Re_1^{1.766} \tag{1.112}$$

In this correlation, dimensionless groups are represented as following:

$$\varphi = \frac{\varepsilon^3}{(1-\varepsilon)^2}\frac{\psi^3 d_{eq}^3\,\rho(\rho_p - \rho)g}{216\mu^2} \tag{1.113}$$

$$Re_1 = \frac{\psi d_{eq}\rho V}{6\mu(1-\varepsilon)} \tag{1.114}$$

Here, ψ represents the sphericity coefficient, d_{eq} is the equivalent diameter (cm), μ is the dynamic viscosity (kg/m/sec), ρ is the water density (kg/m^3).

The use of the calculation method developed by Akgiray and Soyer (2006) and the a numerical solution of equation 1.112 are explained in detail in a recently published course book (Tien, 2012).

It is important to remember that the all methods including equation 1.112 are only applicable for spheres not for the typical filter materials. Although the sphericity coefficient is taken into account in equation 1.112, it is revealed that this equation or more generally the correlations giving φ group as a function of Re_1 group are not valid for the non-spherical particles (Akgiray et al., 2004).

Soyer and Akgiray (2005) are performed experiments with non-spherical particles and proposed an equation representing their data:

$$log\varphi = 0.565013 + 1.15703 log Re_1 + 0.12866 (log Re_1)^2 + 0.02195 (log Re_1)^3 - 0.008 (log Re_1)^4 - (0.8387 + 0.4653 log Re_1)(-log\psi)^{1.15} \quad (1.115)$$

Thereafter, Soyer and Akgiray (2009) studied with spheres having different size and density, and also silica sand, garnet sand, perlite and crushed glass in various size fractions in order to develop more valid and more simple equation and they proposed following equation:

$$log\varphi = \log\left(3.13 Re_1 + 0.673 {Re_1}^{1.766}\right) - (0.930 + 0.274 \log Re_1)(-log\psi)^{1.262} \quad (1.116)$$

In this correlation, ψ represents the particle sphericity and it is calculated using Ergun (1952) equation (Soyer and Akgiray, 2009, 2005). The equation is valid for both spheres and non-spherical filter materials and it is highly coincide with the experimental data obtained from the mentioned study. In the light of experimental data collected by Soyer and Akgiray (2009), this equation is considered to be the most common and most accurate equation among a few equations that have been proposed in the literature for non-spherical materials.

1.4.3 Fluidization of Binary Mixtures

All proposed equations for spherical and non-spherical particles (Akgiray and Saatçi, 2001; Akkoyunlu, 2003; Cleasby and Fan, 1981; Dharmarajah and Cleasby, 1986; Soyer and Akgiray, 2009, 2005) and the equations presented in Table 1.10 are applicable for only monodisperse beds. In other words, only one particle diameter (d_p or d_{eq}) value exists in all of these calculation models. On the other hand, the filter beds in practice are not normally consisted of a mono-sized particles. Instead, they are generally characterized with a particle size distribution. The accepted calculation method for the size distribution by the most widely used Environmental Engineering course (water and wastewater treatment, unit operations) books (AWWA, 1999; Droste, 1997; Metcalf and Eddy, 2004; Peavy et al., 1985; Reynolds, 1996; Weber, 1972)is as following:

The expansion ratio of layers depending on the filter backwash velocity are calculated separately for the all layers. Then, total bed expansion is found by summing expansions of each layer. This calculation method found successful by Cleasby and Baumann (1976) for multi-layered filters composed of anthracite coal and silica sand and it is also confirmed by Hoffman et al. (1960) and Epstein et al. (1981) for the overall bed expansion composed of

different sized spherical particles. Moreover, Cleasby and Woods (1975) are recommended this calculation method. However, Asif (2001, 2012) is performed binary mixtures experiments with spheres. The author reported new data showing that the total expansion is considerably lower than the sum of the expansions of every single material. On the other hand, serial model in which total bed expansion is found by summing the expansions of each separate layer, is recommended by Epstein (2003a) in his comprehensive handbook.

Wen and Yu (1966) performed fluidization experiments with spheres having same density but different diameters. They concluded that the total expansion of the bed can be calculated by defining an equivalent diameter for entire the bed if the particle diameter ratio of the largest to the smallest particle is less than 1.3:

$$d_{pe} = \frac{1}{\sum_{i=1}^{n} \frac{w_i}{d_{pi}}} \tag{1.117}$$

Here, n is the number of different diameters, d_{pi} is the diameter of particle and w_i is the weight fraction ($w_1+w_2+ \ldots + w_n = 1$) of particles having that diameter. Wen and Yu (1966) recommended to use serial model again for the particle systemwith a size ratio above 1.3. These researchers have no suggestions for the particle system having different densities.

Amirtharajah and Cleasby (1972) used d_{60} diameter for the filter beds composed of a uniform material with a size distribution (such as a monomedium sand filter). Here, d_{60} is the sieve size in which the 60 percent of the bed by weight passes through.

Leva et al. (1948) used an arithmetic average diameter to calculate minimum fluidization velocity of filter beds including up to four different particle sizes:

$$d_{pe} = \sum_{i=1}^{n} w_i d_{pi} \tag{1.118}$$

As mentioned above, Epstein et al. (1981) recommend serial model for the calculation of overall bed expansion based on the consistency they observed between the data they produced and the predictions with serial model. In addition to this data, they also cited the study of Cleasby and Baumann (1976) which includes fluidization experiments conducted on anthracite coal and silica sand dual media filter beds. It needs to be emphasized here that: Cleasby and Baumann (1976) studied silica sand filter beds composed of a uniform material with a size distribution. They found that Eq. (1.117) gave the best results for sand beds with

a size distribution (ie, non-uniform), followed by Eq. (1.116), and the serial model gave the highest errors between these three methods. Cleasby and Baumann (1976) did not performed this comparison with any material other than silica sand. Then, they studied with dual media filter beds composed of anthracite coal and silica sand as follows: Expansion of each material (silica sand and anthracite) were separately measured and bed expansion was recorded versus filter backwash rate for the beds having single material. The expansion of dual media filters was then studied and the total expansion was represented in acceptable accuracy by the sum of the expansions of sand and anthracite layers. In summary, in this study, it is found that the serial model was successful for the dual media anthracite-sand filters where the serial model for monolayer filters is not very successful. It may be useful to emphasize that the main objective of the study of Cleasby and Baumann (1976) is to determine the best backwashing methods for wastewater and to compare the quality of water obtained with dual and triple media filters that the total bed extension is not systematically addressed and that no definitive conclusions have been reached.

Erbil et al. (2011) investigated ammonium ion removal in zeolite ion exchange fluidized beds. In the study, monomedium zeolite beds compared with segregated fluidized beds including zeolite with two different particle sizes. Segregated beds were defined as beds in which the layers were not mixed. The authors reported a particle size ratio of 1.7-1.8 to obtain non mixing segregated layers. Serial model was found to produce high agreement with the experimental data.

Consequently, there is no consensus in literature on how to calculate the total fluidized bed expansion for the beds composed of the particles having different dimensions, densities and shapes. There is also no general method of calculation based on extensive experimental data. In addition, the majority of literature studies are based on experiments with spheres. Materials used in rapid filtration are generally not spherical. As a result, there is no comprehensive study made with real filter materials and systematically taking into account the calculation of the total bed expansion.

2 MATERIALS and METHODS

In this section, the experimental apparatus used for fluidization and permeability experiments and the methods employed in preparation and characterization of particle systems are presented.

2.1 Filter Materials

Experiments have been carried out with spherical and non-spherical particles of different size and densities. 20 spherical particles, 5 different types of 4 non-spherical non-porous materials, and 5 different types of 3 non-spherical porous materials were employed as filter materials. Non-spherical particles studied include sand, garnet, crushed glass, perlite, activated carbon, zeolite and anthracite. These are the most commonly used granular materials in filtration, adsorption and ion exchange column operation.

2.1.1 Spherical Particles

20 different spherical particles (made from different materials: cellulose acetate, polyvinyl chloride (PVC), delrin, glass, plastics) having different sizes and densities were investigated in fluidization experiments. List of the spherical particles is given in Table 2.1.

Table 2.1 Spherical particles used in experiments

Materials	Diameter (mm)	Materials	Diameter (mm)
Cellulose Acetate	2.5	Glass	1
Cellulose Acetate	3	Glass	2
Cellulose Acetate	3.5	Glass	3
Cellulose Acetate	4.5	Glass	4
Cellulose Acetate	5	Glass	5
Cellulose Acetate	6	Glass	6
PVC	4.8	Plastics	2
Delrin	2.4	Plastics	2.5
Delrin	3.2	Plastics	3
Delrin	4		
Delrin	4.8		

Spherical particles were used in the study to determine fluidization behavior of spheres. This data was also required for the evaluation of the data of non-spherical particles. Particles (cellulose acetate, PVC and delrin) listed in first column of the table were obtained from a sensitive ball manufacturing company (Engineering Laboratories Inc., USA). The spherical particles (glass and plastics) listed in the right column of the Table 2.1 were obtained from different manufacturers. The Table 2.1 lists the nominal particle sizes given by the manufacturers.

2.1.2 Non-spherical particles

Non-spherical particles used in the study are divided into two groups; (i) non-spherical non-porous materials including sand, garnet, crushed glass and perlite and (ii) non-spherical porous particles including zeolite, activated carbon and anthracite.

2.1.2.1 Non-spherical non-porous particles

Sand, garnet, perlite and crushed glass were used as non-spherical non-porous materials with five different fractions of each material. Only washing and drying were performed as a pretreatment step for the materials and then they were fractionated using standard sieves. Fractions of the natural non-porous materials used in this study are listed in Table 2.2 with sieve size data.

Table 2.2 Fractions of natural materials used in this study

Materials	Sieve size (mm-mm)	Materials	Sieve size (mm-mm)
Sand	1.40-1.18	Crushed glass	1.40-1.18
Sand	1.18-1.00	Crushed glass	1.18-1.00
Sand	1.00-0.85	Crushed glass	1.00-0.85
Sand	0.85-0.71	Crushed glass	0.85-0.71
Sand	0.71-0.60	Crushed glass	0.71-0.60
Garnet	1.40-1.18	Perlite	2.36-2.00
Garnet	1.18-1.00	Perlite	2.00-1.70
Garnet	1.00-0.85	Perlite	1.70-1.40
Garnet	0.85-0.71	Perlite	1.40-1.18
Garnet	0.71-0.60	Perlite	1.18-1.00

2.1.2.2 Non-spherical porous particles

Five different fractions of anthracite, activated carbon and zeolite were investigated as non-spherical porous particles. Fractions of the non-spherical porous materials used in this study are listed in Table 2.3 with sieve size data.

Table 2.3 Fractions of non-spherical porous materials

Materials	Sieve Size (mm)
Activated Carbon	1.40-1.18
Activated Carbon	1.18-1.00
Activated Carbon	1.00-0.85
Activated Carbon	0.85-0.71
Activated Carbon	0.71-0.60
Zeolite	1.40-1.18
Zeolite	1.18-1.00
Zeolite	1.00-0.85
Zeolite	0.85-0.71
Zeolite	0.71-0.60
Anthracite	2.00-1.70
Anthracite	1.70-1.40
Anthracite	1.40-1.18
Anthracite	1.18-1.00
Anthracite	1.00-0.85

2.2 Fluidization System

A schematic diagram of the experimental setup is shown in Figure 2.1. Fluidization experiments were conducted in a 150 cm (only fluidization section) high plexiglass column with an inner diameter of 5.019 cm. Two centrifugal pumps having 1.5 hp and 3 hp pump power were installed and operated with frequency controllers. Two different flowmeters were used for high and low velocities in order to improve sensitivity in flow measurement. Temperature data was recorded for each measurement of fluidization cycle to monitor changes in water temperature. The bed heights were read visually with the help of a ruler attached along the length of the column.

Tap water was used for the all fluidization experiments. The water flow through the column was recirculated back to the storage tank. The water recirculation of the system was continued until the water becomes unclean. A cylindrical tank with a volume of 100L was

used as a water storage tank during fluidization experiments.

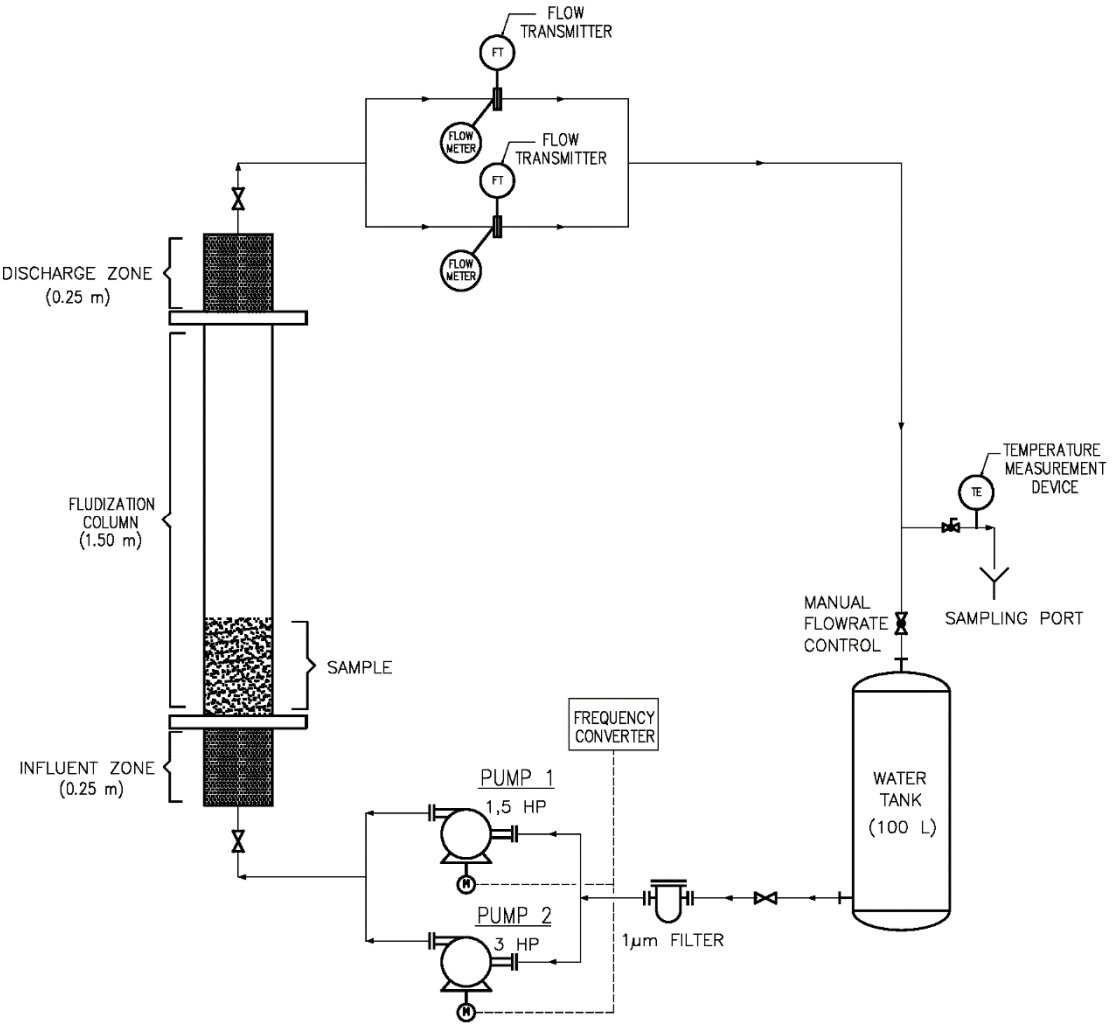


Figure 2.1. Schematic view of experimental set-up

Inlet and discharge sections having 25 cm height were installed to the upper and lower ends of fluidization column with the help of flanges. The aim of using an inlet zone was to avoid negative effects such as channelling and to provide homogenous distribution of water. This calming section was filled with spherical glass beads having 10 mm diameter. Over this section, a 100µm screen filter was placed to prevent the passage of the filter material down and it was fixed to fluidization section with the help of a flange. With same method, on top of column between discharge section with 25 cm height and fluidization column with 150cm height, an additional 100µm screen filter was placed to avoid escaping of filter material.

In order to determine flowrates, the experiments were carried out also using flowmeters. The important point on this measurements was to refrain exceeding flowmeter measurement

ranges. For this reason, two flowmeters (6 mm and 10 mm inner diameters) were used having different measurement ranges (MUT 500, Euromag International). The flowrates were also checked manually to avoid misleading results. The electromagnetic flowmeters used in experiments are shown in the Figure 2.2.



Figure 2.2 The electromagnetic flowmeters used in experiments

There are some significant issues to be considered during the fluidization experiments:

- It is important that the fluidization column should be vertical in flat. The vertical alignment of the column was checked using a level for each time to minimize secondary flows. In the case of misalignment, the necessary adjustments were done before experiments.
- The disposal of air bubbles from the system is important after insertion of the material to the column. For this purpose, the bed was fluidized in higher rates before the experiments start. The porous materials and some other materials were wetted for 24 hours in order to obtain bubble-free experiment.
- During fluidization, expanded bed heights were not recorded without being sure that it becomes stable. When some fluctuations occured in expanded bed, the minimum and maximum oscillation values were noted for every bed height.

- Throughout the fluidization experiments, care was taken to increase the flowrate gradually and proportionally.
- Material bed heights in fluidization column were about 25 cm as a standard height. Also, significant attention was paid to minimize the loss of particles during weighing of materials and installation to the column.
- Flowrate and temperature data were recorded for every expanded bed height. Viscosity and density values were calculated using following functions depending on the temperature data recorded during fluidization experiments.

If temperature value is lower than or equal to 20°C,

$$\mu = 0.001 \times 10^{\left(\frac{1301}{(998.333 + 8.1855\times(\mathrm{T}-20)+0{,}00585\times(T-20)^2)-1{,}30233)}\right)} \quad (2.1)$$

otherwise,

$$\mu = 0.001 \times 10^{\left(\frac{1301}{998.333}-1.30233\right)} \quad (2.2)$$

These two equations were employed to the data to obtain viscosity value on that temperature (Weast et al., 1989).

Density values were calculated as a function of temperature using the equation below (Weast et al., 1989).

$$\rho = (999{,}83952 + 16{,}945176 \times T - 0{,}0079870401 \times T^2 - 0{,}000046170461 \times T^3 + 0{,}00000010556302 \times T^4 - (2{,}8054253E - 10) \times T^5/(1 + 0{,}01687985 \times T) \quad (2.3)$$

Here, μ (kg/m/sn), ρ (kg/m^3) and T(˚C) represent dynamic viscosity, density and temperature respectively.

2.3 Fluidization of Binary Mixtures

Binary mixtures of spherical particles were prepared as 50% mixtures of materials by volume. Table 2.4 lists the thirty three different binary mixtures of spherical materials having different diameters and densities.

Table 2.4 Binary mixtures of different spherical materials

Experiment name	Material 1	Material 2	Experiment name	Material 1	Material 2
Bin1	Delrin 2.4mm	Delrin 3.2mm	Bin18	CA 3mm	CA 4.5mm
Bin2	CA 3.5mm	CA 5mm	Bin19	Glass 1mm	CA 5mm
Bin3	CA 2.5mm	CA 3mm	Bin20	Glass 1mm	Delrin 4mm
Bin4	CA 3mm	Delrin 2.4mm	Bin21	Glass 1mm	PVC 4.8mm
Bin5	CA 2.5mm	Delrin 3.2mm	Bin22	Glass 2mm	CA 5mm
Bin6	Glass 1mm	CA 4.5mm	Bin23	Glass 1mm	Delrin 4.8mm
Bin7	Delrin 4mm	CA 6mm	Bin24	Glass 2mm	Delrin 3.2mm
Bin8	Plastics 2mm	Plastics 2.5mm	Bin25	Glass 2mm	CA 4.5mm
Bin9	Glass 1mm	Delrin 2.4mm	Bin26	Glass 2mm	Delrin 4mm
Bin10	CA 2.5mm	CA 3.5mm	Bin27	Glass 1mm	Plastics 2.5mm
Bin11	PVC 4.8mm	CA 6mm	Bin28	Glass 1mm	Delrin 3.2mm
Bin12	Plastics 3mm	CA 2.5mm	Bin29	Glass 1mm	Plastics 3mm
Bin13	Delrin 2.4mm	CA 3.5mm	Bin30	CA 3mm	Glass 1mm
Bin14	Plastics 2.5mm	CA 3mm	Bin31	Plastics 2mm	Plastics 3mm
Bin15	CA 3 mm	Plastics 3mm	Bin32	Glass 3mm	Glass 5mm
Bin16	CA 2.5mm	Plastics 2mm	Bin33	Glass 3mm	Glass 4mm
Bin17	Glass 1mm	CA 3.5mm			

The fluidization ratio versus fluidization velocity graph of existing spheres were plotted to determine binary mixtures of spheres (Figure 2.3).

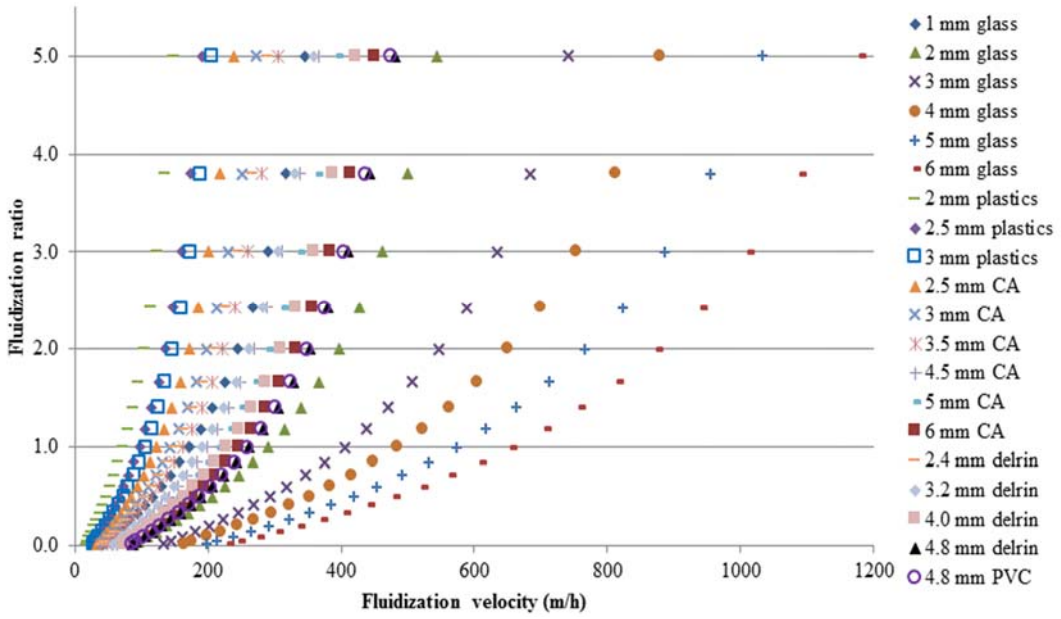


Figure 2.3. Fluidization graph of spheres used in the study

According to Figure 2.3, the mixtures were formed with spheres that would fluidize at same velocities. For example, as it can be clearly seen from the graph, a mixture of 2mm plastics spheres and 5mm glass spheres will not be fluidize at the same time on desired velocities.

2.4 Characterization of particles

Several characterization techniques were applied to the materials. These are particle density, sieve analysis, size determinations, packed bed permeability tests and determination of sphericity as an indication of particle shape.

2.4.1 Density

Particle density is an important particle characteristics for the design and/or operation of a solid-liquid system such as a bed of ion-exchanger or a water treatment granular filter bed. Particle density has significant effects on fluidization (backwashing in granular filters and backwashing and regeneration in ion-exchanger beds) since higher wash rates are required to achieve fluidization of the particles with higher densities but of the same diameter.

2.4.1.1 Density measurement for non-porous materials

The densities of all non-porous materials (spherical particles, and natural non-porous filter materials) were determined by the water displacement technique using 50ml and 100ml pycnometer bottles (Figure 2.4). The procedure of density measurement of spherical particles and calculations are shown in Table 2.5 for the 3.5mm cellulose acetate beads as an example.



Figure 2.4 Different materials prepared for density measurements.

The spherical particles except glass ones were submerged for 24 hours before final weightings to allow the air bubbles to leave material surface. However, for some spherical particles as cellulose acetate, PVC and delrin particles, bubbling on material surface was a significant problem. Figure 2.5 shows the air bubbles in a PVC material surface after 24 hours. To handle this problem a new procedure was derived after different trials. According to this procedure, samples submerged in water in a pycnometer were stirred using a stick to remove bubbles. Stirring was applied when the sample was just filled in the pycnometer and then the sample was waited for 24 hours. The results of measurements after 24 hours waiting period were more applicable.

Table 2.5 The procedure of density measurement of spherical particles and calculations

Material:	3.5mm cellulose acetate beads		
Temperature of water (°C):	15.3	14.6	14.6
(1) Weight of dry pycnometer	30.9718	29.1170	32.9965
(2) Weight of pycnometer full of water	80.9765	79.0230	132.4890
(3) Weight of pycnometer with inside wet	31.1330	29.3438	33.4590
(4) Weight of pycnometer with inside wet + material	39.8489	43.4206	57.6882
(5) Weight of pycnometer with inside wet+ material + water to fill	82.9061	82.1678	137.951
(6) Weight of material = (4) - (3)	8.7159	14.0768	24.2292
(7) Weight of water to fill pycnometer = (2) - (1)	50.0047	49.9060	99.4925
(8) Weight of extra water to fill pycnometer over the material = (5)-(1)-(6)	43.2184	38.9740	80.7251
(9) Weight of equivalent volume of water = (7)-(8)	6.7863	10.9320	18.7674
(10) The specific gravity of material at tested temperature = (6)/(9)	1.2843	1.2877	1.2910
(11) Density of water at tested temperature (kg/m^3)	999.0539	999.1590	999.1590
(12) Density of material (kg/m^3)= (10)*(11)	1283.1	1286.6	1289.9
Average density (g/cc)		1.2865	



Figure 2.5 Air bubbles in material surface

2.4.1.2 Density measurement for porous materials

Particle density was calculated on the basis of either the saturated-surface-dry (SSD) condition or the oven-dry (OD) condition. Three different methods were attempted to reach the SSD condition, giving four different density measurement methods in total. "Saturated-Surface-Dry" (SSD) condition is the state of particles in which the permeable pores of particles are filled with water to the extent achieved by submerging in water for a prescribed period of time, but without free water on the surface of particles (Figure 2.6). The three different methods were tried to reach the SSD condition were (i) The standard cone test, (ii) The Le Chatelier flask method, (iii) The soak-and-strain method.

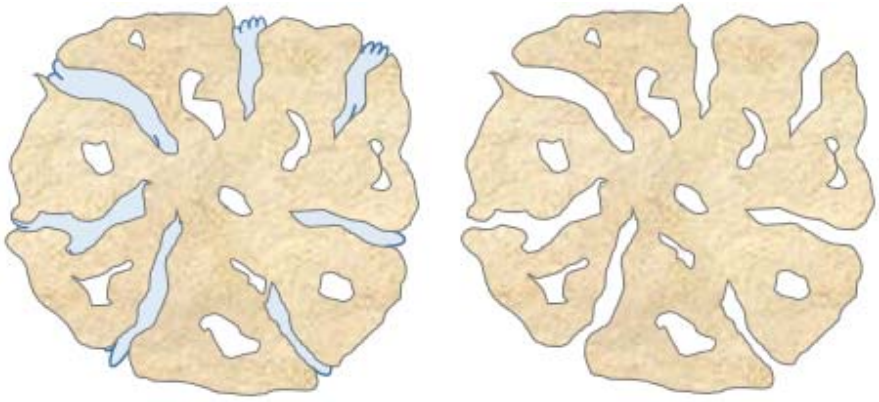


Figure 2.6 Illustrations of saturated surface dry (SSD) and oven dry (OD) particles

Standard cone test: This method is referred to as the "Gravimetric (Pycnometer) Procedure" in the ASTM C128-12 standard. The following is a summary of the procedure and the

standard may be consulted for further details (ASTM C128-12, 2012). The material is initially soaked in water for 24 hours. The excess water is then decanted, the sample is spread over a flat nonabsorbent surface, and it is partially dried exposing it to a gently moving current of warm air. A standard cone-shaped mold is held firmly on a smooth nonabsorbent surface with the large diameter down (Figure 2.7). A portion of the partially dried sample is next placed in the mold by filling it to overflowing and tamped into the mold with several drops of a standard metal tamper. Next, the mold is lifted vertically. Slight slumping of molded sample indicates that the material has reached the SSD condition. If surface moisture is still present, the material will retain the molded shape. In this case, the drying process is continued until the SSD condition is obtained.



Figure 2.7 A photo of mold and tamper used in the study

The pycnometer is partially filled with water. A 500±10 g of the SSD material (which was prepared as described above) is introduced into the pycnometer which is then filled with water to roughly 90 % of its capacity. Pycnometer is rolled manually to eliminate visible air bubbles. After elimination of air bubbles, the water level in the pycnometer is brought to its calibrated capacity and the total mass of pycnometer, material, and water is determined. The water temperature (which is brought to 23±2 °C) is also recorded. Then the material is removed from the pycnometer and dried in the oven to constant mass at temperature of 110±5 °C, is cooled in a desiccator, and the mass is determined. The mass of the empty pycnometer and the mass of the pycnometer filled to its calibrated capacity with water are also recorded for calculations. Sample calculations are given in Table 2.6.

Table 2.6 The calculations of density using cone test method

Material:	Zeolite 1.00-0.85		
Temperature of water (°C)	21.31	24.36	24.38
(1)Weight of volumetric flask (g)	241.73	241.73	241.73
(2)Weight of volumetric flask full of water (g)	1237	1237	1237
(3)Weight of material (SSD) (g)	500.3	500.5	500
(4)Weight of volumetric flask+ material + water to fill	1487.5	1482.5	1483.5
The mass of material after oven drying (OD) (g)	428.0	425.0	423.5
(5)Weight of water to fill volumetric flask (g) = (2) - (1)	995.3	995.3	995.3
(6)Weight of extra water to fill volumetric flask over the material (g) = (4)-(1)-(3)	745.4	740.3	741.8
(7)Weight of equivalent volume of water (g) = (5)-(6)	249.8	255.0	253.5
(8)The specific gravity of material at tested temperature = (3)/(7)	2.003	1.963	1.972
(9)Density of water at tested temperature (kg/m^3)	997.9	997.2	997.2
Density of material (kg/m^3) = (8)*(9)	1998.5	1957.3	1966.9
% Water absorption = (OD)/(3)	16.9	17.8	18.1
Average density of material (kg/m^3)	1974.2	Std. dev.	21.6
Average % water absorption of material	17.6	Std. dev.	0.6

The "cone-test SSD density" of the material is found using the following formula:

$$(\rho_{SSD})_{Conetest} = \frac{M_{SSD}}{(M_{DW})_{SSD}} \times \rho_W \quad (2.4)$$

$(M_{DW})_{SSD}$: mass of the water displaced by the SSD sample

M_{SSD}: SSD mass of the sample

ρ_w: density of water at the test temperature

While the cone test described above conforms to the ASTM standard and it appears to be theoretically the best method for applications involving liquid flow through fixed and fluidized beds, it is tedious to perform and requires a significant amount of experience to obtain reproducible and reliable results. Therefore, two additional, simpler procedures were tested in this work to see if reasonable results could be obtained with less effort and expertise. These are "the Le Chatelier flask method" (developed during the course of this work) and the very simple "soak-and-strain" method. The "soak-and-strain" method is a very simple

procedure one might be tempted to use to get quick and rough answers. Including this method in the present study is expected to give an indication of how much error may be expected as a result of using such a simple procedure. These two methods are explained next.

Le Chatelier flask method: This procedure is employed to determine the water permeable portion of particles (Figure 2.8). Mass of SSD specimen is estimated by adding this pore water mass to the mass of the OD specimen. The flask is first filled with water to a known point between 0 and 1 ml marks. This initial reading and temperature of water are recorded (Figure 2.9).

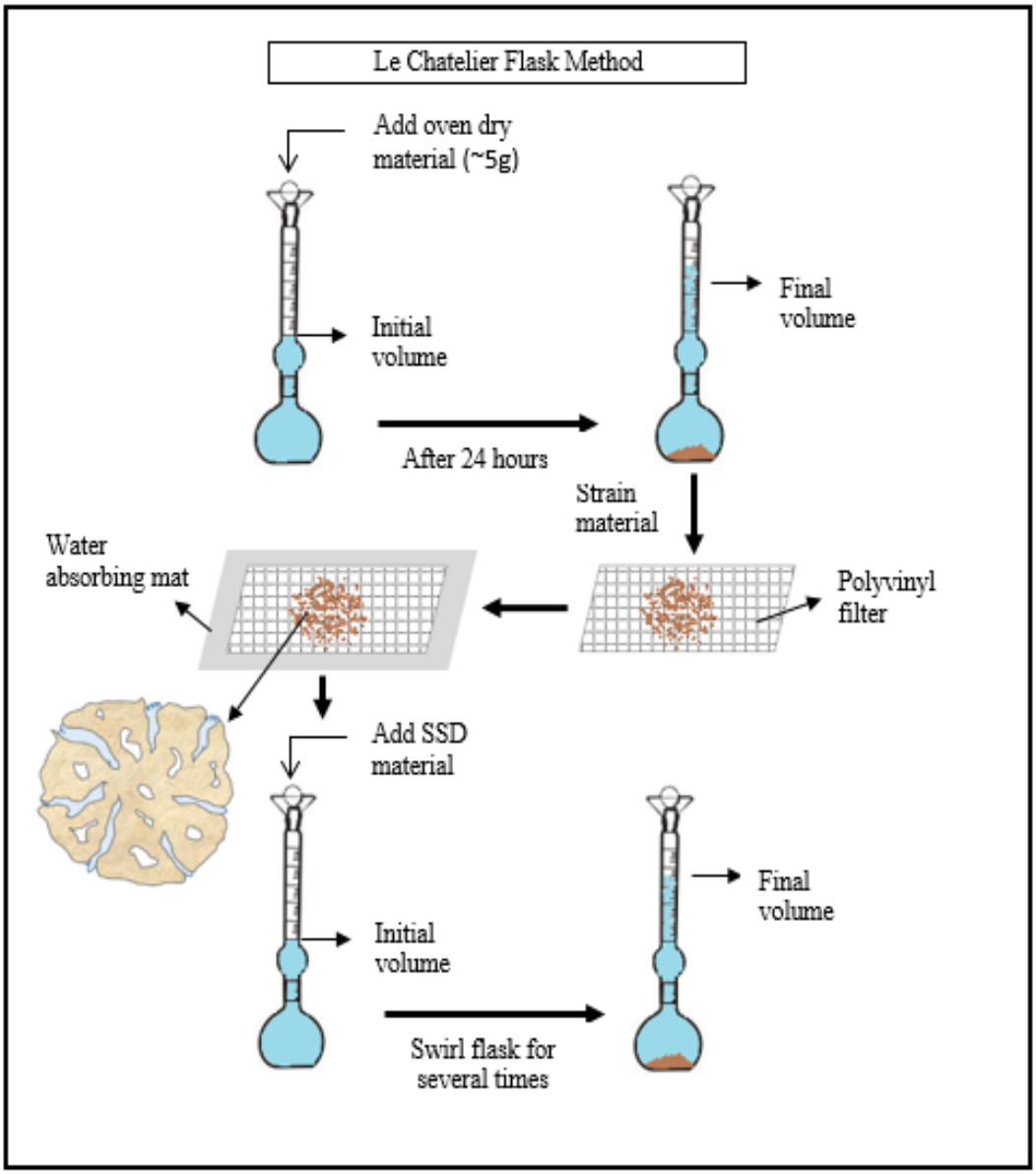


Figure 2.8 Illustration of the procedure of Le Chatelier Flask Method



Figure 2.9 A photo of Le Chatelier flask

A known weight (~5 g) of OD material is then added and a stopper is placed on the flask. The final volume and water temperature are recorded after waiting for 24 hours. Then, the sample is removed from the flask to a polyvinyl filter (100 µm mesh size). Care is taken not to lose any particles during this step. The sample on the filter is placed over a dry water absorbing mat. This arrangement prevents direct contact between particles and the mat which could lead to water drainage from the pores. The material is laid over the filter surface and the filter is moved to the dry parts of the mat for a few times. This process is employed in order to obtain SSD material and takes about 5 minutes. For a second volume determination, the flask is filled with water to a known point between 0 and 1 ml marks again. The SSD material is added and the stopper is placed on the flask. The flask is rolled in an inclined position to remove entrapped air from the particles until no bubbles rise to the water surface. The final volume and temperature are recorded.

The estimation of SSD density with this method is as follows:

$$V_{pore} = \left(V_{2,SSD} - V_{1,SSD}\right) - \left(V_{2,OD} - V_{1,OD}\right) \tag{2.5}$$

$$M_{pore} = V_{pore} \times \rho_W \tag{2.6}$$

$$(\rho_{SSD})_{LeChatelier} = \frac{M_{OD} + M_{Pore}}{\left(V_{2,SSD} - V_{1,SSD}\right)} \tag{2.7}$$

Here, $V_{1,OD}$ is the initial level volume of water for OD particles, $V_{2,OD}$ is the final level volume of water for OD particles, $V_{1,SSD}$ is the initial level volume of water for SSD particles, $V_{2,SSD}$ is the final level volume of water for SSD particles, V_{Pore} is volume of water in pores of material and M_{Pore} is the mass of pore water calculated from V_{Pore} and temperature data. The calculations of density measurement using Le Chatelier flask method are given in Table 2.7 for the zeolite 1.40 mm-1.18 mm fraction as an example.

Soak-and-strain method: Particles submerged in water for 24 hours are simply separated from the water using a strainer without any drying process such as the use of warm air or the application of a blotting paper. The excess water is allowed to drain through the strainer by the action of gravity until one cannot see any additional water passing through the strainer. The wet granular material is mixed slowly with a spoon to facilitate the drainage of excess water. The entire straining and draining process usually takes about 10 minutes. The wet density is then calculated as follows (Table 2.8):

$$\rho_{Straining} = \frac{M_{wet}}{(M_{DW})_{wet}} \times \rho_W \tag{2.8}$$

Here, $(M_{DW})_{wet}$ represents the mass of water displaced by wet sample, M_{wet} is the mass of wet sample after straining and ρ_w is the density of water at the test temperature.

Table 2.7 The calculations of density using Le Chatelier flask method

Zeolite 1.40 mm-1.18 mm	1	2	3	4	5	6
Initial volume of dry material (ml)	17.80	17.80	17.80	17.80	17.80	17.80
Final volume of dry material (ml)	21.90	21.85	21.90	21.90	21.90	21.95
Initial volume of wet material (ml)	17.80	17.80	17.80	17.80	17.80	17.80
Final volume of wet material (ml)	23.70	23.65	23.70	23.60	23.80	23.85
Weight of material (OD) (g)	9.4022	9.4271	9.4475	9.3879	9.3127	9.3857
Temperature (°C)	20.5	20.2	20.2	20.1	20.1	20.1
Density of water (kg/m^3)	998.10	998.16	998.16	998.18	998.18	998.18
% Water absorption	19.1	19.1	19.0	18.1	20.4	20.2
Density (kg/m^3)	1898.1	1918.6	1905.8	1911.2	1868.2	1864.8
Average % absorption	19.3			σ	0.009	
Average density (kg/m^3)	1894.5			σ	0.023	

Table 2.8 The calculations of density using soak-and-strain method

Material	Zeolite 1.40-1.18				
Temperature of water (°C):	22	22	22	22	22
(1) Weight of dry pycnometer (g)	36.6446	36.6446	36.6446	36.6446	36.6446
(2) Weight of pycnometer full of water (g)	136.1128	136.1128	136.1128	136.1128	136.1128
(3) Weight of pycnometer with inside wet (g)	37.1009	36.8904	36.8669	36.9714	36.9608
(4) Weight of pycnometer with inside wet + material (g)	68.6977	60.1553	66.7565	61.7188	57.7939
(5) Weight of pycnometer with inside wet+ material + water to fill (g)	147.5080	145.2356	147.5828	145.5689	144.3224
(6) Weight of material (g)= (4) - (3)	31.5968	23.2649	29.8896	24.7474	20.8331
(7) Weight of water to fill pycnometer (g) = (2) - (1)	99.4682	99.4682	99.4682	99.4682	99.4682
(8) Weight of extra water to fill pycnometer over the material (g)= (5)-(1)-(6)	79.2666	85.3261	81.0486	84.1769	86.8447
(9) Weight of equivalent volume of water (g) = (7)-(8)	20.2016	14.1421	18.4196	15.2913	12.6235
(10) The specific gravity of material at tested temperature = (6)/(9)	1.5641	1.6451	1.6227	1.6184	1.6503
(11) Density of water at tested temperature (kg/m^3)	997.8	997.8	997.8	997.8	997.8
(12) Density of material (kg/m^3)= (10)*(11)	1560.6	1641.4	1619.1	1614.8	1646.7
Average density of material (kg/m^3)	1616.5			σ	34.2

Skeletal density: The mass of OD particles per unit volume of their impermeable portion is defined as "apparent density"(ASTM C128-12, 2012). The term "skeletal density" is used here for this type of density. This method is also based on the gravimetric water displacement technique. The calculation of skeletal density is as follows (Table 2.9):

$$\rho_{Skeletal} = \frac{M_{OD}}{(M_{DW})_{OD}} \times \rho_W \quad (2.9)$$

$(M_{DW})_{OD}$: mass of water displaced by OD material in 24 hours

M_{OD}: oven dry mass of particles

ρ_w: density of water at the test temperature

Table 2.9 The calculations of skeletal density

Material	Zeolite-0.85-0.71				
Temperature of water (°C)	24.35	24.22	24.31	24.27	24.33
(1) Weight of dry pycnometer	32.9955	32.9955	32.9955	32.9955	32.9955
(2) Weight of pycnometer full of water	133.2230	133.2230	133.2230	133.2230	133.2230
(3) Weight of pycnometer with inside wet (g)	33.2452	33.2499	33.2617	33.2726	33.2886
(4) Weight of pycnometer with inside wet + material	54.6821	62.4579	67.2402	60.6458	68.7973
(5) Weight of pycnometer with inside wet+ material + water to fill	142.3312	145.1013	147.0885	144.5742	146.8085
(6) Oven dry weight of material	15.5375	20.3363	23.7114	19.4049	23.2225
(7) Weight of water to fill pycnometer = (2) - (1)	100.2275	100.2275	100.2275	100.2275	100.2275
(8) Weight of extra water to fill pycnometer over the material = (5)-(1)-(6)	93.7982	91.7695	90.3816	92.1738	90.5905
(9) Weight of equivalent volume of water = (7)-(8)	6.4293	8.4580	9.8459	8.0537	9.6370
(10) The specific gravity of material at tested temperature = (6)/(9)	2.4167	2.4044	2.4083	2.4094	2.4097
(11) Density of water at tested temperature (kg/m^3)	997.2096	997.2420	997.2196	997.2296	997.2146
(12) Density of material (kg/m^3) = (10)*(11)	2409.9	2397.8	2401.6	2402.8	2403.0
Average density of material	2403.0	Std. dev.		4.4	

2.4.2 Particle Size

2.4.2.1 Equivalent diameter

Equivalent diameter is defined as the diameter of a sphere which is having same volume with the actual particle. This method is generally used for the determination of particle diameters of fine particles. For the calculation of equivalent diameter, this equation is used:

$$d_{eq} = \sqrt[3]{\frac{6.m}{\pi.\rho_p}} \tag{2.10}$$

d_{eq}: equivalent diameter (cm), m: weight of a particle (gr), ρ_p:density of particle (gr/cm^3)

Equivalent diameter (d_{eq}) of each fraction is calculated by (i) counting and weighing a number of grains, (ii) calculating the volume of one grain using its particle density, (iii) equating the volume of one grain to the volume of equivalent sphere (Equation 2.10). This experiment was repeated three times using representative samples (Figure 2.10). In order to obtain representative samples from non-spherical materials, coning and quartering method (Horwitz, 1990) was employed. While the number of counted spherical particles was determined as 200, it was considered as 600 for non-spherical particles to obtain representative results. An example of equivalent diameter measurement and calculations are given in Table 2.10.



Figure 2.10 A photo of materials counted for equivalent diameter measurement

Table 2.10 An example of equivalent diameter measurement

Material	3.5 mm cellulose acetate		
Density of material	1.272 g/cm^3		
Number of spherical particles	Weight of spherical particles (g)	Weight of a single particle (g)	Equivalent diameter of a spherical particle (mm)
200	5.6723	0.0284	3.479
200	5.6758	0.0284	3.480
200	5.6750	0.0284	3.479
	Average	0.0284	3.479
	Standard deviation of equivalent diameter		0.0004

As can be seen from the relevant equations and explanations, the equivalent diameter obtained depends on how particle density and the mass of the samples (N = 600 for each sample) are measured. It is clear that a self-consistent method should be used. For example, if the SSD-cone test density is used, a sample for equivalent diameter determination should be weighed after being brought to the SSD condition according to the steps detailed in the ASTM standard. Similarly, if the Le Chatelier flask method is employed to estimate the SSD

density, then the sample should be brought to the SSD condition according to the steps of this method before it is weighed to determine m_p (mass of N grains) to be used in Equation 2.10. If the soak-and-strain method is used to approximate the effective density, then particles should be separated from the water using a strainer without any drying and then weighed to determine sample mass m_p to be used in diameter calculation. There are, however, two disadvantages to determining sample masses in this way: (i) Moisture content (and, therefore, the mass) of SSD samples may not remain constant during the time-consuming counting process, (ii) Percent water absorption is already determined for each fraction of each material during density determinations according to all three methods and it would be an unnecessary duplication of work to measure SSD or wet sample masses when they can be calculated from dry sample masses easily. The approach taken here is therefore the following: Oven dry (OD) mass of each sample is measured and the SSD or wet sample masses are then calculated using the percent water absorption values previously determined during density measurements. The same approach is used in calculating the SSD/wet mass of beds of particles used in the fixed and fluidized bed experiments.

2.4.2.1 Diameter measurement using micrometer

Diameters of spherical particles (glass, plastic, delrin, PVC and cellulose acetate spheres) was also measured using micrometer (Figure 2.11). For these measurements, diameters of 20 different beads were evaluated for the determination of the size of a material (e.g. 3mm cellulose acetate). Also for the first 5 beads, 3 different diameter values were recorded for each bead. As an example, diameter measurement of 3.5mm Cellulose Acetate beads using micrometer is given in Table 2.11.



Figure 2.11 A photo of diameter measurement using micrometer

Table 2.11 An example of diameter measurement using micrometer (3.5mm Cellulose Acetate beads).

Number of beads	Diameters (mm)		
1	3.489	3.481	3.503
2	3.496	3.494	3.480
3	3.481	3.495	3.497
4	3.462	3.485	3.495
5	3.458	3.489	3.479
6	3.497		
7	3.512		
8	3.498		
9	3.501		
10	3.468		
11	3.470		
12	3.501		
13	3.502		
14	3.493		
15	3.498		
16	3.500		
17	3.489		
18	3.499		
19	3.479		
20	3.503		
Average Diameter (mm)	3.490	Std. dev.	0.013

2.4.3 Sieving

Sieving process was carried out accordance with the criteria of ASTM (American Society for Testing and Materials) standards (ASTM.2005). After the appropriate sieve sizes (0.60 mm, 0.71 mm, 0.85 mm, 1.00 mm, 1.18 mm, 1.40 mm, 1.7 mm, 2.00 mm) were determined, the sieving process was started to obtain needed fractions. A Ro-Tap sieve shaker (Retsch AS200 tap), in which mechanical action applied to test sieves in two-dimension, was used in sieving process. In addition to horizontal circular motion, this shaker produces a vertical tapping motion to help particulates to pass sieve apertures. A photo of the standard sieves and sieve shaker used in experiments is given in Figure 2.12.

All desired fractions of the material was obtained by this method. The representative samples should be used in the tests for the determination of the material properties. Although the materials are in the range of two standard sieves, the sample taken from the stored material may not be representative.



Figure 2.12 Standard sieves and sieve shaker

After fractionation of materials, coning and quartering process (Horwitz, 1990) was employed to obtain representative samples for characterization experiments (Figure 2.13). According to this technique, the material was poured on a conical shape, and then it was flattened out into a cake. The cake was divided into quarters and two quarters that sit opposite one another are discarded. The other two were combined to constitute the reduced sample. This process was continued until a convenient sample size remains. Characterization experiments were performed with the sample left behind.



Figure 2.13 A photo from coning and quartering process

2.4.4 Permeability Experiments

Permeability tests were conducted for non-spherical non-porous particles (sand, garnet, perlite and crushed glass) and non-spherical porous particles (zeolite, anthracite and activated carbon). For all fractions of non-spherical non-porous particles permeability tests were performed for 5 different bed porosities to evaluate the changes in sphericity values. For the same purpose, the sphericity values of all fractions of non-spherical porous materials were determined using the data for 3 different porosities.

2.4.4.1 Permeability system

Permeability tests were carried out in order to determine sphericities of non-spherical materials. Permeability experiments were performed using "W3 Permeability/ Fluidization Study Apparatus" which was manufactured by Armfield Ltd. The apparatus is designed to measure the characteristics of flow through a bed of particles. The Armfield Apparatus has originally 38 mm internal diameter and 500 mm column length. However, a new column having approximately 40 mm internal diameter and 500 mm column height was used in this study.

Two different manifolds that are on the known levels of this new column were installed to measure headloss values using water manometer. One of the connections was located near the bottom of the bed and the other one was placed considerably over the bed almost near the top of the column (Figure 2.14). Owing to these connections, measurements were accomplished without the need for empty bed headlosses.

A bed of granular particles was placed in the column. The water can flow in either downward or upward directions on this column. Flow was fed from a water tank to the system to prevent air bubbles that may come from tap water. The rate of flow was adjusted using a pump with a frequency converter. Pressure drop across the bed was measured by a 0.5 m length water differential manometer. Permeability experiments for each fraction was performed in different bed heights to determine the effect of porosity on the sphericity coefficient.



Figure 2.14 A photo of modified "Armfield W3 Permeability/Fluidization Study Apparatus"

2.4.4.2 Bed Porosity

The bed porosity is a measure of the empty spaces in a material and is a fraction of the volume of voids over the total volume of bed. Porosity is one of the most significant parameters which is affecting the behavior of a packed bed.

Measurement of porosity is a tough issue for indiscriminately packed beds because of the packing behavior. The most commonly used methods for the determination of bed porosity are water displacement method and weighing method.

In water displacement method, first water is poured to the empty column and the total water volume poured is measured. As a second step material is packed randomly in to the column. And then the whole column is filled with water. The trapped air is escaped with shaking the column. The water is measured using a scaled container. The porosity of material is calculated using this data. The method needs several repetitions of procedure to calculate average porosity. There are practical difficulties of water displacement method such as removal of air bubbles from the materials and soaking of particles before placement to the column.

In weighing method the volume of material is determined weighing particles and using density data. The volume of the empty column is calculated using the column dimensions.

Column diameter, bed height, bed weight and density of material should be measured highly sensitively in order to determine bed porosity using weighing method. Weighing method was used in this study to state porosity of bed.

$$\varepsilon = \frac{V_{voids}}{V_{total}} = \frac{V_{total} - V_{material}}{V_{total}} = 1 - \frac{\mathrm{V_{material}}}{\mathrm{V_{total}}} \quad (2.11)$$

Bed porosity differs between 0 and 1. In this calculation, internal pores of individual grains are disregarded. Average porosity (ε_0) of a fixed bed of filter materials is calculated as follows:

$$\varepsilon_0 = 1 - \frac{M_p / \rho_p}{\frac{\pi D^2}{4} x L_0} \quad (2.12)$$

M_p = mass of particles in bed (kg), ρ_p = particle density (kg/m^3), D = column diameter (m), L_0 = bed depth (m)

2.4.4.3 Sphericity

Sphericity (ψ) is one of the most widely used parameters for defining shape of irregular particles. The sphericity coefficient is a parameter that is used to define the shape of a particle. The sphericity of a particle is calculated as the ratio of the surface volume of a sphere having equal volume with the particle and the surface volume of the particle.

$$\psi = \frac{A_p}{S_p} = \frac{\pi d_{eq}^2}{S_p} \quad (2.13)$$

Sphericity of a perfect sphere is equal to 1 and it differs between 0-1 for all shapes. Sphericities of particle fractions were obtained measuring head loss (h) during the flow through media at varying velocities (V) and were calculated using (Ergun, 1952) equation as given below:

$$\frac{h_L}{L} = 150 \frac{\mu}{\rho g} \frac{(1-\varepsilon)^2}{\varepsilon^3} \left(\frac{S_v}{6}\right)^2 V + 1.75 \frac{1}{g} \frac{(1-\varepsilon)}{\varepsilon^3} \left(\frac{S_v}{6}\right) V^2 \quad (2.14)$$

h : Headloss (m), L : Bed height (m), μ : Dynamic viscosity of fluid (kg/m/s), ρ : Density of fluid (kg/m^3), g : Gravitational acceleration (9.81 m/sec^2), ε : Porosity, S_v : Specific surface, V : Velocity (m/sec)

3 RESULTS AND DISCUSSION

3.1 Spherical Particles

For the characterization of spherical particles, first the densities of spherical materials were determined by the water displacement technique using pycnometer bottles. The average value of minimum three different density experiment results were taken into account for the determination of densities of spheres. Then, this average results were used in equivalent diameter calculations and in other evaluations. Table 3.1 displays the results of density measurements. As seen in the right column of the Table 3.1 standard deviations between experiments are much lower than 0.006 except 2 mm plastics spheres, standard deviation value for that spheres is 0.011.

Table 3.1 The results of density measurements

Materials	Density (g/cm^3)			Average	Standard deviation
	1st experiment	2nd experiment	3rd experiment		
2.5 mm Cellulose Acetate	1.292	1.292	1.298	1.294	0.003
3 mm Cellulose Acetate	1.278	1.286	1.283	1.282	0.004
3.5 mm Cellulose Acetate	1.283	1.287	1.290	1.287	0.003
4.5 mm Cellulose Acetate	1.253	1.252	1.249	1.252	0.002
5 mm Cellulose Acetate	1.283	1.287	1.287	1.285	0.002
6 mm Cellulose Acetate	1.269	1.272	1.264	1.268	0.004
4.8 mm PVC	1.364	1.359	1.351	1.358	0.006
2.4 mm Delrin	1.392	1.387	1.390	1.389	0.002
3.2 mm Delrin	1.417	1.416	1.412	1.415	0.002
4 mm Delrin	1.380	1.384	1.381	1.381	0.002
4.8 mm Delrin	1.381	1.390	1.380	1.384	0.006
2 mm Plastics	1.168	1.187	1.185	1.180	0.011
2.5 mm Plastics	1.205	1.203	1.207	1.205	0.002
2.8 mm Plastics	1.193	1.190	1.191	1.191	0.002
1 mm Glass	2.488	2.487	2.485	2.486	0.002
2 mm Glass	2.566	2.562	2.566	2.565	0.002
3 mm Glass	2.491	2.492	2.499	2.494	0.005
4 mm Glass	2.498	2.496	2.495	2.496	0.001
5 mm Glass	2.530	2.530	2.532	2.531	0.001
6 mm Glass	2.566	2.559	2.558	2.561	0.005

Following the density experiments, equivalent diameter values of the spheres were determined. Three different samples for a uniform size of spheres were counted and weighed as 200 particles. Equivalent diameters of all of the spherical materials were calculated using this procedure. Table 3.2. shows the equivalent diameters of all spheres used in this study. The standard deviations between measurements are also displayed in the most right column of Table 3.2. The values of standard deviations of equivalent diameter measurements were found quite low and it indicates the accuracy and consistency of the used method.

Table 3.2 Equivalent diameters of spherical materials

Materials	Equivalent diameters (mm)				
	1st experiment	2nd experiment	3rd experiment	Average	Standard deviation
2.5 mm Cellulose Acetate	2.435	2.433	2.432	2.433	0.002
3 mm Cellulose Acetate	3.007	3.008	3.008	3.008	0.001
3.5 mm Cellulose Acetate	3.479	3.480	3.479	3.479	0.000
4.5 mm Cellulose Acetate	4.446	4.444	4.448	4.446	0.002
5 mm Cellulose Acetate	4.925	4.926	4.925	4.925	0.001
6 mm Cellulose Acetate	5.971	5.973	5.973	5.972	0.001
4.8 mm PVC	4.789	4.789	4.789	4.789	0.000
2.4 mm Delrin	2.386	2.385	2.384	2.385	0.001
3.2 mm Delrin	3.174	3.176	3.175	3.175	0.001
4 mm Delrin	3.963	3.963	3.970	3.965	0.004
4.8 mm Delrin	4.764	4.763	4.763	4.763	0.000
2 mm Plastics	1.963	1.969	1.965	1.966	0.003
2.5 mm Plastics	2.481	2.483	2.481	2.481	0.001
2.8 mm Plastics	2.860	2.862	2.863	2.862	0.002
1 mm Glass	1.194	1.184	1.195	1.191	0.007
2 mm Glass	2.018	2.022	2.019	2.019	0.002
3 mm Glass	3.192	3.152	3.198	3.181	0.025
4 mm Glass	4.006	4.008	4.024	4.012	0.010
5 mm Glass	4.976	4.974	4.974	4.975	0.001
6 mm Glass	6.027	6.024	6.023	6.025	0.002

Diameters of spherical particles (glass, plastic, delrin, PVC and cellulose acetate spheres) are also measured using micrometer. For the all uniform sizes of spheres, minimum thirty different measurements were conducted and the average values were calculated. Table 3.3 shows the results of diameter measurements using micrometer for the all spherical materials. The results of these diameter measurements are close to the values obtained from equivalent diameter measurements.

Table 3.3 Results of diameter measurements using micrometer of spherical materials

Material	Diameter (mm)	Standard Deviation
2.5 mm Cellulose Acetate	2.444	0.014
3 mm Cellulose Acetate	3.027	0.012
3.5 mm Cellulose Acetate	3.490	0.013
4.5 mm Cellulose Acetate	4.469	0.013
5 mm Cellulose Acetate	4.960	0.018
6 mm Cellulose Acetate	6.000	0.005
4.8 mm PVC	4.813	0.009
2.4 mm Delrin	2.398	0.008
3.2 mm Delrin	3.188	0.009
4 mm Delrin	3.978	0.007
4.8 mm Delrin	4.779	0.008
1 mm Glass	1.204	0.071
2 mm Glass	2.029	0.048
3 mm Glass	3.199	0.180
4 mm Glass	3.895	0.124
5 mm Glass	4.963	0.067
6 mm Glass	6.016	0.122
2 mm Cellulose Acetate	1.950	0.049
2.5 mm Cellulose Acetate	2.454	0.035
2.8 mm Cellulose Acetate	2.786	0.094

Following the characterization experiments of spheres, fluidization experiments were performed. The results of density and equivalent diameter measurements were used to evaluate the fluidization data using different correlations. The sphericity of spherical particles were taken as 1.0 assuming them as a perfect sphere. Although the sphericities of spherical particles were assumed as 1.0, fixed bed permeability experiments were conducted to verify this assumption. The sphericity of particles were calculated as a result of these experiments using Ergun (1952) equation. The sphericity results were found considerably close to 1.0 value as expected. Figure 3.1 shows an example graph of fixed bed experiments for the determination of sphericities. After the fluidization experiments were conducted, the graphs of percent expansion and bed porosity depending on fluidization velocity were plotted. These graphs for all spherical particles are given in Appendix I. On these graphs, experimental data of each spheres was compared with the predicted data obtained from two different correlations. Figure 3.2 displays example graphs of percent bed expansion and fluidized bed porosity depending on fluidization velocity.

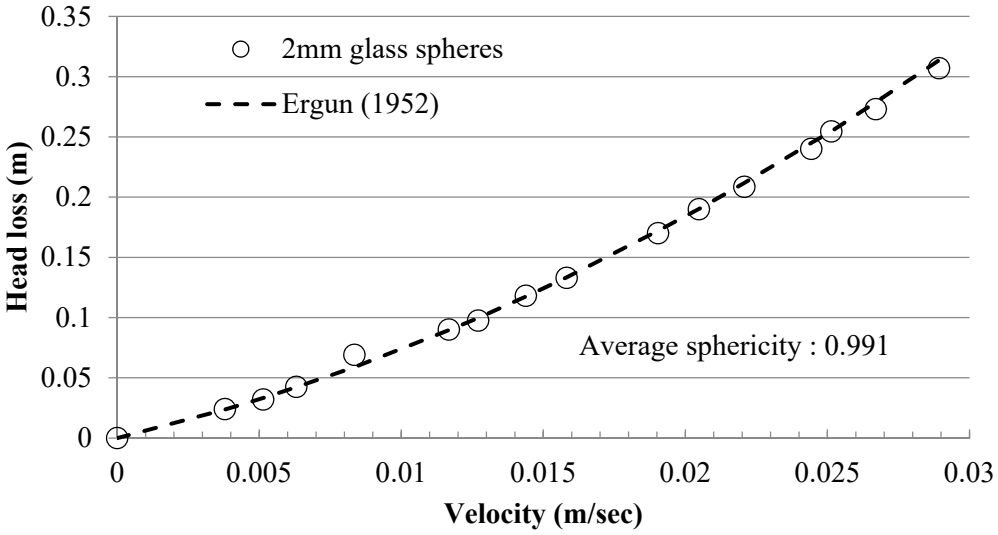
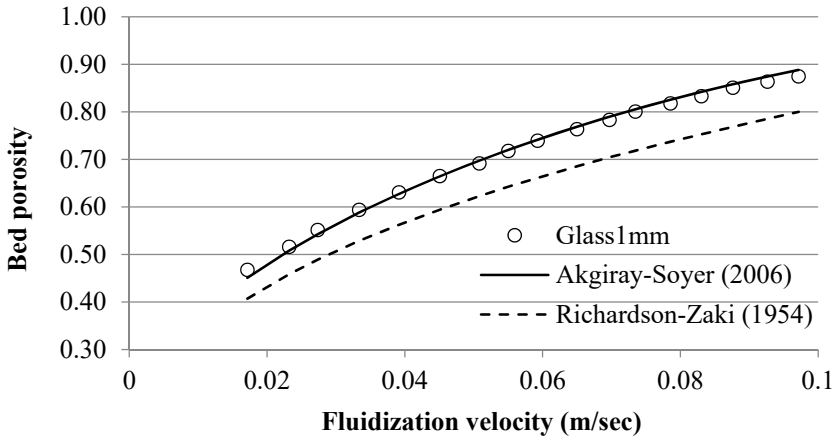


Figure 3.1 An example graph of fixed bed experiments for the determination of sphericities (2mm glass spheres)



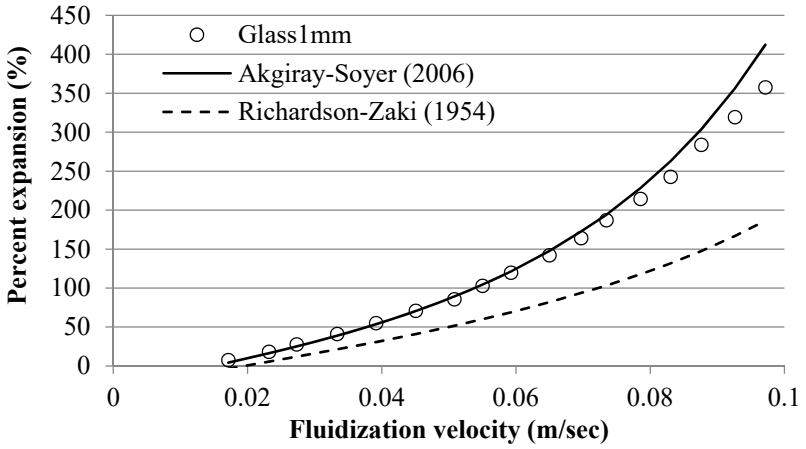


Figure 3.2 Example graphs of percent bed expansion and fluidized bed porosity depending on fluidization velocity (1mm glass spheres)

First of the correlations is the Richardson and Zaki (1954) equation. This equation shows large deviations in both percent expansion and bed porosity graphs. It represents the data more accurately only in some coarse spherical particles (such as 5mm glass and 6mm glass particles) in relatively low bed porosities. The second correlation used to evaluate the data is the Akgiray and Soyer (2006) equation. This correlation has a good consistency with data of this study. As expected, the deviations increase in high percent expansion values. Also, the predicted bed porosity values seem much more consistent than the predicted percent expansion values in graphs.

The number of data points collected from all fluidization experiments with spheres are 351 without any restrictions. In order to evaluate the whole data of spheres the equations proposed in twenty five different studies were employed to the data . Table 3.4 displays the percent errors in terms of porosity of all compared equations for all data points.

According to results, the correlation proposed by Garside and Al-Dibouni (1977) gives the most applicable results with a 1.94% error in porosity. The equations proposed by Dharmarajah and Cleasby (1986), Limas-Ballesteros (1980), Barnea and Mizrahi (1973), Khan and Richardson (1990), Ramamurthy and Subbaraju (1973) and Wen and Fan (1974) have percent error values less than 5%.

The well known equations proposed by Richardson and Zaki (1954) and Wen and Yu (1966) have error results as 6.96% and 6.93% based on porosity, respectively. One of the equations proposed by Kmiec (1982a) gives better results than the other one (Kmiec, 1982b). The equation named by the author as “simple” gives 6.39% error in porosity, since the value for the other equation is 8.24%. The equation used in the most of the Sanitary Engineering books, has a 9.41% error in porosity (Fair et al., 1968). The most unsuitable results were obtained with the equations proposed by Riba and Couderc (1977) as 19.93%, Ganguly (1980) as 23.92% and Patwardhan and Tien (1985) as 24.94% error in porosity.

The all data points were also evaluated using non-dimensional groups. The graphical illustration of this evaluation is given in Figure 3.3 as log φ versus log Re_1 graph. The definitions of these dimensional groups exist in “Introduction” chapter in detail. In Figure 3.3 the consistency of the data with Akgiray and Soyer (2006) equation was also displayed.

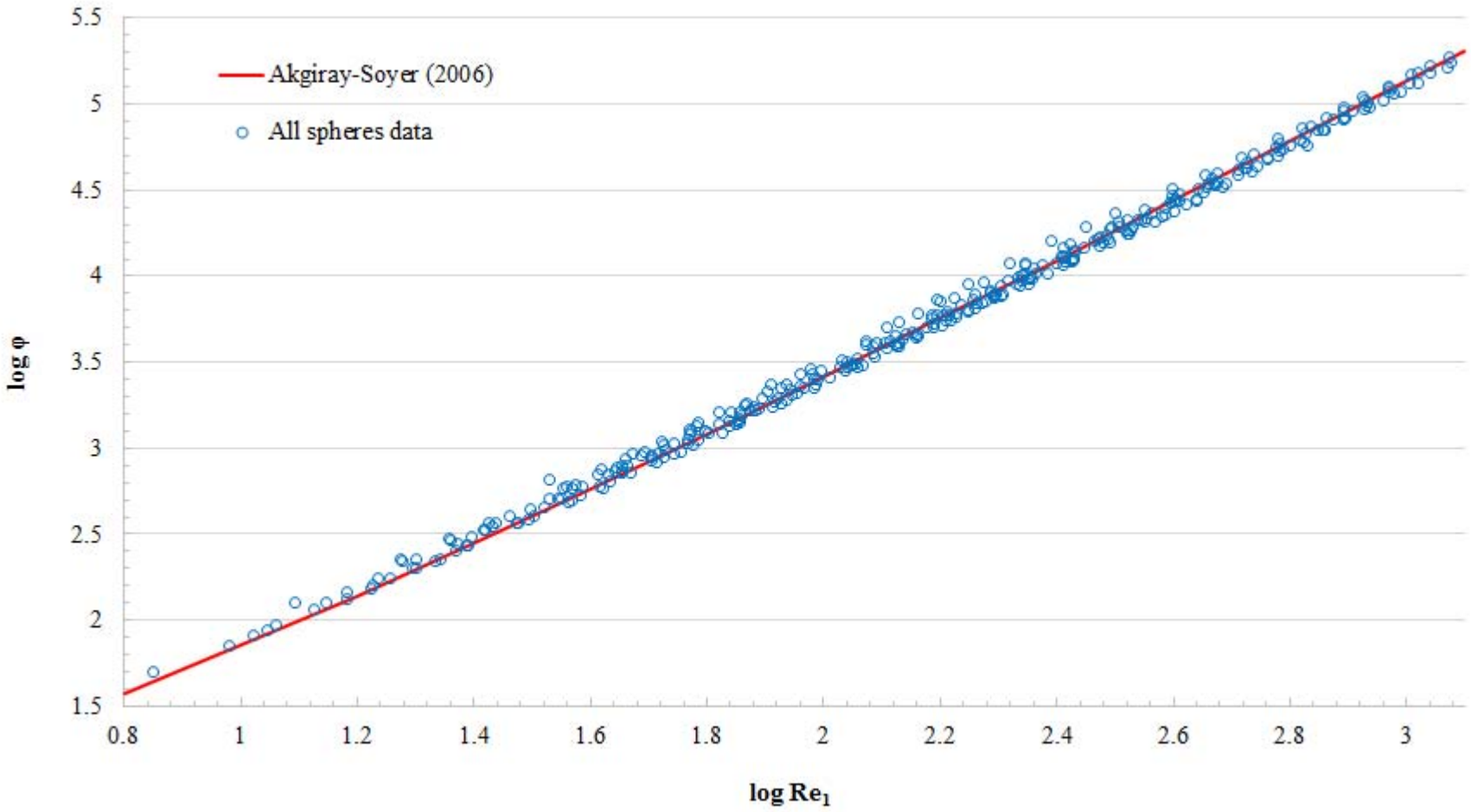


Figure 3.3 The evaluation of all fluidization data of spheres

Table 3.4 Percent errors in porosity of spheres according to different correlations

Correlations	% error in porosity
Garside and Al-Dibouni (1977)	1.94
Akgiray and Soyer (2006)	2.07
Akgiray et al. (2004)	2.15
Limas-Ballesteros (1980)	2.25
Dharmarajah and Cleasby (1986)	2.27
Wen and Fan (1974)	2.53
Barnea and Mizrahi (1973)	2.99
Khan and Richardson (1990)	3.28
Ramamurthy and Subbaraju (1973)	3.90
Lewis and Bowerman (1952)	5.95
Basu and Ghosal (1974)	5.99
Kmiec (1982) (a)	6.39
Hartman et al. (1989)	6.46
Rowe et al. (1961)	6.71
Wen and Yu (1966)	6.93
Richardson and Zaki (1954)	6.96
Lewis et al. (1949)	7.47
Kmiec (1982) (b)	8.24
Fair et al. (1968)	9.41
Gibilaro et al. (1986)	10.55
Singh and Sen Gupta (1980)	10.80
Goroshko et al. (1958)	10.95
Riba and Couderc (1977)	19.93
Ganguly (1980)	23.92
Patwardhan and Tien (1985)	24.94

*Total number of data points: 351 **All data of spherical materials analyzed.

The fluidization data were also evaluated using some restrictions in data. The data point having porosity larger than 0.9 is excluded and the data point having percent expansion lower than 10% is excluded from the data. By this restrictions, the number of data points were decreased to the value of 327. The percent errors in porosity of correlations based on the limitations are given in Table 3.5. These 327 data points are illustrated using non-dimensional groups and the graph of this evaluation is given in Figure 3.4 as log φ versus log Re_1 graph. The correlation of Garside and Al-Dibouni (1977) gives the lowest percent error value as 1.80 and this value is also lower than the value obtained by the data without limitations.

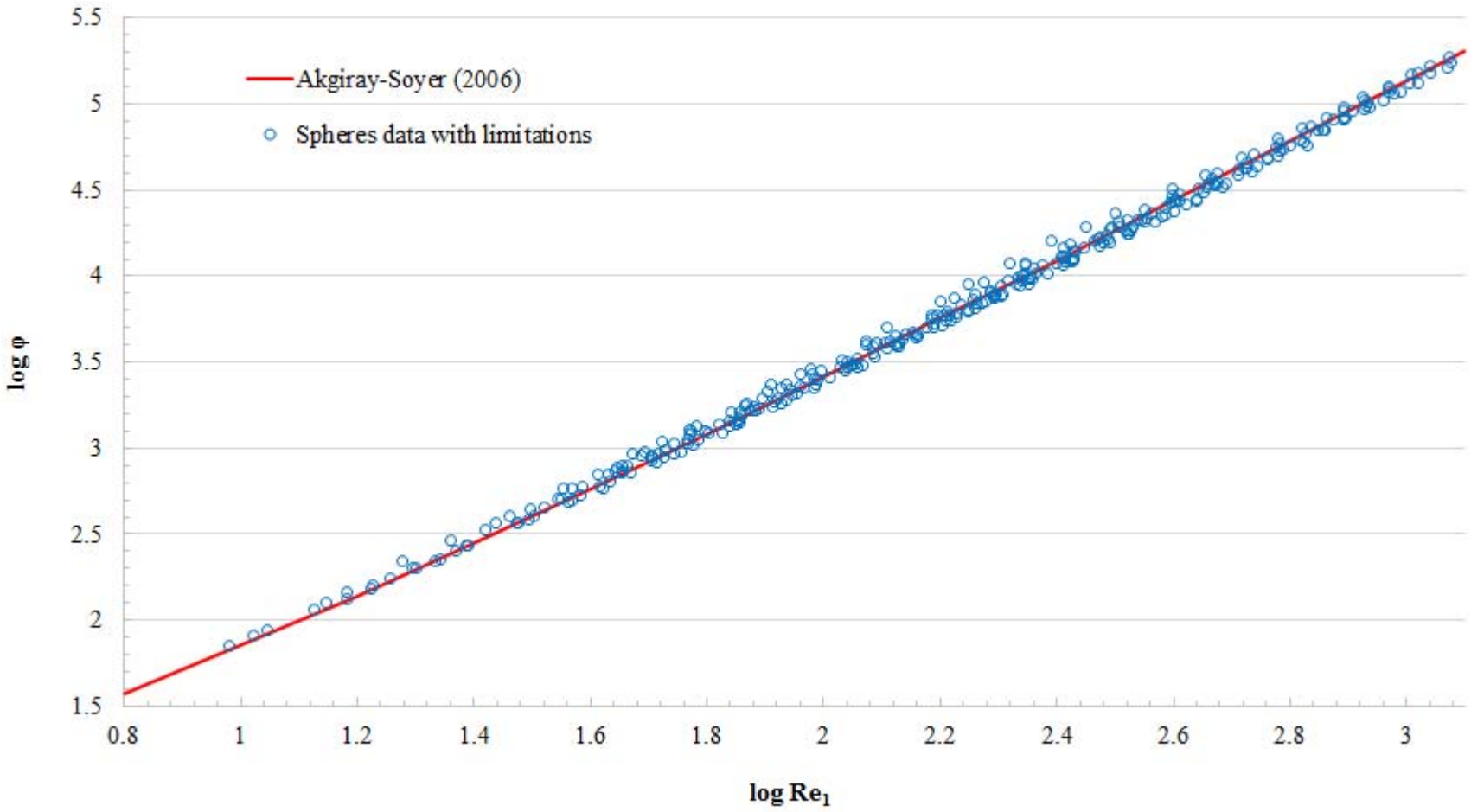


Figure 3.4 The evaluation of fluidization data of spheres with some limitations

The equations proposed by Akgiray and Soyer (2006) and Akgiray et al. (2004) have smaller percent error values by the evaluation using the limitations. The percent error values decrease from 2.07 % to 1.84 % for Akgiray and Soyer (2006) equation and from 2.15 % to 2.03 % for Akgiray et al. (2004) equation. Also the percent error value of Dharmarajah and Cleasby (1986) equation decreases from 2.27 % to 2.0 % by using limitations.

Table 3.5 Percent errors in porosity of spheres according to different correlations (with some limitations in data)

Correlations	**% error in porosity**
Garside and Al-Dibouni (1977)	1.80
Akgiray and Soyer (2006)	1.84
Dharmarajah and Cleasby (1986)	2.01
Akgiray et al., (2004)	2.03
Limas-Ballesteros (1980)	2.08
Wen and Fan (1974)	2.37
Barnea and Mizrahi (1973)	3.02
Khan and Richardson (1990)	3.20
Ramamurthy and Subbaraju (1973)	3.61
Basu and Ghosal (1974)	5.14
Lewis and Bowerman (1952)	6.04
Rowe et al. (1961)	6.69
Kmiec (1982) (a)	6.73
Hartman et al. (1989)	6.80
Richardson and Zaki (1954)	6.89
Wen and Yu (1966)	7.30
Lewis et al. (1949)	7.84
Fair et al. (1968)	7.95
Kmiec (1982) (b)	8.60
Singh and Sen Gupta (1980)	10.28
Gibilaro et al. (1986)	10.35
Goroshko et al. (1958)	11.21
Riba and Couderc (1977)	19.71
Ganguly (1980)	23.33
Patwardhan and Tien (1985)	25.77

*Total number of data points: 327 **Porosities larger than 0.9 excluded.
***Expansions less than 10 % excluded.

Implementation of the limitations to the data was resulted to an increase in percent error values for some equations. The equations proposed by Lewis and Bowerman (1952) Hartman et al. (1989), Kmiec (1982)$_{a,b}$, Lewis et al. (1949), Wen and Yu (1966), Goroshko

et al. (1958) and Patwardhan and Tien (1985) give slightly higher percent error values than the analysis results obtained by all data without any limitations. The increments in percent error values were lower than 1 %. The higher increase were achieved by the equation proposed by Patwardhan and Tien (1985) in which having an increase from 24.94 % to 25.77%. It may be caused from that the equations are more applicable especially for the lower expansion values and /or higher porosities. For this reason, exclusion of data having expansions less than 10% and/or exclusion of the data having larger porosities than 0.9 value, increase the percent error values for this equation.

The limitations were made in order to minimize the experimental errors in low and high bed expansions. Because the milimetric errors for 1-2cm bed expansions result high misleadings. On the other hand, it is difficult to see a sharp expanded bed top to determine the bed height of the highly fluidized bed. So, it also leads to misleadings during the fluidization experiments. For this reason, most of the applied equations give more suitable results using these limitations.

3.2 Binary Mixtures of Spherical Particles

The thirty three different binary mixtures of spheres were composed for the fluidization experiments. The whole list of these mixtures are given in Table 2.4 in previous chapter. The lists of these binary mixtures according to their density difference are given in Table 3.6, Table 3.7 and Table 3.8. Nine of the mixtures were formed from the materials having relatively same density and the retaining twenty four mixtures composed of the materials having different densities. The used spheres in the binary mixture experiments were characterized formerly and the results are given in previous section. Particle size ratio varies from 1.1 to 4.0, and density ratio in these binary combinations varies from 1.1 to 2.1.

The results of fluidization experiments of binary mixtures of materials having same density (type 1) are given in between Appendix II Figure 1 and Appendix II Figure 9. The fluidization results of binary mixtures of spheres produced from different material having slightly different densities (type 2) are also illustrated in between Appendix II Figure 10 and Appendix II Figure 18. The fluidization experiment results of binary mixtures of spheres produced from different material having highly different particle sizes and densities (type 3) are given in between Appendix II Figure 19 and Appendix II Figure 33 as graphical

illustrations.

Table 3.6. The binary mixtures of spheres produced from same material having relatively same density

Experiment name	Material 1	Material 2	Size ratio	Density ratio
Bin1	Delrin 2.4mm	Delrin 3.2mm	1.3	1.0
Bin2	CA 3.5mm	CA 5mm	1.4	1.0
Bin3	CA 2.5mm	CA 3mm	1.2	1.0
Bin8	Plastics 2mm	Plastics 2.5mm	1.3	1.0
Bin10	CA 2.5mm	CA 3.5mm	1.4	1.0
Bin18	CA 3mm	CA 4.5mm	1.5	1.0
Bin31	Plastics 2mm	Plastics 3mm	1.5	1.0
Bin32	Glass 3mm	Glass 5mm	1.6	1.0
Bin33	Glass 3mm	Glass 4mm	1.3	1.0

Table 3.7 The binary mixtures of spheres produced from different material having slightly different densities

Experiment name	Material 1	Material 2	Size ratio	Density ratio
Bin4	CA 3mm	Delrin 2.4mm	1.3	1.1
Bin5	CA 2.5mm	Delrin 3.2mm	1.3	1.1
Bin7	Delrin 4mm	CA 6mm	1.5	1.1
Bin11	PVC 4.8mm	CA 6mm	1.2	1.1
Bin12	Plastics 3mm	CA 2.5mm	1.2	1.1
Bin13	Delrin 2.4mm	CA 3.5mm	1.5	1.1
Bin14	Plastics 2.5mm	CA 3mm	1.2	1.1
Bin15	CA 3 mm	Plastics 3mm	1.1	1.1
Bin16	CA 2.5mm	Plastics 2mm	1.2	1.1

The total predicted bed height of binary mixtures was compared by using three different correlations: i) serial model, ii) Wen and Yu (1966) equation and iii) Leva et al. (1948) equation. Two different methods were employed to calculate total bed expansion observed during each set of experiments by using these correlations. The first method is the serial model in which the expansion of each layer was computed separately by employing Akgiray and Soyer (2006) equation and the sum of each layers expansion was reported as overall bed expansion. The calculations using second way were performed assuming the bed as a

monodispersed bed and employing Akgiray and Soyer (2006) equation by substituting the averaged values of particle properties, i.e mean particle diameter and mean particle density instead of properties of each layer. In this calculations, the mean particle density was taken as the weighted average particle density and mean particle diameter of the binary bed was obtained using two approaches proposed by Wen and Yu (1966) and Leva et al. (1948).

Table 3.8 The binary mixtures of spheres produced from different material having highly different particle sizes and densities

Experiment name	Material 1	Material 2	Size ratio	Density ratio
Bin6	Glass 1mm	CA 4.5mm	3.7	2.0
Bin9	Glass 1mm	Delrin 2.4mm	2.0	1.8
Bin17	Glass 1mm	CA 3.5mm	2.9	1.9
Bin19	Glass 1mm	CA 5mm	4.1	1.9
Bin20	Glass 1mm	Delrin 4mm	3.3	1.8
Bin21	Glass 1mm	PVC 4.8mm	4.0	1.8
Bin22	Glass 2mm	CA 5mm	2.4	2.0
Bin23	Glass 1mm	Delrin 4.8mm	4.0	1.8
Bin24	Glass 2mm	Delrin 3.2mm	1.6	1.8
Bin25	Glass 2mm	CA 4.5mm	2.2	2.0
Bin26	Glass 2mm	Delrin 4mm	2.0	1.9
Bin27	Glass 1mm	Plastics 2.5mm	2.1	2.1
Bin28	Glass 1mm	Delrin 3.2mm	2.7	1.8
Bin29	Glass 1mm	Plastics 3mm	2.4	2.1
Bin30	CA 3mm	Glass 1mm	2.5	1.9

The results are evaluated in two different configurations of graphs for all binary mixtures individually: i) the experimental bed height versus the predicted bed height graph. On these graphs, a 45 degrees line was also illustrated in order to show the accuracy between the actual bed height and predicted one. The accuracy of the approach increases when the data points become closer to this line. ii) the evaluation graphs is the L/L_0 versus percent errors in predicted bed heights. On these graphs, the percent errors of the before mentioned three approaches (serial model, Wen and Yu (1966) and Leva et al. (1948) are displayed for all binary mixtures. The positive and negative errors are given to determine the overestimations and underestimations of the different approaches. The graphical form of Bin 8 mixture results are displayed in Figure 3.5 as an example of these graphs. The predicted bed height

values of Serial model for Bin 8 experiment is almost proportional with experimental bed height values. The results of the other two approaches are better in lower bed expansion values. The deviations increase with the increase in bed expansion. According to the percent error values of Bin8 experiment, the percent errors in predicted bed height differ between 1 % and -3 % for Serial Model. The model gives smaller overestimations and underestimations than Wen and Yu (1966) and Leva et al. (1948) approaches.

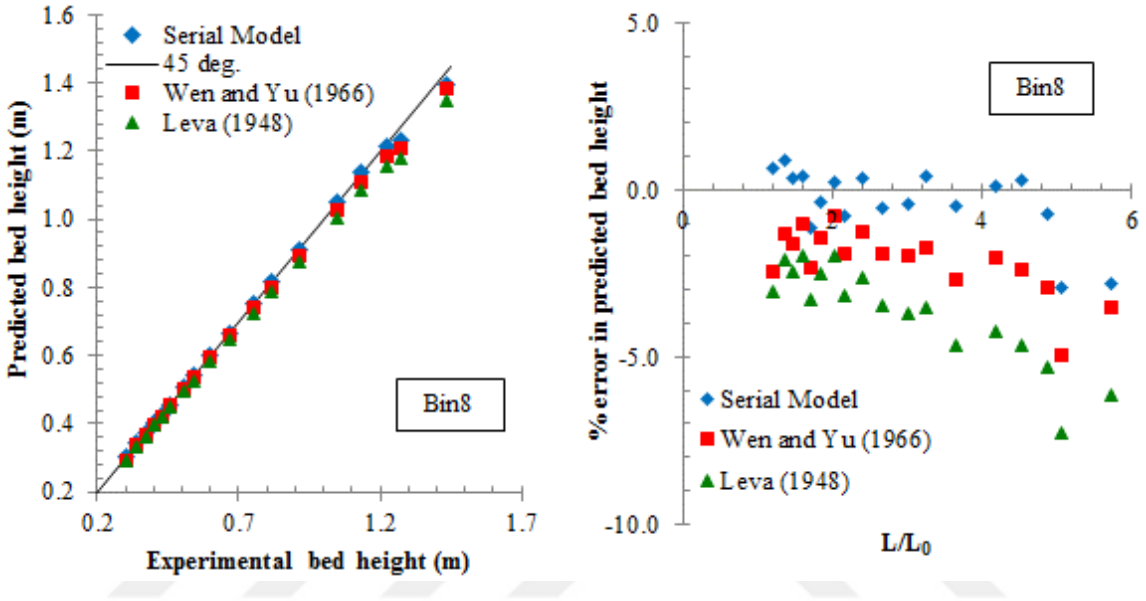


Figure 3.5 Results of fluidization experiment of Bin8 mixture of spheres

Mean percent errors in predicted bed height for the first type of binary mixtures are shown in Table 3.9. The percent errors were calculated and noted as absolute values for the determination of average values. The lowest percent error values are obtained by the mixtures of plastics (Bin 8 and Bin 31) that are also have the closest particle diameters. The mean percent errors for Bin 8 and Bin 31 are 1.38 % and 0.89 % for Serial Model. The use of Serial model gives generally the best results among the other two approaches. Also, the lower percent error results are obtained using Wen and Yu (1966) equation than Leva et al. (1948) equation. Table 3.10 displays the absolute mean percent errors in predicted bed height for the second type of binary mixtures. With an overall perspective, it is seen that the results of Serial model are better than others. However when the table and graphs examined, it also draws attention to the existence of the experiments coming out of the general trend. However when the table and graphs examined, it also draws attention to the existence of the experiments coming out of the general trend. The results of these experiments should be

evaluated by taking into account the characteristics (size, density, etc.) of two materials.

Table 3.9. Absolute mean percent errors in predicted fluidized bed height for the type 1 binary mixtures of spheres

Experiment name	Material 1	Material 2	Absolute mean percent errors in predicted bed height		
			Serial Model	Wen and Yu (1966)	Leva et al. (1948)
Bin1	Delrin 2.4mm	Delrin 3.2mm	3.33	2.21	2.45
Bin2	CA 3.5mm	CA 5mm	3.26	4.09	6.42
Bin3	CA 2.5mm	CA 3mm	2.36	2.41	3.60
Bin8	Plastics 2mm	Plastics 2.5mm	1.38	2.13	3.67
Bin10	CA 2.5mm	CA 3.5mm	2.53	3.47	6.26
Bin18	CA 3mm	CA 4.5mm	3.20	3.31	6.22
Bin31	Plastics 2mm	Plastics 3mm	0.89	3.35	7.09
Bin32	Glass 3mm	Glass 5mm	5.46	3.04	3.86
Bin33	Glass 3mm	Glass 4mm	6.15	5.51	5.04
		Average	3.14	3.29	4.98

Table 3.10 Absolute mean percent errors in predicted fluidized bed height for the type 2 binary mixtures of spheres

Experiment name	Material 1	Material 2	Absolute mean percent errors in predicted bed height		
			Serial Model	Wen and Yu (1966)	Leva et al. (1948)
Bin4	CA 3mm	Delrin 2.4mm	3.16	3.15	3.23
Bin5	CA 2.5mm	Delrin 3.2mm	2.94	8.58	9.87
Bin7	Delrin 4mm	CA 6mm	4.12	3.92	5.30
Bin11	PVC 4.8mm	CA 6mm	6.61	6.45	7.56
Bin12	Plastics 3mm	CA 2.5mm	3.07	2.63	2.83
Bin13	Delrin 2.4mm	CA 3.5mm	3.81	4.36	2.73
Bin14	Plastics 2.5mm	CA 3mm	7.74	2.76	3.59
Bin15	CA 3 mm	Plastics 3mm	3.43	4.74	4.80
Bin16	CA 2.5mm	Plastics 2mm	2.44	14.62	15.75
		Average	4.30	5.25	5.71

For example, for Bin 4 experiment, all three models give an average error value which are also very close together, but the results of experiments are very different for Bin5 experiment. For the Bin16 experiment which the best results obtained by Serial model, the highest percent error values are given by the Wen and Yu (1966) and Leva et al. (1948)

approaches. When the graphs in Appendix II are analyzed, generally underestimated predicted bed height values are obtained by Leva et al. (1948) approach for type 2 binary mixture experiments. This trend is almost same with the results of Wen and Yu (1966) approach for these experiments.

Absolute mean percent error values in predicted fluidized bed height for the binary mixtures of spheres produced from different material having highly different particle sizes and densities are summarized in Table 3.11.

Table 3.11 Absolute mean percent errors in predicted fluidized bed height for the type 3 binary mixtures of spheres

Experiment name	Material 1	Material 2	Absolute mean percent errors in predicted bed height		
			Serial Model	Wen and Yu (1966)	Leva et al. (1948)
Bin6	Glass 1mm	CA 4.5mm	3.51	5.91	19.90
Bin9	Glass 1mm	Delrin 2.4mm	2.71	1.13	8.95
Bin17	Glass 1mm	CA 3.5mm	2.09	2.94	16.75
Bin19	Glass 1mm	CA 5mm	2.07	14.63	18.83
Bin20	Glass 1mm	Delrin 4mm	3.65	19.93	14.35
Bin21	Glass 1mm	PVC 4.8mm	2.74	20.24	18.16
Bin22	Glass 2mm	CA 5mm	4.14	7.61	16.96
Bin23	Glass 1mm	Delrin 4.8mm	4.66	26.59	14.83
Bin24	Glass 2mm	Delrin 3.2mm	2.97	9.93	13.01
Bin25	Glass 2mm	CA 4.5mm	2.58	14.52	21.91
Bin26	Glass 2mm	Delrin 4mm	4.79	3.95	11.35
Bin27	Glass 1mm	Plastics 2.5mm	10.34	20.62	28.21
Bin28	Glass 1mm	Delrin 3.2mm	5.22	14.85	8.11
Bin29	Glass 1mm	Plastics 3mm	4.95	16.02	26.18
Bin30	Glass1mm	CA 3mm	1.51	3.09	17.49
		Average	4.05	12.53	16.98

To evaluate this type of mixtures, it can be said that the Serial model gives better percent error values than the other two approaches. With an overall perspective, the average percent error value in predicted bed height of these fifteen mixtures is found as 4.05 % for Serial model, 12.53 % for Wen and Yu (1966) approach and 16.98 % for Leva et al. (1948) approach.

As it can be seen from the figures in Appendix II, the Leva et al. (1948) approach is resulted generally underestimations for this type of mixtures. However, Wen and Yu (1966) equation is lead to overestimations and underestimations without following any trend.

The percent error values of this type of mixtures are higher than the first two types of mixtures are higher than the first two types of experiments for all models. It could be the result of that the high density differences between particles lead to harder prediction of total bed expansion value. However, the Serial model gives consistent prediction error values for all types of mixtures. These are recorded as 3.14 %, 4.30 %, and 4.05 % for three types of mixtures, respectively. For all of the thirty three binary mixtures, mean percent error in predicted fluidized bed height was found as 3.8 % that is significantly smaller than those obtained from Wen and Yu (1966) and Leva et al. (1948) correlations as 8.02 % and 10.63 %, respectively.

Escudié et al. (2006) was recently evaluated the Serial Model. They recorded that the Serial Model is very well for the prediction of overall bed porosity of binary and ternary species varying only in particle size or in shape. They proposed a further work containing experiments with species differing only in particle density. In the current work, the binary mixtures of particle fractions having same density and shape was studied but the particles have different particle sizes. The obtained results of experiments for this type of binary mixtures have the lowest percent errors.

3.3 Non-spherical Particles

3.3.1 Non-spherical Non-porous Particles

Experiments have been carried out with sieved fractions of sand, garnet, perlite and crushed glass as non-spherical non-porous materials. Five different firactions were obtained from each material type. Then, density and equivalent diameter measurements were performed. Table 3.12 displays the results of density measurements and the standard deviation values between repeated measurements. Also, Table 3.13 shows the results of equivalent diameter measurements.

In order to evaluate the fluidization data of non-spherical materials, the sphericity characterizing the shape of materials used, should be determined first. For this reason,

permeability experiments were performed. During these experiments, fixed bed headlosses were measured for different fluid velocities. Ergun (1952) equation was then used for the determination of sphericities (Figure 3.6). Permeability experiments for each fraction were performed in five different bed heights to determine the effect of porosity on the sphericity. Table 3.14, Table 3.15, Table 3.16 and Table 3.17 display the average sphericities found for sand, garnet, crushed glass and perlite, respectively. The first porosity value ε_1, represents the porosity of the tightly compacted state of the filter bed and the ε_5 represents the loose bed porosity of the filter bed. When applying the models to the data, the sphericity value is taken as the state of ε_4. It means that not a so loose bed and not a so compacted bed porosity value is used for the evaluation.

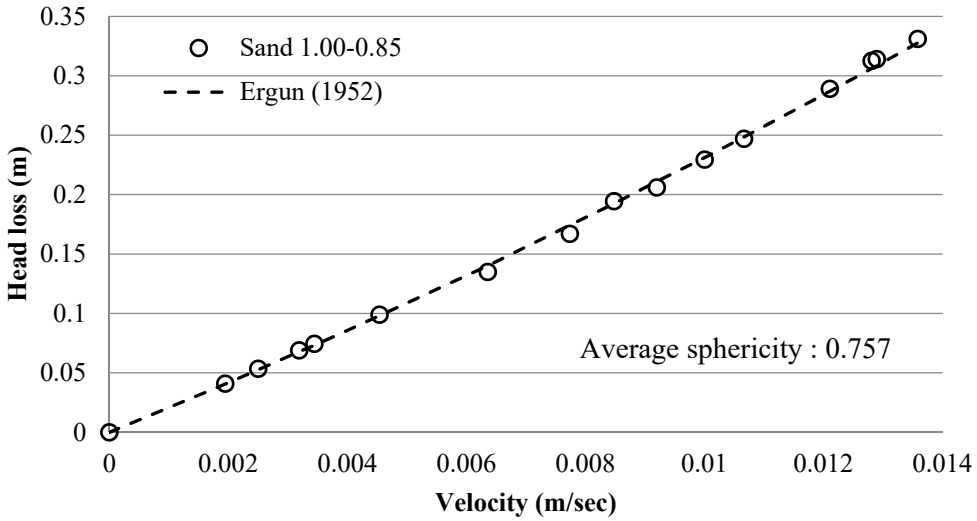


Figure 3.6. An example graph of fixed bed experiments for the determination of sphericities (Sand 1.00-0.85)

Porosity values of sand fractions differ between 0.37 and 0.46 values (Table 3.14). Also the sphericities of sand fractions vary between 0.72 and 0.78 values. The sphericities of relatively coarse fractions of sand are higher than the fines. As it can be seen from the Table 3.15 the porosity values of garnet fractions vary between 0.44 and 0.50 values while the sphericities are in the range of 0.68-0.75. The sphericity values of garnet 0.85mm-0.71mm fraction are shown as relatively higher than the other fractions. Also, the density value of the fraction is different than the other garnet fractions (Table 3.12).

Table 3.12 The results of density measurements of non-spherical non-porous particles

Materials	Sieve size (mm-mm)	Density (g/cm^3)			Average	Standard deviation
		1st experiment	2nd experiment	3rd experiment		
Sand	1.40-1.18	2.636	2.634	2.645	2.638	0.006
Sand	1.18-1.00	2.633	2.629	2.630	2.631	0.002
Sand	1.00-0.85	2.622	2.619	2.615	2.619	0.003
Sand	0.85-0.71	2.619	2.619	2.629	2.623	0.006
Sand	0.71-0.60	2.635	2.629	2.623	2.629	0.006
Garnet	1.40-1.18	3.969	3.981	3.979	3.976	0.006
Garnet	1.18-1.00	3.981	3.973	4.007	3.987	0.018
Garnet	1.00-0.85	4.011	3.999	3.996	4.002	0.008
Garnet	0.85-0.71	3.900	3.945	3.929	3.924	0.023
Garnet	0.71-0.60	3.970	4.004	3.997	3.990	0.018
Crushed glass	1.40-1.18	2.508	2.510	--	2.509	0.002
Crushed glass	1.18-1.00	2.503	2.497	2.505	2.501	0.004
Crushed glass	1.00-0.85	2.514	2.508	2.488	2.503	0.014
Crushed glass	0.85-0.71	2.503	2.484	2.406	2.464	0.052
Crushed glass	0.71-0.60	2.531	2.507	2.472	2.504	0.029
Perlite	2.36-2.00	2.345	2.348	2.354	2.349	0.004
Perlite	2.00-1.70	2.366	2.362	2.361	2.363	0.003
Perlite	1.70-1.40	2.356	2.353	2.366	2.358	0.007
Perlite	1.40-1.18	2.362	2.328	2.361	2.350	0.020
Perlite	1.18-1.00	2.365	2.366	2.398	2.376	0.019

The sphericity values of crushed glass fractions were obtained in the range of 0.49 and 0.55 and the porosities were recorded as between 0.51 and 0.63 (Table 3.16). The range of the difference in sphericity is very small for crushed glass fractions. Porosity values of perlite fractions differ between 0.40 and 0.51 values, and also the sphericities of perlite fractions vary between 0.60 and 0.73 values (Table 3.17). The sphericity values of coarse fractions of perlite are lower than the finer fractions.

Fluidized bed porosity graphs of non-spherical particles are displayed in Appendix III. Figure 3.7 displays an example graph Appendix III as the porosity versus fluidization velocity graph of sand 0.85-0.71 fraction. Porosity versus fluidization velocity graphs were plotted for each fraction. In order to evaluate the data, the predicted porosities obtained from Dharmarajah and Cleasby (1986) equation and Soyer and Akgiray (2009) equation are also displayed on these graphs.

The Dharmarajah and Cleasby (1986) equation was used for the evaluation since it is stated in literature as "state of the art" for the prediction of fluidized bed expansion (AWWA, 1999; Droste, 1997) and also it is the most widely used fluidized bed expansion prediction model for non-spherical materials. The trend of Dharmarajah and Cleasby (1986) approach gives highly different results. This approach generally results with overestimations. In a general point of view, using the Soyer and Akgiray (2009) equation were found to represent data very accurately for the prediction of fluidized bed porosities of non-spherical particles used in the study. When twenty separate measurements of the non-spherical non-porous particle fluidization data are considered together, the mean errors in predicted porosities were found to be 3.3% for Dharmarajah and Cleasby (1986) correlation and 1.8% for Soyer and Akgiray (2009) equation.

Table 3.13 The results of equivalent diameter measurements of non-spherical non-porous particles

Materials	Equivalent diameter			Average	Standard deviation
	1st experiment	2nd experiment	3rd experiment		
Sand (1.40-1.18)	1.395	1.384	1.397	1.392	0.007
Sand (1.18-1.00)	1.210	1.215	1.201	1.209	0.007
Sand (1.00-0.85)	0.974	0.974	0.978	0.975	0.002
Sand (0.85-0.71)	0.865	0.858	0.861	0.862	0.004
Sand (0.71-0.60)	0.817	0.796	0.809	0.807	0.011
Garnet (1.40-1.18)	1.347	1.325	1.357	1.343	0.016
Garnet (1.18-1.00)	1.179	1.167	1.155	1.167	0.012
Garnet (1.00-0.85)	0.981	0.986	0.965	0.977	0.011
Garnet (0.85-0.71)	0.757	0.750	0.753	0.753	0.003
Garnet (0.71-0.60)	0.684	0.699	0.690	0.691	0.007
Crushed glass (1.40-1.18)	1.208	1.188	1.198	1.198	0.010
Crushed glass (1.18-1.00)	1.032	1.073	1.062	1.056	0.021
Crushed glass (1.00-0.85)	0.893	0.912	0.905	0.903	0.010
Crushed glass (0.85-0.71)	0.761	0.766	0.761	0.763	0.003
Crushed glass (0.71-0.60)	0.621	0.614	0.611	0.615	0.005
Perlite (2.36-2.00)	2.245	2.230	2.214	2.230	0.016
Perlite (2.00-1.70)	1.966	1.951	1.958	1.958	0.007
Perlite (1.70-1.40)	1.609	1.749	1.568	1.646	0.095
Perlite (1.40-1.18)	1.366	1.357	1.368	1.364	0.006
Perlite (1.18-1.00)	1.173	1.176	1.163	1.171	0.007

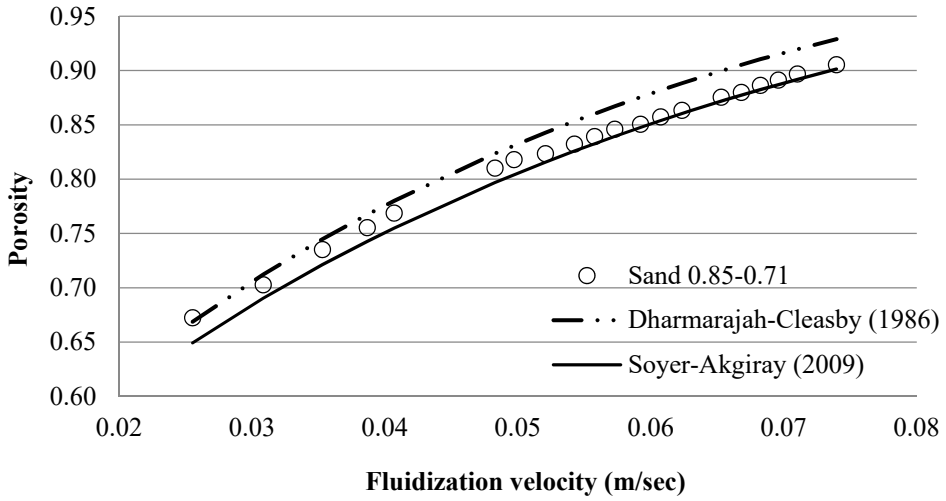


Figure 3.7. The porosity versus fluidization velocity graph of sand 0.85-0.71 fraction as an example graph of Appendix III

Table 3.14 Sphericity values of sand fractions at different bed porosities

Fractions of materials		ε_1	ε_2	ε_3	ε_4	ε_5
Sand 1.40mm-1.18mm	ε	0.368	0.383	0.398	0.414	0.429
	Ψ	0.782	0.780	0.784	0.781	0.788
Sand 1.18mm-1.00mm	ε	0.368	0.385	0.403	0.418	0.436
	Ψ	0.782	0.772	0.773	0.778	0.751
Sand 1.00mm-0.85mm	ε	0.392	0.407	0.424	0.439	0.455
	Ψ	0.750	0.758	0.758	0.757	0.762
Sand 0.85mm-0.71mm	ε	0.400	0.415	0.429	0.448	0.463
	Ψ	0.717	0.713	0.727	0.720	0.732
Sand 0.71mm-0.60mm	ε	0.388	0.406	0.425	0.440	0.456
	Ψ	0.748	0.733	0.741	0.742	0.758

Table 3.15 Sphericity values of garnet fractions at different bed porosities

Fractions of materials		ε_1	ε_2	ε_3	ε_4	ε_5
Garnet 1.40mm-1.18mm	ε	0.442	0.452	0.467	0.476	0.491
	Ψ	0.681	0.685	0.681	0.686	0.691
Garnet 1.18mm-1.00mm	ε	0.440	0.455	0.472	0.482	0.497
	Ψ	0.680	0.680	0.682	0.679	0.686
Garnet 1.00mm-0.85mm	ε	0.440	0.452	0.469	0.483	0.497
	Ψ	0.689	0.679	0.688	0.685	0.693
Garnet 0.85mm-0.71mm	ε	0.439	0.454	0.469	0.483	0.494
	Ψ	0.741	0.742	0.748	0.741	0.756
Garnet 0.71mm-0.60mm	ε	0.445	0.459	0.474	0.489	0.503
	Ψ	0.689	0.674	0.684	0.692	0.698

Table 3.16 Sphericity values of crushed glass fractions at different bed porosities

Fractions of materials		ε_1	ε_2	ε_3	ε_4	ε_5
Crushed glass 1.40mm-1.18mm	ε	0.515	0.536	0.559	0.574	0.599
	Ψ	0.500	0.503	0.519	0.514	0.540
Crushed glass 1.18mm-1.00mm	ε	0.520	0.541	0.565	0.584	0.600
	Ψ	0.493	0.494	0.503	0.498	0.531
Crushed glass 1.00mm-0.85mm	ε	0.520	0.542	0.567	0.587	0.608
	Ψ	0.506	0.512	0.521	0.527	0.534
Crushed glass 0.85mm-0.71mm	ε	0.524	0.545	0.570	0.586	0.607
	Ψ	0.510	0.521	0.530	0.547	0.554
Crushed glass 0.71mm-0.60mm	ε	0.547	0.594	0.610	0.567	0.630
	Ψ	0.495	0.507	0.528	0.491	0.533

Table 3.17 Sphericity values of perlite fractions at different bed porosities

Fractions of materials		ε_1	ε_2	ε_3	ε_4	ε_5
Perlite 2.36mm-2.00mm	ε	0.454	0.467	0.480	0.492	0.508
	Ψ	0.600	0.604	0.612	0.615	0.624
Perlite 2.00mm-1.70mm	ε	0.440	0.453	0.466	0.482	0.494
	Ψ	0.643	0.647	0.643	0.653	0.661
Perlite 1.70mm-1.40mm	ε	0.432	0.444	0.455	0.470	0.487
	Ψ	0.667	0.663	0.668	0.665	0.678
Perlite 1.40mm-1.18mm	ε	0.403	0.414	0.434	0.450	0.468
	Ψ	0.731	0.729	0.721	0.723	0.716
Perlite 1.18mm-1.00mm	ε	0.416	0.430	0.445	0.457	0.473
	Ψ	0.714	0.713	0.720	0.720	0.725

For the fluidization experiments of non-spherical material fractions, the mean percent error values in predicted porosity and in predicted bed expansion were displayed in Table 3.18. These mean percent error values are determined using Soyer and Akgiray (2009) equation.

According to Table 3.18, the fluidization experiments of sand fractions were performed in the modified Reynolds number range of 15.6-122.9. The average percent error in predicted bed porosity and the average percent error in predicted fluidized bed expansion of sand fractions were found as 1.1 % and 7.7 %, respectively. Moreover, the modified Reynolds number range of fluidization experiments of garnet fractions is between 13.6 and 1433.4. For garnet fractions, the percent error values in predicted bed porosity and predicted bed expansion are as 2.0 % and 15.1 %, respectively. The modified Reynolds number range and number of data points of crushed glass fractions are lower than the other material fractions. The average predicted bed porosity value of crushed glass fractions is almost as low as sand fractions'. It was recorded as 1.4 % and the average percent error value in predicted bed

expansion is found as 14.9 %. The highest percent error values in both predicted bed expansion and predicted bed porosity were obtained from the perlite fractions. These are noted as 17.7 % and 2.7 %, respectively.

Fluidization data of all the non-spherical non-porous materials used in this study were also evaluated using non-dimensional groups. Figure 3.8, Figure 3.9, Figure 3.10 and Figure 3.11 were plotted to display the graphical illustrations of this evaluation as log φ versus log Re_l graphs for sand, garnet, crushed glass and perlite fractions, respectively. In addition to data points displayed on the graphs, the curves formed by using Soyer and Akgiray (2009) equation were added to each graph for the highest and the lowest sphericities of materials evaluated in the graphs. Also, the curves of spheres were plotted on each graph.

Table 3.18 Mean percent error values of non-spherical material fractions

Materials	Sieve size (mm-mm)	% error in porosity	% error in expansion	Re range	Number of points
Sand	1.40-1.18	1.3	8.8	36.8-122.9	20
Sand	1.18-1.00	1.3	8.0	27.6-94.4	20
Sand	1.00-0.85	0.9	5.3	23.7-58.5	20
Sand	0.85-0.71	1.0	7.0	15.6-45.5	20
Sand	0.71-0.60	1.2	9.3	19.6-40.3	16
	Average	*1.1*	*7.7*	*Total*	*96*
Garnet	1.40-1.18	2.7	18.5	35.4-143.4	16
Garnet	1.18-1.00	2.7	21.5	24.3-105.4	17
Garnet	1.00-0.85	2.6	18.9	20.8-79.3	17
Garnet	0.85-0.71	0.9	7.4	17.9-52.4	19
Garnet	0.71-0.60	1.3	9.3	13.6-42.5	17
	Average	*2.0*	*15.1*	*Total*	*86*
Crushed glass	1.40-1.18	1.3	16.2	15.7-56.5	16
Crushed glass	1.18-1.00	1.1	11.7	15.1-39.9	15
Crushed glass	1.00-0.85	1	10.6	12.0-30.0	18
Crushed glass	0.85-0.71	1.7	15.5	12.7-22.5	16
Crushed glass	0.71-0.60	2.1	20.6	10.5-15.2	16
	Average	*1.4*	*14.9*	*Total*	*81*
Perlite	2.36-2.00	4.2	29.1	61.6-176.8	16
Perlite	2.00-1.70	3.5	23.4	42.6-149.0	16
Perlite	1.70-1.40	2.4	16.2	31.8-112.8	18
Perlite	1.40-1.18	1.9	11.5	32.3-92.1	21
Perlite	1.18-1.00	1.4	8.4	27.7-75.7	20
	Average	*2.7*	*17.7*	*Total*	*91*

As it can be seen from Figure 3.8, the data points of sand fractions ($0.8 < \log Re_1 < 2.2$) displays a good consistency with curves. There are no significant deviations from the trend. According to Figure 3.9, the fluidization data of garnet fractions ($0.8 < \log Re_1 < 2.4$) shows some small deviations from the general trend. As it can be seen from the Table 3.15, a fraction of garnet material have higher sphericity value than others. It could be the reason of the situation. Figure 3.10 displays the fluidization data of crushed glass fractions based on dimensionless groups. As noted before, the mean percent error values in predicted bed porosity values of crushed glass fractions are very low (1.4 %). Therefore, any significant deviations from the general trend exists. The fluidization data of perlite fractions based on dimensionless groups is shown in Figure 3.11. The perlite fractions consist of coarse fractions (in the range of 2.36 mm- 1.40 mm sieve sizes) and relatively fine fractions (in the range of 1.40 mm- 1.00 mm sieve sizes). As it can be seen from the Table 3.17, the sphericities of the fine and coarse fractions also differ and so the trend of the data have some clear deviations. The data points were not located between the highest and the lowest sphericity curves, as expected.

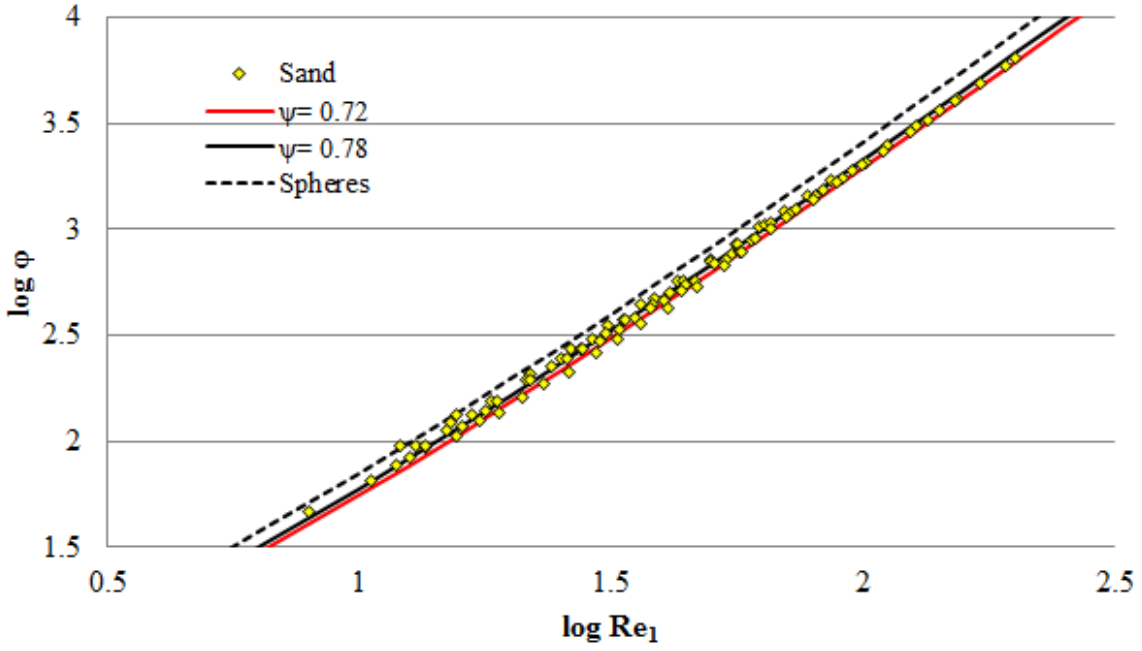


Figure 3.8 The fluidization data of sand fractions based on dimensionless groups

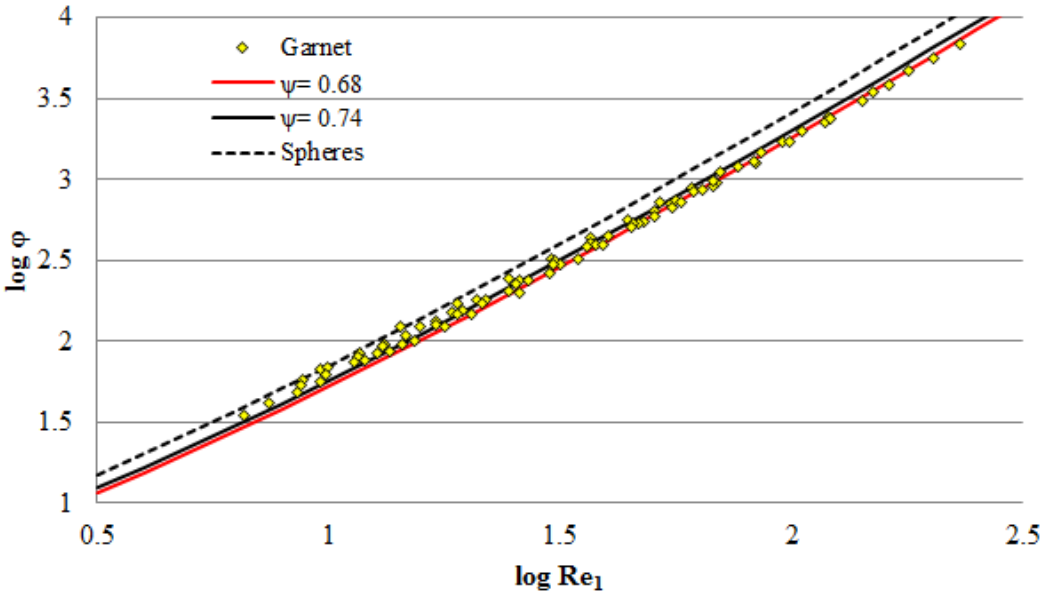


Figure 3.9 The fluidization data of garnet fractions based on dimensionless groups

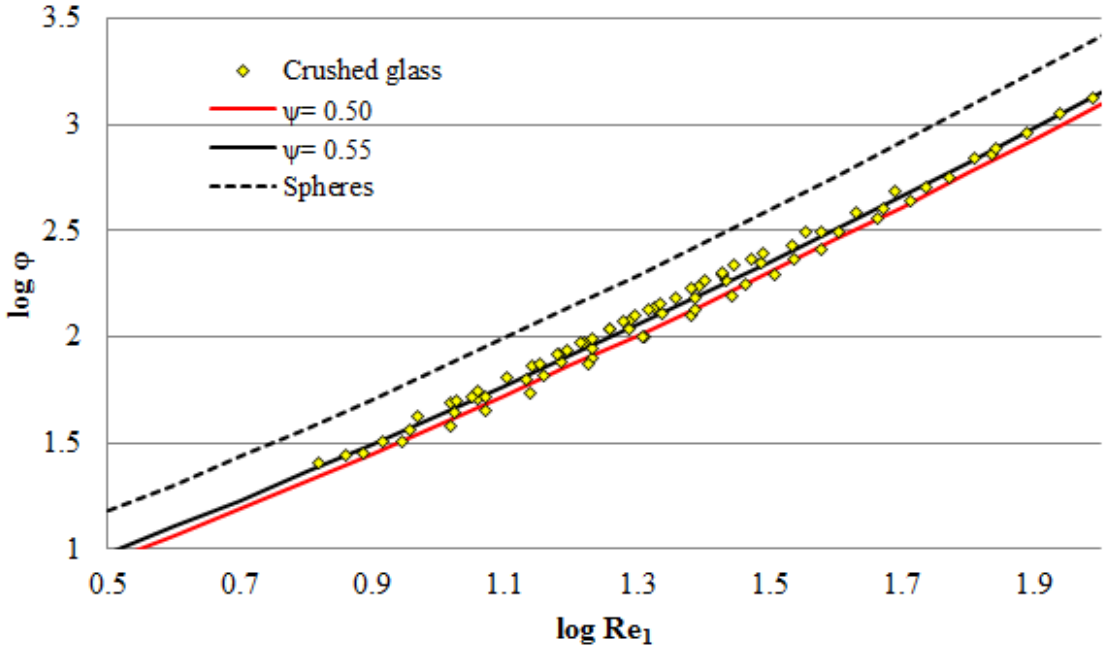


Figure 3.10 The fluidization data of crushed glass fractions based on dimensionless groups

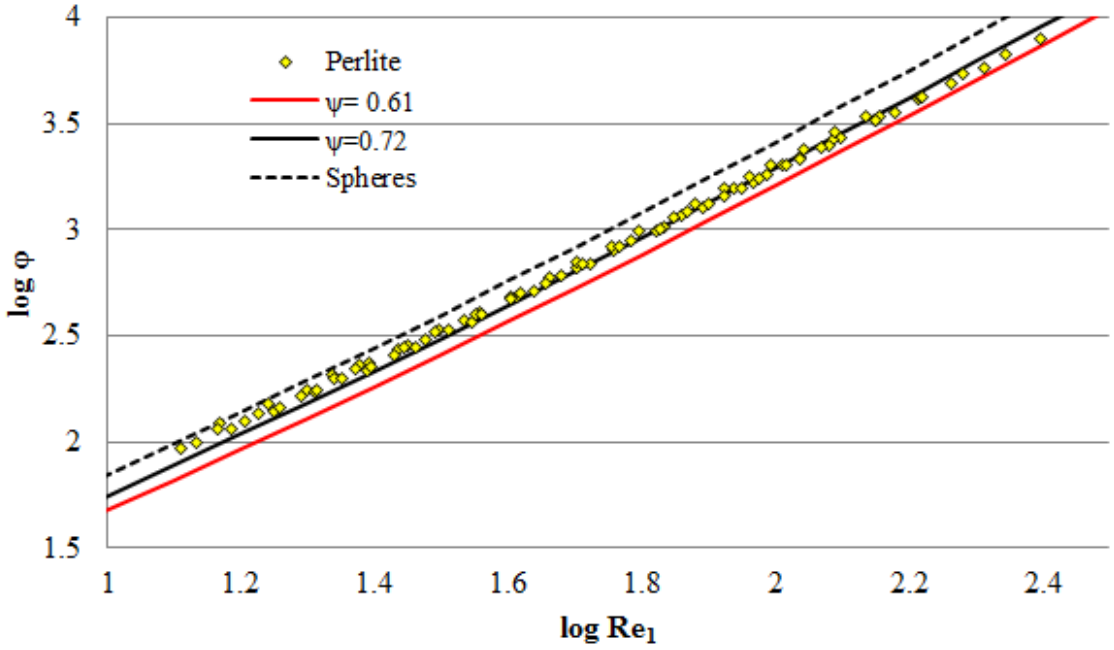


Figure 3.11 The fluidization data of perlite fractions based on dimensionless groups

3.3.2 Non-spherical Porous Particles

The experimental results of non-spherical porous particles for particle density, percent water absorption, equivalent diameter, sphericity, and fixed-bed porosity are displayed in Figure 3.12, Figure 3.13, Figure 3.14, Figure 3.15 and Figure 3.16.

The Figure 3.12 shows the effective density values according to the three different methods used to prepare water-saturated particles plus the skeletal density of each fraction. As expected, the skeletal density is always higher than the effective density. It is also seen that the skeletal density tends to increase as particle size decreases. This is also reasonable, since some of the closed pores are converted to open pores and the ratio of the solid part of the skeletal volume increases as particle size decreases.

Percent water absorption (A) was calculated as the percent increase in the mass of a sample after soaking in water for 24 h, expressed as percentage of the dry mass:

$$A = 100\frac{(M_{WET} - M_{OD})}{M_{OD}} \tag{3.1}$$

where M_{OD} and M_{WET} are the mass of particles in oven-dry and wet (soaked in water) condition, respectively.

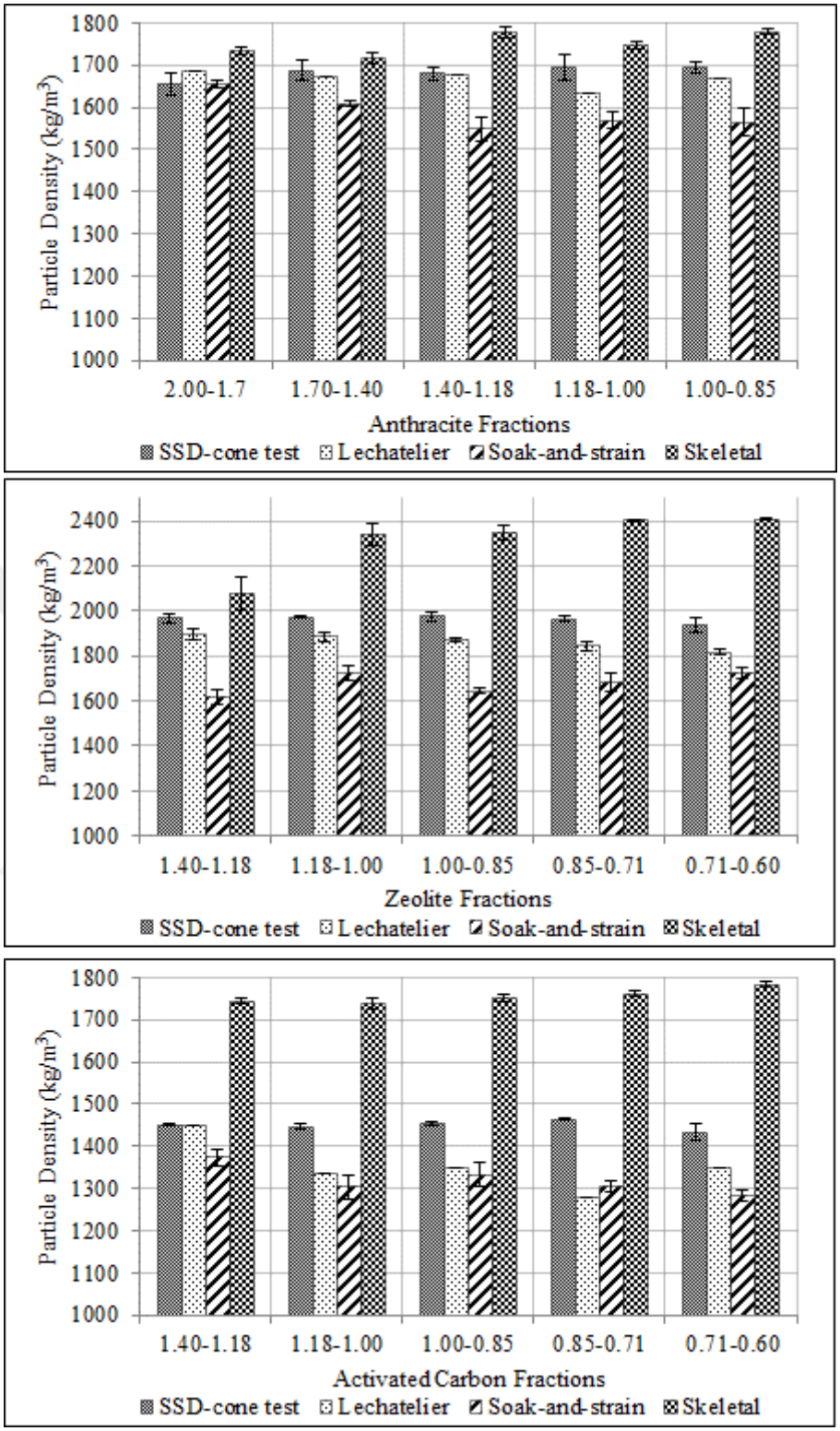


Figure 3.12 Particle density of zeolite, activated carbon, and anthracite fractions

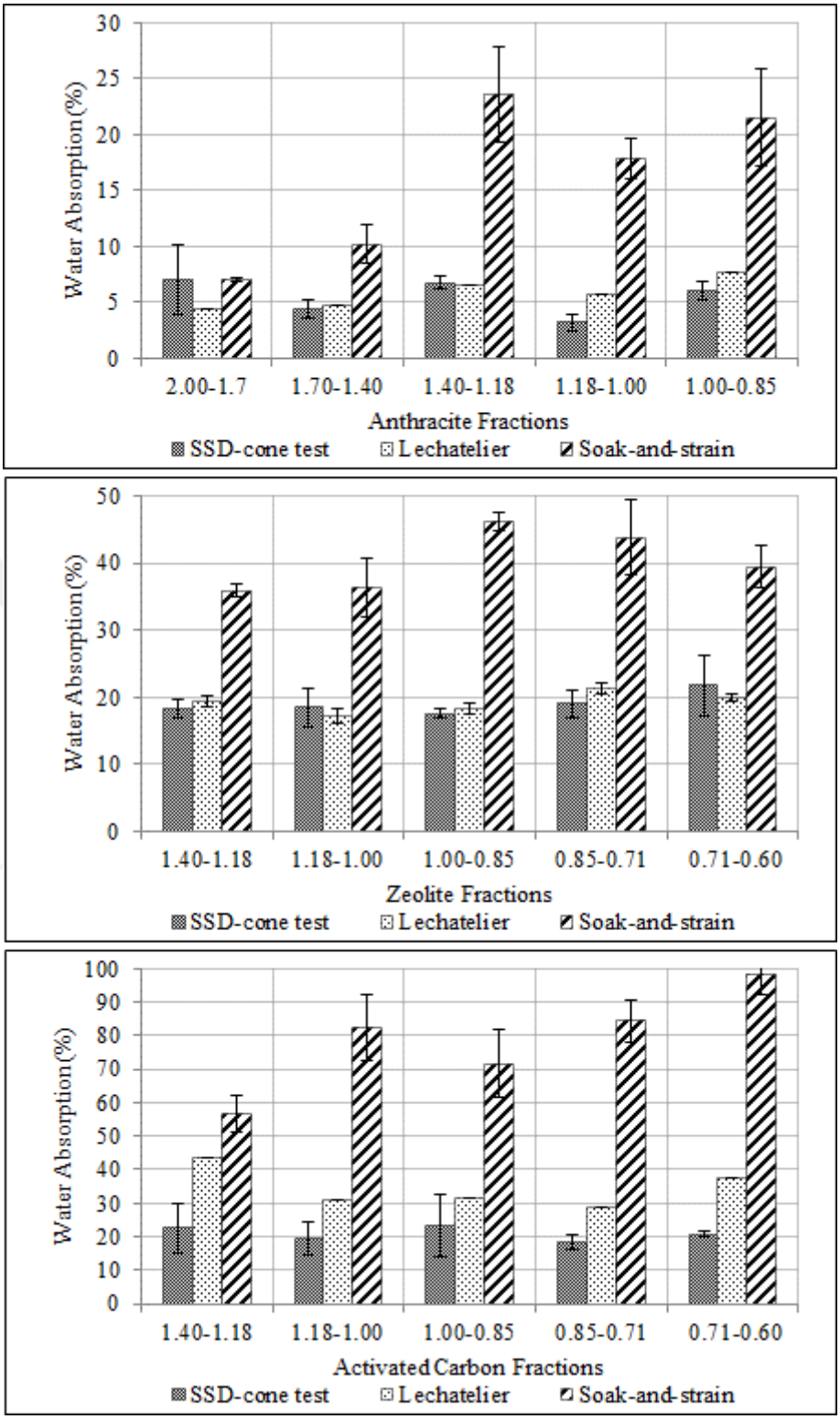


Figure 3.13 Water absorption of porous material fractions

As explained before, the “wet” condition is obtained by three different methods. Figure 3.13 displays and compares water absorption values obtained with the three methods. The percent absorption values for each fraction were obtained during density measurements and are based on at least three repetitions for each method. The following are observed: Focusing on the standard cone test (the leftmost bar within each group of three bars in the figure), water absorption ratio was lowest for anthracite coal (about 3-7%) followed by zeolite (about 18-22%), and highest for activated carbon (about 19-23%). A similar trend is observed with the other two methods. Comparing the three methods, it is seen that the simple soak-and-strain approach leads to absorption of significantly higher amounts of water compared to the other two methods: Water absorption values as high as 8-23% for anthracite, 36-46% for zeolite, and 56-98% for activated carbon were observed with this method (Figure 3.13). Higher water retentions in turn generally yield smaller density values (cf. the third bar within each group of 4 bars in Figure 3.12). This may be explained by noting that excessively wet particles contain larger percentages of water and -since the density of water is less than that of the solid matrix – the effective density is smaller for such particles.

The results obtained with the Le Chatelier flask method are closer to those of the cone test, but a similar general trend (i.e. higher water absorption and lower density values compared to the cone test) is also observed with this method. The results in Figure 3.13 already indicate that the water retained on the particles is too high when the soak-and-strain method is used. It will be seen that this methods leads to the calculation of higher than expected diameter values as well as physically impossible sphericities.

Figure 3.14 displays the equivalent diameters based on the three effective density estimation methods plus the values obtained with oven-dry masses and skeletal densities. Dashed lines on the figure indicate passing and retaining sieve sizes. All methods except the soak-and-strain method resulted in particle diameters that generally fall within the passing-retaining size range. The equivalent diameter based on the skeletal volume (which excludes internal open pores) is the smallest in each case, as expected. It is seen that the soak-and-strain method yields the largest diameter values among the three methods that use water-soaked particles. These diameter values are generally significantly larger than the passing sieve size, another indication that excessive amounts of water are retained on particle surfaces when this method is used.

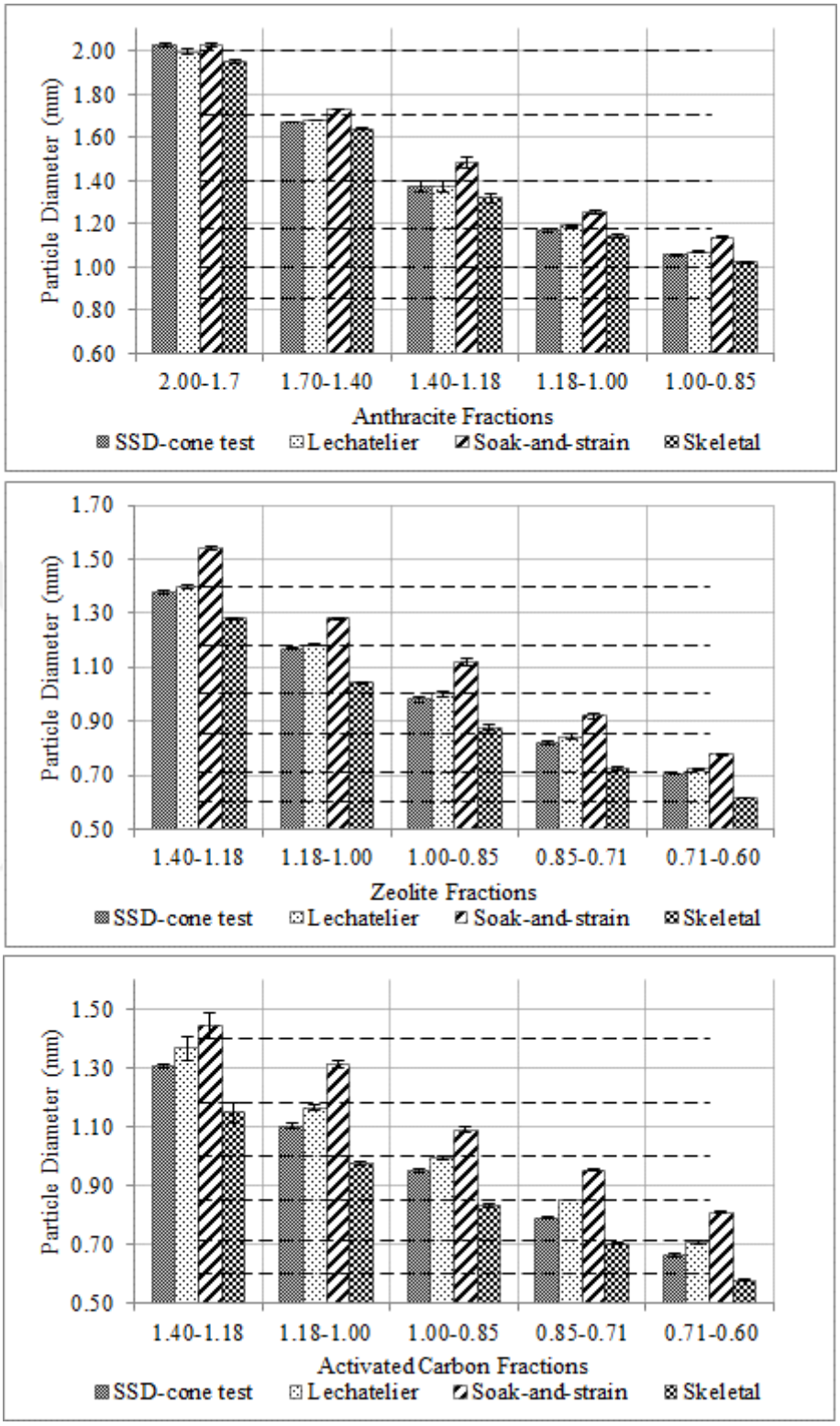


Figure 3.14 Particle equivalent diameters of porous material fractions

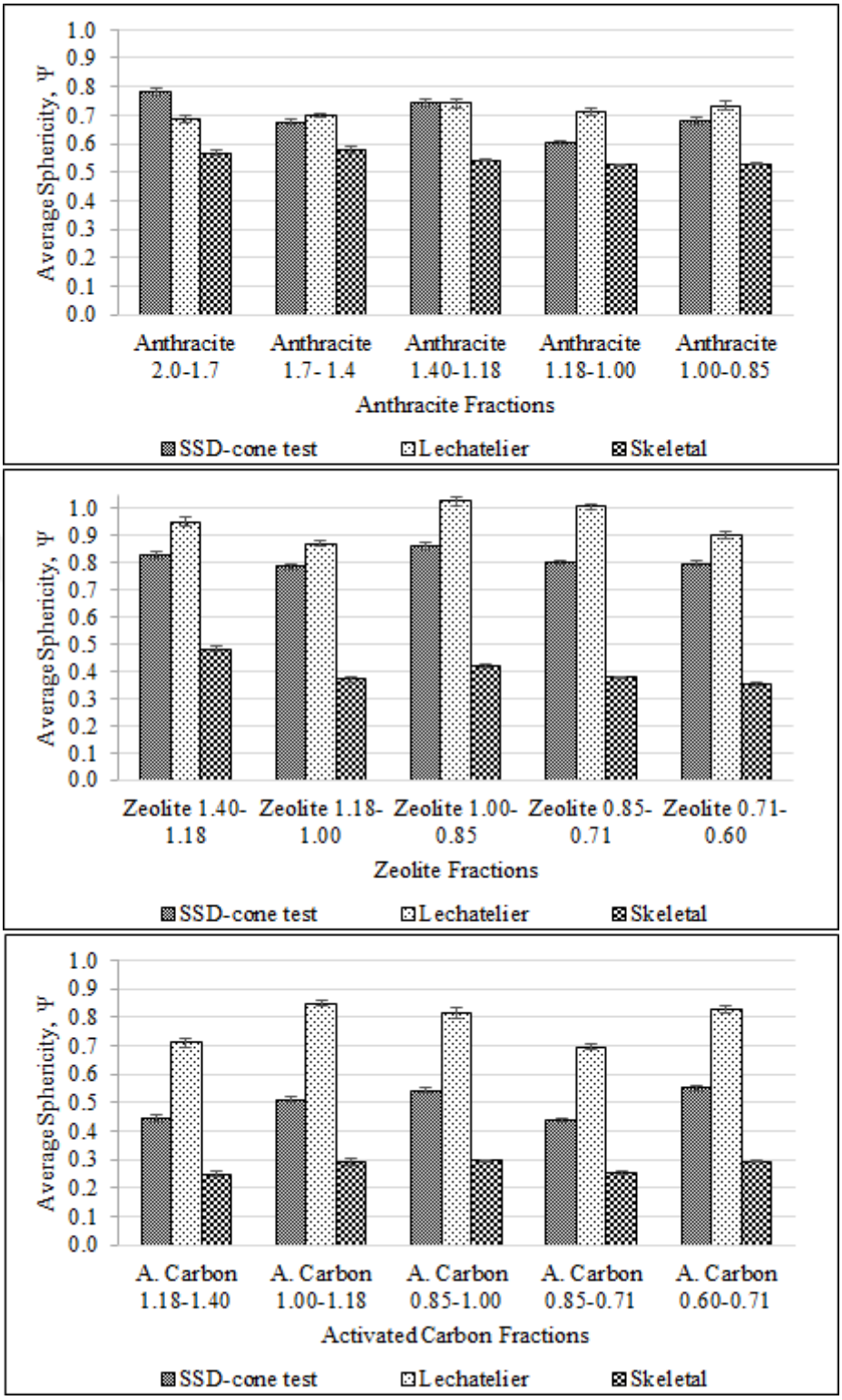


Figure 3.15 Sphericities of porous material fractions

The deviations between the different methods increase as water absorption increases (smallest for anthracite, largest for activated carbon). For anthracite coal, the Le Chatelier flask method gives diameter and effective density values in reasonable agreement with the standard cone test (see topmost graphs in Figure 3.12 and Figure 3.14), but the agreement deteriorates for zeolite and activated carbon materials which absorb higher amounts of water. The diameter values calculated by the Le Chatelier flask method are in general slightly larger than those obtained using the cone test. This indicates that more water is retained on particle surfaces when this method is used instead of the standard cone test.

Figure 3.15 shows the sphericity values (see also Table 3.19, Table 3.20 and Table 3.21) obtained with wet weights and densities based on the cone test and the Le Chatelier flask test. The sphericity values calculated using OD mass and skeletal density are also shown. The sphericities based on the soak-and-strain method were physically meaningless and are therefore not shown. The fact that the soak-and-strain method yields unreasonable sphericity factors leads to the conclusion that this method is not suitable for fixed and fluidized bed applications.

From Figure 3.15, it is seen that sphericities of zeolite and anthracite fractions are found to be in the range of 0.78-0.86 and 0.61-0.78, respectively, when SSD sample masses are determined and densities are measured according the standard cone test. On the other hand, sphericities of activated carbon fractions were found to be in the range of 0.44-0.55. This finding is consistent with the visual observation that activated carbon particles appeared more angular and less spherical compared to the other materials used in this study. While the anthracite coal sphericities based on the Le Chatelier flask test (middle bars) are found to be in reasonable agreement with those based on the cone test (the leftmost bars), this method tended to yield significantly larger sphericities for activated carbon and zeolite fractions. Since zeolite fractions already had high sphericities (in the range of 0.78-0.86), those based on the Le Chatelier flask test exceeded unity slightly in two cases (Figure 3.15 and Table 3.20). These values were rounded down to unity during the fluidization calculations discussed below.

.

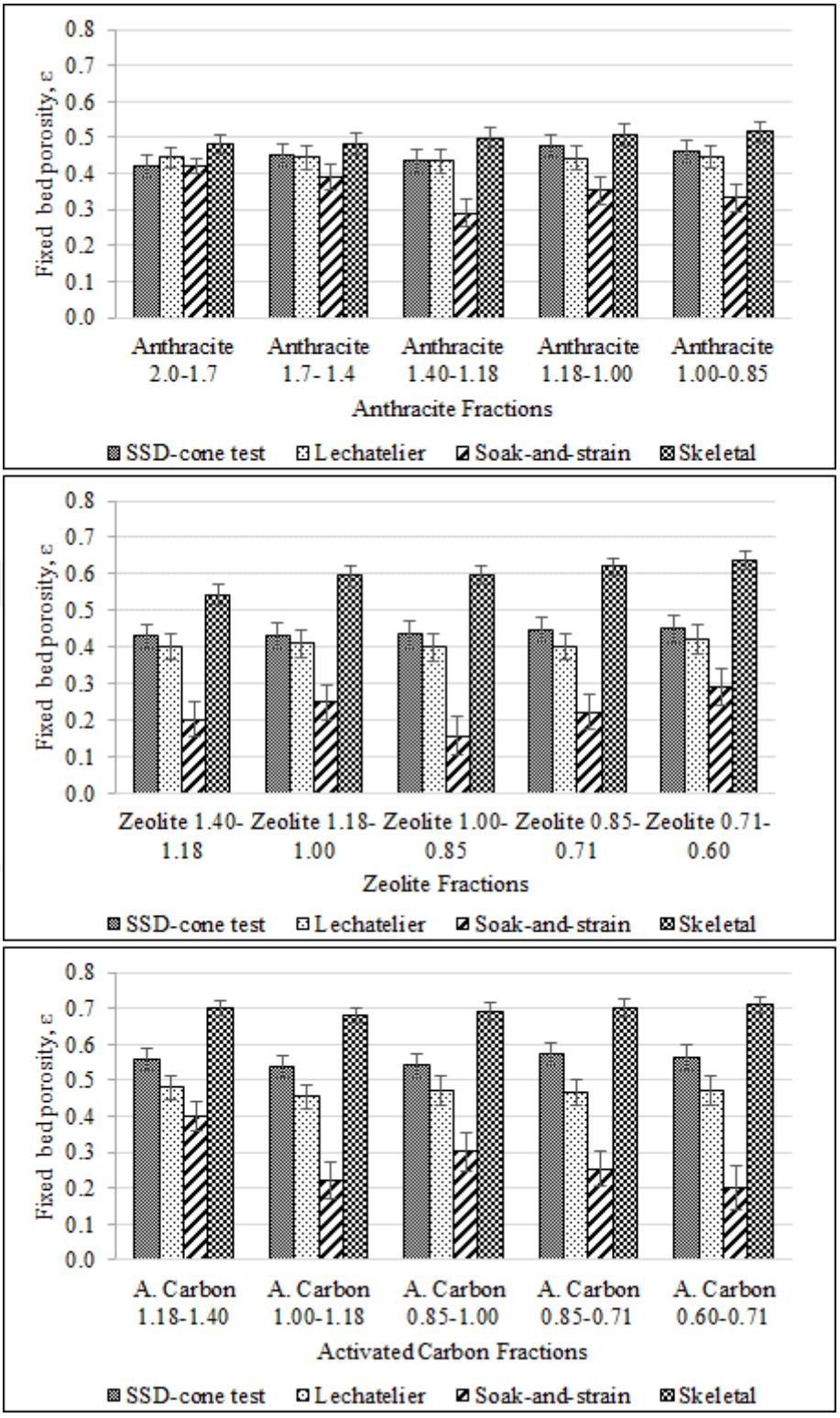


Figure 3.16 Median fixed-bed porosities of porous material fractions (loose-bed and compacted-bed porosities are shown as variation on the bars)

Fixed-bed porosity values are shown in Figure 3.16. Fixed-bed head loss is very sensitive to porosity and using correct porosity values is absolutely necessary to obtain accurate results in such calculations. For anthracite and zeolite fractions, the Le Chatelier flask method leads to porosity values in reasonable agreement with the cone test, but the deviation increases as water absorption increases, leading to poor agreement between the two methods for activated carbon fractions. The soak-and-strain method leads to significantly lower values of porosity for all three materials. Since particle surfaces remain excessively wet and the volume of excess water layers is included in "particle volume fraction" when this method is used, it is reasonable that this method would yield smaller than true external porosities. The extent of deviation, however, is probably much larger than one might expect without experimental evidence such as that given in Figure 3.16. The rightmost bars in Figure 3.16 show that the use of skeletal density and OD bed mass leads to the largest porosity values. This is because internal pores are also included in the calculation of bed porosity in this case.

As noted before, the fixed-bed head loss measurements were performed with three different bed porosities (loose, median, and compacted) for all fractions. In order to compare sphericities of different fractions and materials, the sphericities based on the median bed porosities (which are thought to be close the values in practical applications, as explained before) are used in Figure 3.15 and detailed results are reported in Table 3.19 to Table 3.21.

Figure 3.17 shows the raw experimental data for water fluidization of anthracite, zeolite, and activated carbon fractions. The fluidization data were employed in a number of calculations as explained next.

Equation 1.116 was previously found to be very accurate for non-porous materials of both spherical (Akgiray and Soyer, 2006) and irregular non-spherical shapes (Soyer and Akgiray, 2009). Porosity and expanded bed heights were therefore predicted with Equation 116 using the two methods of determining wet sample mass and effective density, i.e. the cone test and the Le Chatelier flask method, to see which method will give better agreement with the fluidization data (see Figure 3.18 and Table 3.22).

An examination of these results shows that the Le Chatelier method leads to reasonable agreement with the standard cone test, i.e. the two methods of determining wet sample mass and effective density give similar agreement (or, deviation) of the model (Equation 1.116) from the experimental fluidization data for anthracite and zeolite fractions. This is consistent

with the observation that the density, diameter, and sphericity values obtained with the two methods are in approximate agreement.

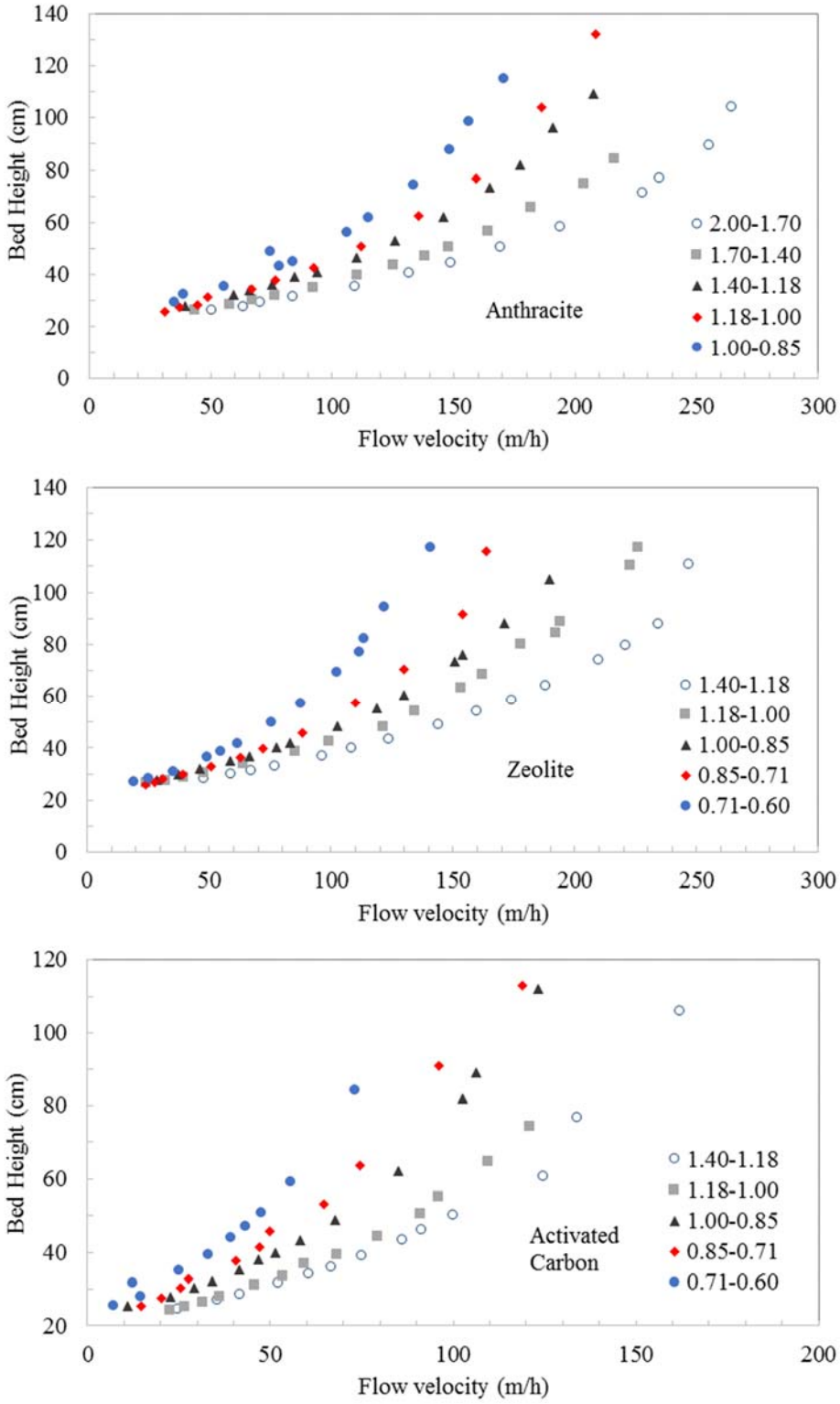


Figure 3.17 Fluidization data for anthracite, zeolite, and activated carbon fractions

For activated carbon, however, there are significant deviations between the two methods. The standard cone test leads to much better agreement with the model predictions, whereas calculations based on the Le Chatelier flask method yields greatly varying errors for different fractions and a large overall mean error.

Based on these results, it may be conjectured that a method such as the Le Chatelier flask method that approximates the SSD condition may be satisfactory for materials that absorb relatively small amounts of water, but as the amount of water absorbed increases, such approximate methods will be less satisfactory. The standard cone test is seen to consistently yield good results for all the materials tested in this work (see Figure 3.18 and Table 3.22 as well as Figure 3.19, Figure 3.20, Figure 3.21).

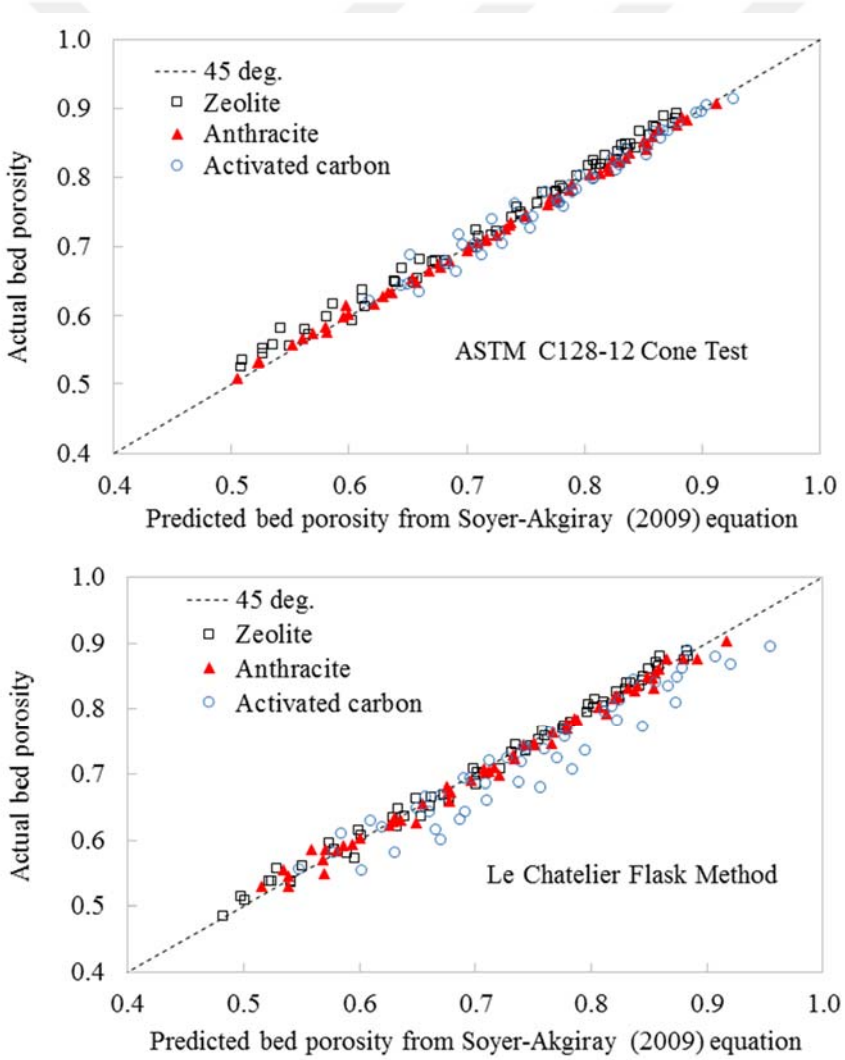


Figure 3.18. Predicted versus actual bed porosity based on two methods of determining wet sample mass and effective density

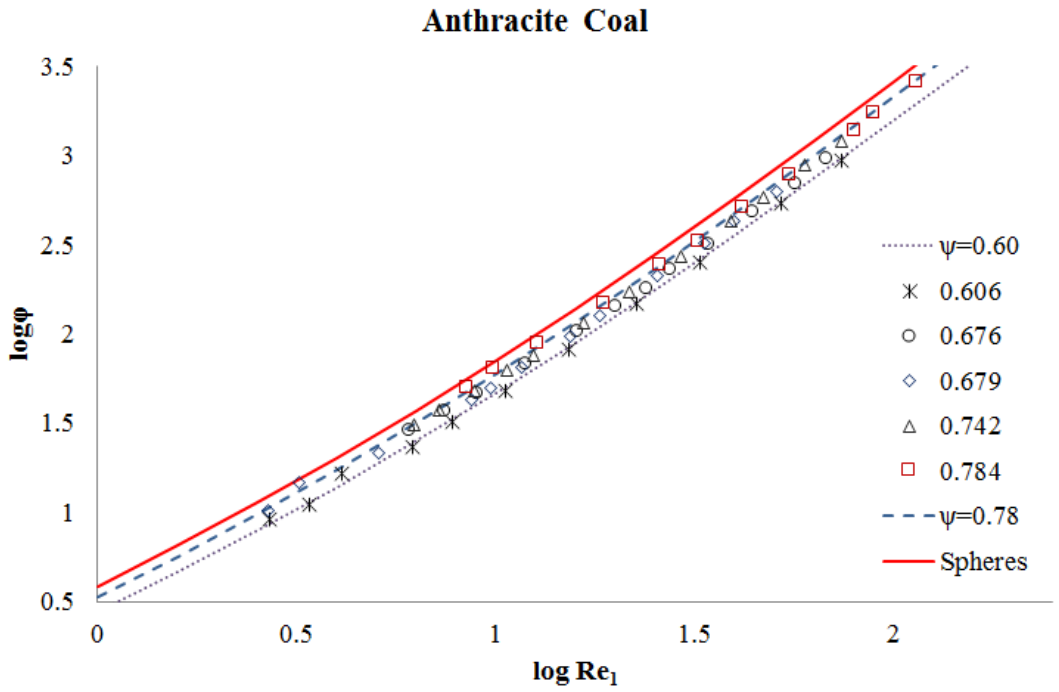


Figure 3.19 Experimental data for anthracite coal fractions and model lines for different sphericity values (properties based on the standard cone test)

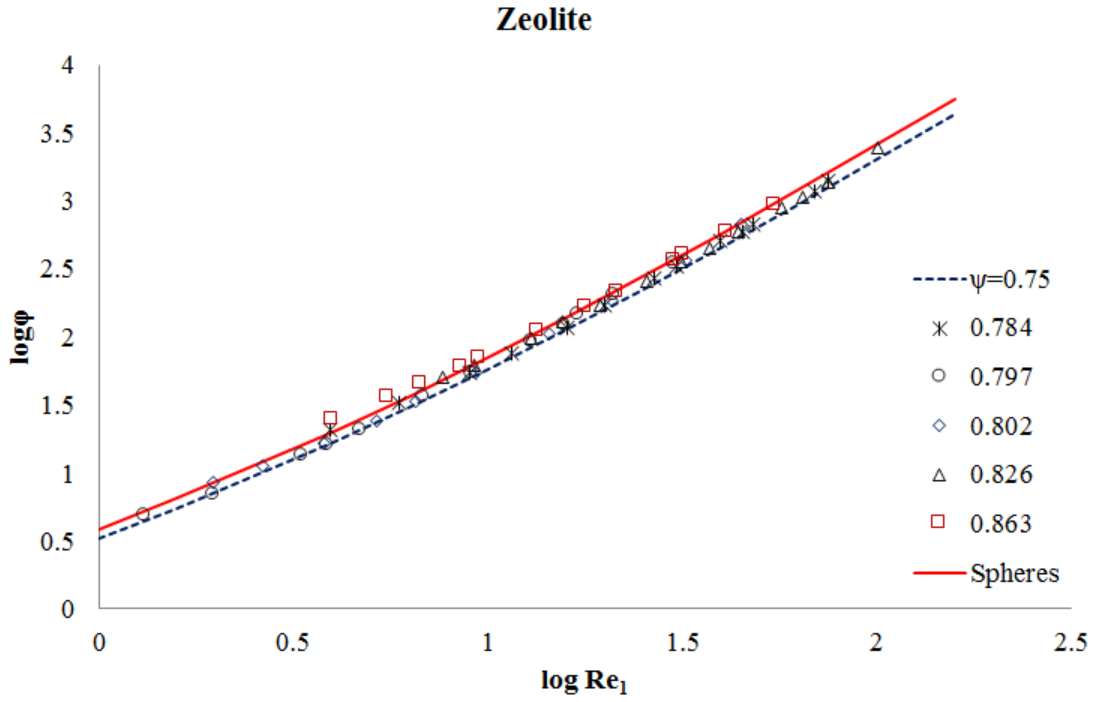


Figure 3.20 Experimental data for zeolite fractions and model lines for different sphericity values (properties based on the standard cone test)

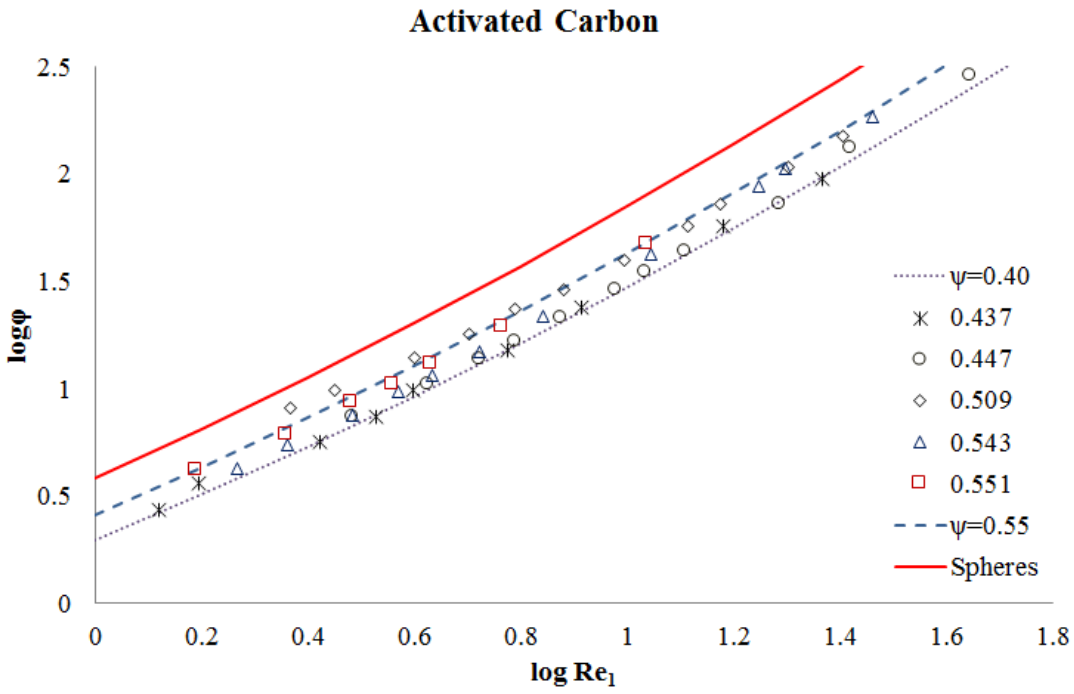


Figure 3.21 Experimental data for activated carbon fractions and model lines for different sphericity values (properties based on the standard cone test).

Figure 3.18, Figure 3.19 and Figure 3.20 are based on the same fluidization data discussed above and show logφ versus $\log Re_1$ data. All three figures were generated using the particle properties based on the standard cone test. The solid curves in these figures represent the fluidization of spheres and are obtained by setting $\psi = 1$ in Equation 1.116. These results confirm the previous finding (Akgiray et al., 2004; Soyer and Akgiray, 2009, 2005) that non-spherical particle data fall below the curve for spherical particles in such a plot and that the deviation increases as sphericity decreases.

This trend can be seen not only as one proceeds from higher sphericity materials to materials with lower sphericities (from zeolite to anthracite and then to activated carbon), but also as one proceeds from higher sphericity fractions of a given material to lower sphericity fractions of the same material. In Figure 3.21, for example, the data points for the activated carbon fraction (0.85-0.71 mm) with $\psi = 0.437$ are clearly below the data points for the activated carbon fraction (0.71-0.60 mm) with $\psi = 0.551$. Furthermore, the positions of the data for the various fractions relative to each other and relative to the spherical particle curve are in excellent agreement with Equation 1.116.

Figure 3.22 shows the results obtained when, in addition to Equation 1.116, the Dharmarajah-Cleasby and Richardson-Zaki correlations are applied in conjunction with the particle properties based on the standard cone test for the SSD condition. While the Dharmarajah-Cleasby correlation takes sphericity into account explicitly, the Richardson-Zaki correlation does not take sphericity into account directly. For the non-spherical media studied here, equivalent diameter values were substituted for the diameter term in the Richardson-Zaki correlation and the Haider and Levenspiel (1989) correlation was used to estimate the particle terminal settling velocities which in turn were used to calculate the index *n* in the Richardson-Zaki correlation.

Table 3.19 Sphericities at different porosities for anthracite fractions using cone test and Le Chatelier flask density measurement methods

Material Fractions	Cone Test					Le Chatelier Flask Method					# of points
	ε		Ψ		σ	ε		Ψ		σ	
Anthracite 2.0-1.70	ε_1	0.449	Ψ_1	0.784	0.008	ε_1	0.472	Ψ_1	0.692	0.011	14
	ε_2	0.420	Ψ_2	0.784	0.014	ε_2	0.445	Ψ_2	0.686	0.016	15
	ε_3	0.388	Ψ_3	0.788	0.017	ε_3	0.414	Ψ_3	0.683	0.019	15
Anthracite 1.70- 1.40	ε_1	0.479	Ψ_1	0.691	0.011	ε_1	0.473	Ψ_1	0.713	0.011	15
	ε_2	0.451	Ψ_2	0.676	0.017	ε_2	0.444	Ψ_2	0.699	0.016	15
	ε_3	0.416	Ψ_3	0.689	0.022	ε_3	0.409	Ψ_3	0.715	0.022	15
Anthracite 1.40-1.18	ε_1	0.467	Ψ_1	0.752	0.020	ε_1	0.467	Ψ_1	0.752	0.020	15
	ε_2	0.434	Ψ_2	0.742	0.017	ε_2	0.434	Ψ_2	0.741	0.017	15
	ε_3	0.404	Ψ_3	0.748	0.019	ε_3	0.405	Ψ_3	0.747	0.019	15
Anthracite 1.18-1.00	ε_1	0.506	Ψ_1	0.622	0.012	ε_1	0.474	Ψ_1	0.722	0.011	15
	ε_2	0.475	Ψ_2	0.606	0.016	ε_2	0.442	Ψ_2	0.712	0.016	15
	ε_3	0.443	Ψ_3	0.606	0.015	ε_3	0.408	Ψ_3	0.722	0.016	15
Anthracite 1.00-0.85	ε_1	0.493	Ψ_1	0.679	0.009	ε_1	0.478	Ψ_1	0.730	0.009	15
	ε_2	0.463	Ψ_2	0.679	0.011	ε_2	0.447	Ψ_2	0.734	0.011	15
	ε_3	0.431	Ψ_3	0.662	0.013	ε_3	0.414	Ψ_3	0.721	0.013	15

From Figure 3.22, it is seen that both correlations deviate significantly from the experimental data. The deviation of the Dharmarajah-Cleasby correlation increases as sphericity decreases. This observation is consistent with earlier findings for non-porous non-spherical particles (Soyer and Akgiray, 2009). Although the Richardson-Zaki correlation yielded relatively reasonable results for zeolite (which has the highest sphericity values among the three materials), it yielded deviations even larger than those of the Dharmarajah-Cleasby correlation for anthracite coal and activated carbon. That the Richardson-Zaki correlation does not fit the non-spherical particle data well is not surprising, as it has been developed using spherical particle data only.

Table 3.20 Sphericities at different porosities for zeolite fractions using cone test and Le Chatelier flask density measurement methods.

Material Fractions	Cone Test					Le Chatelier Flask Method					# of points
		ε		Ψ	σ		ε		Ψ	σ	
Zeolite 1.40-1.18	ε_1	0.459	Ψ_1	0.832	0.012	ε_1	0.434	Ψ_1	0.947	0.013	15
	ε_2	0.429	Ψ_2	0.826	0.012	ε_2	0.402	Ψ_2	0.951	0.015	15
	ε_3	0.391	Ψ_3	0.856	0.017	ε_3	0.362	Ψ_3	1.002	0.020	15
Zeolite 1.18-1.00	ε_1	0.469	Ψ_1	0.787	0.010	ε_1	0.450	Ψ_1	0.863	0.011	15
	ε_2	0.430	Ψ_2	0.784	0.010	ε_2	0.410	Ψ_2	0.869	0.009	15
	ε_3	0.397	Ψ_3	0.815	0.012	ε_3	0.376	Ψ_3	0.913	0.010	15
Zeolite 1.00-0.85	ε_1	0.466	Ψ_1	0.852	0.013	ε_1	0.434	Ψ_1	0.997	0.017	15
	ε_2	0.434	Ψ_2	0.863	0.012	ε_2	0.399	Ψ_2	1.026	0.018	15
	ε_3	0.395	Ψ_3	0.883	0.016	ε_3	0.358	Ψ_3	1.073	0.021	15
Zeolite 0.85-0.71	ε_1	0.478	Ψ_1	0.800	0.055	ε_1	0.434	Ψ_1	0.985	0.068	15
	ε_2	0.448	Ψ_2	0.802	0.007	ε_2	0.402	Ψ_2	1.007	0.011	15
	ε_3	0.412	Ψ_3	0.810	0.004	ε_3	0.362	Ψ_3	1.045	0.006	15
Zeolite 0.71-0.60	ε_1	0.482	Ψ_1	0.784	0.013	ε_1	0.456	Ψ_1	0.876	0.015	15
	ε_2	0.449	Ψ_2	0.797	0.011	ε_2	0.422	Ψ_2	0.901	0.013	15
	ε_3	0.404	Ψ_3	0.802	0.010	ε_3	0.374	Ψ_3	0.924	0.013	15

Table 3.21 Sphericities at different porosities for activated carbon fractions using cone test and Le Chatelier flask density measurement methods

Material Fractions	Cone Test					Le Chatelier Flask Method					# of points
		ε		Ψ	σ		ε		Ψ	σ	
Activated Carbon 1.40-1.18	ε_1	0.587	Ψ_1	0.468	0.045	ε_1	0.514	Ψ_1	0.725	0.069	15
	ε_2	0.557	Ψ_2	0.447	0.016	ε_2	0.479	Ψ_2	0.709	0.017	15
	ε_3	0.527	Ψ_3	0.432	0.013	ε_3	0.443	Ψ_3	0.706	0.014	15
Activated Carbon 1.18-1.00	ε_1	0.567	Ψ_1	0.528	0.019	ε_1	0.487	Ψ_1	0.855	0.022	15
	ε_2	0.539	Ψ_2	0.509	0.015	ε_2	0.453	Ψ_2	0.847	0.016	15
	ε_3	0.507	Ψ_3	0.511	0.013	ε_3	0.416	Ψ_3	0.886	0.013	15
Activated Carbon 1.00-0.85	ε_1	0.575	Ψ_1	0.547	0.014	ε_1	0.511	Ψ_1	0.798	0.016	15
	ε_2	0.541	Ψ_2	0.543	0.012	ε_2	0.472	Ψ_2	0.813	0.013	15
	ε_3	0.504	Ψ_3	0.533	0.009	ε_3	0.430	Ψ_3	0.825	0.013	15
Activated Carbon 0.85-0.71	ε_1	0.596	Ψ_1	0.431	0.014	ε_1	0.496	Ψ_1	0.666	0.021	15
	ε_2	0.573	Ψ_2	0.437	0.005	ε_2	0.468	Ψ_2	0.694	0.007	15
	ε_3	0.538	Ψ_3	0.442	0.003	ε_3	0.425	Ψ_3	0.737	0.003	15
Activated Carbon 0.71-0.60	ε_1	0.598	Ψ_1	0.516	0.007	ε_1	0.513	Ψ_1	0.745	0.010	15
	ε_2	0.563	Ψ_2	0.551	0.011	ε_2	0.471	Ψ_2	0.827	0.018	15
	ε_3	0.531	Ψ_3	0.550	0.007	ε_3	0.431	Ψ_3	0.860	0.015	15

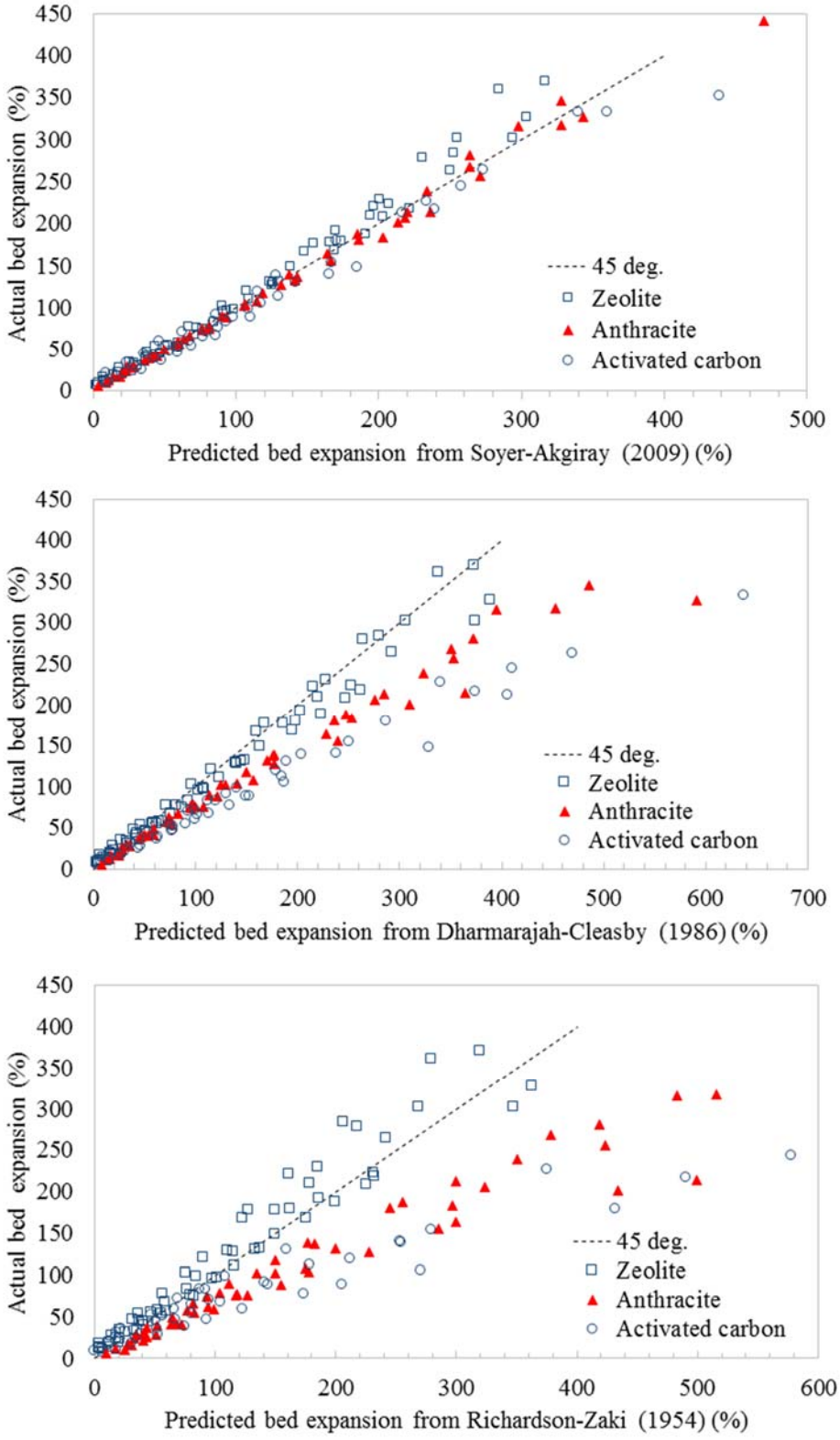


Figure 3.22 Experimental versus predicted bed expansions based on three different correlations (properties based on the standard cone test)

Table 3.22 Mean percent errors in expansion and porosity predicted with Equation 1.116

Material	Sieve size (mm)	Mean % errors in expansion		Mean % errors in porosity		Number of points
		Cone Test	Le Chatelier Method	Cone Test	Le Chatelier Method	
Anthracite	2.00-1.70	6.8	9.1	0.95	1.10	12
Anthracite	1.70-1.40	4.5	5.5	0.61	0.82	12
Anthracite	1.40-1.18	3.0	3.2	0.45	0.49	12
Anthracite	1.18-1.00	8.8	18.7	1.13	2.42	11
Anthracite	1.00-0.85	6.7	5.8	0.87	0.85	12
Average (Anthracite)		**5.9**	**8.3**	**0.80**	**1.11**	**59**
Zeolite	1.40-1.18	9.9	6.2	1.28	0.82	13
Zeolite	1.18-1.00	11.5	7.1	1.33	0.85	13
Zeolite	1.00-0.85	22.4	14.7	3.24	2.24	12
Zeolite	0.85-0.71	9.0	7.5	1.02	1.11	10
Zeolite	0.71-0.60	8.8	10.2	1.15	1.52	12
Average (Zeolite)		**12.4**	**9.1**	**1.61**	**1.30**	**60**
A. Carbon	1.40-1.18	11.3	4.9	1.30	0.68	11
A. Carbon	1.18-1.00	22.3	16.1	2.07	1.77	11
A. Carbon	1.00-0.85	24.8	51.4	2.89	6.60	11
A. Carbon	0.85-0.71	12.2	100.8	1.16	9.21	9
A. Carbon	0.71-0.60	15.2	21.6	1.66	3.01	8
Average (A. Carbon)		**17.5**	**37.5**	**1.85**	**4.13**	**50**
Average (All Materials)		**11.6**	**17.2**	**1.40**	**2.07**	**169**

The initial and main motivation for this work was to study water fluidization of granular materials with internal pores and to ascertain the applicability of the previously developed correlation (Equation 1.116) to such materials. Therefore, the results reported in Figure 3.18-Figure 3.22 and Table 3.22 are considered to be particularly important. The version of Equation 1.116 applicable to spheres (which can be recovered by setting $\psi = 1$ in Equation 1.116) was developed (Akgiray and Soyer, 2006) using spherical particle data (600 measurements) from the literature and then tested against new spherical particle data (332 measurements) collected in that work. With a mean error of 2.26 % in porosity (based on 600 + 332 = 932 data points in the ranges $-1.96 < log\ Re_I < 3.54$ and $0.37 < \varepsilon < 0.90$), it was found to represent the spherical particle data better than any of the other correlations evaluated in that study. Equation 1.116 was then developed (Soyer and Akgiray, 2009) as an extension of the earlier equation (Akgiray and Soyer, 2006) to non-spherical particles by collecting new data (a total of 1486 measurements with 10 sieved fractions of silica sand, 11

sieved fractions of crushed glass, 5 sieved fractions of perlite, and 4 sieved fractions of garnet sand in the ranges $0.40 < \varepsilon < 0.90$, $-0.76 < log\ Re_1 < 2.51$, and $0.40 < \psi < 1.0$). Equation 1.116 was found to represent the non-spherical particle data (the mentioned 1486 data points) with a mean error of 1.83 % in porosity. It is believed that the mean error of 1.40 % in porosity found in the present work serves not only as a strong verification of the applicability of Equation 1.116 to media with internal pores, but also as a further verification of its accuracy for non-spherical media in general.

4 CONCLUSIONS

In this study, expansion behavior of particle beds containing spherical and non-spherical particles was studied experimentally. The most commonly used filter materials in water treatment include both non-porous (sand, garnet, perlite) and porous (e.g. zeolite, activated carbon, anthracite coal) particles. All of the materials studied in this work were characterized carefully and the most reliable techniques were reported.

- The results obtained from the experiments conducted on monodispersed beds of twenty different sizes of spherical particles indicated that the experimental data was very well correlated by the Garside and Al-Dibouni (1977) and Akgiray and Soyer (2006) equations. Mean errors in bed porosity for the Garside and Al-Dibouni and Akgiray and Soyer models are 1.94 % and 2.07 %, respectively. The most widely used correlation that was referenced in many of the textbooks and handbooks in this area is the correlation proposed by Richardson and Zaki (1954). When applied to the new data collected in this work, the Richardson and Zaki correlation has been found to be much less accurate than the two correlations mentioned above.
- In addition to experiments conducted with monodispersed bed of spheres, expansion behavior of binary mixtures of spherical particles was also studied experimentally. Thirty three different binary mixtures of spheres were prepared. These include i) nine different binary mixed beds with the spheres of same density but with a size ratio ranging between 1.2 and 1.6, ii) twenty four different binary beds that were composed of spheres at different size and density ratios. Particle size ratio varies from 1.1 to 4.0, and density ratio in these binary combinations varies from 1.1 to 2.1. Total bed expansion observed during each set of experiments was compared with those calculated in two ways: i) serial model in which the expansion of each layer was computed separately by employing Akgiray and Soyer (2006) equation and the sum of each layers expansion was reported as overall bed expansion. ii) assuming the bed as a monodispersed bed and employing Akgiray and Soyer (2006) equation by substituting the averaged values of particle properties, i.e mean particle diameter and mean particle density instead of properties of each layer. Here, the mean particle density is the weighted average particle density; mean particle diameter of the binary bed was obtained using two approaches proposed by Wen and Yu (1966) and Leva

et al. (1948). Results indicated that serial model by employing Akgiray and Soyer equation to determine the individual expansion of each layer is the most accurate method. Mean percent error in predicted fluidized bed height for all of the thirty three binary mixtures was found as 3.8 % which is significantly smaller than those obtained when Wen and Yu (1966) (8.02 %) and Leva et al. (1948) (10.63 %) methods have been used.

- The fluidization experiments were also performed with the most commonly used filter materials including non-porous (sand, garnet, perlite and crushed glass) and porous particles (granular activated carbon, anthracite and zeolite). A total of 35 different fractions of materials were studied during the experiments, all of which were carefully prepared by sieving and characterized by employing several techniques to measure density, particle size, porosity and sphericity. Sphericity of each material was determined using the Ergun equation and fixed bed head loss data. Particle densities were measured by a water displacement technique. Equivalent diameters have been measured by counting and weighing minimum 200 grains of each fraction.
- The correlation that was proposed for the expansion of non-spherical media by Dharmarajah and Cleasby (1986) has been included in AWWA's Water Quality Handbook (AWWA, 1999). For non-spherical materials, Dharmarajah and Cleasby (1986) correlation and the equation published by Soyer and Akgiray (2009) were assessed. It is seen that the Soyer and Akgiray (2009) correlation, which is considerably simpler in form, was very accurate, whereas the use of Dharmarajah and Cleasby (1986) correlation leads to large errors. When all the non-spherical non-porous particle data (20 separate measurements) are considered together, the mean errors in predicted porosities were found to be 3.3% (Dharmarajah and Cleasby, 1986) and 1.8% (Soyer and Akgiray, 2009).
- All the relevant particle and bed properties of porous particles depend on how particle density and the mass of a sample of particles are measured. Particles with internal pores filled with the liquid of interest should be used in these measurements. Three different methods of particle density and sample mass measurement are explained and tested: i) the standard cone test (ASTM C128-12), ii) the soak-and-strain method, and ii) the Le Chatelier flask method. On the basis of the findings obtained in this work, it is concluded that the standard cone test (ASTM C128-12) is the most reliable method

among the methods considered for the determination of percent water absorption and effective density values of porous particles.

- (i) Particle and bed characteristics important in hydraulic calculations for fixed and fluidized beds of porous particles (i.e. particles with internal pores) are elucidated.
- (ii) It is explained that all the relevant particle and bed properties of porous particles depend on how particle density and the mass of a sample of particles are measured and it is argued that particles with internal pores filled with the liquid of interest should be used in these measurements.
- (iii) Three different methods of particle density and sample mass measurement are explained and tested: (a) The standard cone test (ASTM C128-12), which is theoretically the best method, but is tedious and somewhat difficult to carry out. (b) The soak-and-strain method which perhaps represents a "naive" approach -with its simplicity and directness- one might be tempted to use to obtain quick and approximate answers. (c) The Le Chatelier flask method developed herein to approximate the theoretical correctness of the ASTM standard density test while avoiding the more difficult steps of that test.
- (iv) The standard cone test (ASTM C128-12) is the most reliable method among the methods considered here for the determination of percent water absorption and effective density values of porous particles. This conclusion is further supported by the finding that the correlation developed by Soyer and Akgiray (2009) using non-porous particles only is in excellent agreement with fluidization data collected in the present work when particle properties based on the standard cone test are employed in the calculations.
- (v) The correlation by Soyer and Akgiray (2009) was developed using (both spherical and non-spherical, but) non-porous particles only. An important finding of the present study is that the predictions of this correlation are in excellent agreement with the fluidization data for the three porous media studied in this work. The Dharmarajah-Cleasby correlation –which is the only other general correlation that takes fluid and particle properties including sphericity into account explicitly- manifests increasing deviations from the data as sphericity decreases. The Richardson-Zaki correlation –which does not

take particle shape or sphericity into account-yields even greater deviations from the data for the non-spherical media studied in this work.

This work addresses certain open questions in the liquid solid fluidization literature. It should also be mentioned that a number of questions regarding fluidized bed hydraulics remains unanswered. There is a great deal of experimental work and analysis of data which still need be carried out. Investigation of wall effects on fluidization, investigation of intermixing and inversion phenomena in fluidization of mixtures and employment of the proposed porous filter material characterization technique to multiple porous particle types (natural porous materials, ion exchange resins, etc.) can be a continuation of this work.

REFERENCES

Akgiray, Ö, Saatçi, A. M., 2001. A new look at filter backwash hydraulics. Water Sci. Technol. Water Supply 1, 65–72.

Akgiray, Ö., Soyer, E., Yüksel, E., 2004. Prediction of filter expansion during backwashing. Water Sci. Technol. Water Supply 4, 131–138.

Akgiray, Ö., Soyer, E., 2006. An evaluation of expansion equations for fluidized solid-liquid systems. Aqua 55, 517–525.

Akgiray, Ö., Soyer, E., Yüksel, E., 2004. Prediction of filter expansion during backwashing. Water Sci. Technol. Water Supply 4, 131–138.

Akkoyunlu, A., 2003. Expansion of Granular Water Filters During Backwash. Environ. Eng. Sci. 20, 655–665.

Allen, T., 2003. Powder Sampling and Particle Size Determination, 1st Editio. ed. Elsevier.

American Water Works Association) AWWA, 1999. Water Quality and Treatment: A Handbook of Community Water Supplies, 5th ed. McGraw-Hill.

Amirtharajah, A., 1970. Expansion of Graded Sand Filters during Backwashing. Iowa State University, Ames, IA.

Amirtharajah, A., Cleasby, J.L., 1972. Predicting expansion of filters during backwash. J. Am. Water Work. Assoc. 64, 52–59.

Asif, M., 2012. Volume-change of mixing at incipient fluidization of binary-solid mixtures: Experimental data and predictive models. Powder Technol. 217, 361–368.

Asif, M., 2001. Expansion Behavior of a Binary-Solid Liquid Fluidized Bed with Large Particle Size Difference. Chem. Eng. Technol. 24, 1019–1024.

Astarita, G., 1993. Forces acting on particles in a fluidised bed. Chem Eng Sci 48, 3438–3440.

ASTM C128-12, 2012. Standard Test Method for Density, Relative Density (Specific Gravity), and Absorption of Fine Aggregate. West Conshohocken, PA. doi:10.1520/E0336-11.the

ASTM C136, 2005. Standard test methods for sieve analaysis. West Conshohocken, PA.

B100-01, 2001. Standard for Granular Filter Material. Denver, CO.

Babu, S.P., Shah, B., Talwalkar, A., 1978. Fluidization correlations for coal gasification materials-minimum fluidization velocity and fluidized bed expansion ratio. AIChE Symp Ser 74, 176–186.

Barnea, E., Mizrahi, J., 1973. A generalized approach to the fluid dynamics of particulate systems: Part 1. General correlation for fluidization and sedimentation in solid multiparticle systems. Chem. Eng. J. 5, 171–189.

Basu, J., Ghosal, S.K., 1974. Velocity-voidage relationship in fluidizing and sedimenting beds. Indian Chem. Eng. 3, 29.

Benyahia, F., O'Neill, K.E., 2005. Enhanced Voidage Correlations for Packed Beds of

Various Particle Shapes and Sizes. Part. Sci. Technol. 23, 169–177.

Blake, F.C., 1922. The resistance of packing to fluid flow. Trans. Am. Inst. Chem. Eng. 14, 3.

Bourgeois, P., Grenier, P., 1968. The ratio of terminal velocity to minimum fluidizing velocity for spherical particles. Can. J. Chem. Eng. 46, 325–334.

Brown, G.G., 1966. Unit Operations. John Wiley, New York.

Carlos, C., Richardson, J., 1968. Solids movement in liquid fluidised beds -I. Particle velocity distribution. Chem Eng Sci 23, 813–824.

Carman, P.C., 1937. Fluid flow through granular beds. Trans. Inst. Chem. Eng. 15, 150–166.

Carvalho, W.J., 1970. Fluidization of Crushed Anthracite Coal. Iowa State University, Ames, IA.

Chang, M., Trussell, R.R., Guzman, V., Martinez, J., Delaney, C.K., 1999. Laboratory studies on the clean bed headloss of filter media. Aqua 48, 137–145.

Chen, J.J., 1987. Comments on "'Improved equation for the calculation of minimum fluidization velocity.'" Ind. Eng. Chem. Res. 26, 633–634.

Chitester, D.C., Kornosky, R.M., Fan, L.S., Danko, J.P., 1984. Characteristics of fluidization at high pressure. Chem. Eng. Sci. 39, 253–261.

Chyang, C., Huang, W., 1988. Characteristics of large particle fluidization. J Chin Inst Chem Engrs 19, 81–89.

Cleasby, J.L., 1973. Backwash of granular filters used in wastewater filtration, Annual Progress Report on EPA Project R802140. Cincinnati, OH.

Cleasby, J.L., Baumann, A.R., 1976. Backwash of granular filters used in waste water filtration, Final Report on EPA Project R802140. Engineering Research Institute, Iowa State University.

Cleasby, J.L., Fan, K.S., 1981. Predicting fluidization and expansion of filter media. J. Environ. Eng. 107, 455–471.

Cleasby, J.L., Woods, C.F., 1975. Intermixing of Dual Media and Multi-media Granular Filters. J. Am. Water Work. Assoc. 67, 197–203.

Clift, R., Grace, J.R., Weber, M.E., 1978. Bubbles, Drops and Particles, 1st ed. Academic Press, New York.

Clift, R., Seville, J., Moore, S., Chavarie, C., 1987. Comments on buoyancy in fluidized beds. Chem Eng Sci 42, 191–194.

Couderc, J.P., 1985. Incipient fluidization and particulate systems, in: Davidson, J.F., Clift, R., Harrison, D. (Eds.), Fluidization. Academic Press: London, pp. 1–46.

Coulson, J.M., 1949. The flow of fluids through granular beds: effect of particle shape and voids in streamline flow. Trans. Inst. Chem. Eng 27, 237–257.

Darcy, H., 1856. Les Fontaines publiques de la ville de Dizon. Paris.

Dharmarajah, A.H., 1982. Effect of particle shape on prediction of velocity-voidage relationship in fluidized solid-liquid systems. Ph.D. thesis, Iowa State University,

Ames, IA.

Dharmarajah, A.H., Cleasby, J.L., 1986. Predicting the expansion behavior of filter media. J. Am. Water Work. Assoc. 78, 66–76.

Dixon, A., 1988. Correlations for wall and particle shape effects on fixed bed bulk voidage. Can. J. Chem. Eng. 66, 705–708.

Droste, R.L., 1997. Theory and Practice of Water and Wastewater Treatment. John Wiley & Sons, Inc, New York.

Eastwood, J., Matzen, E., Young, M., Epstein, N., 1969. Random loose porosity of packed beds. Brit Chem Eng 14, 1542–1545.

Edzwald, J.K., 2011. Water Quality and Treatment: A Handbook on Drinking Water, 6th ed. McGraw-Hill : New York.

El-Temtamy, S., Epstein, N., 1986. Effect of low velocity liquid pulstions on some hydrodynamic characteristics of liquid and gas–liquid fluidized beds. AIChE J. 32, 509–512.

Epstein, N., 2003. Applications of Liquid-Solid Fluidization. Int. J. Chem. React. Eng. 1, 1–16.

Epstein, N., Leclair, B.P., Pruden, B.B., 1981a. Liquid fluidization of binary particle mixtures—I. Chem. Eng. Sci. 36, 1803–1809. doi:10.1016/0009-2509(81)80128-5

Epstein, N., Leclair, B.P., Pruden, B.B., 1981b. Liquid fluidization of binary particle mixtures—I. Chem. Eng. Sci. 36, 1803–1809.

Erbil, A.Ç., Soyer, E., Beler Baykal, B., 2011. Ammonium Ion Removal with a Natural Zeolite in Monodispersed and Segregated Fluidized Beds. Ind. Eng. Chem. Res. 50, 6391–6403.

Ergun, S., 1952. Fluid Flow Through Packed Columns. Chem. Eng. Prog. 48, 89–94.

Ergun, S., 1951. Determination of Particle Density of Crushed Porous Solids. Anal. Chem. 23, 151–156.

Ergun, S., Orning, A.A., 1952. Fluid Flow through Randomly Packed Columns and Fluidized Beds. Ind. Eng. Chem. 41, 1179–1184.

Escudié, R., Epstein, N., Grace, J.R., Bi, H.T., 2006. Layer inversion phenomenon in binary-solid liquid-fluidized beds: Prediction of the inversion velocity. Chem. Eng. Sci. 61, 6667–6690.

Fair, G., Geyer, J., Okun, D., 1968. Water and wastewater engineering, Vol. 2, Water purification and wastewater treatment and disposal. Wiley, New York.

Fair, G.M., Geyer, J.C., Okun, D.A., 1971. Elements of Water Supply and Wastewater Disposal, 2nd editio. ed. John Wiley and Sons, Inc., New York.

Fidleris, V., Whitmore, R.L., 1961. Experimental determination of the wall effect for spheres falling axially in cylindrical vessels. Br. J. Appl. Phys. 12, 490.

Foscolo, P.U., Gibilaro, L.G., Waldram, S.P., 1983. A unified model for particulate expansion of fluidised beds and flow in fixed porous media. Chem. Eng. Sci. 38, 1251–1260.

Furnas, C., 1929. Flow of gases through beds of broken solids, Bulletin 3. ed. US Bureau of Mines.

Ganguly, U.P., 1980. Direct method for prediction of expanded bed height in liquid-solid fluidization. Can. J. Chem. Eng. 58, 559–563.

Garside, J., Al-Dibouni, M.R., 1977. Velocity-voidage relationships for fluidization and sedimentation in solid-liquid systems. Ind. Eng. Chem. Process. Des. Dev 16, 206–214.

Gibilaro, L., Di Felice, R., Waldram, S., Foscolo, P., 1987. Authors' reply to Clift et al. Chem Eng Sci 42, 194–196.

Gibilaro, L., F, Di Felice, R., Waldram, S., Foscolo, P., 1985. Generalized friction factor and drag coefficient correlations for fluid-particle interactions. Chem. Eng. Sci. 40, 1817–1823.

Gibilaro, L., Waldram, S., Foscolo, P., 1984. Authors' reply to comments by N. Epstein. Chem Eng Sci 39, 1819–1820.

Gibilaro, L.G., Di Felice, R., Waldram, S.P., Foscolo, P.U., 1986. A predictive model for the equilibrium composition and inversion of binary-solid liquid fluidized beds. Chem. Eng. Sci. 41, 379–387.

Goroshko, V.D., Rozenbaum, R.B., Todes, O.M., 1958. Approximate hydraulic laws of a suspended layer. Izv Vyss. Uchebn Zaved Neft Gaz 1, 125.

Grace, J., 1982. Fluidized bed hydrodynamics, in: Hetsroni, G. (Ed.), Handbook of Multiphase Systems. New York, pp. 6–8.

Gunasingham, K., Lekkas, T.D., Fox, G.T.J., Graham, N.J.D., 1978. Predicting the expansion of granular filter beds. Filtr. Sep. 619.

Haider, A., Levenspiel, O., 1989. Drag coefficient and terminal velocity of spherical and nonspherical particles. Powder Technol. 58, 63–70.

Handley, D., Doraisamy, A., Butcher, K., Franklin, N., 1966. A study of the fluid and particle mechanics in liquid-fluidized beds. Trans Instn Chem Engrs 44, 260–273.

Handley, D., Heggs, P., 1968. Momentum and het transfer mechanism in regular shaped packings. Trans Inst Chem Eng 46, 251–264.

Hartman, M., Havlin, V., Svoboda, K., Kozan, A.P., 1989. Predicting voidage for particulate fluidization of spheres by liquids. Chem Eng Sci 44, 2770–2775.

Haughey, D.P., Beveridge, G.G., 1966. Local voidage variation in a randomly packed bed of equal-sized spheres. Chem. Eng. Sci. 21, 905–916.

Hicks, R.E., 1970. Pressure drop in packed beds of spheres. Ind. Eng. Chem. Fundam. 9, 500–502.

Hoffman, R.F., Lapidus, L., Elgin, J.C., 1960. The mechanics of vertical moving fluidized systems: IV. Application to batch-fluidized systems with mixed particle sizes. AIChE J. 6, 321–324.

Horwitz, W., 1990. Nomenclature for sampling in analytical chemistry. Pure Appl. Chem. 62, 1193–1208.

Inglezakis, V.J., Poulopoulos, S.G., 2006. Adsorption, Ion Exchange and Catalysis: Design

of Operations and Environmental Applications. Elsevier: Amsterdam 602.

Jean, R.-H., Fan, L.-S., 1998. Multiphase flow: liquid/solid fluidized bed systems, in: Johnson, R. (Ed.), Handbook of Fluid Dynamics. CRC Press, pp. 19.1–19.25.

Khan, a. R., Richardson, J.F., 1990. Pressure gradient and friction factor for sedimentation and fluidisation of uniform spheres in liquids. Chem. Eng. Sci. 45, 255–265.

Kmiec, A., 1982. Equilibrium of forces in fluidized bed — experimental verification. Chem. Eng. J. 23, 133–136.

Kmiec, A., 1978. Particle distributions and dynamics of particle movement in solid–liquid fluidized beds. Chem Eng J 15, 1–12.

Kozeny, J., 1927. About capillaries conducting water in the earth, Sitzber. Akd. Wiss. Wien, Math. Naurv. Kasse.

Latif, B., Richardson, J., 1972. Circulation patterns and velocity distributions for particles in a liquid fluidised bed. Chem Eng Sci 27, 1933–1949.

Leva, M., 1959. . Fluidization. McGraw-Hill, New York.

Leva, M., 1947. Pressure drop through packed tubes: Part I. Chem. Eng. Prog. 43, 549–554.

Leva, M., Grummer, M., Weintraub, M., Pollchick, M., 1948. Introduction to Fluidization. Chem.Eng.Prog. 44, 511–520.

Leva, M., Weintraub, M., Grummer, M., Pollchik, M., 1949. Fludization of Anthracite Coal. Ind. Eng. Chem. 41, 1206–1212.

Lewis, E.W., Bowerman, E.W., 1952. Fluidization of solid particles in liquids. Chem. Eng. Prog. 48, 603.

Lewis, W.K., Gilliland, E.R., Bauer, W.C., 1949. Characteristics of Fluidized Particles. Ind. Eng. Chem. 41, 1104–1117.

Limas-Ballesteros, R., 1980. Fluidisation de particules non spheriques. Transfert de matiere entre le solide et le liquide. Institut National Polytechnique, Toulouse.

Lin, T.J., Fan, L.S., 1997. Characteristics of high pressure liquid-solid fluidization. AIChE J. 43, 45–57.

Loeffler, A.L., 1953. Mechanism of hindered settling and fluidization. Iowa State University of Science and Technology.

Logsdon, G.S., Hess, A.F., Chipps, Michael, J., Rachwal, A.J., 2002. Filter Maintenance and Operations Guidance Manual. Denver, CO.

Lucas, A., Arnaldos, J., Casal, J., Puigjaner, L., 1986. Improved equation for the calculation of minimum fluidization velocity. Ind. Eng. Chem. Process Des. Dev. 25, 426–429.

Metcalf&Eddy, 2004. Wastewater Engineering: Treatment Disposal Reuse. McGraw-Hill.

Morcom, A.R., 1946. Fluid Flow Through Granular Materials. Trans. Inst. Chem. Eng. 30–43.

Nakamura, M., Hamada, Y., Toyama, S., Fouda, A.E., Capes, C.E., 1985. An experimental investigation of minimum fluidization velocity at elevated temperatures and pressures. Can. J. Chem. Eng. 63, 8–13.

Narsimhan, G., 1965. On a generalized expression for prediction of minimum fluidization velocity. AIChE J. 11, 550–554.

Oman, A.O., Watson, K.M., 1944. Pressure drops in granular beds. Natl. Pet. News 36, 795–801.

Patwardhan, V.S., Tien, C., 1985. Sedimentation and liquid fluidization of solid particles of different sizes and densities. Chem. Eng. Sci. 40, 1051–1060.

Peavy, H.S., Rowe, D.R., Tchobanoglous, G., 1985. Environmental Engineering, Internatio. ed. McGraw Hill.

Pettyjohn, E.S., Christiansen, E.B., 1948. Effect of particle shape on free-settling rates of isometric particles. Chem. Eng. Prog. 44, 157–172.

Ramamurthy, K., Subbaraju, K., 1973. Bed Expansion Characteristics of Annular Liquid-Fluidized Beds. Ind. Eng. Chem. Process. Des. Dev 12, 184–189.

Reynolds, T.D., 1996. Unit Operations and Proceses in Environmental Engineering, 2nd ed. PWS Publishing Company.

Riba, J., Routie, R., Couderc, J., 1978. Conditions minimales de mise en fluidisation par un liquide. Can. J. Chem. Eng. 56, 26–30.

Riba, J.P., Couderc, J.P., 1977. Expansion de couches fluidisees par des liquids. Can. J. Chem. Eng. 55, 118–121.

Richardson, J.F., 1971. Incipient fluidization and particulate systems, in: Davidson, J.F., Harrison, D. (Eds.), Fluidization. Academic Press: London, pp. 25–64.

Richardson, J.F., Zaki, W.N., 1954. The sedimentation of a suspension of uniform spheres under conditions of viscous flow. Chem. Eng. Sci. 3, 65–73.

Rose, H., Rizk, M., 1949. Further researches in fluid flow through beds of granular material, in: Proc Inst Mech Eng. London, pp. 493–503.

Rowe, P.N., A.M.C.T., D.I.C., Henwood, G.A., 1961. Drag forces in a hydraulic model of a Fluidized bed-Part I. Trans Instn Chem Engrs 39, 43–54.

Saxena, S.C., Vogel, G.J., 1977. The measurement of incipient fluidisation velocities in a bed of coarse dolomite at temperature and pressure. Trans. Inst. Chem. Eng 55, 184–189.

Scott, G.D., 1960. Packing of spheres. Nature 188, 908–911.

Sholji, I., Johnson, F.A., 1987. Comparison of Backwash Models for Granular Media. J. Environ. Eng. 113, 532–549.

Singh, A.N., Sen Gupta, P., 1980. Expansion behaviour of liquid-solid fluidized bed systems. Can. J. Chem. Eng. 58, 116.

Soyer, E., Akgiray, Ö., 2009. A new simple equation for the prediction of filter expansion during backwashing. J. Water Supply Res. Technol. - Aqua 58, 336–345.

Soyer, E., Akgiray, Ö., 2005. Expansion of non-spherical media during fluidization, in: Proceedings of IWA International Conference on Particle Separation,Seoul, Sourth Korea, June 1-5. pp. 579–586.

Stevenson, D.G., 1994. The specification of filtering materials for rapid gravity filtration, in: Water Environ. J. pp. 527–534.

Subramanian, P., Arunachalam, V.R., 1980. A simple device for the determination of sphericity factor. Ind. Eng. Chem. Fundam 19, 436–437.

Tallmadge, J., 1970. Packed bed pressure drop-an extension to higher Reynolds numbers. AIChE J. 16, 1092–1093.

Tien, C., 2012. Principles of Filtration, 1st ed. Elsevier.

Tilton, J.N., 2008. Fluid and Particle Dynamics, in: Perry, R.H., Green, D.W. (Eds.), Perry's Chemical Engineers' Handbook. McGraw-Hill : New York.

Turton, R., Levenspiel, O., 1986. A short note on the drag correlation for spheres. Powder Technol. 47, 83–86.

Wadell, H., 1935. Volume, shape, and roundness of quartz particles. J. Geol. 43, 250–280.

Wadell, H., 1933. Sphericity and Roundness of Rock Particles. J. Geol. 41, 310–331.

Weast, R.C., Astle, M.J., Beyer, W.H., 1989. CRC Handbook of Chemistry and Physics, 69th Editi. ed. Florida.

Weber, W., 1972. Physicochemical Processes for Water Quality Control. Wiley-Interscience.

Wen, C., Yu, Y., 1966. Mechanics of fluidization. Chem Eng Prog Symp Ser 62, 100–111.

Wen, C.Y., Fan, L.S., 1974. Some Remarks on the Correlation of Bed Expansion in Liquid-Solid Fluidized Beds. Ind. Eng. Chem., Process Des. Dev. 13, 194–197.

Wen, C.Y., Yu, Y.H., 1966. A generalized method for predicting the minimum fluidization velocity. AIChE J. 12, 610–612.

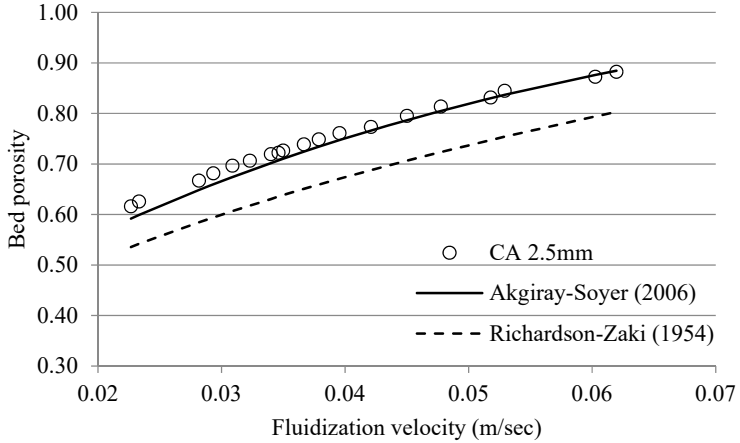
Wilhelm, R.H., Kwauk, M., 1948. Fluidization of solid particles. Chem. Eng. Prog. 44, 201.

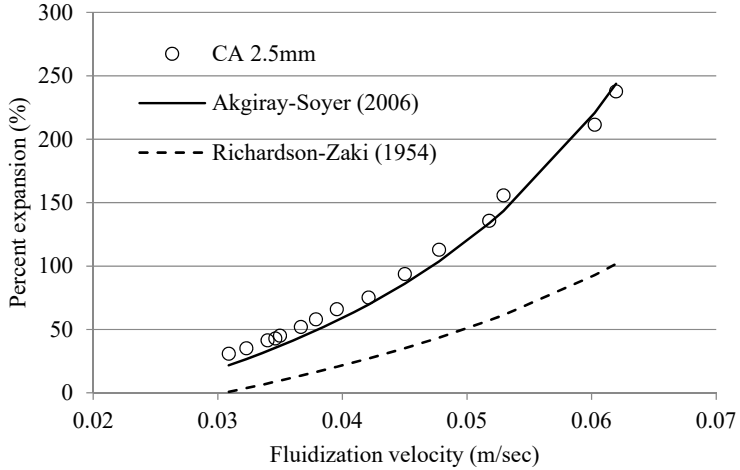
Yang, W.C., 2003. Handbook of Fluidization and Fluid-Particle Systems, Chemical Engineering. Marcel Dekker: New York.

Zou, R.., Yu, A.B., 1996. Evaluation of the packing characteristics of monosized nonspherical particles. Powder Technol. 88, 71–76.

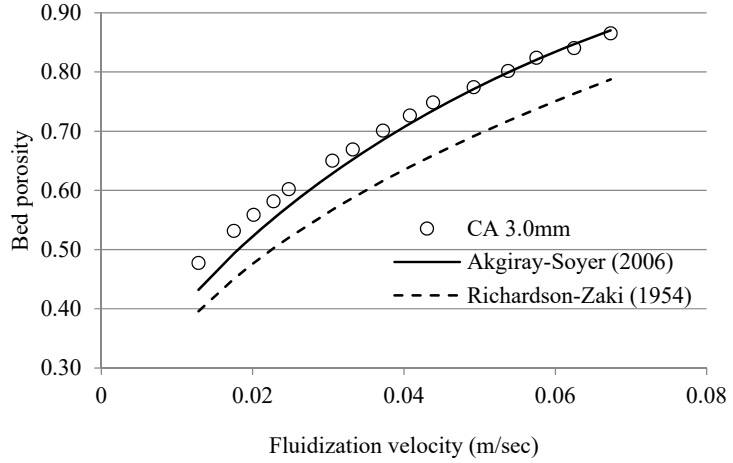
APPENDIX I

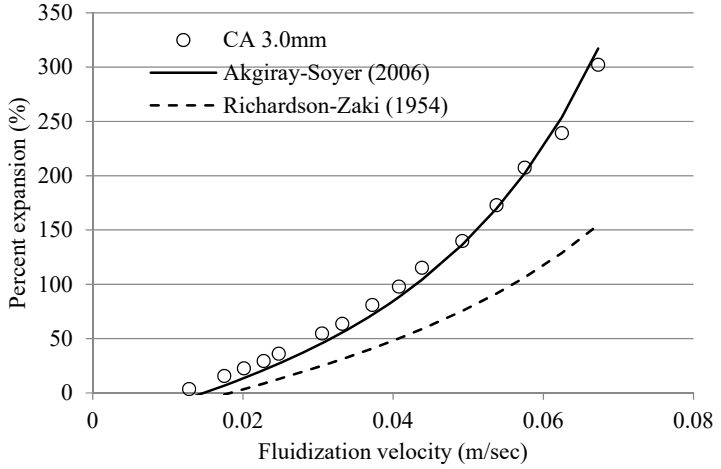
Percent Expansion and Bed Porosity Graphs of Spherical Particles



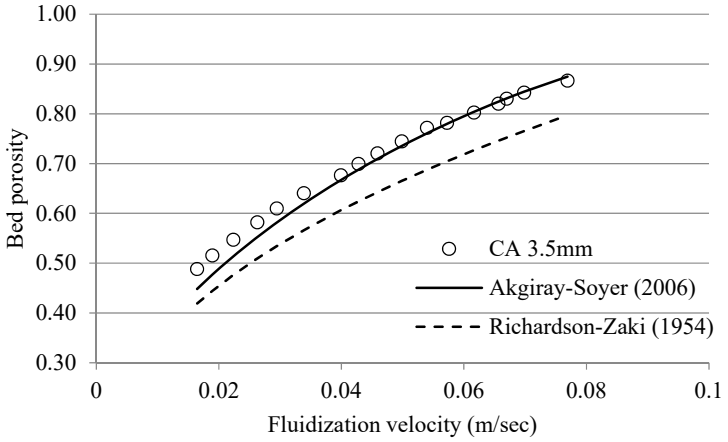


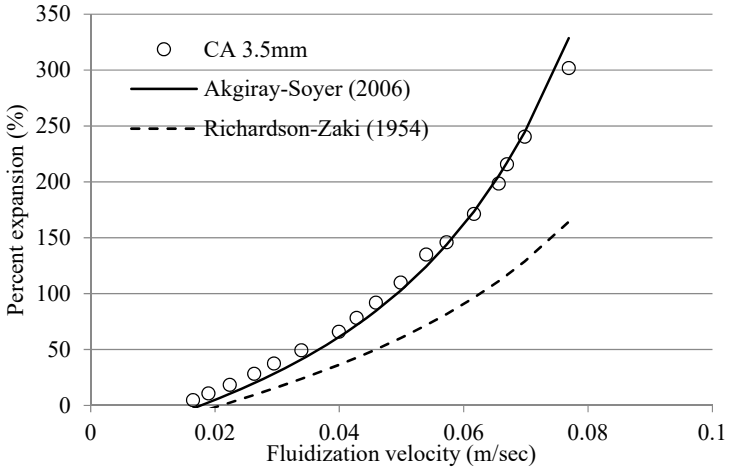
Appendix I-Figure 1. Percent expansion and bed porosity graphs of 2.5mm cellulose acetate beads



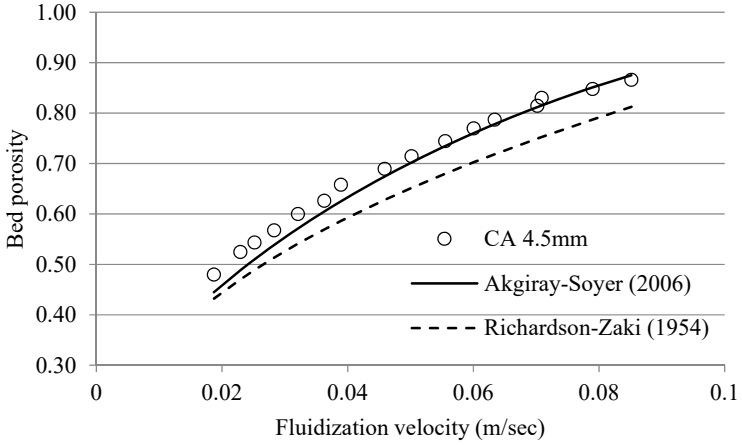


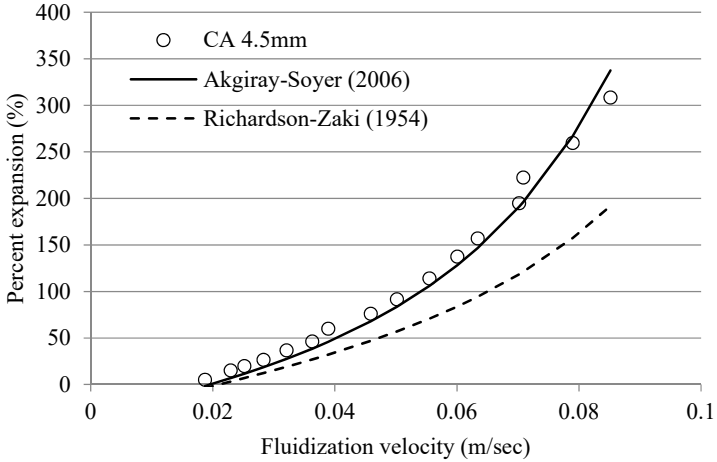
Appendix I-Figure 2. Percent expansion and bed porosity graphs of 3mm cellulose acetate beads



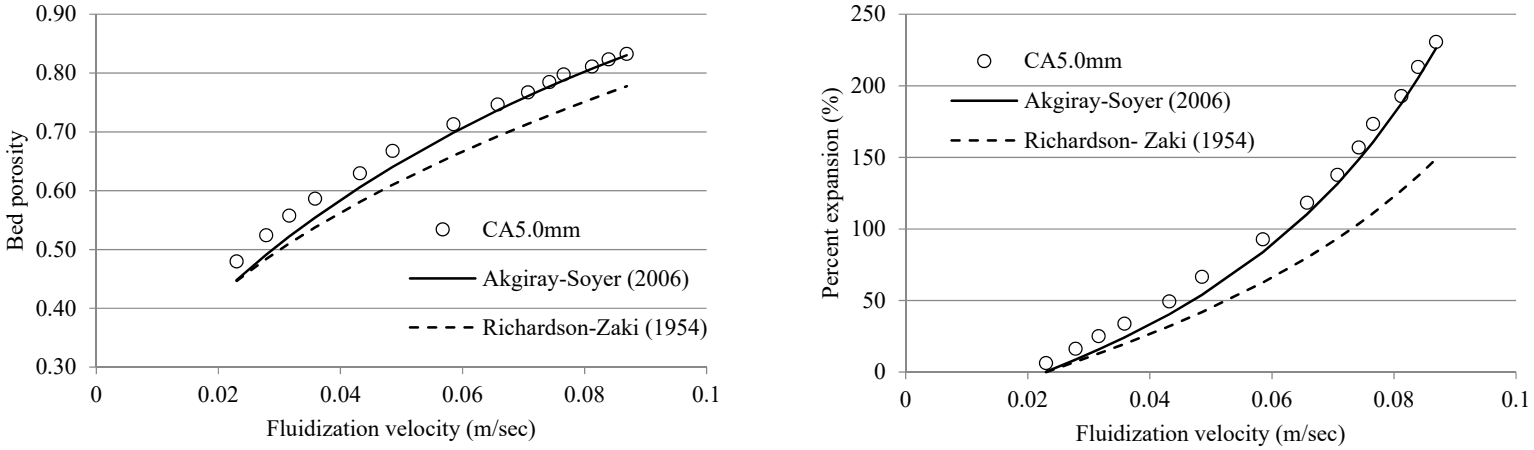


Appendix I-Figure 3 Percent expansion and bed porosity graphs of 3.5mm cellulose acetate beads

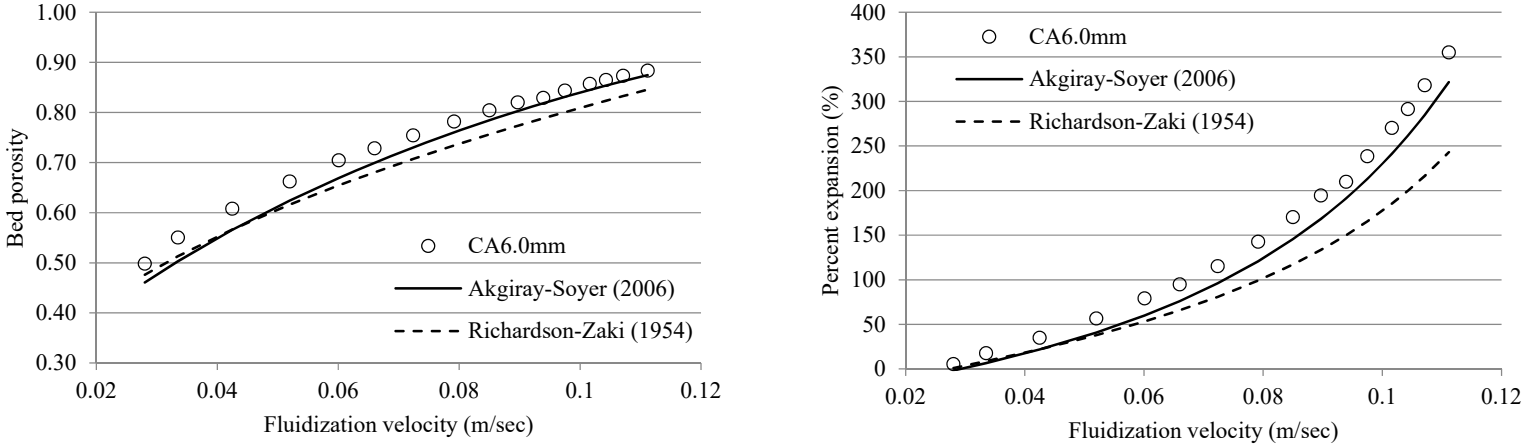




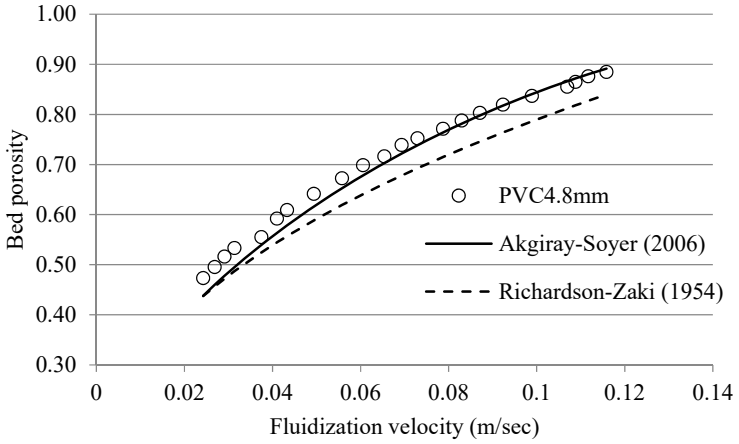
Appendix I-Figure 4 Percent expansion and bed porosity graphs of 4.5mm cellulose acetate beads

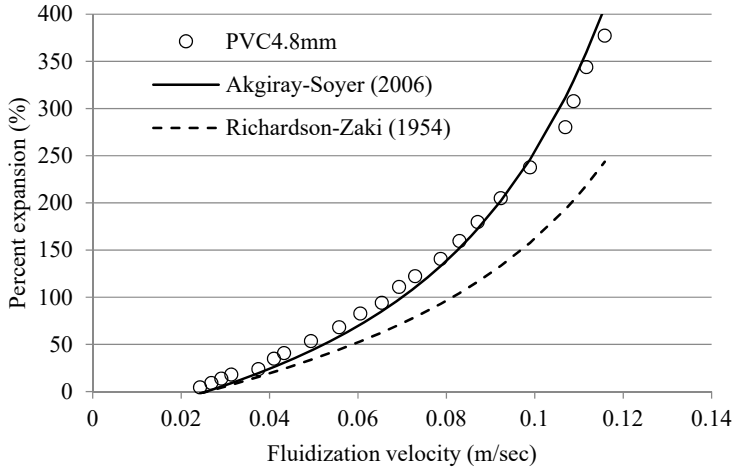


Appendix I-Figure 5 Percent expansion and bed porosity graphs of 5mm cellulose acetate beads

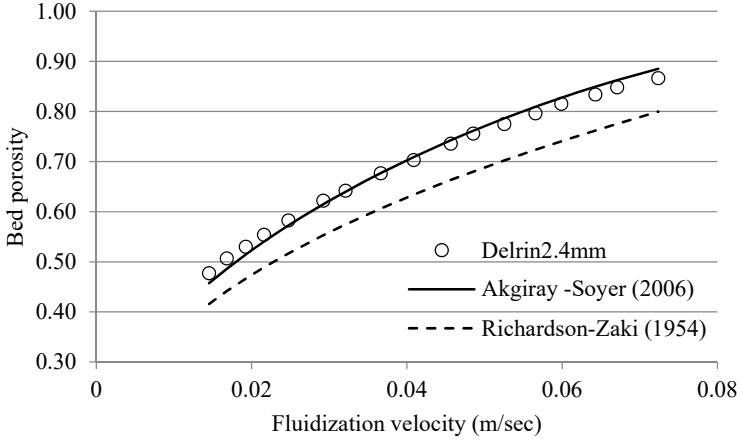


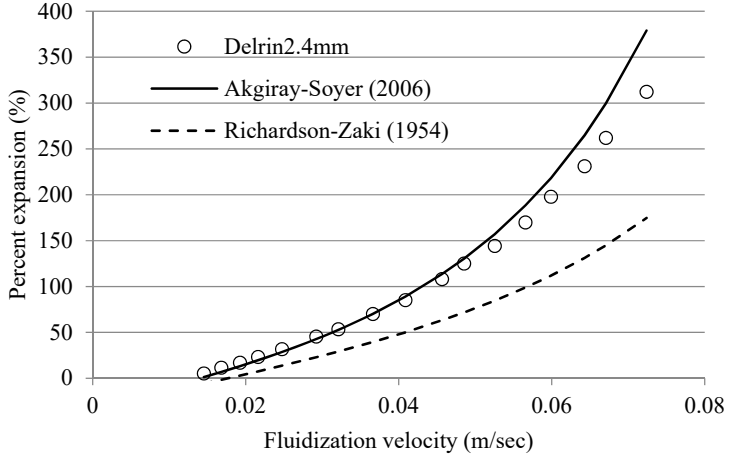
Appendix I-Figure 6 Percent expansion and bed porosity graphs of 6mm cellulose acetate beads



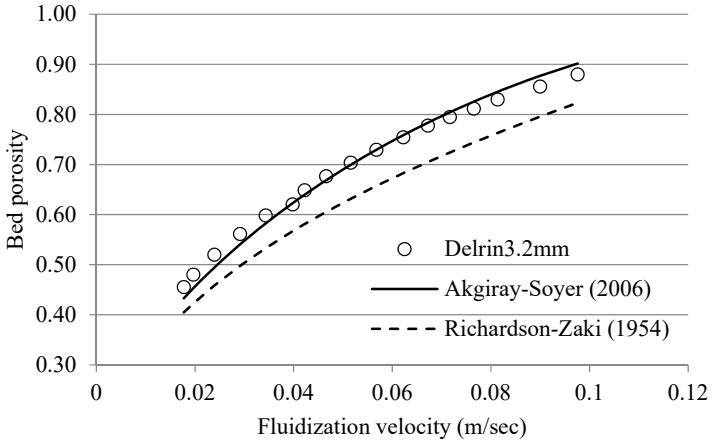


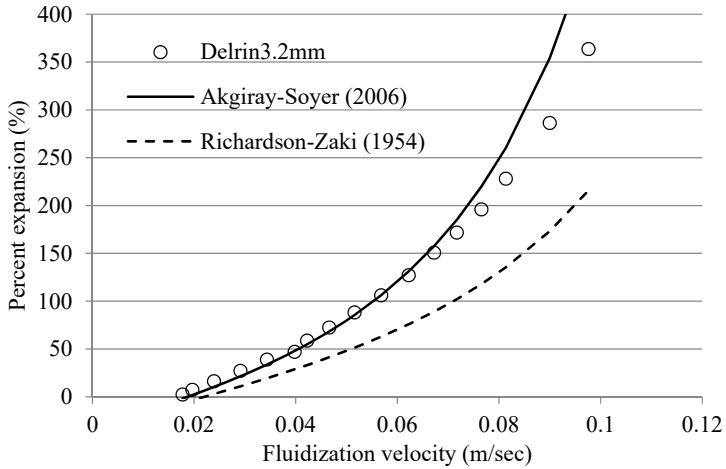
Appendix I-Figure 7 Percent expansion and bed porosity graphs of 4.8mm PVC beads



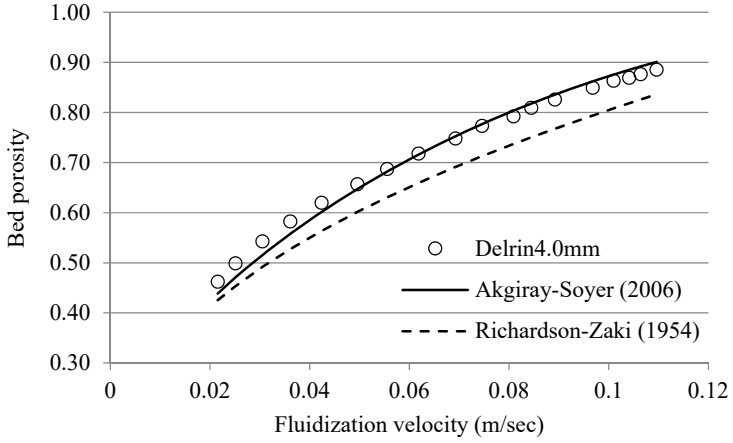


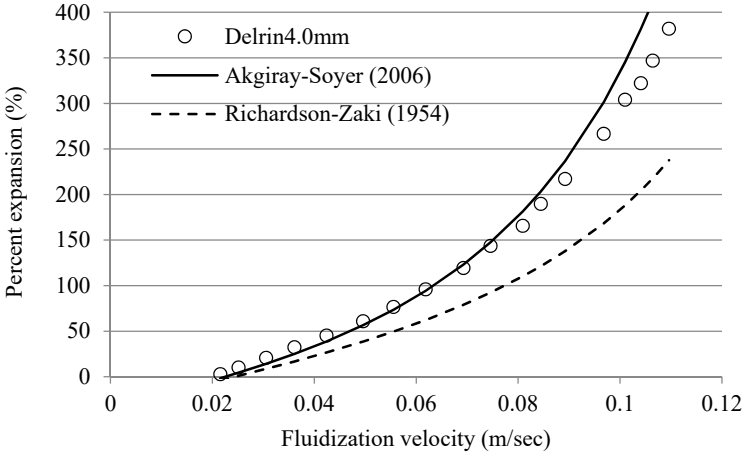
Appendix I-Figure 8 Percent expansion and bed porosity graphs of 2.4mm delrin beads



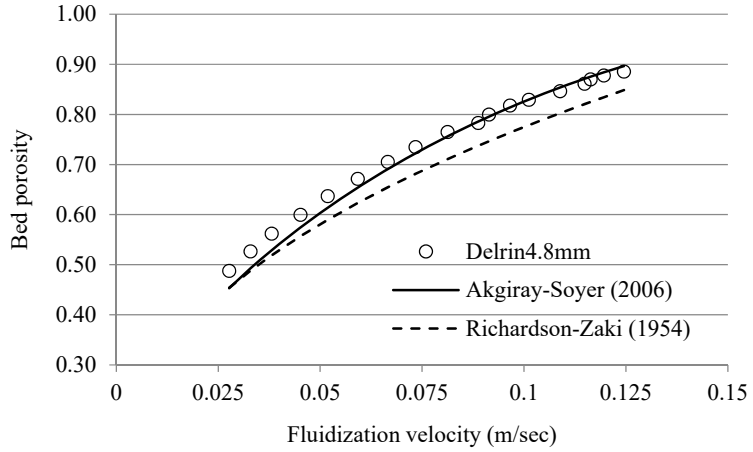


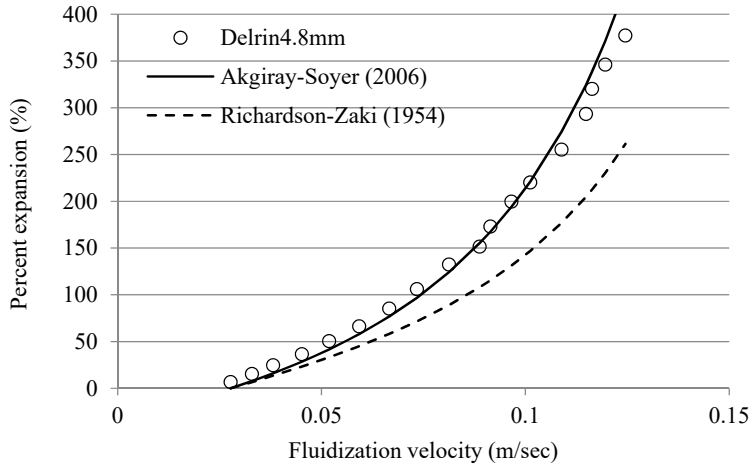
Appendix I-Figure 9 Percent expansion and bed porosity graphs of 3.2mm delrin beads



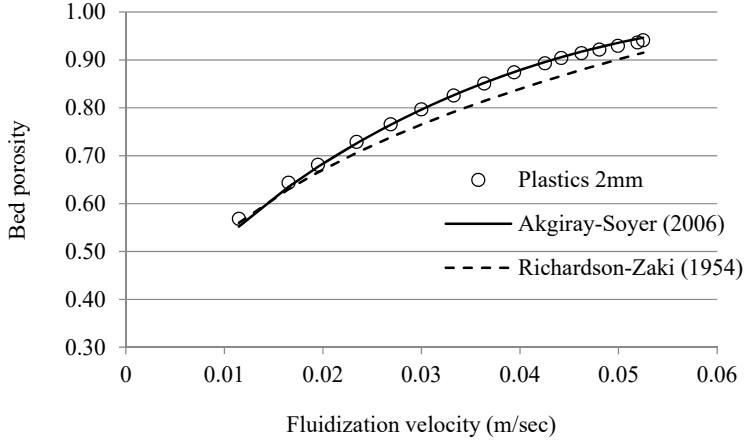


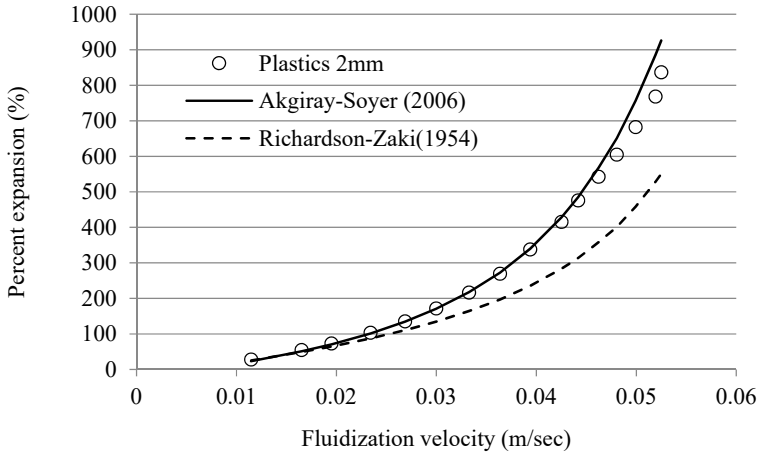
Appendix I-Figure 10 Percent expansion and bed porosity graphs of 4mm delrin beads



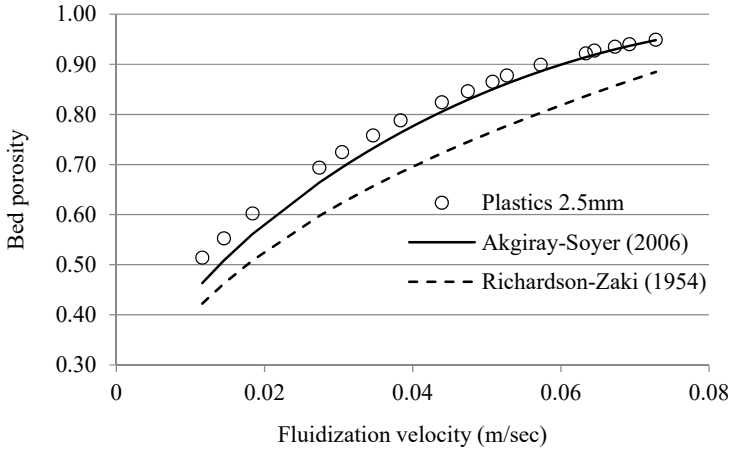


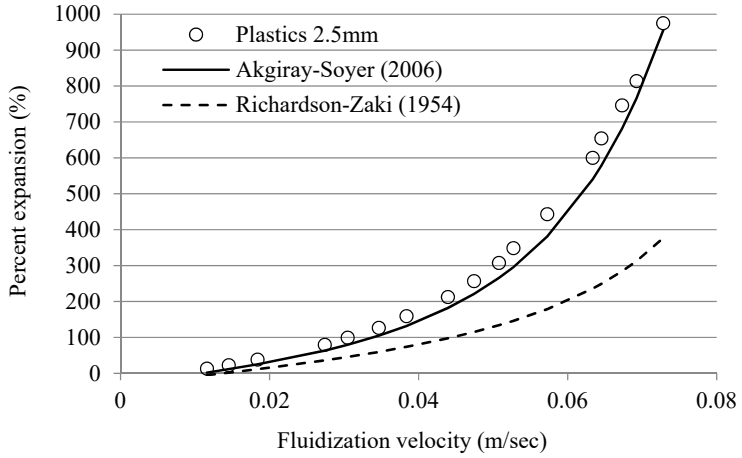
Appendix I-Figure 11 Percent expansion and bed porosity graphs of 4.8mm delrin beads



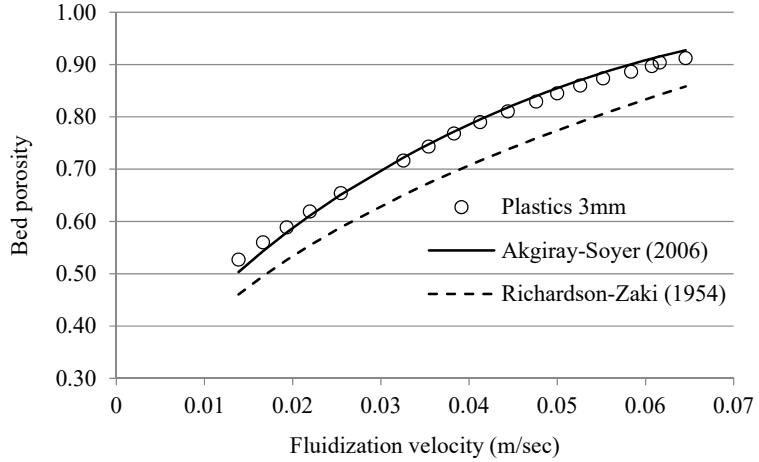


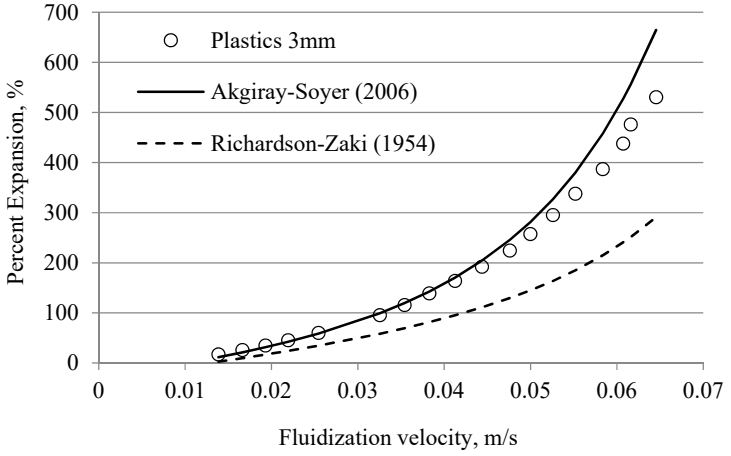
Appendix I-Figure 12 Percent expansion and bed porosity graphs of 2mm plastics beads



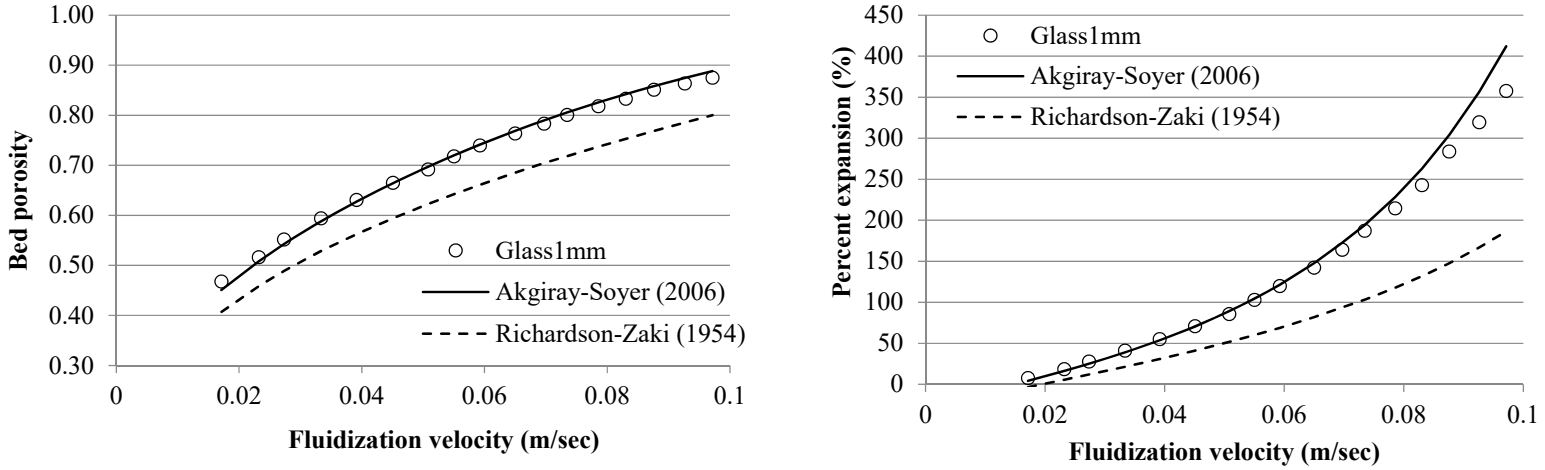


Appendix I-Figure 13 Percent expansion and bed porosity graphs of 2.5mm plastics beads

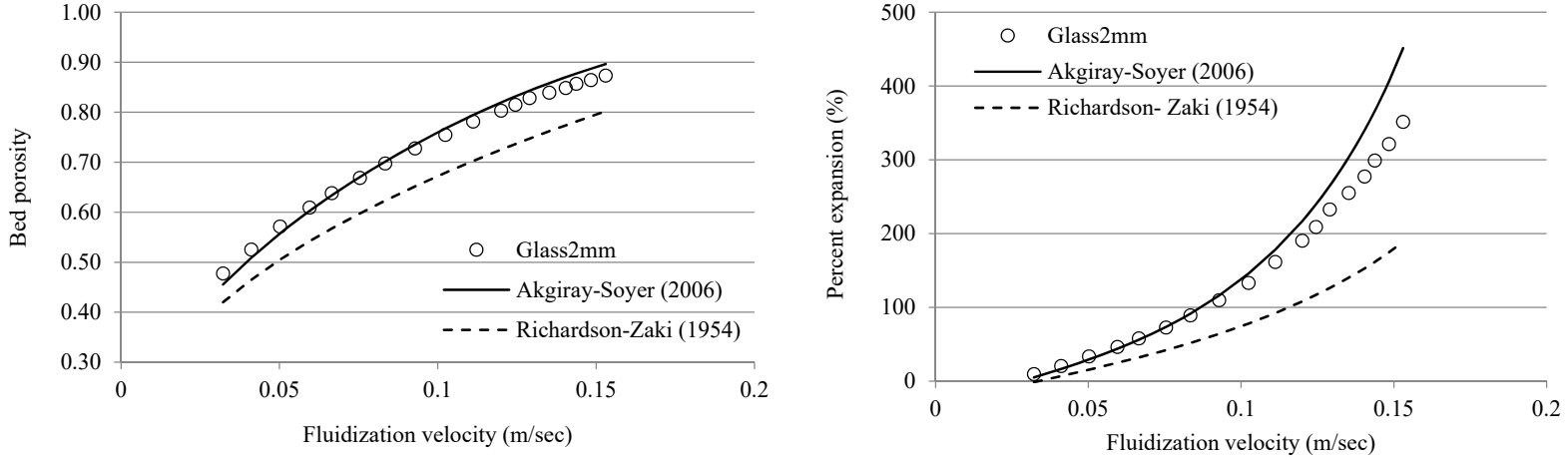




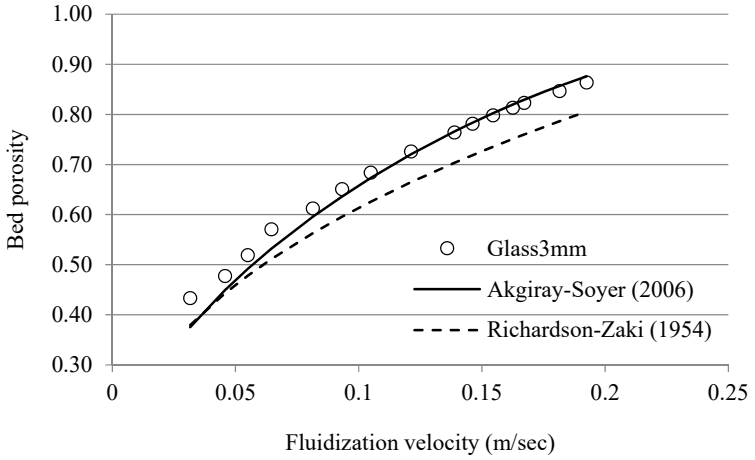
Appendix I-Figure 14 Percent expansion and bed porosity graphs of 3mm plastics beads

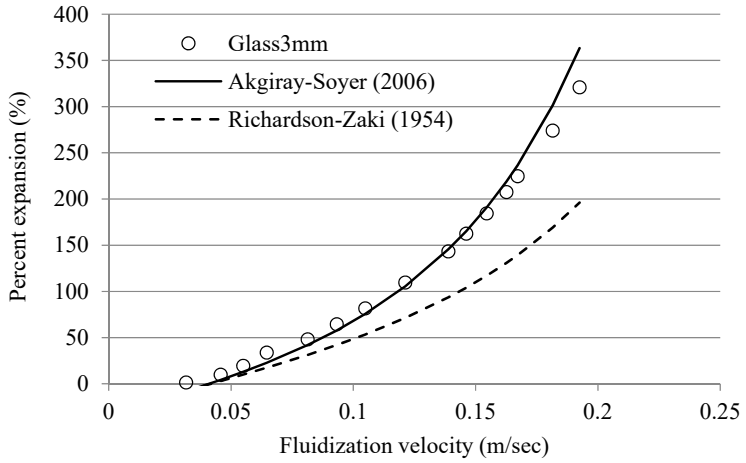


Appendix I-Figure 15 Percent expansion and bed porosity graphs of 1mm glass beads

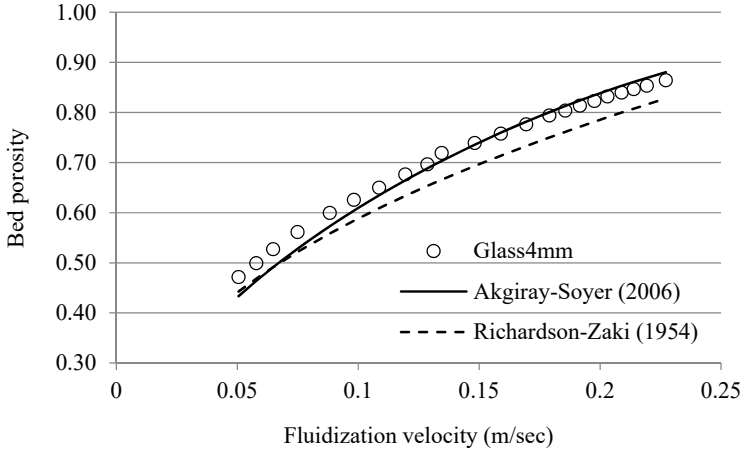


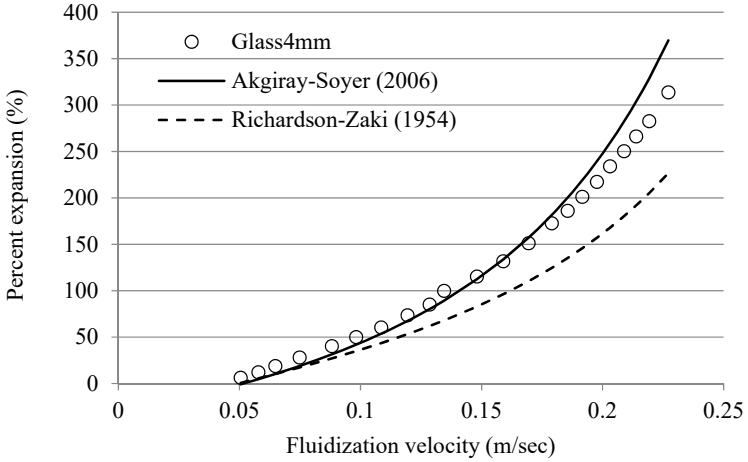
Appendix I-Figure 16 Percent expansion and bed porosity graphs of 2mm glass beads



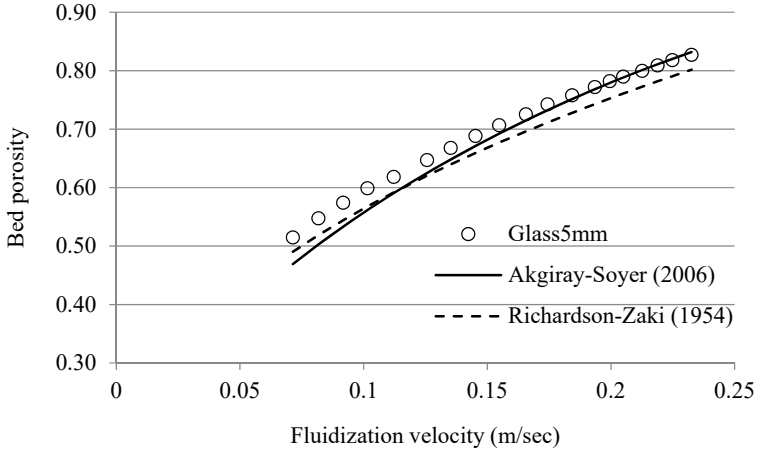


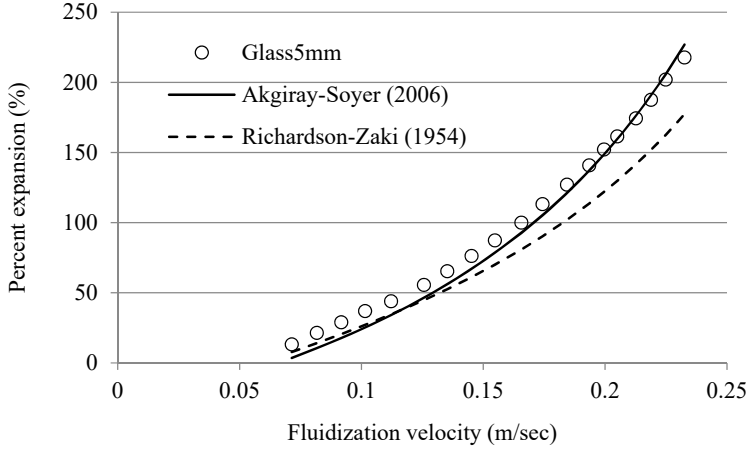
Appendix I-Figure 17 Percent expansion and bed porosity graphs of 3mm glass beads



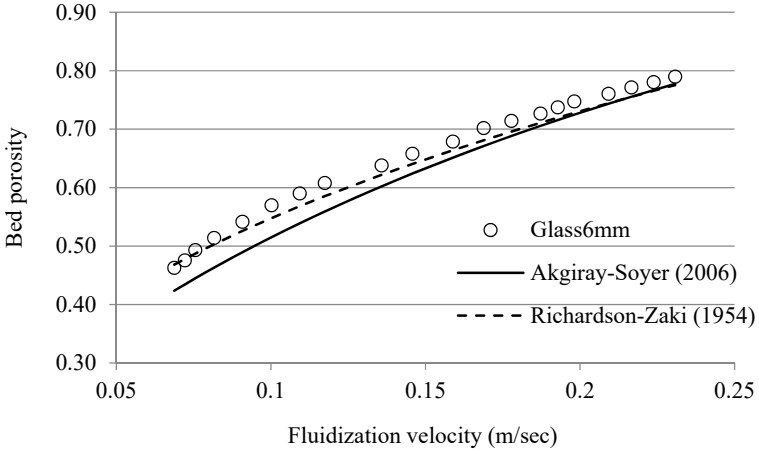


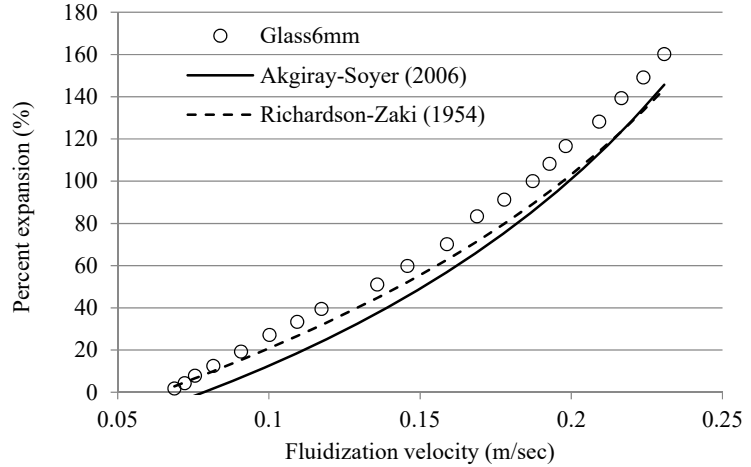
Appendix I-Figure 18 Percent expansion and bed porosity graphs of 4mm glass beads





Appendix I-Figure 19 Percent expansion and bed porosity graphs of 5mm glass beads

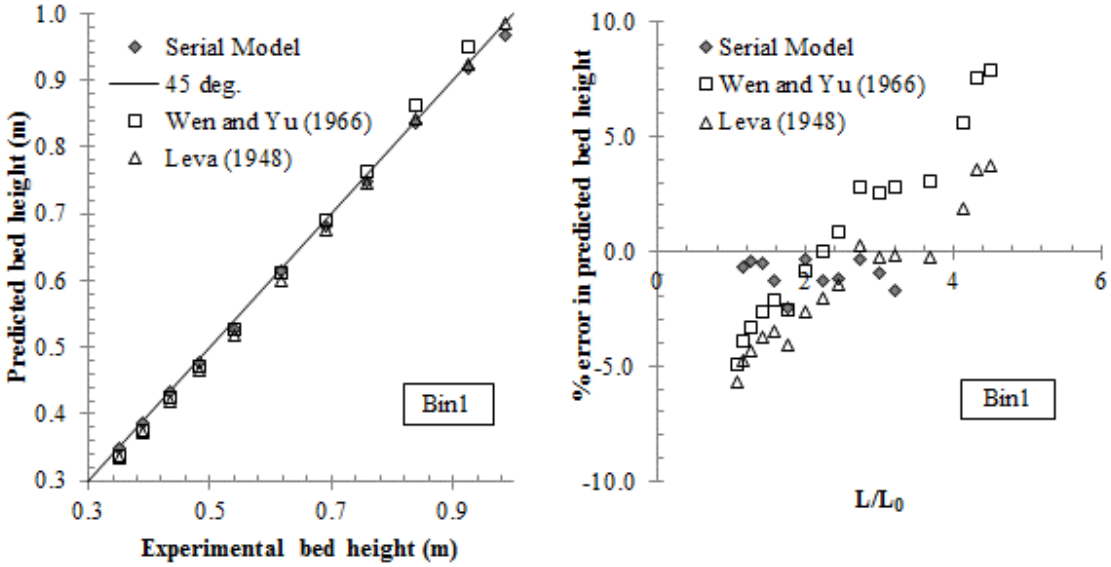




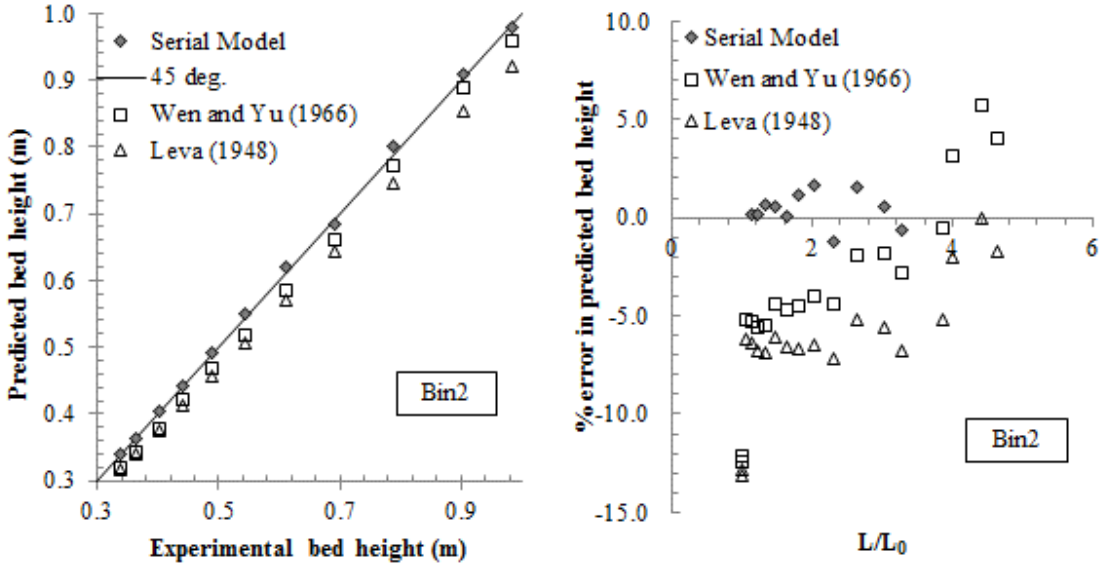
Appendix I-Figure 20 Percent expansion and bed porosity graphs of 6mm glass bead

APPENDIX II

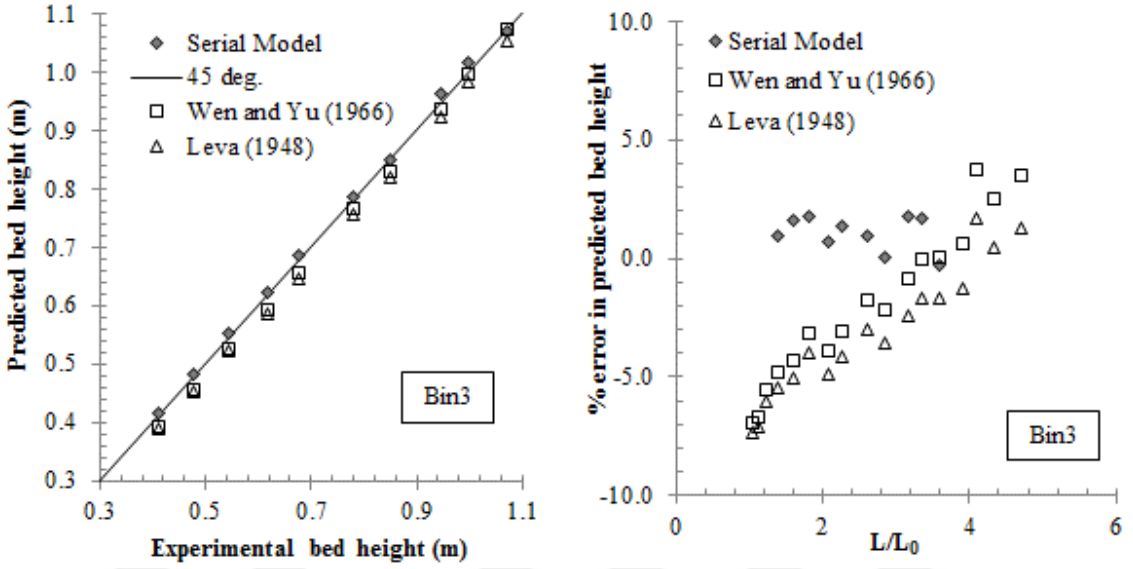
Fluidization graphs of Binary Mixtures of Spherical Particles



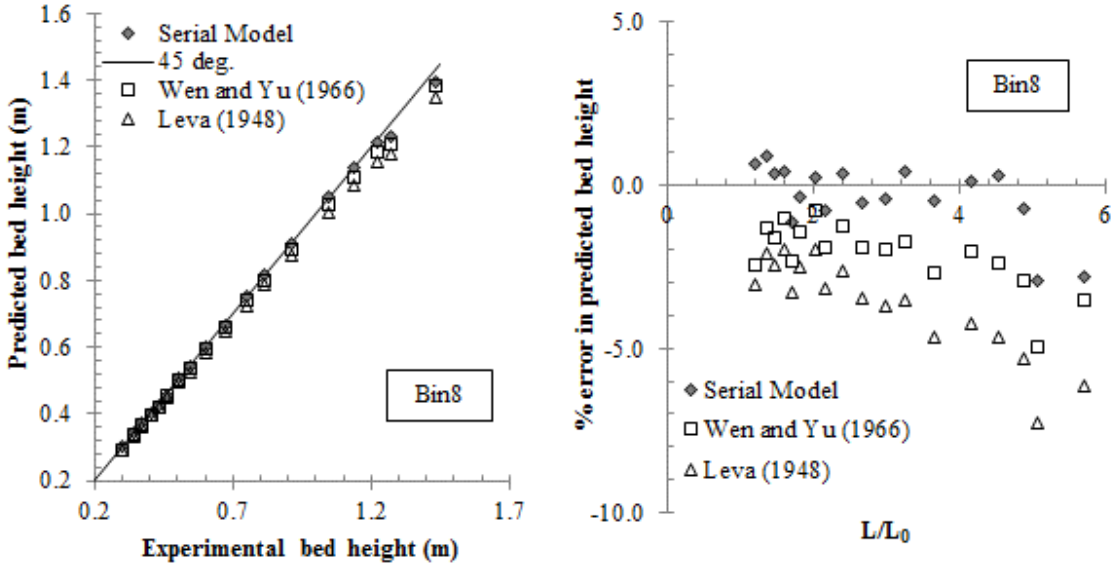
Appendix II-Figure 1 Results of fluidization experiment of binary mixture 1



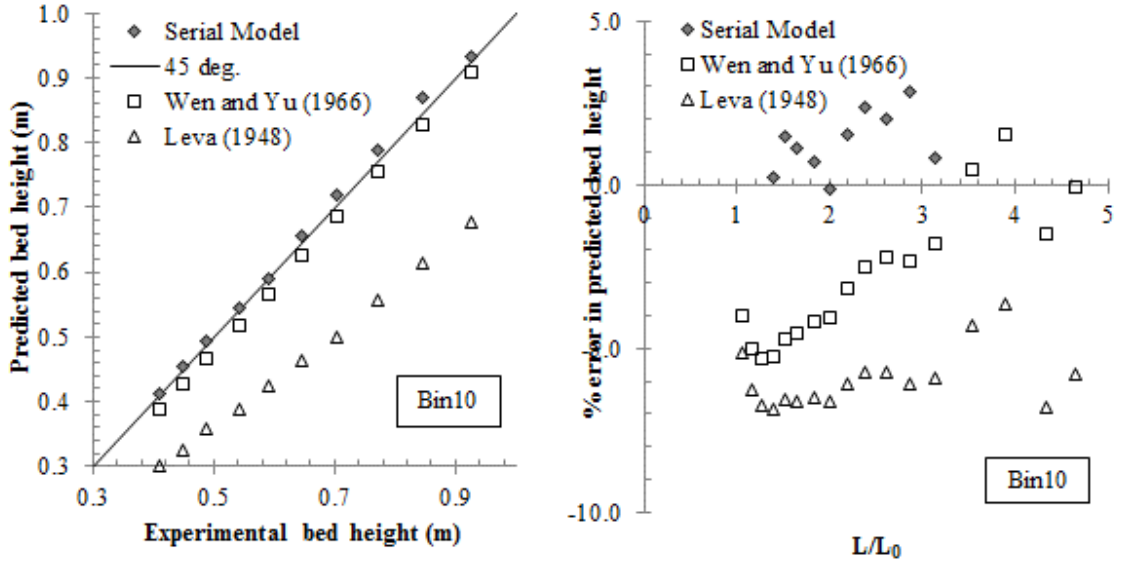
Appendix II-Figure 2 Results of fluidization experiment of binary mixture 2



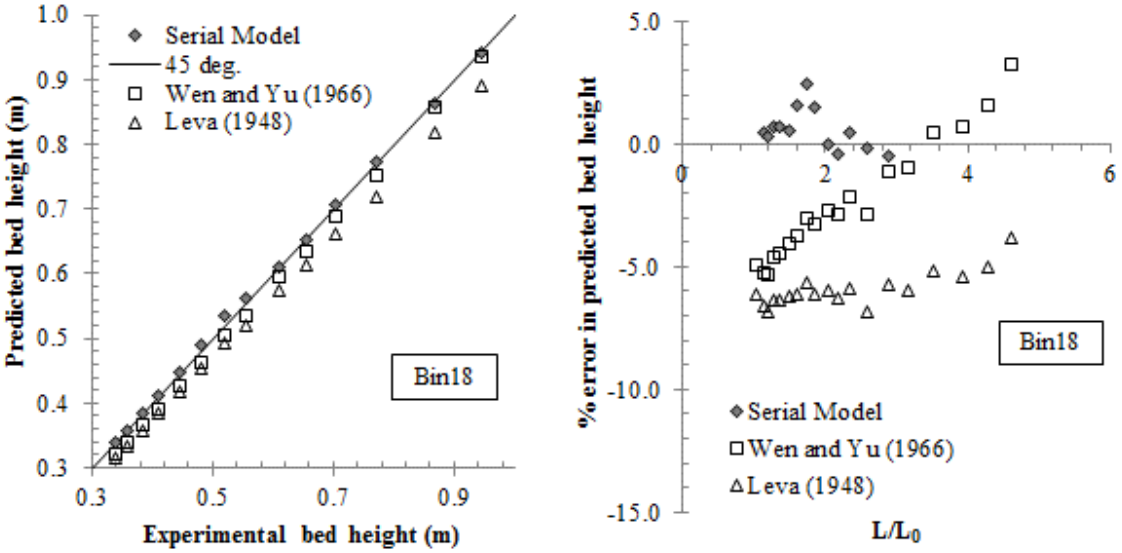
Appendix II-Figure 3 Results of fluidization experiment of binary mixture 3



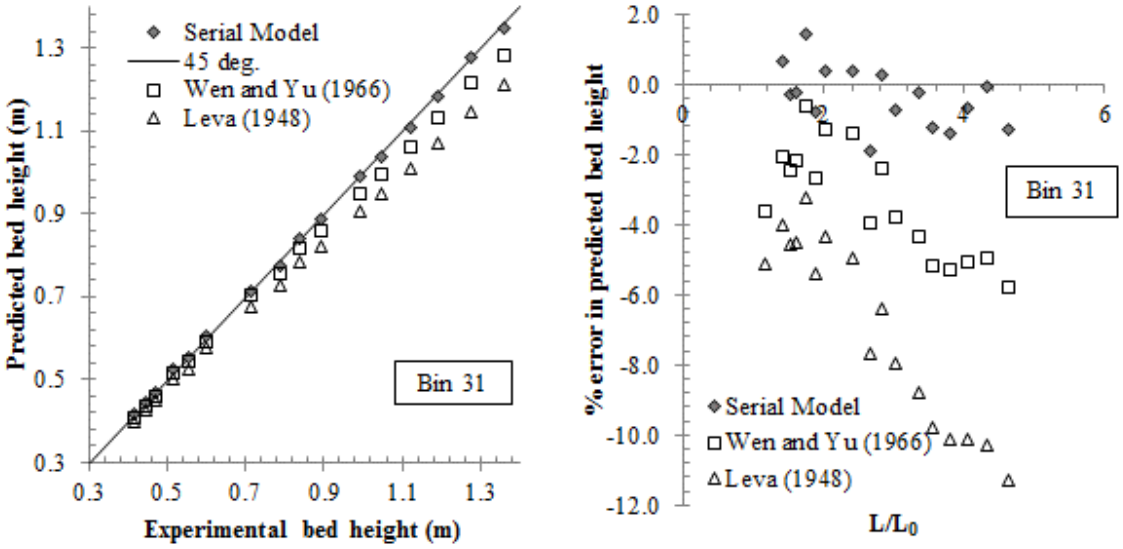
Appendix II-Figure 4 Results of fluidization experiment of binary mixture 8



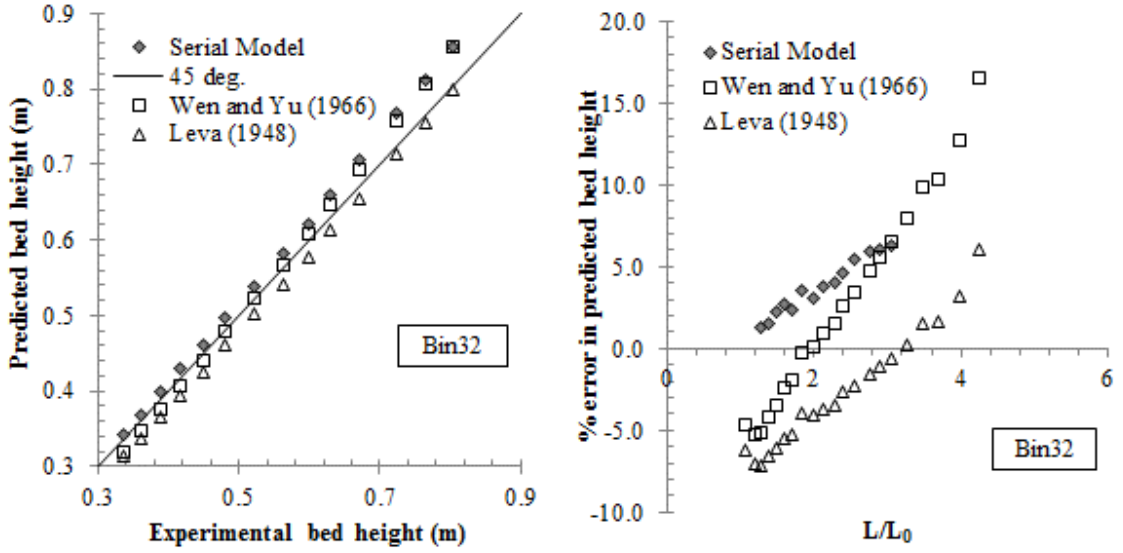
Appendix II-Figure 5 Results of fluidization experiment of binary mixture 10



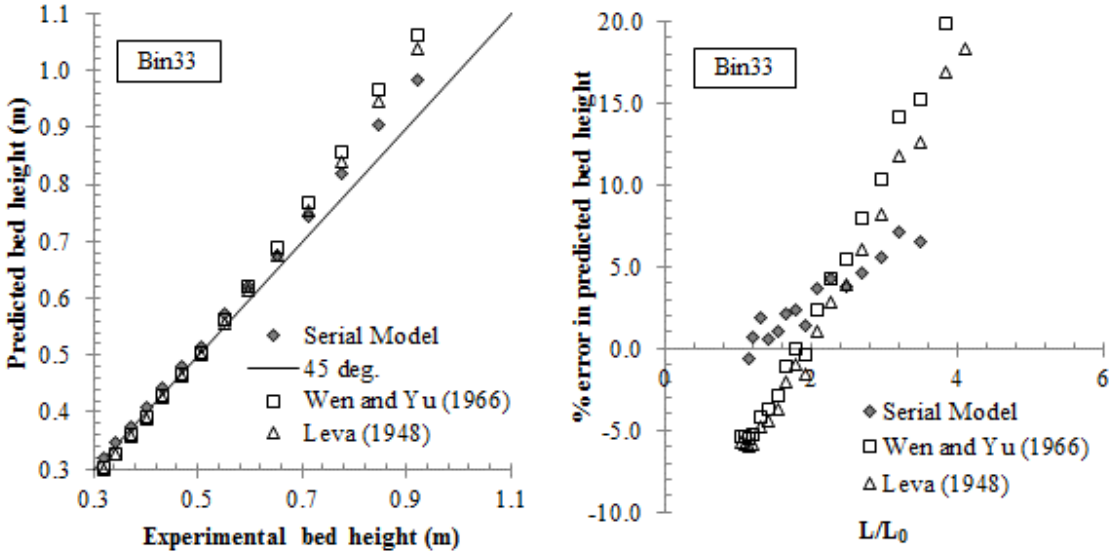
Appendix II-Figure 6 Results of fluidization experiment of binary mixture 18



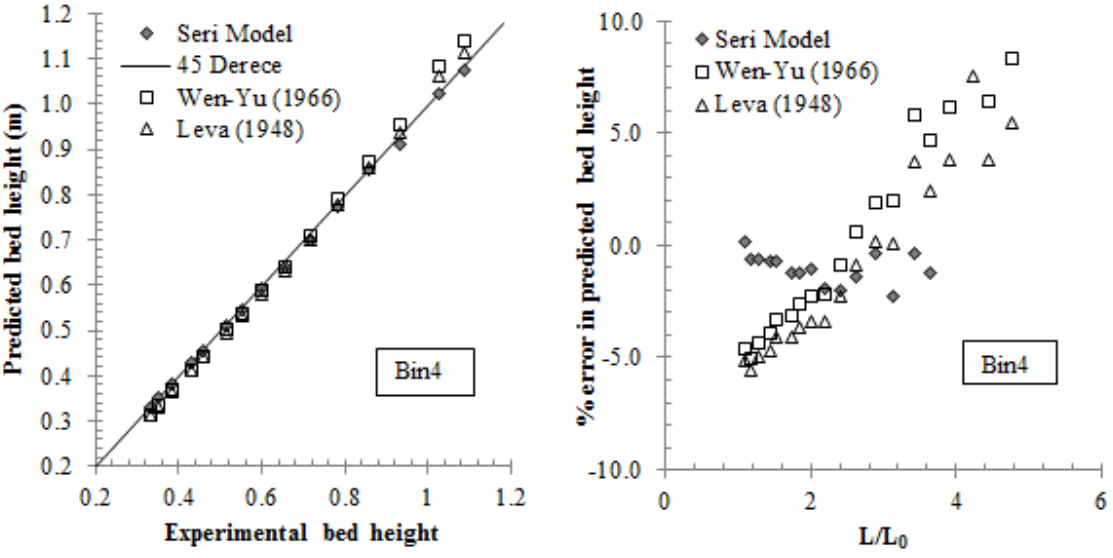
Appendix II-Figure 7 Results of fluidization experiment of binary mixture 31



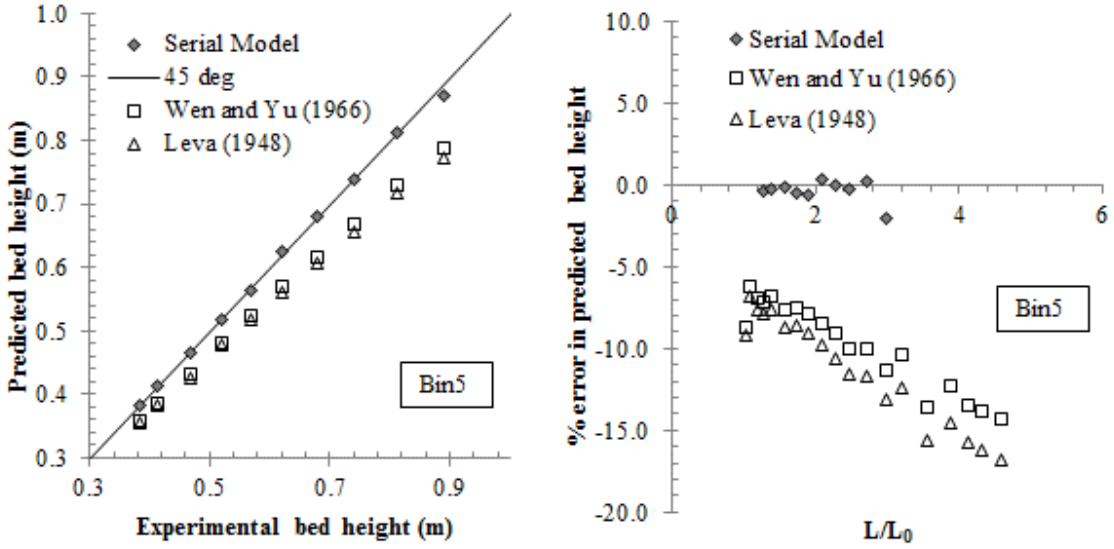
Appendix II-Figure 8 Results of fluidization experiment of binary mixture 32



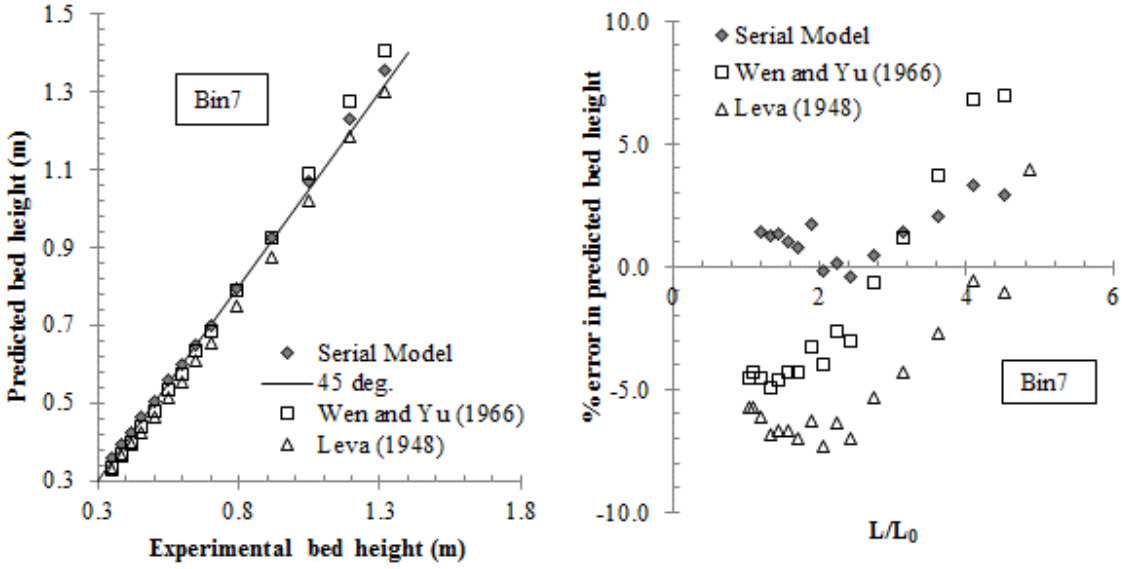
Appendix II-Figure 9 Results of fluidization experiment of binary mixture 33



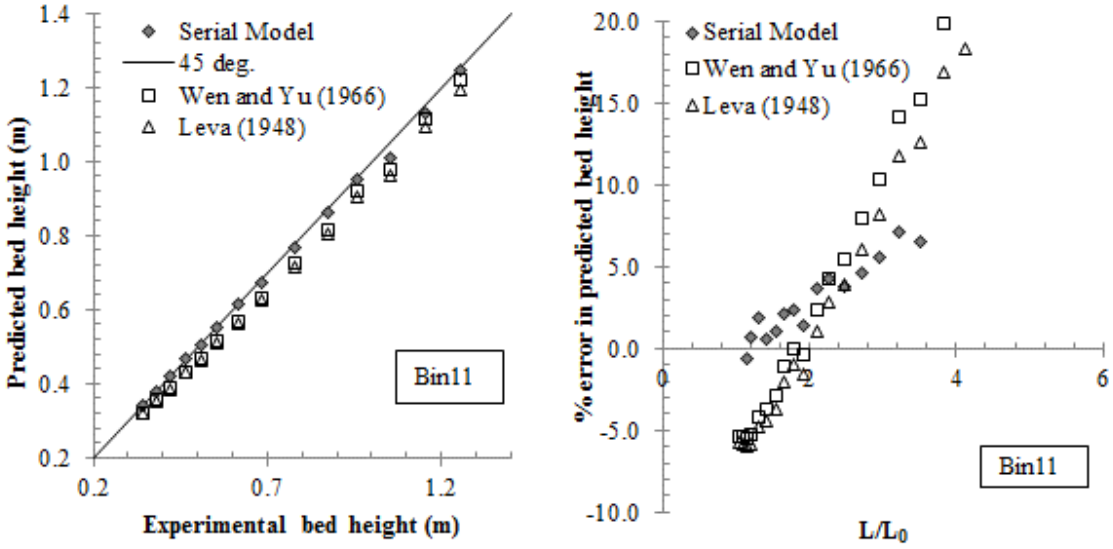
Appendix II-Figure 10 Results of fluidization experiment of binary mixture 4



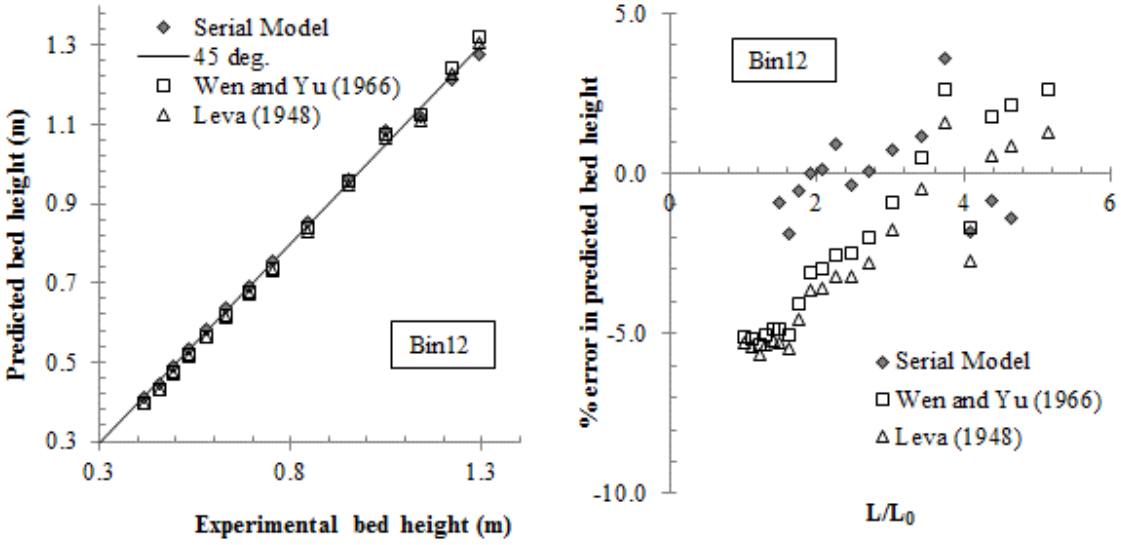
Appendix II-Figure 11 Results of fluidization experiment of binary mixture 5



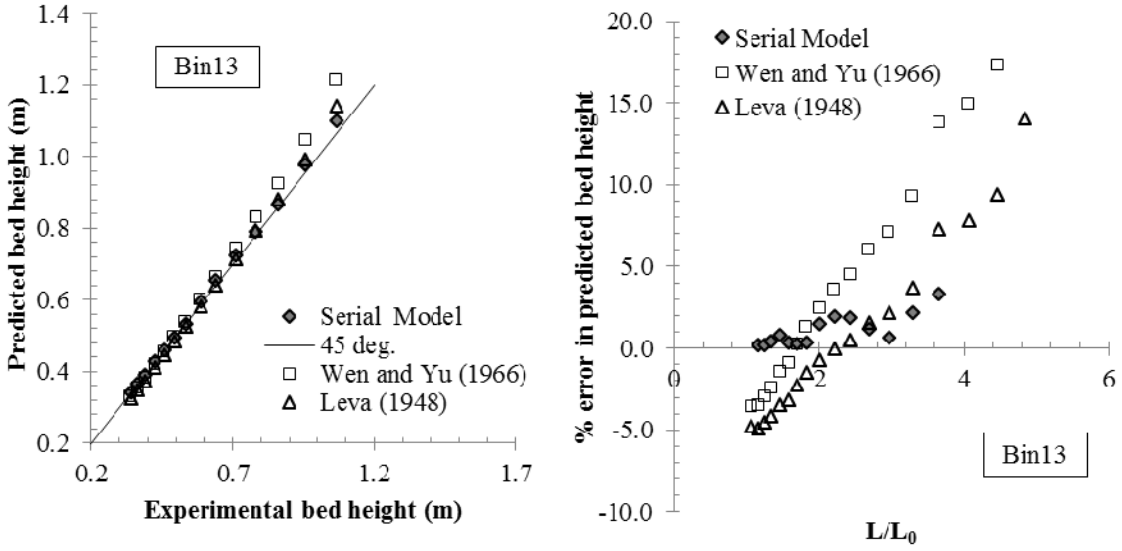
Appendix II-Figure 12 Results of fluidization experiment of binary mixture 7



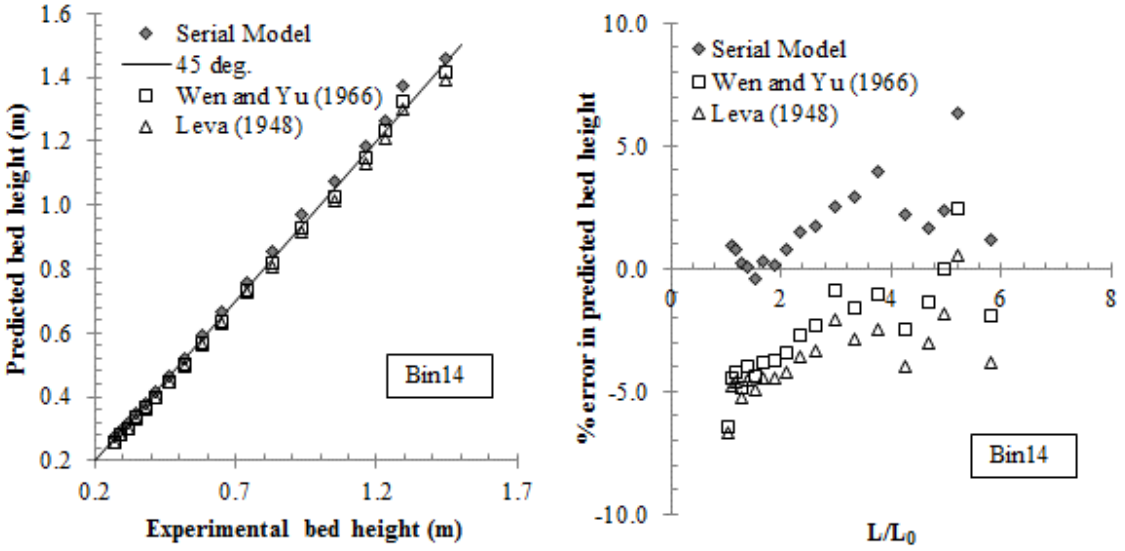
Appendix II-Figure 13 Results of fluidization experiment of binary mixture 11



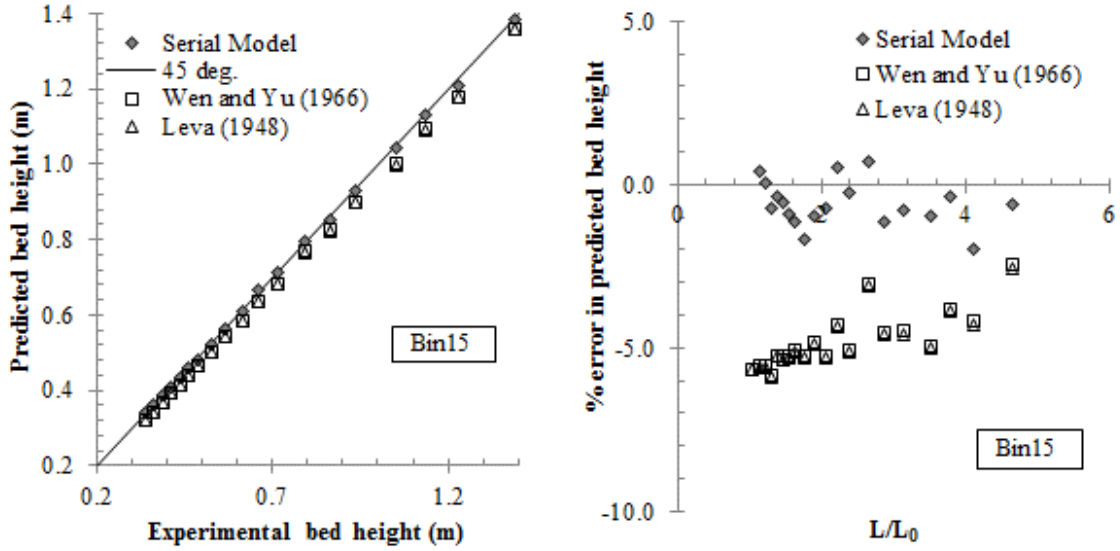
Appendix II-Figure 14 Results of fluidization experiment of binary mixture 12



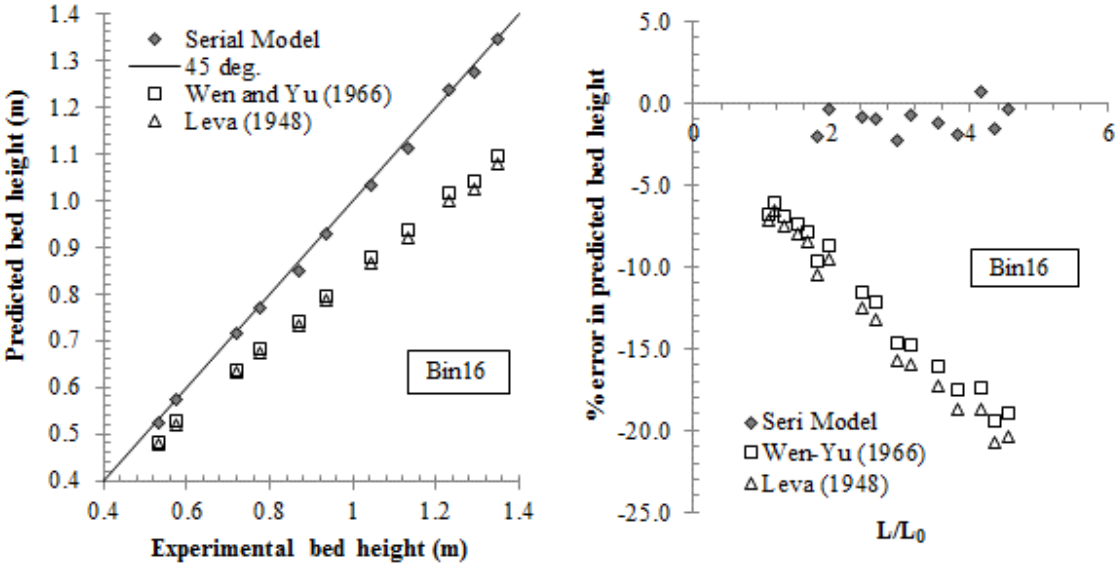
Appendix II-Figure 15 Results of fluidization experiment of binary mixture 13



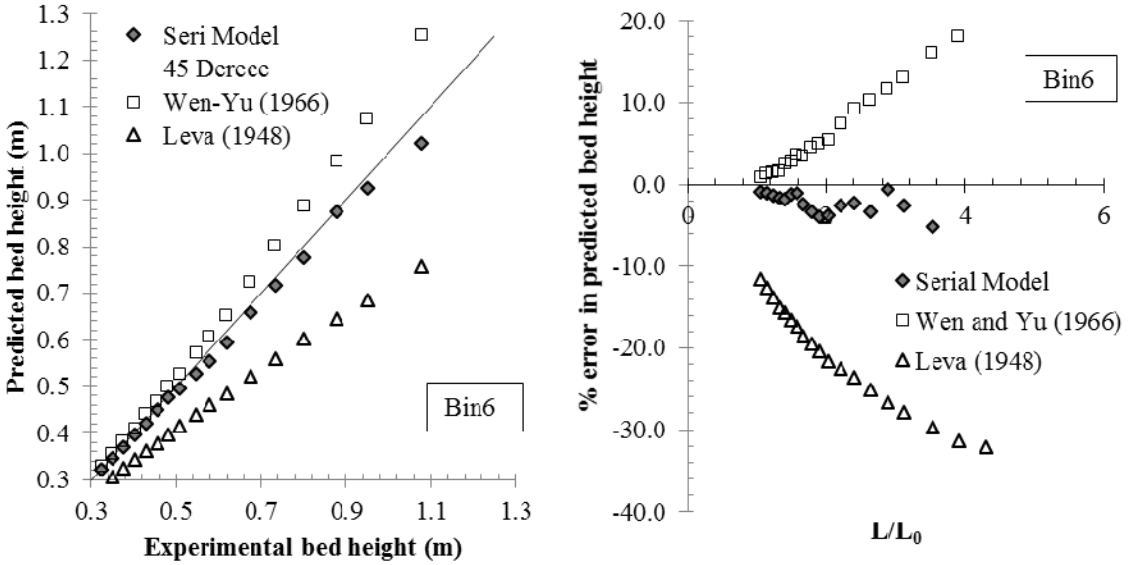
Appendix II-Figure 16 Results of fluidization experiment of binary mixture 14



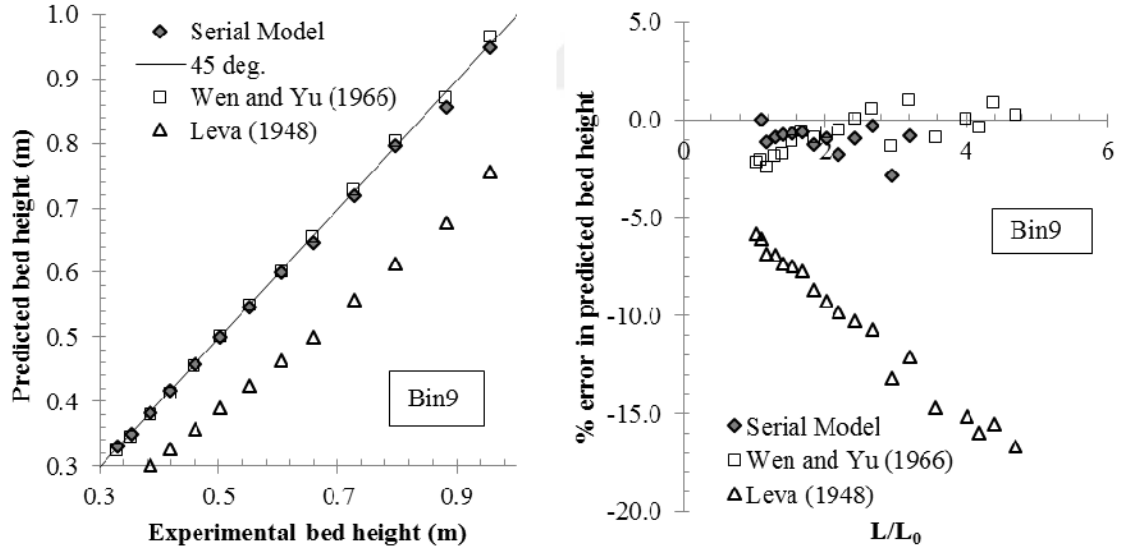
Appendix II-Figure 17 Results of fluidization experiment of binary mixture 15



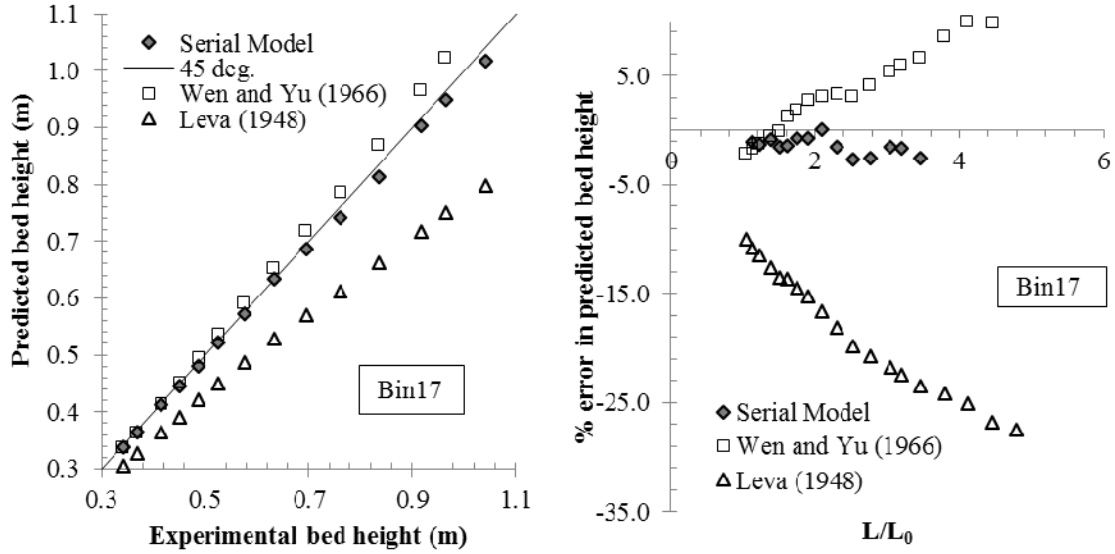
Appendix II-Figure 18 Results of fluidization experiment of binary mixture 16



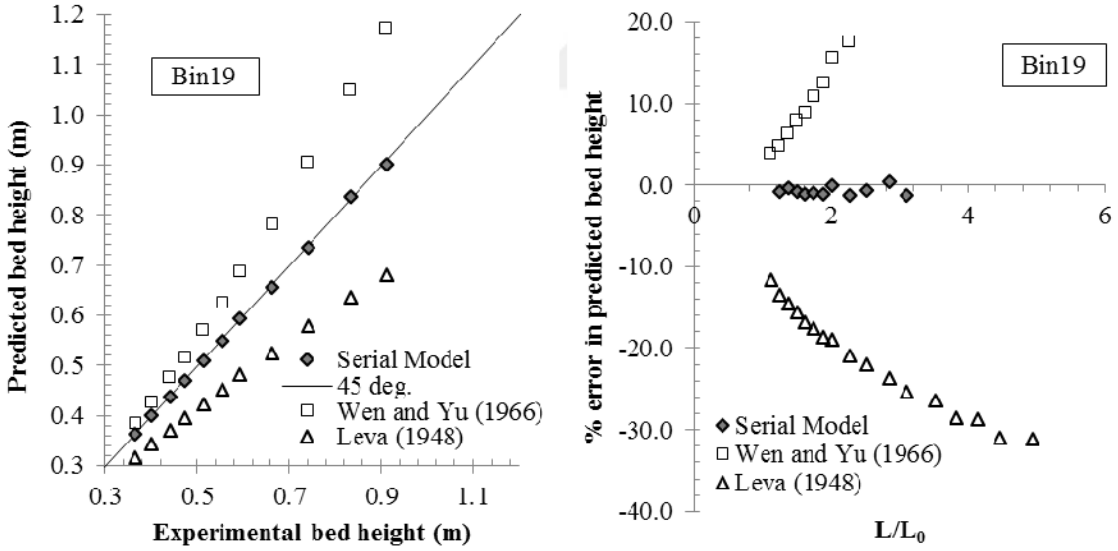
Appendix II-Figure 19 Results of fluidization experiment of binary mixture 6



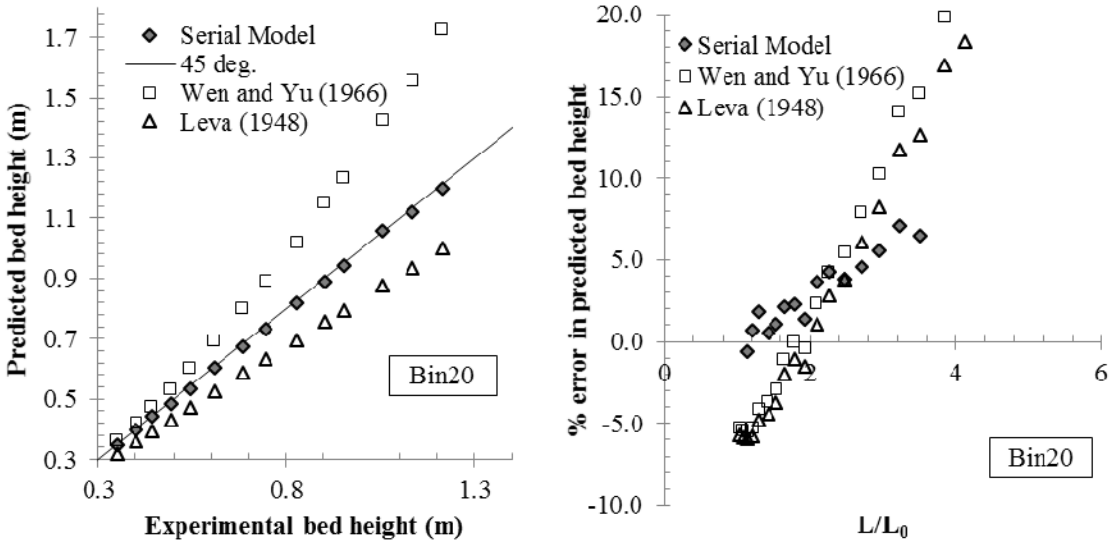
Appendix II-Figure 20 Results of fluidization experiment of binary mixture 9



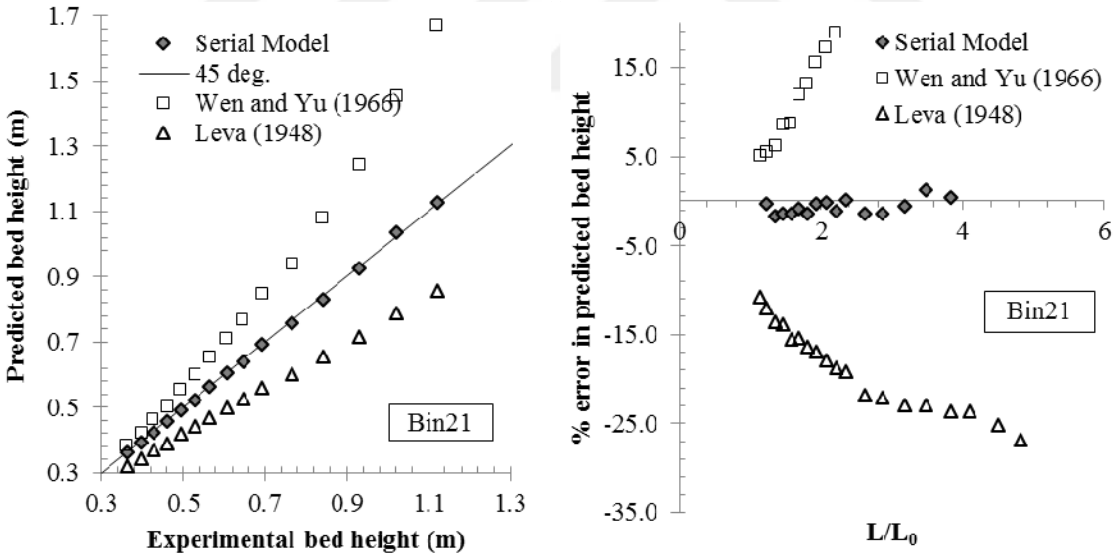
Appendix II-Figure 21 Results of fluidization experiment of binary mixture 17



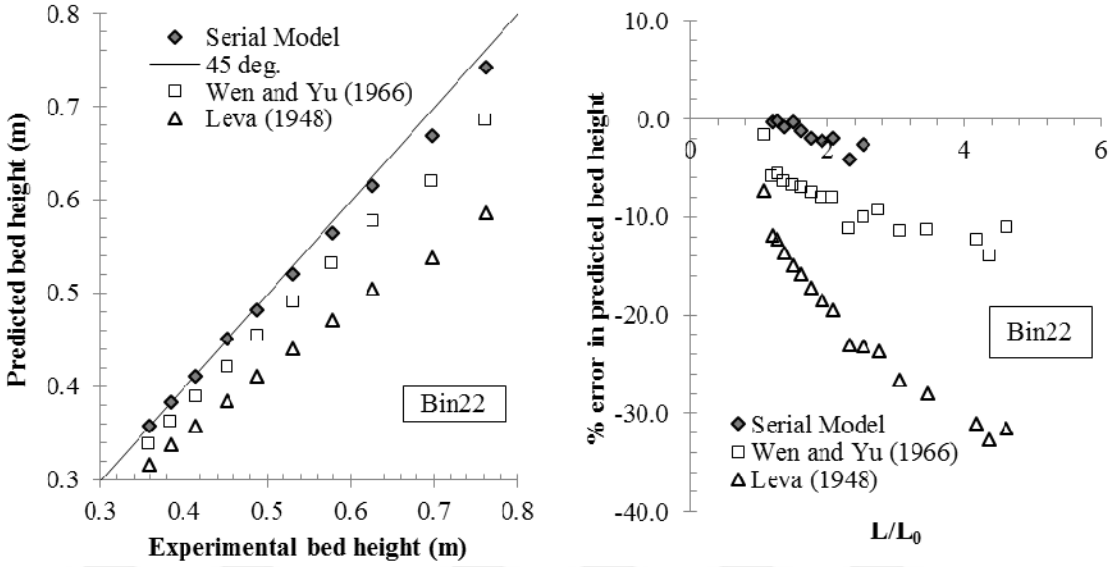
Appendix II-Figure 22 Results of fluidization experiment of binary mixture 19



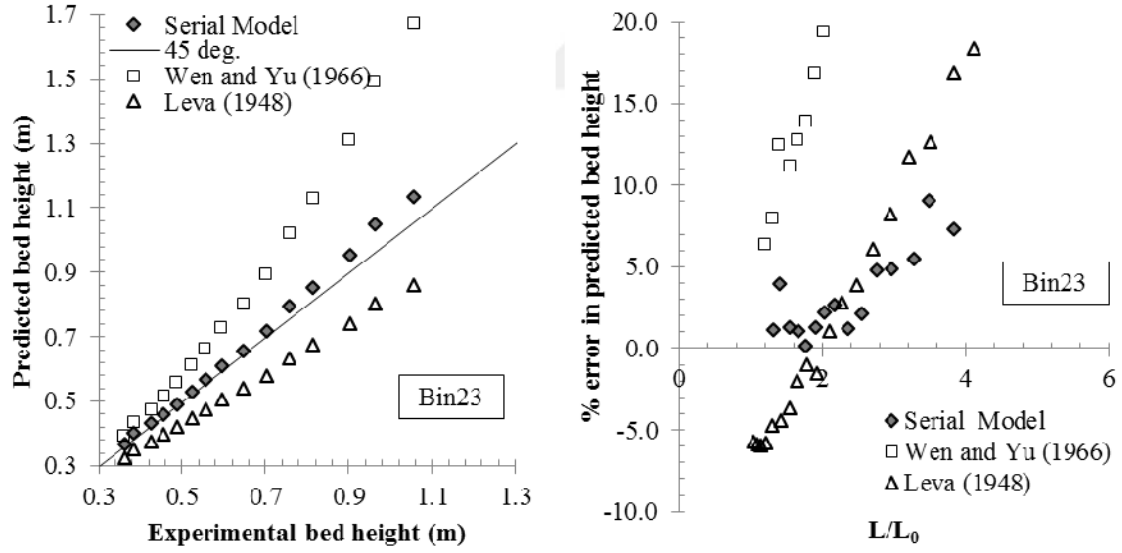
Appendix II-Figure 23 Results of fluidization experiment of binary mixture 20



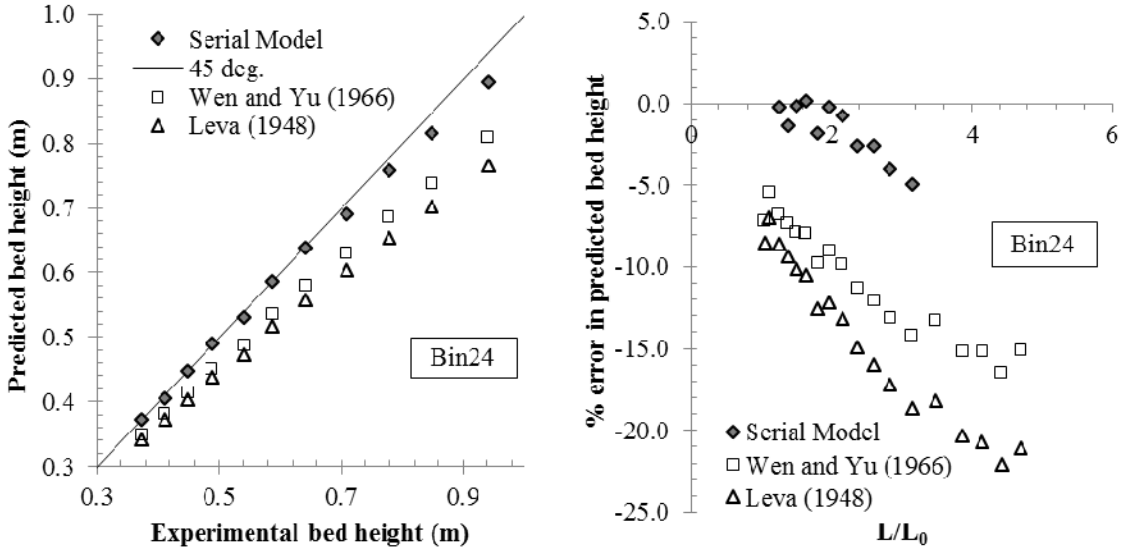
Appendix II-Figure 24 Results of fluidization experiment of binary mixture 21



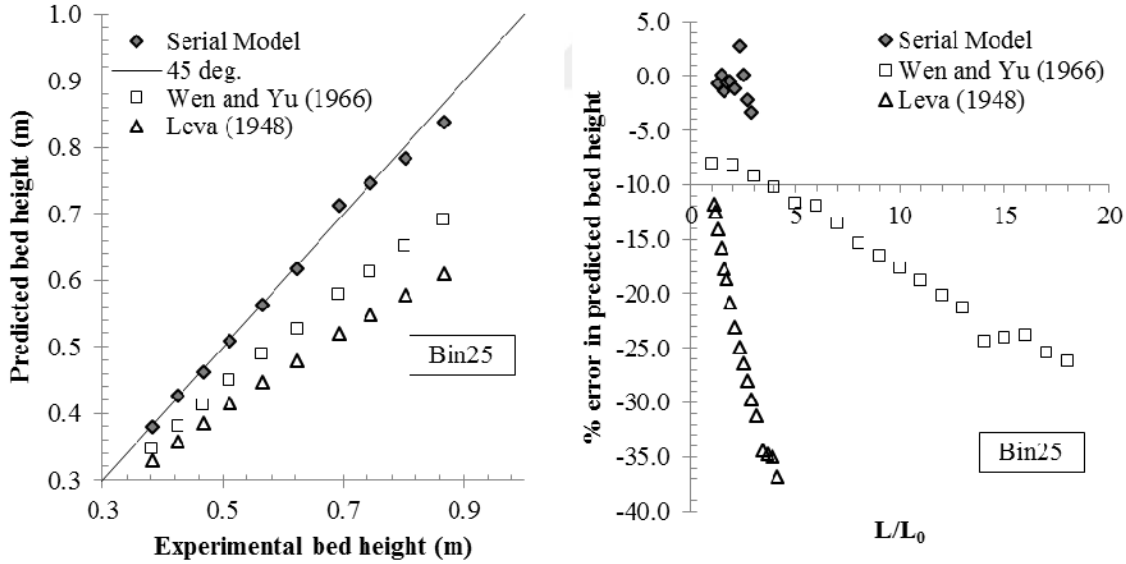
Appendix II-Figure 25 Results of fluidization experiment of binary mixture 22



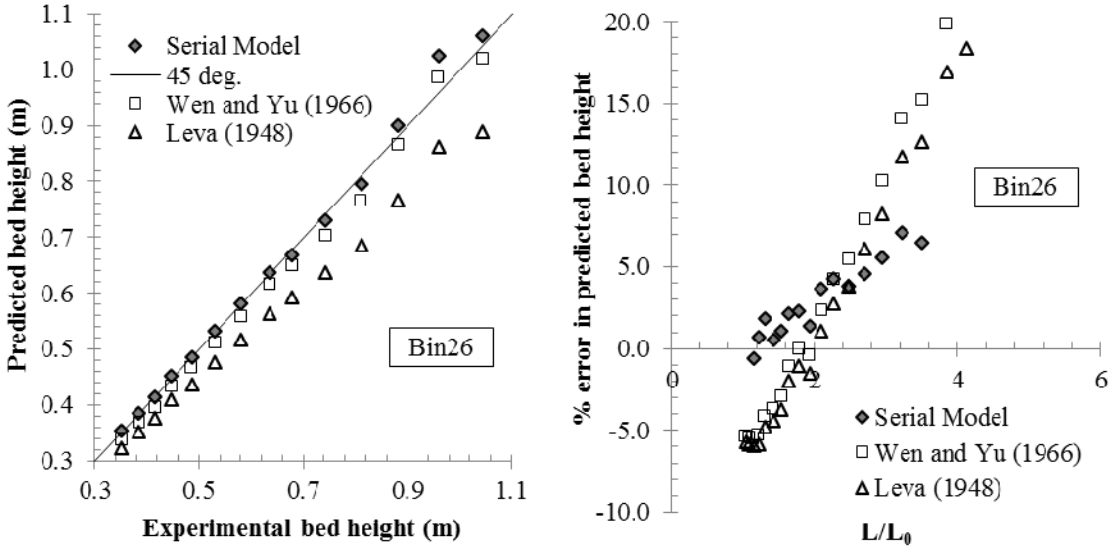
Appendix II-Figure 26 Results of fluidization experiment of binary mixture 23



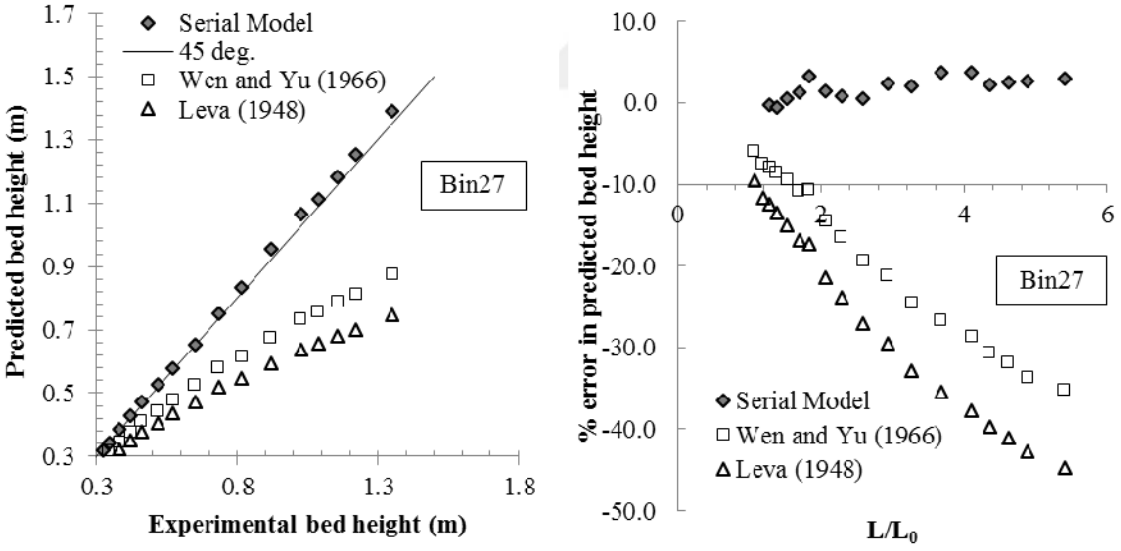
Appendix II-Figure 27 Results of fluidization experiment of binary mixture 24



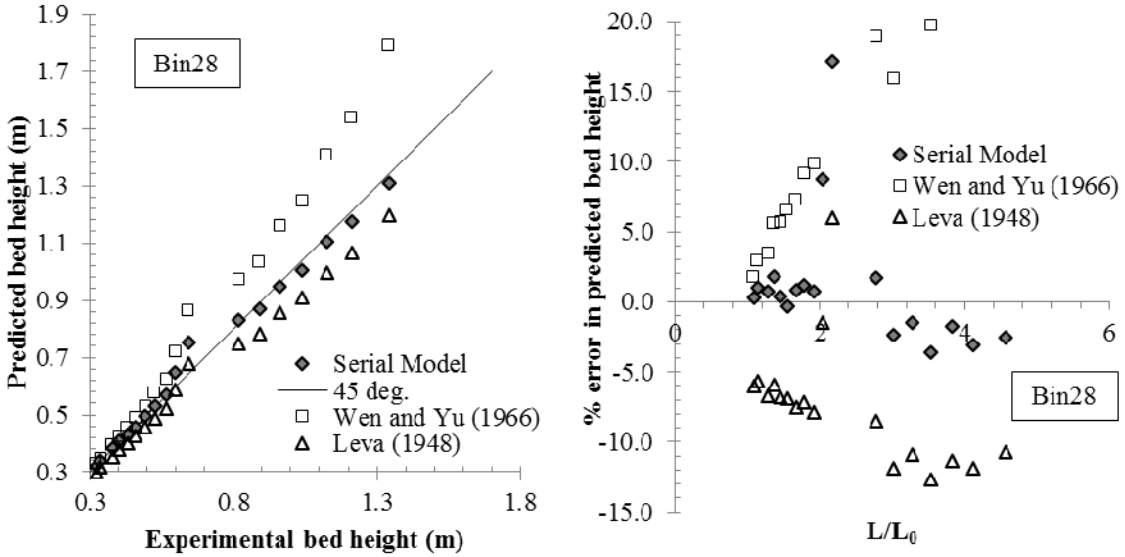
Appendix II-Figure 28 Results of fluidization experiment of binary mixture 25



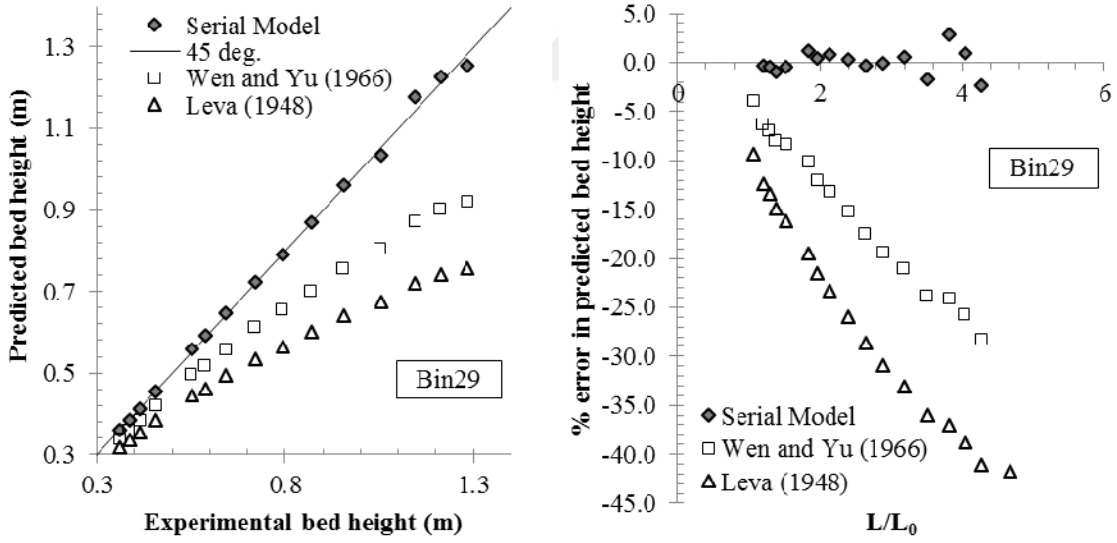
Appendix II-Figure 29 Results of fluidization experiment of binary mixture 26



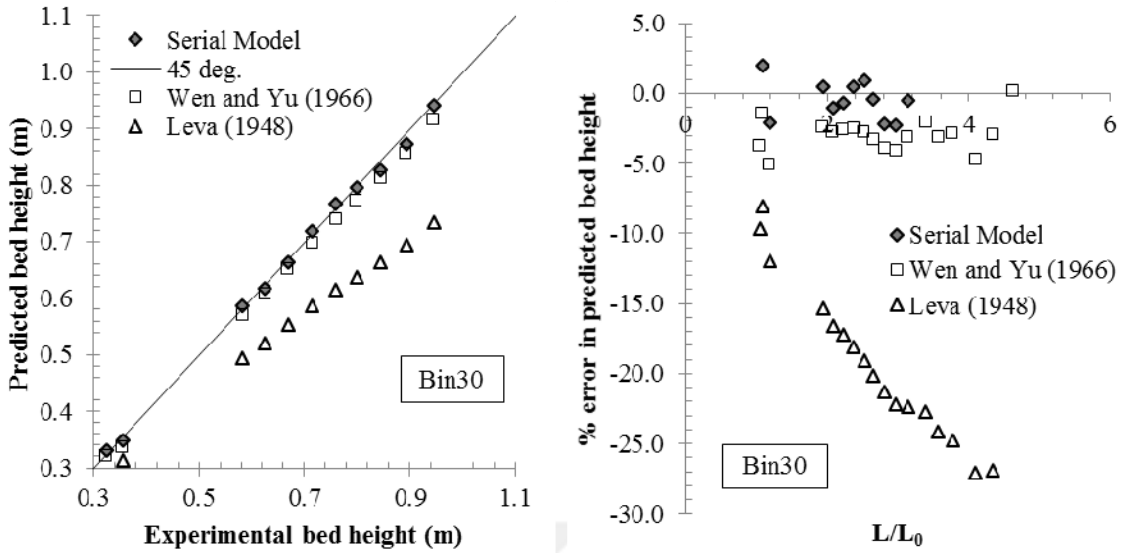
Appendix II-Figure 30 Results of fluidization experiment of binary mixture 27



Appendix II-Figure 31 Results of fluidization experiment of binary mixture 28



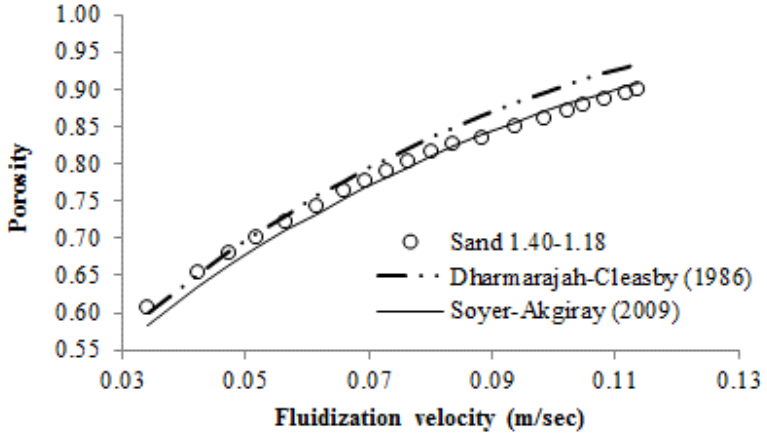
Appendix II-Figure 32 Results of fluidization experiment of binary mixture 29

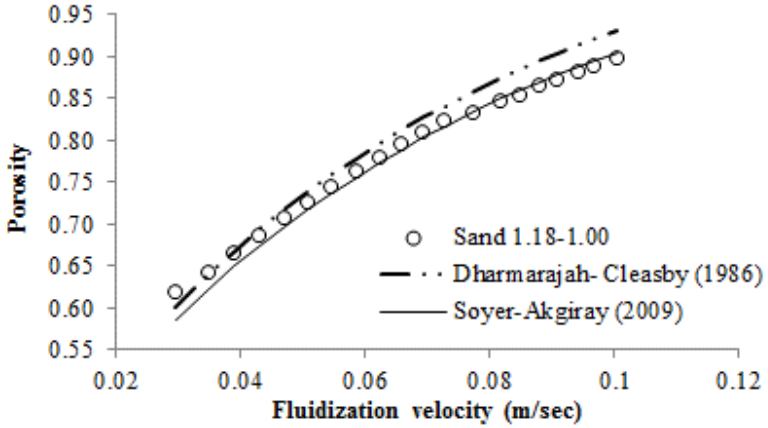


Appendix II-Figure 33 Results of fluidization experiment of binary mixture 30

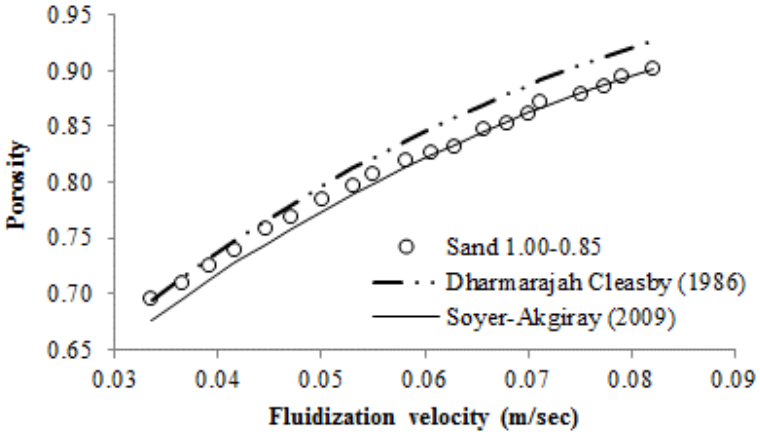
APPENDIX III

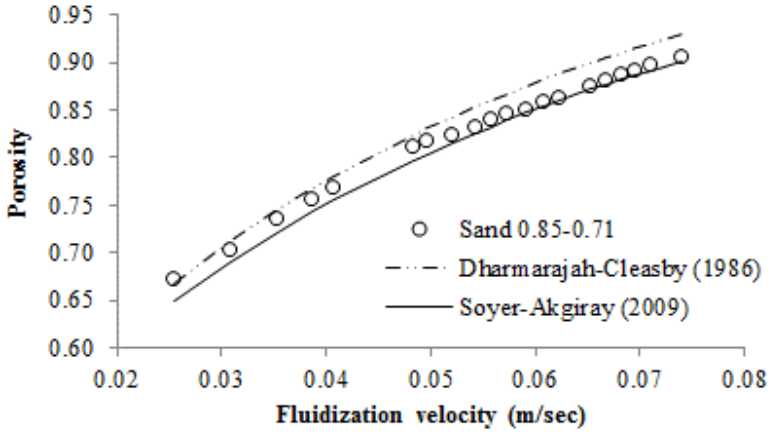
Fluidized Bed Porosity Graphs of Non-Spherical Particles



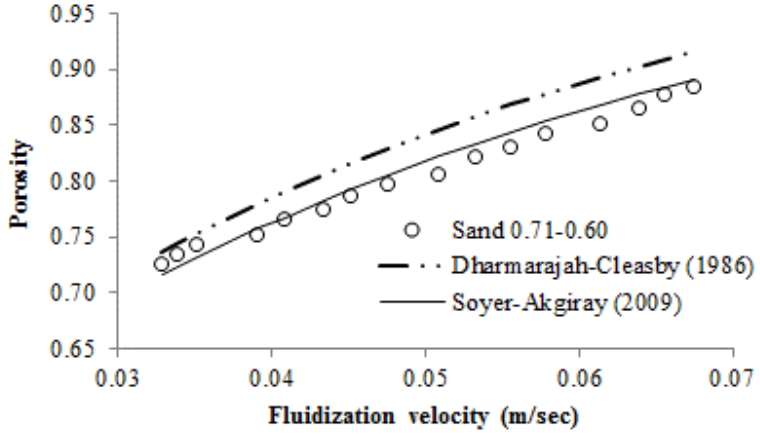


Appendix III-Figure 1 Fluidization graphs of 1.40-1.18 and 1.18-1.00 fractions of sand

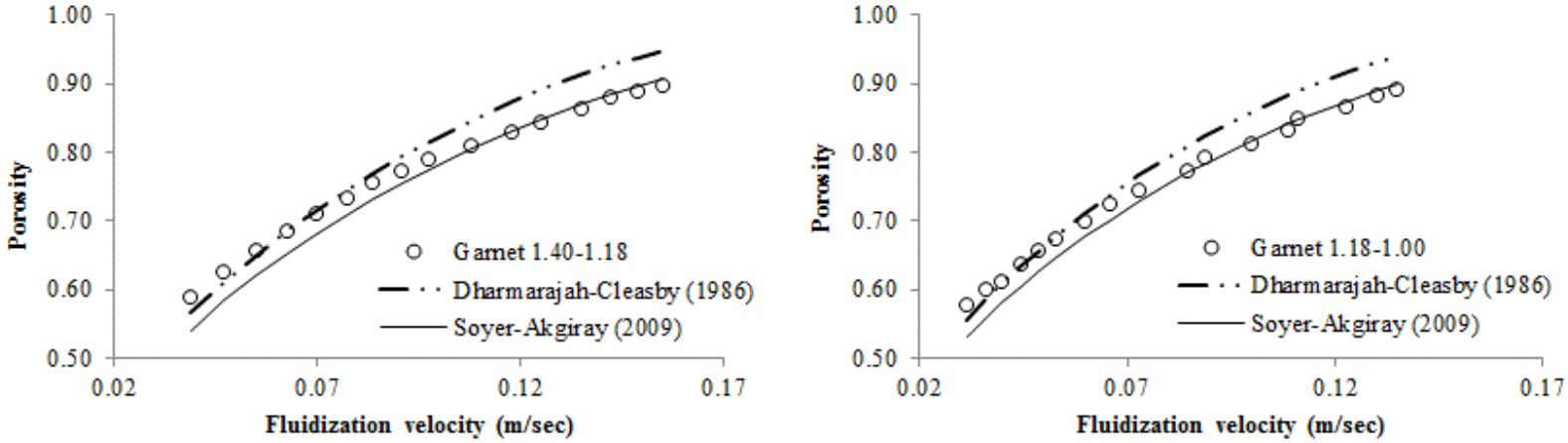




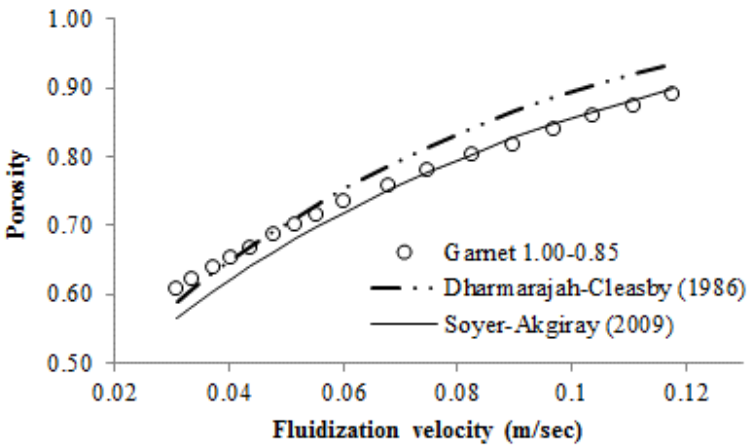
Appendix III-Figure 2 Fluidization graphs of 1.00-0.85 and 0.85-0.71 fractions of sand

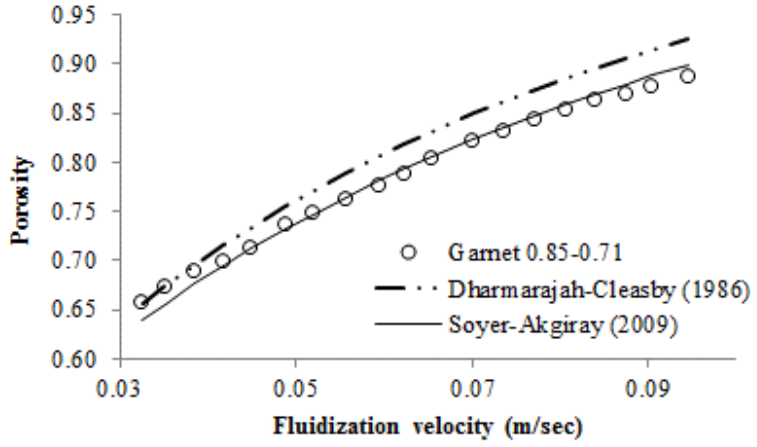


Appendix III-Figure 3 Fluidization graph of 0.71-0.60 fraction of sand

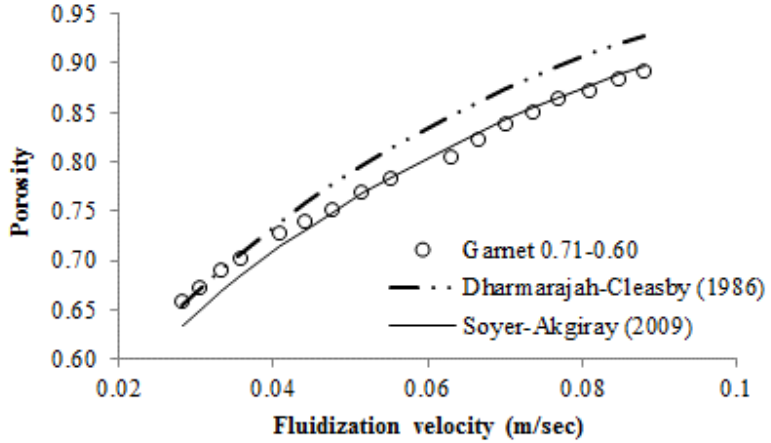


Appendix III-Figure 4 Fluidization graphs of 1.40-1.18 and 1.18-1.00 fractions of garnet

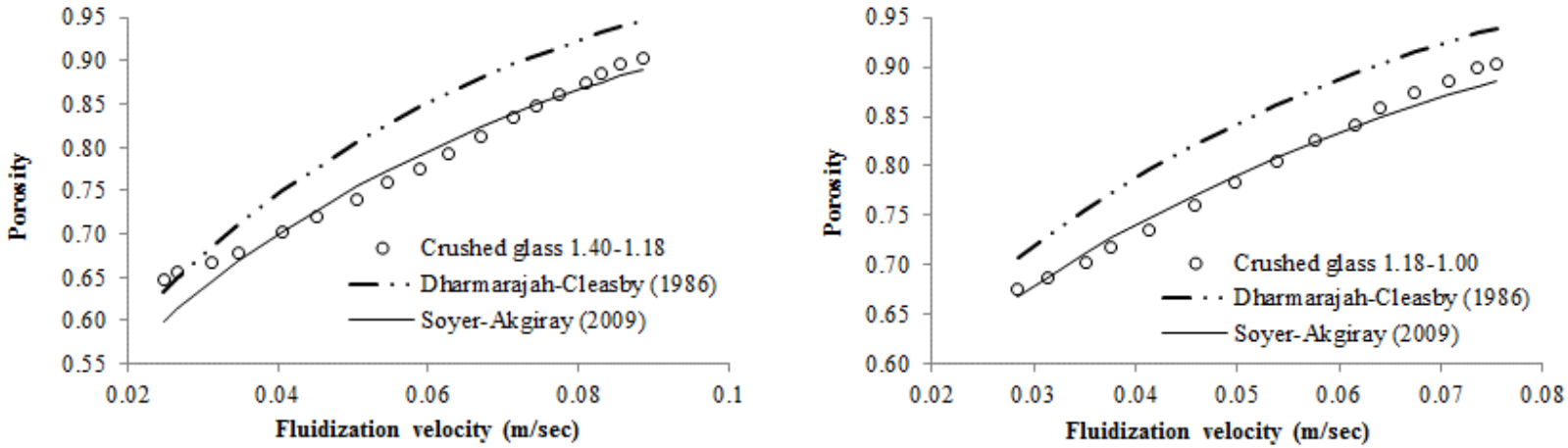




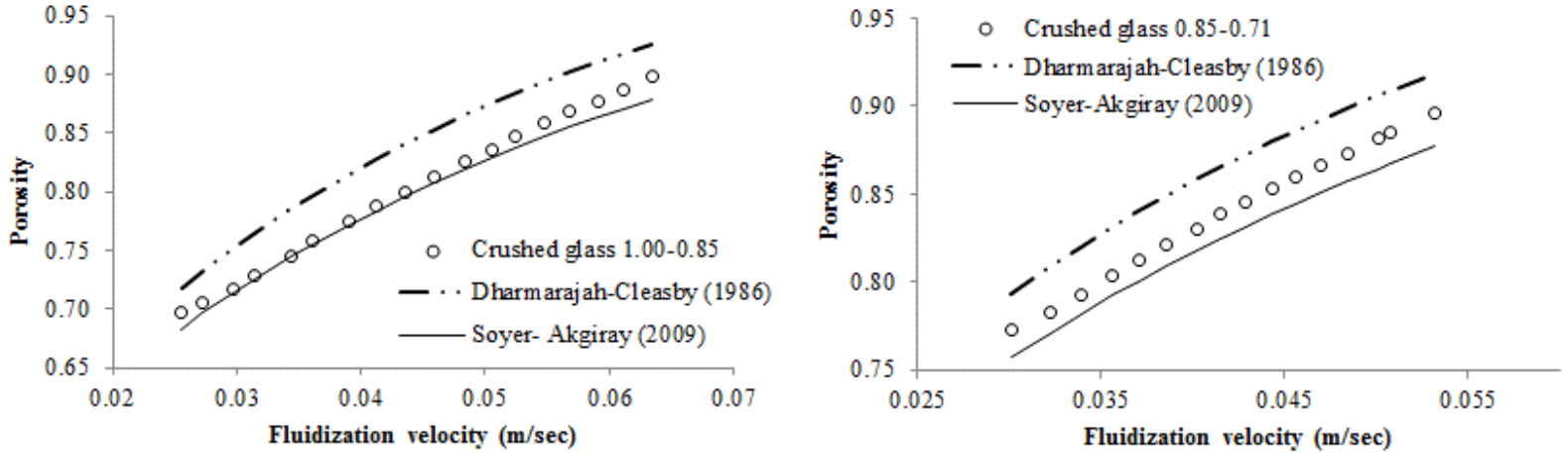
Appendix III-Figure 5 Fluidization graphs of 1.00-0.85 and 0.85-0.71 fractions of garnet



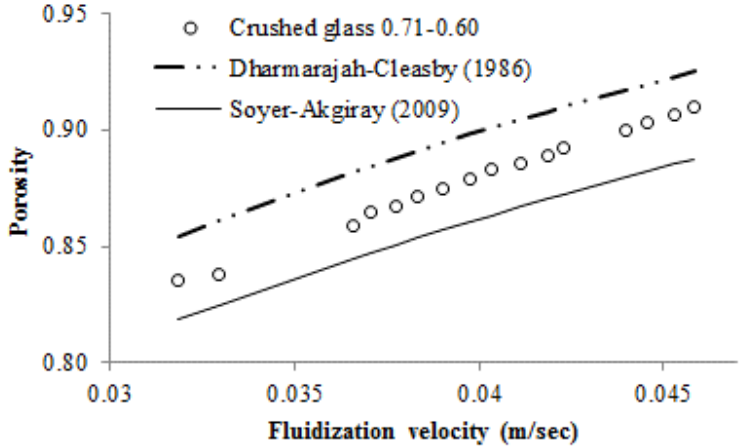
Appendix III-Figure 6 Fluidization graph of 0.71-0.60 fraction of garnet



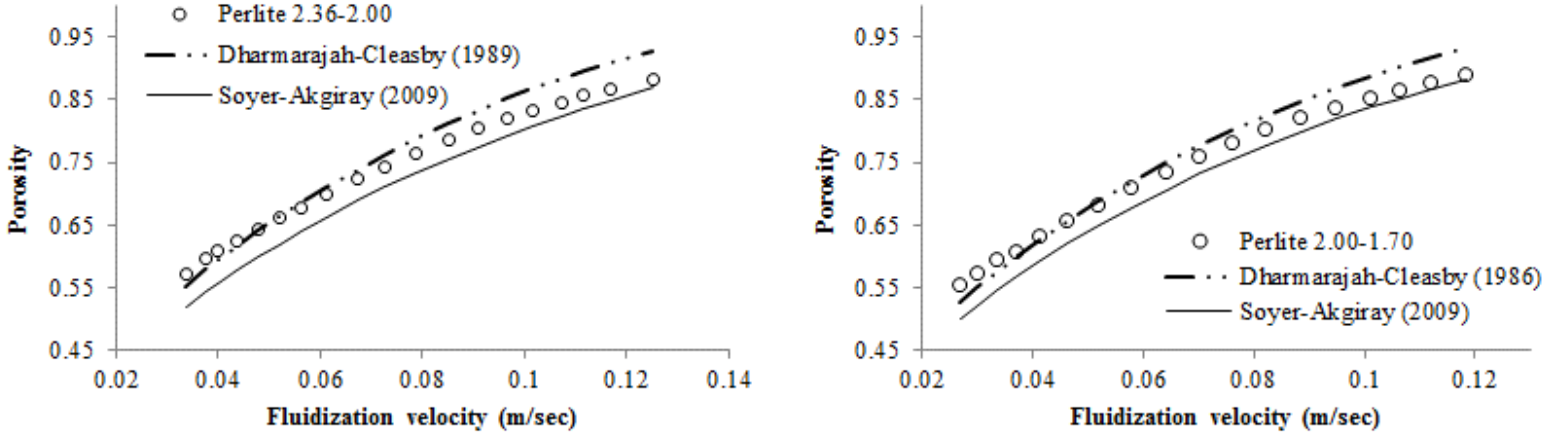
Appendix III-Figure 7 Fluidization graphs of 1.40-1.18 and 1.18-1.00 fractions of crushed glass



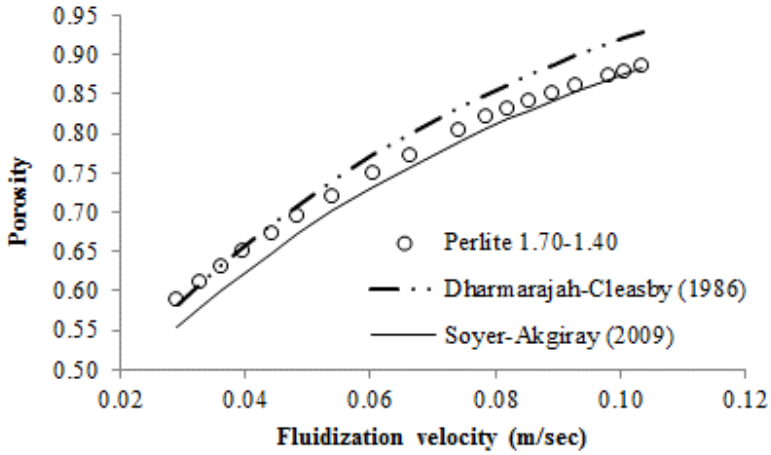
Appendix III-Figure 8 Fluidization graphs of 1.00-0.85 and 0.85-0.71 fractions of crushed glass

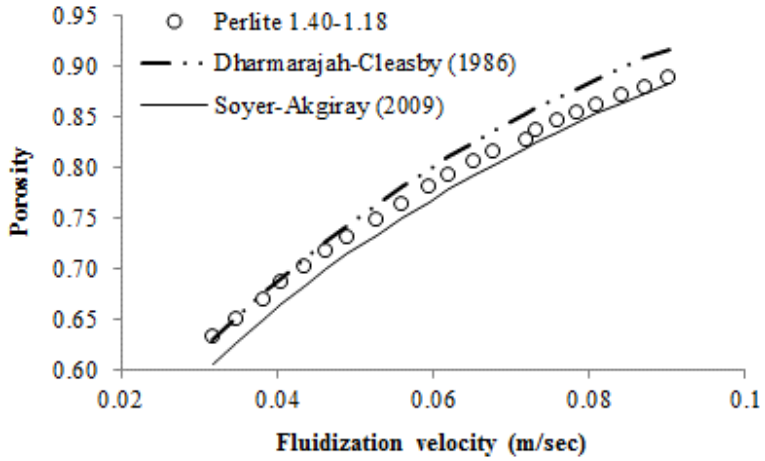


Appendix III-Figure 9 Fluidization graph of 0.71-0.60 fraction of crushed glass

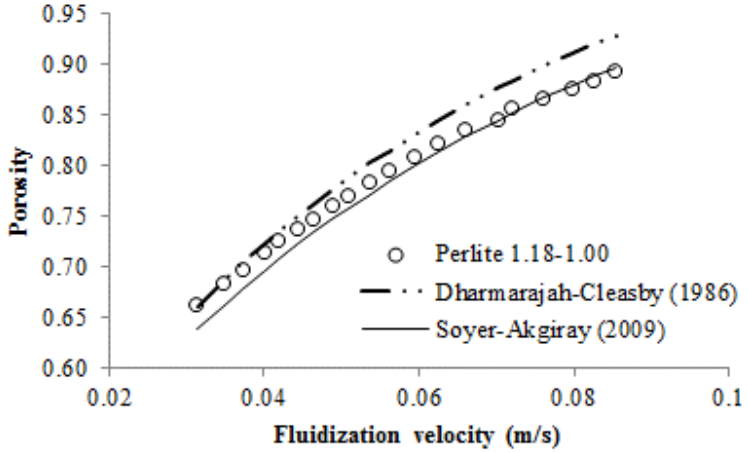


Appendix III-Figure 10 Fluidization graphs of 2.36-2.00 and 2.00-1.70 fractions of perlite





Appendix III-Figure 11 Fluidization graphs of 1.70-1.40 and 1.40-1.18 fractions of perlite



Appendix III-Figure 12 Fluidization graph of 1.18-1.00 fraction of perlite

ÖZGEÇMİŞ

1. Adı Soyadı : SELDA YİĞİT HUNCE

2. Doğum Tarihi : 1985

3. Unvanı : Arş.Gör.

4. Öğrenim Durumu

Derece	Alan	Üniversite	Yıl
Lisans	Çevre Mühendisliği	MARMARA ÜNİVERSİTESİ	2008
Yüksek Lisans	Çevre Mühendisliği	MARMARA ÜNİVERSİTESİ	2010
Doktora	Çevre Mühendisliği	MARMARA ÜNİVERSİTESİ	2017

5. Akademik Unvanlar

Görev Unvanı	Alan	Üniversite	Yıl
Arş.Gör.	Çevre Mühendisliği	BAHÇEŞEHİR ÜNİVERSİTESİ	2008-2010
Arş.Gör.	Çevre Mühendisliği	İSTANBUL ÜNİVERSİTESİ	2014-

7. Yayınlar

7.1 Uluslararası Hakemli Dergilerde Yayınlanan Makaleler

Yiğit Hunce S. , Soyer E., Akgiray Ö., "Characterization of Granular Materials with Internal Pores for Hydraulic Calculations Involving Fixed and Fluidized Beds", INDUSTRIAL & ENGINEERING CHEMISTRY RESEARCH, vol.55, pp.8636-8651, 2016

Yiğit Hunce S. , Akgul D., Demir G., Mertoglu B., "Solidification/stabilization of landfill leachate concentrate using different aggregate materials", WASTE MANAGEMENT, vol.32, pp.1394-1400, 2012

Yiğit Hunce S. , Demir G., Ozdemir H., Borucu G., Saral A., "Elemental Concentrations of Atmospheric Aerosols and the Soil Samples on the Selected Playgrounds in Istanbul", JOURNAL OF RESIDUALS SCIENCE, vol.7, pp.123-130, 2010

Yiğit Hunce S. , "Examining the Particulate Matter (PM2.5 ve PM10) Pollution on the Playgrounds in Istanbul", EKOLOJI, vol.19, pp.72-79, 2010

Borucu G., Yiğit Hunce S. , Ozdemir H., Demir G., Ozcan H.K., "Quantification of Atmospheric Particle Number Concentration for Selected Children Playgrounds: A Case Study in Istanbul", JOURNAL OF RESIDUALS SCIENCE, vol.7, pp.147-152, 2010

7.2 Uluslararası Bilimsel Toplantılarda Sunulan ve Bildiri Kitabında (Proceedings) Basılan Bildiriler

Yiğit Hunce S. , Soyer E., Akgiray Ö., "Characterızatıon of Natural Zeolıte For Granular-Bed Fılters", International Porous and Powder Materials Symposium and Exhibition, PPM 2015, İZMİR, TÜRKIYE, 15-18 Eylül 2015, pp.294-298

Yiğit Hunce S. , Soyer E., Akgiray Ö., "Particle Characterization of Crushed Recycled Glass", 2nd International Conference on Recycling and Reuse, İSTANBUL, TÜRKIYE, 4-6 Haziran 2014, pp.169-170

Soyer E., Yiğit Hunce S. , Yılmaz Z., Babaoğlu C., Ülkü Z.M., Akgiray Ö., "Recycled Material in Water Filtration: The Efect of Media Grain Shape", 2nd International Conference on Recycling and Reuse, İSTANBUL, TÜRKIYE, 4-6 Haziran 2014, pp.171-172

Çoban A., Yiğit Hunce S. , Demir G., "Sürdürülebilir Su Yönetimi Çerçevesinde Evsel Atıksuların Arıtım Teknolojileri ve Yeniden Kullanımının Değerlendirilmesine Genel Bir Bakış", International Symposium On Environment, Bişkek, KIRGIZISTAN, 20-23 Mayıs 2009, pp.1-1

Yiğit Hunce S. , Çoban A., Demir G., "Dezenfeksiyonun Çevre Mühendisliği'ndeki Değişik Uygulamaları ve Dezenfeksiyon Yöntemlerinin Değerlendirilmesi", International Symposium On Environment, Bişkek, KIRGIZISTAN, 20-23 Mayıs 2009, pp.1-1

7.4 Ulusal Hakemli Dergilerde Yayınlanan Makaleler

Yiğit Hunce S. , Çoban A., Demir G., "Comparative Evaluation of Various Advanced Oxidation Processes for the Treatment of Textile Industry Effluents", Beykent University Journal of Science and Technology, cilt.3, ss.149-160, 2009

7.5 Ulusal Bilimsel Toplantılarda Sunulan ve Bildiri Kitabında Basılan Bildiriler

Yiğit Hunce S. , Elmaslar Özbaş E., Özcan H.K., Öngen A., Gazi S., "Küçükçekmece İlçesi Sınırları İçerisinde Oluşan Evsel ve Endüstriyel Atık Miktarlarının İncelenmesi", 8. Ulusal Katı Yönetimi Kongresi, UKAY'2016, KASTAMONU, TÜRKIYE, 11-14 Mayıs 2016, ss.0-0

Yiğit Hunce S. , Çoban A., Demir G., Ozdemir H., Borucu G., Ak N., "Partiküler Maddeler ve İklim Değişikliği Üzerine Etkilerinin Değerlendirilmesi", II. Türkiye İklim Değişikliği Kongresi, İSTANBUL, TÜRKIYE, 16-18 Haziran 2010, ss.307-316

Çoban A., Yiğit Hunce S. , Demir G., Ak N., "Küresel İklim Değişikliği ve Su Kaynakları Üzerine Etkisi: Türkiye Örneği", II. Türkiye İklim Değişikliği Kongresi, TİKDEK, İSTANBUL, TÜRKIYE, 16-18 Haziran 2010, ss.155-164

Yapsaklı K. , Yiğit Hunce S. , Yılmaz A.G., Mertoglu B., "Zeolit Dolgulu Filtrelerde Anammox Kültürünün Yetiştirilmesi", ÇEVKOS VI, Türkiye'de Çevre Kirlenmesi Öncelikleri Sempozyumu, İSTANBUL, TÜRKIYE, 28-29 Mayıs 2009, ss.378-382

Çoban A., Yiğit Hunce S. , Demir G., "Kompostlaştırma Prosesinde Yöntem Seçiminin Kompost Kalitesi Üzerindeki Etkisinin Değerlendirilmesi", TÜRKAY 2009 Türkiye'de Katı Atık Yönetimi Sempozyumu, İSTANBUL, TÜRKIYE, 15-17 Haziran 2009, ss.0-0

7.6 Yazılan Ulusal Kitaplar veya Kitaplarda Bölümler

Saatçı A.M., Akgiray Ö. , Soyer E., Erdim E., Yiğit Hunce S. , "Su Arıtma Tesisleri İşletimi El Kitabı", Türkiye Belediyeler Birliği, ANKARA, 2015

8. Projeler

"İstanbul Kenti Evsel Arıtma Çamurlarından Termokimyasal Yöntemlerle Enerji Geri Kazanım Potansiyelinin Belirlenmesi", Diğer Kamu Kuruluşlarınca Desteklenen, TR10/14/EVK/0022, Araştırmacı, 2015